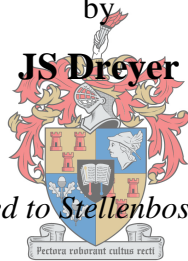

INVESTIGATING THE INFLUENCE OF LOW-
LEVEL OUTLET SHAPE ON THE SCOUR
CONE FORMED DURING PRESSURE
FLUSHING OF SEDIMENTS IN
HYDROPOWER PLANT RESERVOIRS

by

JS Dreyer



Thesis submitted to Stellenbosch University in

fulfilment of the requirements for the degree of

UNIVERSITEIT
iYUNIVESITHI
STELLENBOSCH
UNIVERSITY

Master of Engineering

100

1918 · 2018

Division of Water and Environmental Engineering

Department of Civil Engineering

Stellenbosch University

Private Bag X1, Matieland, 7602

Stellenbosch, South Africa

Supervisor: Prof GR Basson

December 2018

DECLARATION

1. Plagiarism is the use of ideas, material and other intellectual property of another's work and to present it as my own.
2. I agree that plagiarism is a punishable offence because it constitutes theft.
3. I also understand that direct translations are plagiarism.
4. Accordingly, all quotations and contributions from any source whatsoever (including the internet) have been cited fully. I understand that the reproduction of text without quotation marks (even when the source is cited) is plagiarism.
5. I declare that the work contained in this thesis, except where otherwise stated, is my original work and that I have not previously (in its entirety or in part) submitted it for grading in this module/assignment or another module/assignment.

Signed: _____

Initials and surname: _____

Date: _____

ABSTRACT

The global shift to renewable energy sources has led to the exponential growth of hydropower in the 21st century. Hydropower will continue to play an important role in electricity supply in the near future and as such the sustainable development of new hydropower plants (HPPs) is of utmost importance. Major hydropower plants require a reservoir (dam or weir) to be constructed on a river to temporarily store water and generate the required head for power generation. However, due to the reduction in flow velocity and sediment transport capacity when a river enters a reservoir, all or part of the incoming sediment load is trapped. The sedimentation of a reservoir essentially decreases the live storage capacity and potentially leads to sediment-laden water entering the hydropower intakes, thereby damaging turbines and causing generation losses.

Several sediment management strategies, such as watershed management, sluicing, flushing and turbidity current venting, have been employed all over the world with varying degrees of success. Pressure flushing is generally not regarded as an efficient means to regain lost storage capacity, but is often implemented in drier climates where reservoirs trap most of the incoming sediment and no additional water is available for implementing other sediment management strategies. More specifically, pressure flushing is often used in HPPs to scour out deposited sediment through a low-level outlet located below the hydropower intake.

In spite of the advances in pressure flushing studies, more information on the effect of the low-level outlet shape on the scour cone geometry is needed since almost all studies have been conducted on circular outlets. The dimensions of the scour cone are essential for the proper design of low-level outlets so that sediment-free conditions can be maintained at the power intake. In this study, the scour cone geometry associated with different outlet shapes under changing water depths and sediment levels were experimentally investigated. Four outlet shapes (circular, square, flat rectangular and upright rectangular) were tested at three water depths (1.75, 1.125 and 0.5 *m*) and three sediment levels (0, 0.1 and 0.2 *m*). Fine, non-cohesive silica sand with an effective diameter of 0.09 *mm* was used to pack a horizontal bed. Scour cone measurements were taken using a handheld three-dimensional laser scanner and the geometrical characteristics of the scour cone were analysed.

Non-dimensional equations for computing the scour cone dimensions and volume were developed using a multi-linear regression analysis. The developed equations fit the experimental data well and also take the outlet shape into account. The centreline and cross-

sectional bed profiles of the scour cones were also analysed and dimensionless equations defining the bed profile shape were developed. The results indicated that an increase in water depth (and thus also discharge) led to an increase in scour cone dimensions. Increasing the sediment level was also associated with an increase in scour cone size. Overall, the outlet shape had a significant effect on the scour cone geometry. The widest and largest scour cones were generally associated with the flat rectangular outlet, especially in cases where the sediment level was above the outlet invert.

OPSOMMING

Die wêreldwye skuif na hernubare energiebronne het gelei tot die eksponensiële groei van hidrokragsentrales in die 21^{ste} eeu. Hidrokragsentrales sal in die nabye toekoms, soos vandag, 'n belangrike rol in die voorsiening van elektrisiteit vervul. Daarom is die volhoubare ontwikkeling van nuwe hidrokragsentrales van kardinale belang. Groot hidrokragsentrales benodig 'n dam of keerwal wat in 'n rivier gebou word om water tydelik op te gaar en die benodigde waterhoogte vir kragopwekking te skep. As gevolg van die afname in vloeisnelheid en sedimentvervoerkapasiteit wanneer 'n rivier 'n dam binnegaan, word al die sediment of 'n deel van die inkomende sedimentlading gedeponeer. Die toeslikking van 'n dam verminder die bruikbare stoorkapasiteit en lei daartoe dat sediment-draende water die hidrokragsentrales binnedring. Dit kan skade veroorsaak aan turbines en opwekkingsverliese veroorsaak.

Verskeie sedimentbestuurstrategieë (soos opvanggebiedbestuur, deurspoel van sediment, uitspoeling, deurlating van digtheidstrome, ens.) is wêreldwyd onderneem met verskillende mates van sukses. Drukspoeling word oor die algemeen nie as 'n doeltreffende strategie beskou om verlore opgaarkapasiteit te herwin nie. Dit word egter dikwels in droër klimate geïmplementeer waar damme meeste van die inkomende sediment terughou en daar geen ekstra water beskikbaar is vir die implementering van ander sedimentbestuurstrategieë nie. Drukspoeling word dikwels in hidrokragsdamme gebruik om gedeponeerde sediment deur 'n laevlak-uitlaat, wat onder die kraginlate geleë is, te spoel.

Ten spyte van die vordering wat gemaak is met drukspoelnavorsing, is meer inligting nodig oor die invloed van die laevlak-uitlaatvorm op die sedimentuitskuurkeël, aangesien bykans alle vorige studies met sirkelvormige uitlate uitgevoer is. Die afmetings van die uitskuurkeël is noodsaaklik vir die behoorlike ontwerp van laevlak-uitlate, sodat sedimentvrye toestande by die hidrokragsentrales gehandhaaf kan word. In hierdie studie is die uitskuurkeëlafmetsings van verskillende uitlaatvorms onder veranderende waterdieptes en sedimentvlakke, eksperimenteel ondersoek. Vier uitlaatvorms (sirkelvormig, vierkantig, plat reghoekig en regop reghoekig) is getoets op drie waterdieptes (1.75, 1.125 en 0.5 m) en drie sedimentvlakke (0, 0.1 en 0.2 m). Fyn, nie-kohesiewe silika sand met 'n effektiewe deursnee van 0.09 mm is gebruik om 'n horisontale sediment bed te pak. Die skuurkeëls is opgemeet met behulp van 'n drie-dimensionele laserskandeerder en die geometriese eienskappe van die keëls is ondersoek.

Dimensielose vergelykings vir die berekening van die uitskuurkeëlafmetsings en volume is ontwikkel met behulp van 'n multi-lineêre regressie-ontleding. Die vergelykings wat ontwikkel

is pas die eksperimentele data goed en neem ook die uitlaatvorm in ag. Die lengte- en dwarsnitte van die skuurkeëls is ook ontleed en dimensielose vergelykings wat die bodemprofielvorm definieer, is ontwikkel. Die resultate het getoon dat 'n toename in waterdiepte (en dus ook deurstroming) lei het tot 'n toename in uitskuurkeëlafmeters. Die verhoging van die sedimentvlak is ook gekoppel aan 'n toename in die uitskuurkeëlgrootte. Die uitlaatvorm het 'n beduidende invloed op die uitskuurkeëlafmeters. Die wydste en grootste uitskuurkeëls is oor die algemeen verwant aan die plat reghoekige uitlaat, veral in gevalle waar die sedimentvlak bo die uitlaat was.

ACKNOWLEDGEMENTS

Above all, I would like to thank God for giving me the good health, intellect and the physical abilities required to complete this study.

To my supervisor, Prof. Gerrit Basson, thank you for your valuable guidance and support throughout my study. I truly admire your knowledge and expertise in the field of hydraulic engineering.

To the laboratory manager, Mr. Ning Ma, thank you for your assistance with the design and construction of the physical model.

To the laboratory technical staff, Mr. Johan Nieuwoudt and Mr. Illiyaaz Williams, thank you for your assistance during the construction and testing phases of the physical model.

Stellenbosch University and the Water Research Commission (WRC) for funding of the physical model which was required for this study.

To my parents and brother, Jaco, Greta and Gerrit, thank you for your incredible love, motivation and support throughout my studies. I wish to thank my parents for inspiring me to further my studies and instilling the values of hard work and perseverance in me. I would also like to express my sincere gratitude to you for the financial support over the years.

Finally, I would like to thank my friends and loved ones for your encouragement and emotional support throughout my study. A special thank you to my colleagues in S407, thank you for your friendship and motivation over the past two years.

CONTENTS

1 Introduction	1
1.1 Background Information	1
1.2 Aim of Study	2
1.3 Problem Statement	2
1.4 Research Methodology	5
1.5 Thesis Overview	5
2 Literature Review	6
2.1 Introduction	6
2.2 Reservoir Sedimentation	6
2.2.1 Introduction	6
2.2.2 Sediment Properties.....	6
2.2.3 Sediment Transport	15
2.2.4 Sediment Deposition	17
2.2.5 Impacts of Reservoir Sedimentation	19
2.2.6 Reservoir Sedimentation in South Africa	21
2.3 Hydropower Reservoirs.....	22
2.3.1 Introduction	22
2.3.2 Classification of Hydropower Plants.....	22
2.3.3 HPP Turbine Damage.....	28
2.3.4 Hydropower Intake Structure Design.....	35
2.4 Low-Level Outlet Design.....	40
2.4.1 Criteria for Low-Level Outlet Design.....	41
2.4.2 Discharge Capacity	42
2.4.3 Shape and Geometry	43
2.4.4 Layout.....	44
2.4.5 Abrasion and Cavitation.....	45
2.4.6 Gates and Operation	46
2.4.7 Blockage by Sediment and Debris	49
2.4.8 Maintenance and Inspection.....	50
2.4.9 Typical Design	50
2.4.10 Chinese Low-Level Outlets.....	51
2.5 Sedimentation Management Strategies	54

2.5.1 Reduce Sediment Inflow from Upstream.....	55
2.5.2 Route Sediments to Minimize Deposition	55
2.5.3 Remove Accumulated Sediment Deposits	57
2.5.4 Sediment Management for Different Types of Dams	58
2.6 Reservoir Desiltation by Means of Flushing.....	58
2.6.1 Drawdown Flushing	60
2.6.2 Pressure Flushing	60
2.6.3 Applications and Limitations	62
2.7 Low-Level Outlet Flushing Under Pressure.....	62
2.7.1 Orifice Flow Theory.....	62
2.7.2 Pressure Flushing Process	64
2.7.3 Scour Cone Geometry	65
2.7.4 Previous Hydraulic Model Studies.....	71
2.8 Laws of Hydraulic Similarity for Physical Models.....	79
2.8.1 Similarity Laws	80
2.8.2 Scaling of Sediment	83
3 Experimental Setup.....	85
3.1 Objectives.....	85
3.2 Dimensional Analysis	85
3.3 Experiment Design	88
3.4 Physical Model Design.....	90
3.5 Sediment.....	93
3.6 Measurement Techniques.....	95
3.6.1 Scour Measurements	95
3.6.2 Discharge Measurement.....	97
3.6.3 Water Level Measurement	99
3.7 Experimental Procedure	99
3.8 Determining Experimental Time.....	100
3.9 Improvements from Previous Pressure Flushing Physical Models	101
3.10 Visual Observations	103
3.11 Limitations	103
4 Experimental Results	105
4.1 Data Processing and Analysis	105
4.2 Outlet Comparison	105

4.3 Scour Cone Results	106
4.3.1 Tests 1 to 12 with $H_s = 0$ m.....	106
4.3.2 Tests 13 to 24 with $H_s = 0.1$ m.....	109
4.3.3 Tests 25 to 36 with $H_s = 0.2$ m.....	110
4.3.4 Scour Cone Geometry Results	111
4.4 Repeatability.....	113
5 Analysis and Discussion of Results	114
5.1 Analysis of Scour Cone Geometry.....	114
5.1.1 Cone Length	114
5.1.2 Cone Width	117
5.1.3 Cone Height.....	120
5.1.4 Cone Depth.....	123
5.1.5 Cone Volume.....	126
5.1.6 Summary	128
5.2 Comparison with Literature	129
5.3 Regression Analysis	131
5.3.1 Simplification Process.....	131
5.3.2 Models.....	132
5.3.3 Scour Cone Length.....	134
5.3.4 Scour Cone Width	135
5.3.5 Scour Cone Height	136
5.3.6 Scour Cone Depth	137
5.3.7 Scour Cone Volume	138
5.3.8 Sensitivity Analysis.....	142
5.3.9 Regression Analysis for Each Outlet Shape.....	143
5.3.10 Summary	145
5.4 Centreline Bed Profiles	145
5.5 Cross-Sectional Bed Profiles.....	149
5.6 Scour Cone Aspect Ratio Analysis	154
5.7 Flushing Efficiency	157
5.8 Practical Application of Results	158
5.8.1 Scaled Results for Application.....	158
5.8.2 Proposed Layout of Flushing and HPP Intake	162
6 Conclusions and Recommendations	164

6.1 Conclusions from the Literature Review	164
6.2 Conclusions from the Physical Model Experiments	165
6.3 Recommendations for Further Research	166
7 References	168
8 Appendices	178
Appendix A Summary of Tunnel Spillways	179
Appendix B Experimental Setup Photos	182
Appendix C Sediment Specification Sheet	185
Appendix D Scanner Specifications	186
Appendix E Scour Cone Photos	187
Appendix F Scour Cone Contour Plots	190
Appendix G Comparison with Other Studies	196
Appendix H Statistical Parameters Definitions	202
Appendix I Statistical Parameters of the Regression Analysis	204
Appendix J Statistical Parameters for the Outlet Specific Regression Analysis	205
Appendix K Centreline Bed Profiles	207
Appendix L Cross-Sectional Bed Profiles	212
Appendix M Scour Cone Slope Comparison	217
Appendix N Prototype Scaled Graphs	218

LIST OF FIGURES

Figure 2.1 Normal and cumulative frequency curves of sediment distributions (adapted from Yang, 2003)	7
Figure 2.2 Sphericity, roundness and sorting of sediment particles (adapted from Morris & Fan, 1998).....	11
Figure 2.3 Settling velocity as a function of sediment size for spherical particles in water at 15°C	14
Figure 2.4 Sediment transport in rivers (adapted from Dey, 2014)	16
Figure 2.5 Turbidity current in a reservoir (adapted from Morris <i>et al.</i> , 2008)	17
Figure 2.6 Longitudinal deposition shapes (adapted from Morris & Fan, 1998).....	18
Figure 2.7. Reservoir deposition patterns (adapted from Shen, 1999).....	19
Figure 2.8 General HPP layout and its components (adapted from Daware, 2016)	22
Figure 2.9 Typical storage scheme layout (adapted from Kumar <i>et al.</i> , 2011).....	25
Figure 2.10 Typical run-of-river scheme with pondage (adapted from Kumar <i>et al.</i> , 2011)...	26
Figure 2.11 Layout of a pumped storage scheme (adapted from Kumar <i>et al.</i> , 2011).....	27
Figure 2.12 Comparison between impulse and reaction turbines (adapted from Rathore <i>et al.</i> , 2015).....	29
Figure 2.13 Definition sketch for intake submergence (Johnson, 1988)	38
Figure 2.14. Trash rack parameters and bar shape factors (adapted from ESHA, 2004).....	39
Figure 2.15. Low-level outlet and intake layout of Gebidem Dam (adapted from Morris & Fan, 1998).....	45
Figure 2.16 Low-level outlet configuration of the Cerro del Águila Dam showing the syphon structure to assist in sediment flushing (adapted from Sayah <i>et al.</i> , 2015).....	49
Figure 2.17 Typical low-level outlet arrangement (adapted from Vischer & Hager, 1998)....	51
Figure 2.18 Graph showing the height versus width plots of for 31 major dams with rectangular shaped tunnel outlets	53
Figure 2.19. A summary of sediment control measures (adapted from Morris, 2015).....	55
Figure 2.20 Comparison of pressure and drawdown flushing (adapted from Shen, 1999).....	59
Figure 2.21 Flow through an orifice (Chadwick <i>et al.</i> , 2013).....	63
Figure 2.22 Scour cone formed by pressure flushing (Lai & Shen, 1996)	65
Figure 2.23 Scour limit in static water for different outlets (adapted from White & Bettess, 1984).....	66
Figure 2.24 Simplified flow pattern at a low-level outlet (adapted from Scheuerlein, 1993)..	67

Figure 2.25. Flushing actions at water level drawdown (adapted from Scheuerlein <i>et al.</i> , 2004)	69
Figure 2.26 Modified Liu Diagram (adapted from SANRAL, 2013)	84
Figure 3.1 Schematic drawing of the experimental setup	90
Figure 3.2 View from downstream of steel plate installation with supports	90
Figure 3.3 Steel discs with different shaped outlets	91
Figure 3.4 Connections at the downstream end of the plate	92
Figure 3.5 Sediment bed and plate viewed from upstream	93
Figure 3.6 Grain size distribution curve with five percentage bands	94
Figure 3.7 DPI-8 handheld three-dimensional (3D) scanner	96
Figure 3.8 Coordinate system of the experimental setup	97
Figure 3.9 Upstream inflow control setup	98
Figure 3.10 Stage-discharge relationship for the round outlet	99
Figure 3.11 Sediment in water samples taken at different times during the test	101
Figure 4.1 Photo showing the scour cone of Test 6	106
Figure 4.2 Scour cone contour plots of the square outlet for $H_s = 0$ m	107
Figure 4.3 Scour cone contour plots for different outlets at $H_w = 1.75$ m and $H_s = 0$ m	108
Figure 4.4 Photo showing the scour cone of Test 19 with different scour cone features	109
Figure 4.5 Scour cone contour plots of the flat rectangular outlet for $H_s = 0.1$ m	110
Figure 4.6 Scour cone of Test 36	110
Figure 4.7 Scour cone contour plots of the flat rectangular outlet for $H_s = 0.2$ m	111
Figure 5.1 Cone length comparison for different outlet shapes and sediment levels	115
Figure 5.2 Discharge effect on cone length	116
Figure 5.3 Cone width comparison for different outlet shapes and sediment levels	118
Figure 5.4 Cone height comparison for different outlet shapes and sediment levels	121
Figure 5.5 Scour depth versus sediment level plot for $H_w = 1.125$ m	125
Figure 5.6 Cone volume comparison for different outlet shapes and sediment levels	126
Figure 5.7 Comparison of measured and predicted results by Meshkati Shahmirzadi <i>et al.</i> (2010) for (a) cone length and (b) cone width	129
Figure 5.8 Measured versus predicted cone volume from Emamgholizadeh <i>et al.</i> (2006)	130
Figure 5.9 Scatter plots comparing observed and predicted values for the cone length	135
Figure 5.10 Scatter plots comparing observed and predicted values for the cone width	136
Figure 5.11 Scatter plots comparing observed and predicted values for the cone height	137
Figure 5.12 Scatter plots comparing observed and predicted values for the cone depth	138

Figure 5.13 Scatter plots comparing observed and predicted values for the cone volume ...	139
Figure 5.14 Scatter plots comparing observed and predicted values for the improved cone volume regression.....	141
Figure 5.15 Observed versus predicted cone volume	141
Figure 5.16 Calibrated cone volume prediction	142
Figure 5.17 Centreline bed profiles for flat rectangular outlet at $H_s = 0$ m.....	146
Figure 5.18 Comparison of centreline profiles for $H_s = 0$ m and $H_w = 1.75$ m	147
Figure 5.19 Centreline bed profile data for Test 1 to 12 ($H_s = 0$ m)	147
Figure 5.20 Centreline bed profile data for Test 13 to 36 ($H_s = 0.1$ & 0.2 m).....	148
Figure 5.21 Cross-sectional profiles for Test 7–Flat rectangular outlet, $H_s=0$ m, $H_w=1.75$ m	150
Figure 5.22 Non-dimensional transverse scour cone profiles for Test 1 to 12 ($H_s = 0$ m)	151
Figure 5.23 Non-dimensional transverse scour cone profiles for Test 13 to 36 ($H_s > 0$ m) ..	151
Figure 5.24 Non-dimensional shape of top of scour hole	153
Figure 5.25 Graph showing the length to half-width of all tests.....	154
Figure 5.26 Isovelocity contours upstream of different shaped orifices	156
Figure 5.27 Sediment scaling for a 1:50 scale using the modified Liu diagram.....	160
Figure 5.28 Prototype scour cone volume at different water depths for flat rectangular outlet at 1:50 scale (determined using Equation 5-28 and Table 5.26).....	161
Figure 5.29 Elevation view of proposed layout of intake and outlet works.....	162
Figure 5.30 Elevation view of proposed layout of one low-level outlet and intakes.....	163
Figure A.1 Tunnel spillway types according to ICOLD (2017)	181
Figure B.1 View downstream towards plate showing concrete flow straighteners in flume.	182
Figure B.2 View downstream towards plate showing the levelled sediment bed at the invert level ($H_s = 0$ m) before the start of Test 1	182
Figure B.3 View of levelled sediment bed with thin steel plate used to keep sediment out of the outlet (acting as a control gate)	183
Figure B.4 (a) SAFMAG flow meter used for measuring outflowing discharge (b) butterfly valve used to control outflow	183
Figure B.5 Settling basin used to trap outflowing sediment	184
Figure B.6 Outflow at settling basin during testing	184
Figure C.1 Sediment specification sheet as provided by supplier.....	185
Figure D.1 DPI-8 handheld 3D scanner specifications (DotProduct, 2017).....	186
Figure E.1 Scour cone photos for the first set of tests where $H_s = 0$ m.....	187
Figure E.2 Scour cone photos for the first set of tests where $H_s = 0.1$ m.....	188

Figure E.3 Scour cone photos for the first set of tests where $H_s = 0.2$ m.....	189
Figure F.1 Scour cone contour plots for Tests 1 to 3 (Round outlet).....	190
Figure F.2 Scour cone contour plots for Tests 4 to 6 (Square outlet)	190
Figure F.3 Scour cone contour plots for Tests 5 to 7 (Flat rectangular outlet)	191
Figure F.4 Scour cone contour plots for Tests 10 to 12 (Upright rectangular outlet).....	191
Figure F.5 Scour cone contour plots for Tests 13 to 15 (Round outlet).....	192
Figure F.6 Scour cone contour plots for Tests 16 to 18 (Square outlet)	192
Figure F.7 Scour cone contour plots for Tests 19 to 21 (Flat rectangular outlet)	193
Figure F.8 Scour cone contour plots for Tests 22 to 24 (Upright rectangular outlet).....	193
Figure F.9 Scour cone contour plots for Tests 25 to 27 (Square outlet)	194
Figure F.10 Scour cone contour plots for Tests 28 to 30 (Flat rectangular outlet)	194
Figure F.11 Scour cone contour plots for Tests 31 to 33 (Upright rectangular outlet).....	195
Figure F.12 Scour cone contour plots for Tests 34 to 36 (Round outlet).....	195
Figure K.1 Centreline bed profiles for $H_w = 1.75$ m and $H_s = 0$ m	207
Figure K.2 Centreline bed profiles for $H_w = 1.125$ m and $H_s = 0$ m	207
Figure K.3 Centreline bed profiles for $H_w = 0.5$ m and $H_s = 0$ m	208
Figure K.4 Centreline bed profiles for $H_w = 1.75$ m and $H_s = 0.1$ m	208
Figure K.5 Centreline bed profiles for $H_w = 1.125$ m and $H_s = 0.1$ m	209
Figure K.6 Centreline bed profiles for $H_w = 0.5$ m and $H_s = 0.1$ m	209
Figure K.7 Centreline bed profiles for $H_w = 1.75$ m and $H_s = 0.2$ m	210
Figure K.8 Centreline bed profiles for $H_w = 1.125$ m and $H_s = 0.2$ m	210
Figure K.9 Centreline bed profiles for $H_w = 0.5$ m and $H_s = 0.2$ m	211
Figure L.1 Cross-sectional bed profiles for $H_w = 1.75$ m and $H_s = 0$ m.....	212
Figure L.2 Cross-sectional bed profiles for $H_w = 1.125$ m and $H_s = 0$ m.....	212
Figure L.3 Cross-sectional bed profiles for $H_w = 0.5$ m and $H_s = 0$ m.....	213
Figure L.4 Cross-sectional bed profiles for $H_w = 1.75$ m and $H_s = 0.1$ m.....	213
Figure L.5 Cross-sectional bed profiles for $H_w = 1.125$ m and $H_s = 0.1$ m.....	214
Figure L.6 Cross-sectional bed profiles for $H_w = 0.5$ m and $H_s = 0.1$ m.....	214
Figure L.7 Cross-sectional bed profiles for $H_w = 1.75$ m and $H_s = 0.2$ m.....	215
Figure L.8 Cross-sectional bed profiles for $H_w = 1.125$ m and $H_s = 0.2$ m.....	215
Figure L.9 Cross-sectional bed profiles for $H_w = 0.5$ m and $H_s = 0.2$ m.....	216
Figure N.1 Prototype scour cone length at different water depths for flat rectangular outlet at 1:50 scale (determined using Equation 5-27 and coefficients in Table 5.26)	218

Figure N.2 Prototype scour cone width at different water depths for flat rectangular outlet at 1:50 scale (determined using Equation 5-27 and coefficients in Table 5.26) 218

Figure N.3 Prototype scour cone height at different water depths for flat rectangular outlet at 1:50 scale (determined using Equation 5-27 and coefficients in Table 5.26) 219

Figure N.4 Prototype scour cone depth at different water depths for flat rectangular outlet at 1:50 scale (determined using Equation 5-27 and coefficients in Table 5.26) 219

LIST OF TABLES

Table 2.1 Sediment size classes (Morris & Fan, 1998).....	7
Table 2.2 Definition of small hydropower as defined by various countries	23
Table 2.3 Summary of the application ranges of different turbines.....	32
Table 2.4 Constants defining bell mouth shape of different inlets.....	36
Table 2.5 Correction factor k for flow at an angle to the bars (Bratko & Doko, 2013).....	40
Table 2.6 Comparison of the advantages and disadvantages of different control gate locations (USACE, 2003)	48
Table 2.7 Low-level outlets of Chinese hydropower projects (Guo, 2012).....	52
Table 2.8 Comparison of sluicing and turbidity current venting (from Fan & Morris, 1992a).....	57
Table 2.9 Comparison of pressure and drawdown flushing (from Fan & Morris, 1992a).....	61
Table 2.10 Field data of scour cone slope angles in Chinese reservoirs	70
Table 2.11 Scalar relationships for Froude Law	81
Table 3.1 Range of tests conducted.....	89
Table 3.2 Parameters for calculating weighted settling velocity	94
Table 3.3 Sediment characteristics	95
Table 3.4 Data accuracy of the DPI-8 handheld scanner	96
Table 3.5 Improvements made in this study compared to other physical model studies.....	103
Table 4.1 Observed average discharge coefficient for different outlets	106
Table 4.2 Scour cone geometry results for all tests.....	112
Table 4.3 Results of repeated tests	113
Table 5.1 Cone length comparison of different outlet shapes compared to round outlet	114
Table 5.2 Comparison of the cone length increase with increasing discharge	116
Table 5.3 Comparison of the cone length increase with increasing sediment level.....	117
Table 5.4 Cone width comparison of different outlet shapes compared to round outlet	119
Table 5.5 Comparison of the cone width increase with increasing discharge	120
Table 5.6 Comparison of the cone width increase with increasing sediment level	120
Table 5.7 Cone height comparison of different outlet shapes compared to round outlet	122
Table 5.8 Comparison of the cone height increase with increasing discharge	123
Table 5.9 Comparison of the cone height increase with increasing sediment level.....	123
Table 5.10 Cone depth comparison of different outlet shapes compared to round outlet.....	124
Table 5.11 Comparison of the cone depth increase with increasing discharge.....	124
Table 5.12 Comparison of the cone depth decrease with increasing sediment level	125

Table 5.13 Cone volume comparison of different outlet shapes compared to round outlet ..	127
Table 5.14 Comparison of the cone volume increase with increasing discharge	127
Table 5.15 Comparison of the cone volume increase with increasing sediment level.....	128
Table 5.16 Range of parameters in regression analysis	131
Table 5.17 Range of dimensionless parameters	132
Table 5.18 Regression analysis summary for scour cone length	134
Table 5.19 Regression analysis summary for scour cone width	135
Table 5.20 Regression analysis summary for scour cone height	136
Table 5.21 Regression analysis summary for scour cone depth	137
Table 5.22 Regression analysis summary for scour cone volume	139
Table 5.23 Regression summary for improved volume prediction.....	140
Table 5.24 Sensitivity analysis of the parameters used in the regression analysis	143
Table 5.25 Maximum and minimum errors of proposed equations for different outlets.....	143
Table 5.26 Coefficients for the separate regression equations.....	144
Table 5.27 Explicit equations for scour cone geometry prediction.....	145
Table 5.28 Longitudinal slope angle comparison for all tests.....	149
Table 5.29 Transverse slope angle comparison for all tests.....	152
Table 5.30 Aspect ratios for all tests conducted.....	155
Table 5.31 Average aspect ratios for the sediment levels and water depths	157
Table 5.32 Flushing efficiency for all tests (10^{-3})	158
Table 5.33 Prototype sediment sizes for different scales	159
Table 5.34 Range of parameters for different scales.....	160
Table 5.35 Scour cone dimensions for example scenario	161
Table A.1 Characteristics of typical large scale tunnel spillways ordered by height ICOLD (2017)	179
Table G.1 Scour cone length comparison between observed values from this study and predicted values from the equations of other authors (<i>mm</i>)	196
Table G.2 Scour cone width comparison between observed values from this study and predicted values from the equations of other authors (<i>mm</i>)	197
Table G.3 Scour cone depth comparison between observed values from this study and predicted values from the equations of other authors (<i>mm</i>)	198
Table G.4 Scour cone volume comparison between observed values from this study and predicted values from the equations of other authors ($10^{-3} m^3$)	199

Table G.5 Scour cone length comparison between observed values for the round outlet from this study and predicted values from the equations of other authors (<i>mm</i>).....	200
Table G.6 Scour cone width comparison between observed values for the round outlet from this study and predicted values from the equations of other authors (<i>mm</i>).....	200
Table G.7 Scour cone volume comparison between observed values for the round outlet from this study and predicted values from the equations of other authors ($10^{-3} m^3$) ...	201
Table I.1 Regression analysis summary for the Linear Model	204
Table I.2 Regression analysis summary for the Linear Logarithmic Model.....	204
Table I.3 Regression analysis summary for the Logarithmic Transformed Model	204
Table J.1 Regression analysis summary for the square outlet.....	205
Table J.2 Regression analysis summary for the flat rectangular outlet.....	205
Table J.3 Regression analysis summary for the round outlet.....	205
Table J.4 Regression analysis summary for the upright rectangular outlet	206
Table M.1 Longitudinal and transverse slopes of the scour cones for all tests.....	217

LIST OF SYMBOLS

a	=	relative length of the longest particle axis
a_g	=	gate height (m)
α	=	angle between conduit centreline and the wall surface
A_o	=	outlet cross-sectional area (m^2)
b	=	relative length of the intermediate particle axis
b_b	=	width between bars (mm)
b_g	=	gate width (m)
b_{oc}	=	outlet width over centreline (m)
b_{oe}	=	outlet width at the edge (m)
β	=	submerged angle of repose of deposits (<i>degrees</i>)
c	=	relative length of the shortest particle axis
C	=	constant for different approach conditions
C_c	=	coefficient of contraction
C_d	=	discharge coefficient
C_D	=	drag coefficient
d_s	=	particle diameter (m)
d_{16}	=	diameter at which 16% of the sample is smaller than this value
d_{50}	=	diameter at which 50% of the sample is smaller than this value (median)
d_{84}	=	diameter at which 84% of the sample is smaller than this value
D	=	diameter of the conduit at the end of the entrance transition (m)
D_c	=	scour cone depth (m)
D_{sc}	=	diameter of PSC structure (m)
E	=	Euler number
E_f	=	flushing efficiency
F_D	=	fluid drag force (N)
Fr	=	Froude number
G_r	=	gradation coefficient
G_s	=	specific gravity
h_t	=	head loss (mm)

h_{oc}	=	outlet height over centreline (m)
h_{oe}	=	outlet height at the edge (m)
h_{pi}	=	piezometric head (m)
h_1	=	head upstream of V-notch crest, measured $5h_1$ upstream (m)
H_c	=	scour height, distance from top of sediment bed to lowest point (m)
H_h	=	hydraulic head of the reservoir, from the gate's horizontal axis (m)
H_s	=	horizontal sediment level above outlet invert (m)
H_w	=	available head above outlet (m)
ΔH	=	head losses from intake to gate (m)
K_b	=	coefficient for bar shape
K_x, K_y	=	constants for different conditions as defined in Table 2.4
λ	=	scale between prototype and model
L	=	characteristic linear dimension
L_c	=	scour cone length (m)
L_{sc}	=	length of PSC structure (m)
m	=	model
M	=	mass of sediment particle (kg)
M_t	=	total mass of sample (kg)
n	=	number of outlets
\emptyset	=	porosity
p	=	prototype
$p_{1,2}$	=	pressure at specified point (Pa)
Δp	=	change in pressure (kN/m^2)
ρ	=	density of water (kg/m^3)
ρ_s	=	mass density of sediment particle (kg/m^3)
ρ_{wb}	=	wet bulk density (kg/m^3)
φ	=	angle of inclination from horizontal ($degrees$)
P_o	=	outlet perimeter (m)
Q	=	flow rate (m^3/s)
Q_d	=	dominant discharge in the river (m^3/s)

Q_m	=	maximum free discharge of the outlets without flood detention (m^3/s)
Q_o	=	discharge through the outlet (m^3/s)
Q_0	=	dependent variable
$Q_{1,2,3}$	=	independent variables
r_c	=	distance of flushing cone without drawdown from Equation 2-37 (m)
R^2	=	coefficient of determination
Re	=	Reynolds number
Re_s	=	Reynolds number of sediment particle
R_o	=	hydraulic radius of the outlet (m)
σ	=	geometric standard deviation
σ_t	=	surface tension (N/m)
S	=	minimum submergence from the top of the intake (m)
SF	=	shape factor
S_n	=	slope of the line connecting the upstream end of the maximum pool level with the low-level outlets
S_0	=	original gradient of the river
t	=	time (s)
t_b	=	bar thickness (mm)
θ	=	angle of V-notch (<i>degrees</i>)
U	=	arbitrary parameter defined by $\frac{V}{\sqrt{gD}}$, where V and D are the average
U_o	=	velocity through the outlet (m/s)
ν	=	kinematic viscosity, $1.13 \times 10^{-6} m^2/s^2$ for water at $15^\circ C$ (m^2/s)
V	=	velocity (m/s)
V_a	=	approach velocity (m/s)
V_c	=	scour cone volume (m^3)
V_{*c}	=	critical shear velocity (m/s)
V_h	=	threshold velocity, equal to approach flow velocity V_a (m/s)
V_p	=	velocity in the conduit or penstock (m/s)
V_R	=	total volume of the reservoir (m^3)
V_s	=	volume of sediment without voids (m^3)
V_{sp}	=	volume of sediment particle (m^3)

V_{SS}	=	sediment settling velocity (m/s)
V_t	=	total volume of sample (m^3)
V_w	=	volume of water used during flushing (m^3)
$V_{1,2}$	=	velocity at specified point (m/s)
w	=	half-width of profile (m)
ω	=	settling velocity (m/s)
$\bar{\omega}$	=	effective settling velocity (m/s)
ω_n	=	settling velocity of associated diameter (m/s)
W	=	width at specific location (m)
We	=	Weber number
W_c	=	scour cone width (m)
W_m	=	maximum width of scour hole (m)
W_s	=	submerged weight of sediment (N)
x	=	distance from outlet along centreline (m)
x_c	=	coordinates whose x-x axis are parallel to and 0.65D from the conduit centreline
y	=	position along profile (m)
y_c	=	coordinates whose y-y axis are normal the conduit centreline and 0.5D downstream from the entrance face
γ_s	=	specific weight of sediment particle (kN/m^3)
γ_s'	=	submerged specific weight (kN/m^3)
γ_w	=	specific weight of water (kN/m^3)
$z_{1,2}$	=	elevation of the specified point above the datum (m)
Z	=	depth at position along profile (m)
Z_{CL}	=	centreline depth (m)
Z_{CL-max}	=	maximum centreline depth (m)

LIST OF ABBREVIATIONS AND ACRONYMS

ADV	Acoustic Doppler Velocimeter
ASCE	American Society of Civil Engineers
CFD	Computational Fluid Dynamics
CFRD	Concrete faced rockfill dam
ER	Rock-filled dam
ESHA	European Small Hydropower Association
FMC AG	Fichtner Management Consulting AG
HPP	hydropower plant
ICOLD	International Commission on Large Dams
IHA	International Hydropower Association
IRENA	International Renewable Energy Agency
MAE	Mean absolute error
MAF	Mean annual flow
MAR	Mean annual runoff
PG	Gravity dam
PSC	Projecting semi-circular structure
PVC	Polyvinyl chloride
RCC	Roller compacted concrete dam
RMSE	Root mean squared error
RoR	Run-of-river
SANRAL	South African National Roads Agency Ltd
TE	Earth-filled dam
USACE	United States Army Corps of Engineers
USBR	United State Bureau of Reclamation
VA	Arch dam

1 INTRODUCTION

1.1 Background Information

The word hydro is a combining form which comes from the Ancient Greek word for water. More specifically, hydropower refers to the energy generated by falling or moving water that could be harnessed for useful purposes.

For thousands of years human civilizations have utilised the power from flowing water for numerous daily tasks (Gatte & Kadhim, 2012). The first use dates back to the third century BC, where Greeks used water to power the Perachora wheel used for grinding corn and wheat (Tomlinson, 1976).

Hydropower has been closely associated with economic growth and globally played a major role in increasing development. A good example of this is the industrial revolution in England which was initiated by hydropower (International Hydropower Association, 2015).

Nowadays, the term hydropower is used exclusively to refer to electricity generation from water movement and will thus be used according to this definition for the remainder of this document. The force of flowing water was first used for the generation of electricity in 1878, when it was used to power a lamp in an English country house. Within the next decade hundreds of hydropower plants (HPPs) were in operation and the technology rapidly spread across the globe. The United States and Canada were initially the global leaders in hydropower, but in the past few decades China and Brazil have become the leaders (Campbell, 2010; International Hydropower Association, 2015). In 2015 China had 296 GW hydropower capacity, which accounted for 28% of the world's hydropower generation. China is also still the global leader in terms of commissioning new hydropower capacity with 16 GW of new projects commissioned in 2015 (Wetstone, Thornton, Hinrichs-rahlwes, Sawyer, Sander, Taylor, Rodgers, Alers, Lehmann, Eckhart & Hales, 2016).

At the end of 2015, hydropower was by far the greatest source of renewable energy, with a 16.6% contribution to the total global electricity production (Wetstone *et al.*, 2016). According to Gatte & Kadhim (2012), hydroelectric power is the cheapest source of electrical power, with the added benefit that it is renewable. Into the 21st century, hydropower will continue to play an integral role in electricity supply, especially as focus has shifted to renewable energy (International Hydropower Association, 2015).

1.2 Aim of Study

The main objective of this research is to contribute to the sustainable design of future reservoirs for sediment management by means of pressure flushing through low-level outlets located near the hydropower intakes. A better understanding of sediment flushing through low-level outlets is vital in order to decrease the coarse sediment load passing through hydropower intakes. This study aims to experimentally investigate the influence of the low-level outlet shape on the scour cone that forms during pressure flushing of sediments.

1.3 Problem Statement

Hydropower generation is the conversion of kinetic energy of moving water to electrical energy and is dependent on the flow of water from a higher level to a lower level, namely hydraulic potential energy. This difference in elevation is referred to as the *head* (Cleveland & Morris, 2014). A natural head such as a waterfall or a river running down a steep hill could be utilised for hydropower. Very often, however, artificial head is created by constructing a dam or weir, forming a reservoir, in order to raise the water to the desired level (Breeze, 2014). The result is greater potential energy, resulting in increased electricity output (FMC AG, 2011).

The construction of a reservoir also provides the operators with better control of the outflow of water and thus also the power generation (USBR, 2005). However, there are several disadvantages associated with reservoirs in general. With advances in dam engineering, modern dam failures have been reduced to acceptable limits, but the next major threat to the longevity and productivity of dams is reservoir sedimentation (Sumi & Hirose, 2000). The sedimentation problems experienced in hydropower reservoirs are of specific concern for this study.

Sedimentation essentially decreases the live storage capacity and if not managed properly, also leads to sediment-laden water entering the intakes. When non-cohesive coarse sediments enter the power intakes it results in severe turbine damage and generation losses (Sharma & Sharma, 1977).

Reservoirs constructed in the previous century were almost all designed with the conventional engineering concept of “design life”. The design life approach means that the structure will serve its purpose for a finite period, after which it is disposed of. This approach works well for conventional civil infrastructure that is easily refurbished, such as buildings and roads, but not for dams. This is due to the fact that after reservoirs are filled with sediment, they are often deemed useless, unless extreme measures can be taken. The problem that designers now face is that most of the world’s best reservoir sites have already been utilised and many have been

Chapter 1: Introduction

partially or completely filled with sediment. New dams should be designed with a “life cycle approach” in which implementation of sediment management strategies allow continued use and thus eliminating the element of disposal (Annandale, Morris & Karki, 2016).

Sedimentation must therefore be managed in all hydropower projects. Basson & Rooseboom (1999) stated that there are three ways to manage sediment accumulation in a reservoir, namely:

- reduce sediment load through watershed management;
- pass incoming sediment through the reservoir; or
- remove sediment after deposition.

This study focuses on the latter, namely removing sediments after deposition in the reservoir. Deposited sediment can be removed by mechanical (dredging or dry excavation) or hydraulic (flushing) methods (Annandale *et al.*, 2016). Two types of flushing are commonly used, namely drawdown flushing and pressure flushing, with high and low reservoir water levels respectively. The latter is done by opening the low-level outlets which allows the formation of a local scour hole. This is mainly done to keep the area in front of a hydropower intake free of sediment and is considered ineffective for restoring the live storage capacity in large reservoirs (Atkinson, 1996; Fan & Morris, 1992a; Lai & Shen, 1996; Morris & Fan, 1998; Shen, 1999; White & Bettess, 1984).

Even though this method of sediment removal is generally considered ineffective, several studies have been conducted to improve the flushing efficiency and create a better understanding of the scour cone formation associated with flushing under pressure.

Many regions across the world have dry climates or are prone to multi-year droughts (such as Southern Africa, Northern Africa, Middle East, Western Asia, Western America and Australia), and therefore rely on over-year storage for power generation and water supply. In these countries the ratio of reservoir storage volume to mean annual flow (MAF) is generally large in order to capture occasional major floods and store enough water for dry periods (Annandale *et al.*, 2016). Due to the scarcity of water, these countries cannot afford to empty a reservoir for flushing and thus pressure flushing is often the only viable option for clearing the area in front of the intakes.

Hydropower plant reservoirs do not always require a large storage capacity, because power generation is mainly dependent on the available head and flow rate. With sufficient measures to keep the intakes sediment free, a hydropower plant can silt up to a high level, without major impact on operation and power generation.

Chapter 1: Introduction

The main problems this study aims to address are:

- poor understanding of low-level outlet design for pressure flushing of non-cohesive sediment, and
- lack of design guidelines regarding the optimal low-level outlet shape for pressure flushing of sediments (local).

Several pressure flushing experimental model studies have been conducted over the years, but due to physical and time constraints, the results of many of these studies are only applicable under very specific conditions. Some of the problems associated with previous model studies include:

- Most studies used circular outlets and the influence of different outlet shapes on the scour cone has been overlooked or not taken into account (Dodaran, Park, Mardashti & Noshadi, 2012; Emamgholizadeh, Bina, Fathi-Moghadam & Ghomeysi, 2006; Emamgholizadeh & Fathi-Moghadam, 2014; Fathi-Moghadam, Emamgholizadeh, Bina & Ghomeshi, 2010a; Lai & Shen, 1996; Madadi, Rahimpour & Qaderi, 2017; Meshkati Shahmirzadi, Dehghani, Sumi, Mosaedi & Meftah H, 2010; Sawadogo, 2015; Shahraki, Ahadpour & Mardashti, 2014; Shen, 1999).
- Many studies used a single sediment level (Dodaran *et al.*, 2012; Emamgholizadeh, Bateni & Jeng, 2013; Emamgholizadeh *et al.*, 2006; Emamgholizadeh & Fathi-Moghadam, 2014; Fathi-Moghadam *et al.*, 2010a; Madadi *et al.*, 2017; Meshkati, Dehghani, Naser, Emamgholizadeh & Mosaedi, 2009; Meshkati Shahmirzadi, Dehghani, Sumi, Mosaedi, *et al.*, 2010; Meshkati Shahmirzadi, Dehghani, Sumi, Naser & Ahadpour, 2010; Shahraki *et al.*, 2014).
- Water depths in previous studies have not been very high, with the highest being 1.2 m in three previous model studies (Emamgholizadeh *et al.*, 2006; Emamgholizadeh & Fathi-Moghadam, 2014; Fathi-Moghadam *et al.*, 2010a).

This study addresses the above-mentioned problems by investigating orifice gravity flow (without pumping) through different low-level outlet shapes at varying sediment levels and water depths up to 1.75 m in the model. The model does not represent a specific prototype, but results can be scaled appropriately. For example, at a scale of 1:50 this could represent a prototype water depth of 87.5 m.

1.4 Research Methodology

A thorough review of the literature on hydropower reservoir sedimentation, hydropower intakes and low-level outlet flushing was followed by laboratory experiments to assess the extent of local scour in front of different low-level outlets during pressure flushing. An experimental model was designed and tested at the Civil Engineering Department Hydraulics Laboratory of Stellenbosch University.

Four different low-level outlet shapes were tested with three different water depths and three different sediment levels, in order to establish which shape is most effective in terms of flushing efficiency and scour cone dimensions. The flushing experiments were conducted by allowing water to flow out under gravity and no pumping was required.

Based on the experimental results, the best low-level outlet shape was identified. The experimental results were compared to other similar studies found in the literature. Using the results, equations describing the scour cone geometry were developed by regression analysis. Finally, the practical application of the results was demonstrated.

1.5 Thesis Overview

The thesis is structured as follows:

- **Chapter 2** presents the literature review, which includes topics on hydropower reservoirs, low-level outlet design, reservoir sedimentation and its management as well as more detailed discussions on pressure flushing through low-level outlets.
- **Chapter 3** contains information regarding the laboratory experiments which were conducted, including model design, experimental procedures and measurement techniques.
- **Chapter 4** presents the methods for processing the experimental data as well as the results from the tests.
- **Chapter 5** contains an in-depth analysis of the scour cone geometry results followed by a comparison with the literature. The regression analysis from the obtained results is also discussed and numerous equations for the dimensions of the scour cone are presented. The scour cone bed profiles are presented and analysed as well as the scour cone aspect ratio and the flushing efficiency.
- **Chapter 6** summarises the conclusions and gives recommendations for further study.

2 LITERATURE REVIEW

2.1 Introduction

In this chapter, relevant information from the literature regarding pressure flushing is reviewed. Background information about reservoir sedimentation and sedimentation management strategies are provided, followed by in-depth research on flushing of reservoirs. Specific focus is placed on pressure flushing through low-level outlets and the studies of several authors are reviewed.

2.2 Reservoir Sedimentation

2.2.1 Introduction

Reservoir sedimentation is the complex process whereby a reservoir behind a dam is filled with sediment carried by the incoming river. The rate of sedimentation in a reservoir depends on numerous factors including catchment characteristics, reservoir characteristics and climate. The average global sedimentation rate is about 0.8% of the original storage capacity per year, but is much higher in some regions such as Asia (ICOLD Sedimentation Committee, 2009). Sedimentation not only reduces the storage capacity of a reservoir, but also influences water supply, hydropower, flood control, navigation, recreation and the environment. Reservoir sedimentation is influenced by the sediment properties, characteristics of sediment transport and the patterns of deposition in the reservoir (Morris & Fan, 1998).

2.2.2 Sediment Properties

2.2.2.1 Size Classification

Sediment particles transported by water vary greatly in size ranging over seven orders of magnitude from clay particles to boulders. With grain size being the most important parameter for describing the behaviour of a sediment in water, it is important to distinguish between the various size ranges when considering sediment transport (Julien & Tuzson, 2002). Sediments are also broadly classified as either coarse or fine, with the former referring to sand and larger particles and the latter to silts and clays (Morris & Fan, 1998). The general sediment size classification is shown in **Table 2.1**.

Table 2.1 Sediment size classes (Morris & Fan, 1998)

Sediment type		Grain diameter range (mm)
Coarse	Boulders	4000-250
	Cobbles	250-64
	Gravel	64-2
	Sand	2-0.062
Fine	Silt	0.062-0.004
	Clay	<0.004

Although the properties of individual sediment particles are important, most sediment samples are not uniform, but rather made up of a mixture of grain sizes. It is therefore of interest to determine the particle size distribution which is commonly done through a sieve analysis. This method requires a sediment sample to be passed through a series of different mesh sized sieves whereafter the weighted fraction in each sieve is computed. The results of the sieve analysis can then be plotted as a grain size distribution curve, where the vertical axis represents the cumulative weight percentage and the horizontal axis represents the particle size as shown in **Figure 2.1**.

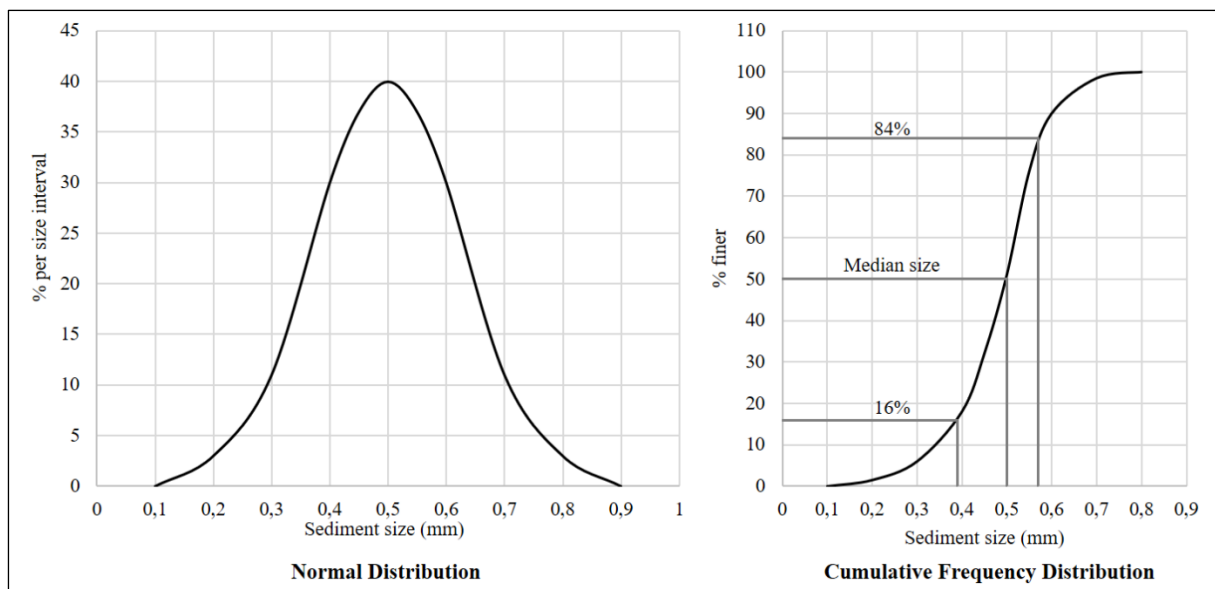


Figure 2.1 Normal and cumulative frequency curves of sediment distributions (adapted from Yang, 2003)

For simplification, it is often desirable to describe the behaviour of a sediment using a single diameter. The median diameter (d_{50}), is often used and is the diameter at which 50% of the sample's mass consists of particles with a diameter smaller than this value. If the grain size

Chapter 2: Literature Review

distribution curve is S-shaped, the gradation coefficient (Gr) and standard deviation (σ) can be calculated using **Equation 2-1** and **Equation 2-2** to give an indication of uniformity in the sample (Morris & Fan, 1998).

$$Gr = \frac{1}{2} \left(\frac{d_{84}}{d_{50}} + \frac{d_{50}}{d_{16}} \right) \quad 2-1$$

$$\sigma = \left(\frac{d_{84}}{d_{16}} \right)^{\frac{1}{2}} \quad 2-2$$

where:

G_r = gradation coefficient

σ = geometric standard deviation

d_{84} = diameter at which 84% of the sample is smaller than this value

d_{50} = diameter at which 50% of the sample is smaller than this value

d_{16} = diameter at which 16% of the sample is smaller than this value

2.2.2.2 Density

The density of a sediment particle, ρ_s , is an expression of its mass per unit volume, shown in **Equation 2-3**, and is related to the particle's mineral composition. The density of quartz particles is approximately 2650 kg/m^3 and is typically used for sediment calculations because natural river sands consist mostly of quartz.

$$\rho_s = \frac{M}{V_{sp}} \quad 2-3$$

where:

ρ_s = density of sediment particle (kg/m^3)

M = mass of sediment particle (kg)

V_{sp} = volume of sediment particle (m^3)

A sediment sample's density, known as the bulk density, is often an important parameter and includes both solid particles and voids. The bulk density of sediment is mostly a function of the mineral composition and the degree of compaction, with higher compaction being associated with a higher bulk density. Bulk density is distinguished into two main types, namely wet bulk density (or total bulk density) and dry bulk density, where the latter is calculated after the sample is oven-dried. The wet bulk density of reservoir sediment deposits is of specific interest in sediment scour investigations and can be determined using **Equation 2-4**. Numerous studies

Chapter 2: Literature Review

on bulk density of deposited sediments have been conducted over the years and several authors have presented empirical relationships for prediction thereof (Boroujeni, Fathi-Moghadam & Shafaei-Bejestan, 2009; Lane & Koelzer, 1943; Lara & Pemberton, 1963; Miller, 1953). Boroujeni *et al.* (2009) stated that these empirical relationships often underpredict the bulk density and that more studies should be conducted to develop an accurate empirical method that accounts for depth variation effects.

$$\rho_{wb} = \frac{M_t}{V_t} \quad 2-4$$

where:

$$\begin{aligned} \rho_{wb} &= \text{wet bulk density (kg/m}^3\text{)} \\ M_t &= \text{total mass of sample (kg)} \\ V_t &= \text{total volume of sample (m}^3\text{)} \end{aligned}$$

The specific weight of a particle is the product of mass density and gravitational acceleration as shown in **Equation 2-5**. The submerged specific weight can then be expressed as the difference between the specific weights of the particle and the fluid surrounding it, shown in **Equation 2-6**.

$$\gamma_s = \rho_s \cdot g \quad 2-5$$

$$\gamma'_s = \gamma_s - \gamma_w \quad 2-6$$

where:

$$\begin{aligned} \gamma_s &= \text{specific weight of sediment particle (kN/m}^3\text{)} \\ \gamma'_s &= \text{submerged specific weight (kN/m}^3\text{)} \\ \gamma_w &= \text{specific weight of water (kN/m}^3\text{)} \end{aligned}$$

The specific gravity (G_s) of a solid, typically 2.65, is a commonly used dimensionless ratio to indicate the density of the particle, shown in **Equation 2-7**.

$$G_s = \frac{\gamma_s}{\gamma_w} = \frac{\rho_s}{\rho} \quad 2-7$$

where:

$$\begin{aligned} G_s &= \text{specific gravity} \\ \rho &= \text{density of water (kg/m}^3\text{)} \end{aligned}$$

2.2.2.3 Porosity

The porosity (\emptyset) of deposited sediments quantifies the fraction of a given sediment sample that consists of voids and is an important parameter in determining the volume occupied by the sediments. Porosity is defined by **Equation 2-8**. Well-sorted sands tend to have a porosity of between 0.3 and 0.4, whilst poorly sorted gravels have porosity values as low as 0.2 due to finer grains filling the spaces between coarser grains.

$$\emptyset = \frac{V_t - V_s}{V_t} \quad 2-8$$

where:

\emptyset = porosity

V_s = volume of sediment without voids (m^3)

2.2.2.4 Cohesive and Non-cohesive Classification

Besides classification by size, sediments are also classified as either non-cohesive or cohesive. Cohesiveness renders sediments more resistant to erosion but is only displayed by clay particles with sizes less than 0.002 mm (Garcia, 2008). According to Partheniades (2009), cohesive grains are subjected to electrochemical surface forces that arise due to mineralogical sediment properties. Cohesive sediments generally have a high surface to volume ratio and the surface forces become dominant over the submerged weight of the particle (gravitational forces), leading to flocculation. As a result, the sediment transport and erosional processes of cohesive sediments are much harder to predict. In contrast, the sediment properties such as settling velocity, angle of repose and critical shear stress for non-cohesive sediments are determined by gravitational forces which are functions of particle size. Although reservoir deposits often contain a high clay content and have cohesive properties, this study focuses on non-cohesive sediment only due to the complexities and uncertainties involved in modelling cohesive sediment.

2.2.2.5 Angle of Repose

The angle of repose, also called the friction angle, of a sediment is the slope angle formed with the horizontal at the critical condition of incipient sliding (Morris & Fan, 1998). Simply put by Carter (1950), it is the maximum slope angle a heap or embankment can have without sliding.

For non-cohesive sediment the angle of repose is measured in the uncompacted state and is dependent on the grain size, shape and sorting (Miller & Byrne, 1966). Particle shape is roughly defined by roundness and sphericity, which are defined as:

Chapter 2: Literature Review

- Roundness – the smoothness of the grain corners and edges
- Sphericity – the relative length of the particle along the three axes

The effect of roundness on the hydraulic behaviour of a particle is relatively small but plays a major role in determining the abrasiveness to hydraulic equipment, which is discussed in **Section 2.3.3**. The sphericity of a particle has been studied extensively in settling velocity studies and can be expressed by the shape factor (SF) presented in **Equation 2-9**. The shape factor for a spherical particle is 1.0 and typically about 0.7 for natural sands (Vanoni, 2006).

$$SF = \frac{c}{\sqrt{ab}} \quad 2-9$$

where:

- SF = shape factor
 a = relative length of the longest particle axis
 b = relative length of the intermediate particle axis
 c = relative length of the shortest particle axis

Particle sorting simply refers to the distribution of grain sizes present in a sediment sample. **Figure 2.2** visually explains the concepts of sphericity, roundness and sorting. Miller & Byrne (1966) state that the angle of repose of sediment generally increases with a decrease in particle size, sphericity, roundness and sorting. Typically, the angle of repose for well-sorted sand is 30°, increasing gradually to 40° for gravel (Garcia, 2008; Julien & Tuzson, 2002).

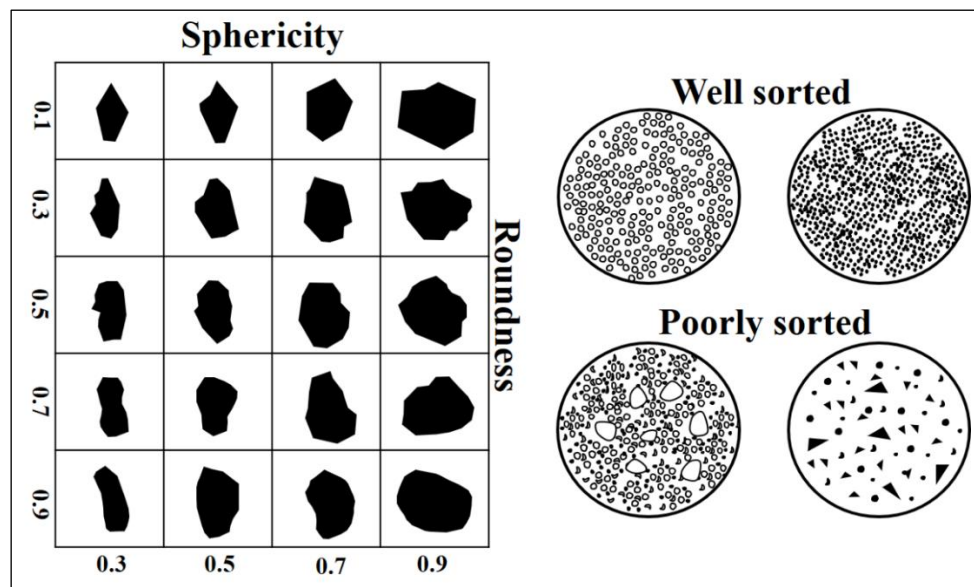


Figure 2.2 Sphericity, roundness and sorting of sediment particles (adapted from Morris & Fan, 1998)

Chapter 2: Literature Review

If non-cohesive sediment has accumulated against a low-level outlet, and the outlet is opened, the side slope angle of the scour cone will be similar to the submerged angle of repose of the deposits. However, if cohesive materials are present, the slope is generally steeper, but could also be less steep in cases where the sediment liquefies under certain conditions (Morris & Fan, 1998).

2.2.2.6 Settling Velocity

The settling velocity of a particle is a fundamental property determining the behaviour of the sediment in a fluid and is of special importance in sediment transport and deposition. Settling velocity is dependent on sediment-fluid interaction and is thus influenced by sediment size, shape, concentration and density as well as fluid temperature, salinity, density and viscosity (Morris & Fan, 1998). Settling velocity can be described by the balance between the submerged weight of the particle and the drag force induced by the fluid. According to Jenzer Althaus, Cesare & Schleiss (2015) the submerged weight of a spherical sediment particle can be calculated using **Equation 2-10**.

$$W_s = \frac{\pi}{6} \cdot d_s^3 \cdot (\rho_s - \rho) \cdot g \quad 2-10$$

where:

W_s = submerged weight of sediment (N)

d_s = particle diameter (m)

The fluid drag force can simply be described by

$$F_D = \frac{C_D \cdot \rho \cdot d_s^2 \cdot \omega^2 \cdot \pi}{8} \quad 2-11$$

where:

F_D = fluid drag force (N)

C_D = drag coefficient

ω = settling velocity (m/s)

For the particle to reach terminal velocity, the submerged weight must therefore be equal to the drag force, giving

$$\omega = \sqrt{\frac{4 \cdot (\rho_s - \rho) \cdot d_s \cdot g}{3 \cdot \rho \cdot C_D}} \quad 2-12$$

Chapter 2: Literature Review

In **Equation 2-12** the drag coefficient C_D , is the only remaining unknown required for calculating the settling velocity. The first analytical expressions for C_D were developed based on the assumption that the sediment particle is spherical and were later modified to take particle shape into consideration. The drag coefficient is strongly related to the particle Reynolds number, Re_s , and for the laminar settling region is

$$C_D = \frac{24}{Re_s} \quad 2-13$$

where:

$$Re_s = \frac{\omega \cdot d_s}{\nu} \quad 2-14$$

Re_s = Reynolds number of sediment particle

ν = kinematic viscosity (m^2/s)

Substituting **Equation 2-13** into **Equation 2-12** leads to the well-known Stoke's Law for settling velocity (given in **Equation 2-18**) which is applicable to spherical particles ranging in size from 1 to 100 μm .

For Reynolds numbers outside the laminar region, several empirical relationships between C_D and Re_s are presented in the literature. The Oseen and Kaskas formulae (**Equation 2-15** and **Equation 2-16** respectively) are two of the most commonly used and are applicable for $0.1 < Re_s < 1$ and $1 < Re_s < 200\,000$ respectively (Jenzer Althaus *et al.*, 2015).

$$C_D = \frac{24}{Re_s} \left[1 + \frac{3}{16} Re_s \right] \quad 2-15$$

$$C_D = \frac{24}{Re_s} + \frac{4}{\sqrt{Re_s}} + 0.4 \quad 2-16$$

A thorough analysis and comparison of existing drag coefficient equations was done by Brown & Lawler (2003) which yielded an improved and more sophisticated equation that holds for all $Re_s < 200\,000$.

$$C_D = \frac{24}{Re_s} (1 + 0.15 \cdot Re_s^{0.681}) + \frac{0.407}{1 + \frac{8710}{Re_s}} \quad 2-17$$

The relations given above between settling velocity, drag coefficient and Reynolds number are only valid for spherical particles and therefore cannot be applied to natural sediment particles because of shape differences. In these cases, the shape factor (SF) described in **Section 2.2.2.5**

Chapter 2: Literature Review

needs to be considered. For a shape factor between 0.5 and 1, experiments have shown that the fall velocity can differ up to 30%. Van Rijn (1993) presents the following settling velocity equations

for $1 < d_s \leq 100 \mu\text{m}$:

$$\omega = \frac{(G_s - 1) \cdot g \cdot d_s^2}{18 \cdot \nu} \quad 2-18$$

for $100 < d_s < 1000 \mu\text{m}$:

$$\omega = \frac{10\nu}{d_s} \cdot \left[\left(1 + \frac{0.01 \cdot (G_s - 1) \cdot g \cdot d_s^3}{\nu^2} \right)^{0.5} - 1 \right] \quad 2-19$$

for $d_s \geq 1000 \mu\text{m}$:

$$\omega = 1.1 \sqrt{(G_s - 1) \cdot g \cdot d_s} \quad 2-20$$

A more detailed analysis of several settling velocity equations is beyond the scope of this literature review, but can be found in Brown & Lawler (2003). A relationship between settling velocity and sediment particle size was determined using **Equations 2-18, 2-19** and **2-20**, and is shown in **Figure 2.3**. Note that this figure does not take the shape factor into consideration.

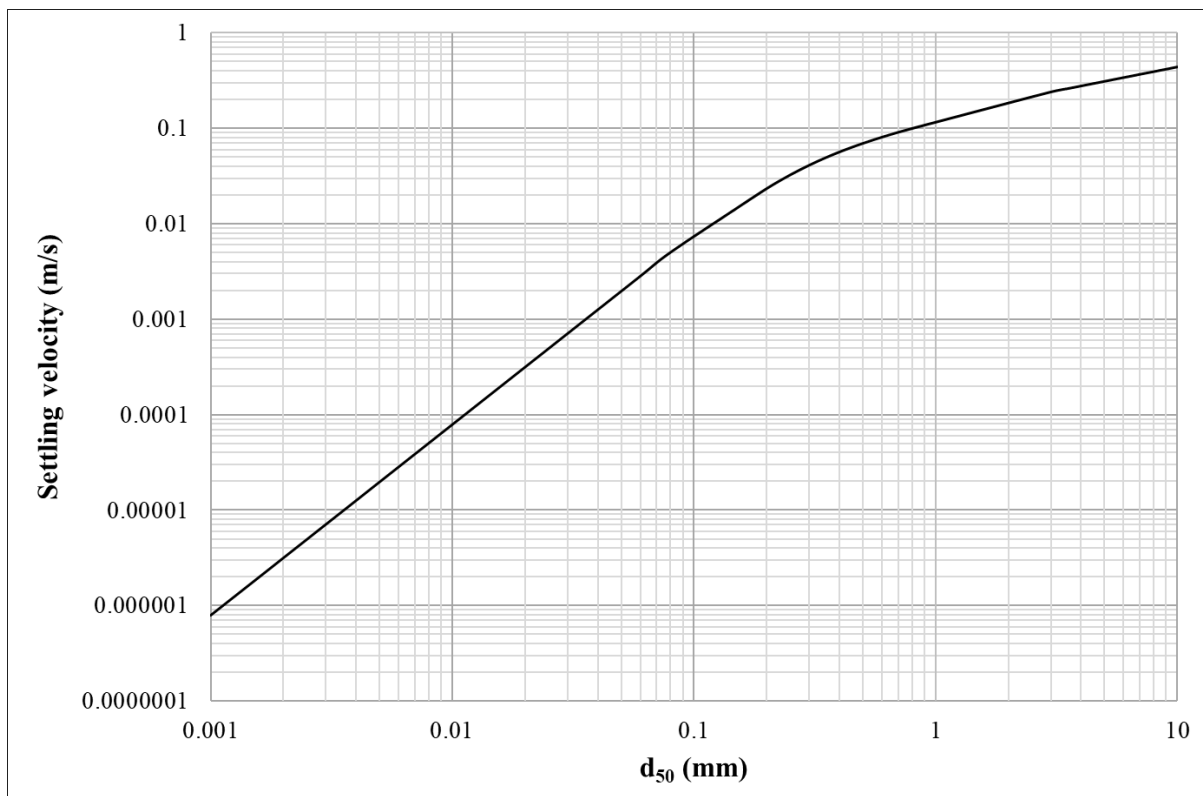


Figure 2.3 Settling velocity as a function of sediment size for spherical particles in water at 15°C

2.2.3 Sediment Transport

According to Kondolf (1997) the sediment processes in a watershed can be divided into three main categories: sediment production, sediment transport and sediment deposition. Sediment production is the first part of the sediment cycle and comprises of weathering and erosion of surfaces in a catchment as well as the displacement of river bed material by flow induced shear stress. The removal of detached sediment particles then occurs by entrainment and transport by water, which is often initiated by rainfall that results in sheet erosion (Garcia, 2008).

A substantial portion of the removed sediment is not transported out of the drainage basin, but instead are deposited on slopes, flood plains or in channels (Mahmood, 1987). The sediment that reaches the river is initially transported by the stream, but when the river enters a reservoir the sediment transport capacity reduces and the hydraulic conditions in the reservoir determine the sediment load (Basson & Rooseboom, 2007). The transport of sediment in rivers and reservoirs are thus discussed separately.

2.2.3.1 Transport in Rivers

The transport of sediment in rivers can be in the form of bed load and suspended load, depending on the catchment parameters (i.e. slope and vegetation), flow conditions (i.e. discharge and depth) and the sediment characteristics (i.e. size and shape). Van Rijn (1993) distinguishes three modes of particle motion: (1) rolling and sliding motion; (2) suspended motion; and (3) saltation motion.

Rolling and sliding motion occurs where the particles' critical value for initiation of motion is just exceeded by the bed-shear velocity, but they remain in continuous contact with the bed, forming the bed-load.

When the bed-shear velocity increases, the particles will start to move along the bed by regular jumps, called saltations which are also part of the bed load. If the settling velocity of the particles is exceeded by the bed shear velocity, they can be lifted off the bed and possibly be at a depth where the turbulence could be strong enough to keep the particles in suspension.

Another load, called wash load, can be contained in the suspended load and consists of very fine particles (silt and clay), usually less than 0.05 mm. The wash load mainly consists of particles from land surface erosion and abrasion of particles in transport, not from bed material (Van Rijn, 1993). The total transported load in a river is simply a combination of bed-load, suspended load and wash load as illustrated in **Figure 2.4**.

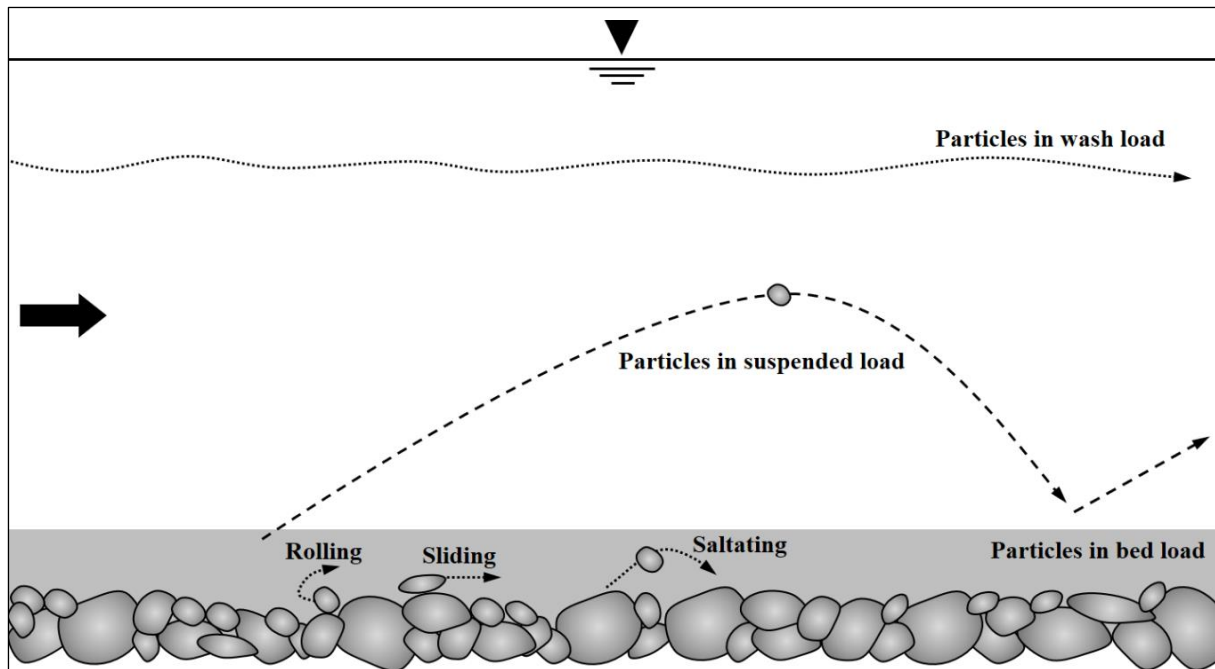


Figure 2.4 Sediment transport in rivers (adapted from Dey, 2014)

2.2.3.2 Transport in Reservoirs

As long as the sediment transport capacity of the flowing water is high enough, sediment will continue to be transported, even in a reservoir. Basson & Rooseboom (2007) mention three mechanisms of sediment transport in reservoirs, namely (1) turbulent suspension; (2) density currents; and (3) colloidal suspension.

Similar to the case in rivers, the dominant transport mechanism is turbulent suspension, where sediment particles remain in suspension due to turbulent forces in the flow (Basson & Rooseboom, 2007). The suspended sediment, comprising of sand, silt and clay, is distributed throughout the water column and some of it may be deposited and some transported through the reservoir and released downstream (Annandale *et al.*, 2016). Several studies on the development of suspended load formulas are found in the literature but are beyond the scope of this study.

Density currents are gravitationally induced flows that arise due to the density differences between the sediment-laden inflow and the cleaner water in the reservoir (Basson & Rooseboom, 2007). Various types of density currents are described in the literature, such as overflow, underflow and interflow, but underflow, also called turbid density currents are by far the most common (Mahmood, 1987). **Figure 2.5** illustrates the typical actions of a turbidity current in a reservoir. The presence of suspended sediments in the inflowing water causes a density difference and triggers a plunging current, thereby producing stratified flow (Chamoun,

Chapter 2: Literature Review

De Cesare & Schleiss, 2016). The point where the turbid water plunges beneath the clear water is called the *plunge point* and is often detected by a dramatic change in water colour and the presence of floating debris which accumulates at this point due to the convergence of the downstream-moving dense current and the upstream-moving clear water that travels along the surface (Mahmood, 1987; Morris & Fan, 1998).

These currents can travel very long distances (more than 100 km in some cases) along the reservoir bed, usually transporting fine to very fine sediment all the way to the dam (Annandale *et al.*, 2016). A turbidity current can even move up the dam wall and recirculate in the reservoir (Annandale, 2005). The venting of turbidity currents through low-level outlets has long been considered an effective sedimentation management technique in many reservoirs. Several field and laboratory observations and measurements were presented by Fan (1985) and more lately by Chamoun *et al.* (2016, 2017). Density current venting is briefly discussed in **Section 2.5.2**.

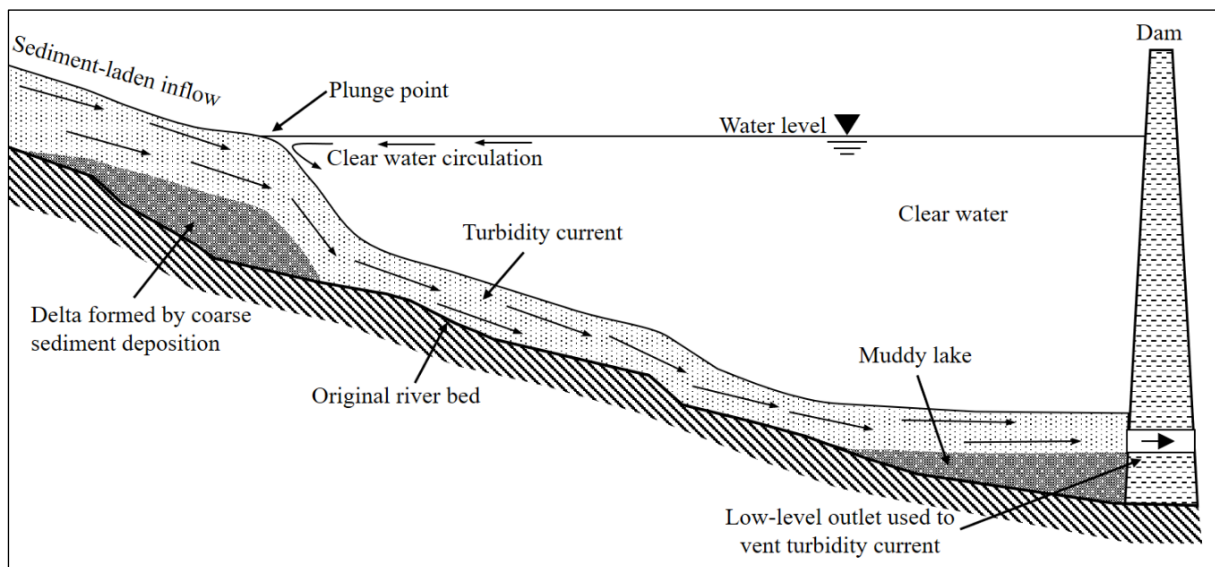


Figure 2.5 Turbidity current in a reservoir (adapted from Morris *et al.*, 2008)

Colloidal suspension is the suspension of fine particles (between 0.001 and 1 μm) due to electrostatic forces and is largely dependent on water quality. These suspensions are normally present at concentrations lower than 100 ppm and typically contribute less than 3% to the total load (Basson & Rooseboom, 2007).

2.2.4 Sediment Deposition

As a river enters a reservoir, the flow area increases and the flow velocity decreases, leading to a reduction in sediment transport capacity and therefore sediment deposition (Annandale, 2005). Not all of the sediment will always deposit, since some of it may pass through the

Chapter 2: Literature Review

reservoir and be released downstream. The proportion of the inflowing sediment that is trapped behind the dam is described by the reservoir's unique trap efficiency, which is dependent on sediment characteristics (such as particle size, shape and settling velocity) and reservoir parameters (shape, size, slope and flow) (Rulot, Dewals, Erpicum, Archambeau & Piroton, 2012). Reservoirs with a low capacity to MAR ratio can have trap efficiencies of less than 20%, but for large reservoirs it is typically close to 100% (ICOLD Sedimentation Committee, 2009). Four longitudinal depositional shapes are typically found in reservoirs as shown in **Figure 2.6**. These shapes often occur concurrently and are predominantly determined by sediment size, flooding, density currents and reservoir operating rules (Annandale *et al.*, 2016). Laterally the sediment deposits in the deepest part of the cross-section first, regardless of the original river cross-sectional shape, and over time forms a near-horizontal surface that spreads across the submerged floodplain (Morris & Fan, 1998; Rulot *et al.*, 2012).

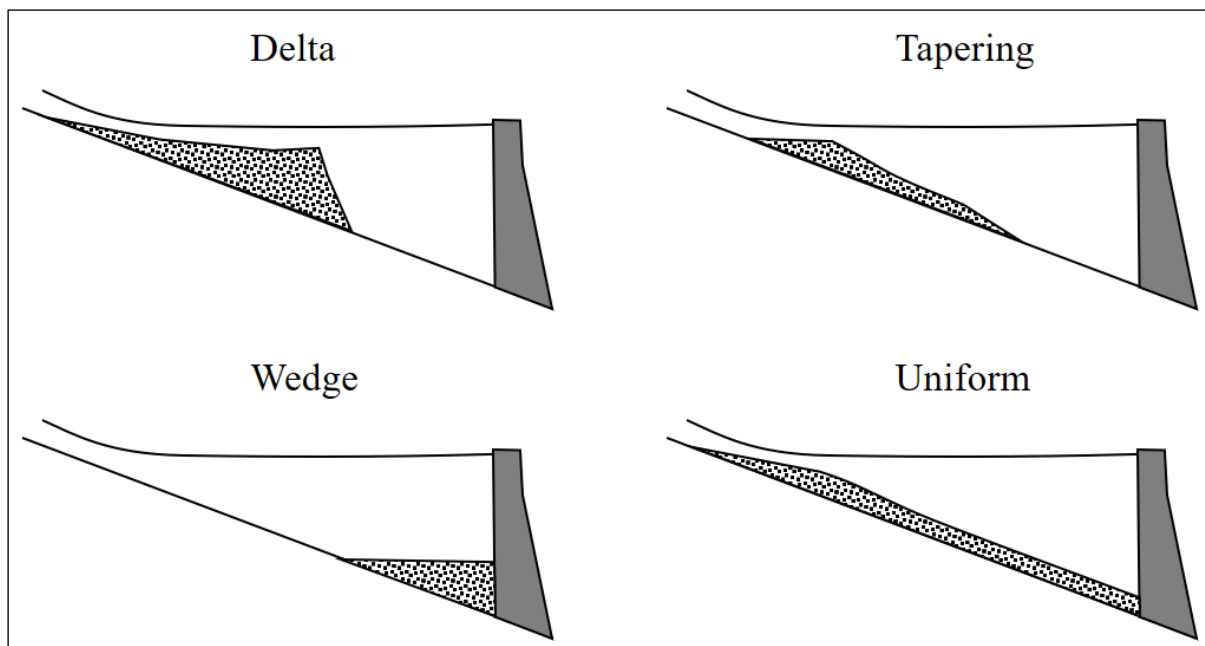


Figure 2.6 Longitudinal deposition shapes (adapted from Morris & Fan, 1998)

In general, large particles transported by the bed load and the coarse fraction of the suspended load settle first, forming a delta at the upstream end of the reservoir (Annandale, 2005). As shown in **Figure 2.7**, the delta is divided into two zones, namely the topset bed and the foreset bed, where the transition of the two coincides with the plunge point (Fan & Morris, 1992b). The topset deposits are dominated by bed material and have a milder slope than the original river bed, whereas the foreset is the face of the delta and is characterised by decreased grain size and increased slope. Downstream of the foreset bed is the bottomset bed which contains

Chapter 2: Literature Review

fine sediment deposits that have lower settling velocities and were carried by non-stratified flow and/or density currents (Morris & Fan, 1998).

Sometimes a muddy lake forms just upstream of the dam and is an indication that turbidity currents are likely present (Annandale *et al.*, 2016). Occasional events such as reservoir drawdown or extreme flooding may however carry coarser material towards the dam, forming deposit layers that vary in grain size (Morris & Fan, 1998).

Figure 2.7 shows the typical deposition pattern in a reservoir. If the sedimentation is not managed properly, the deposits can fill the reservoir and essentially eliminate the benefits for which it was built (Morris & Fan, 1998).

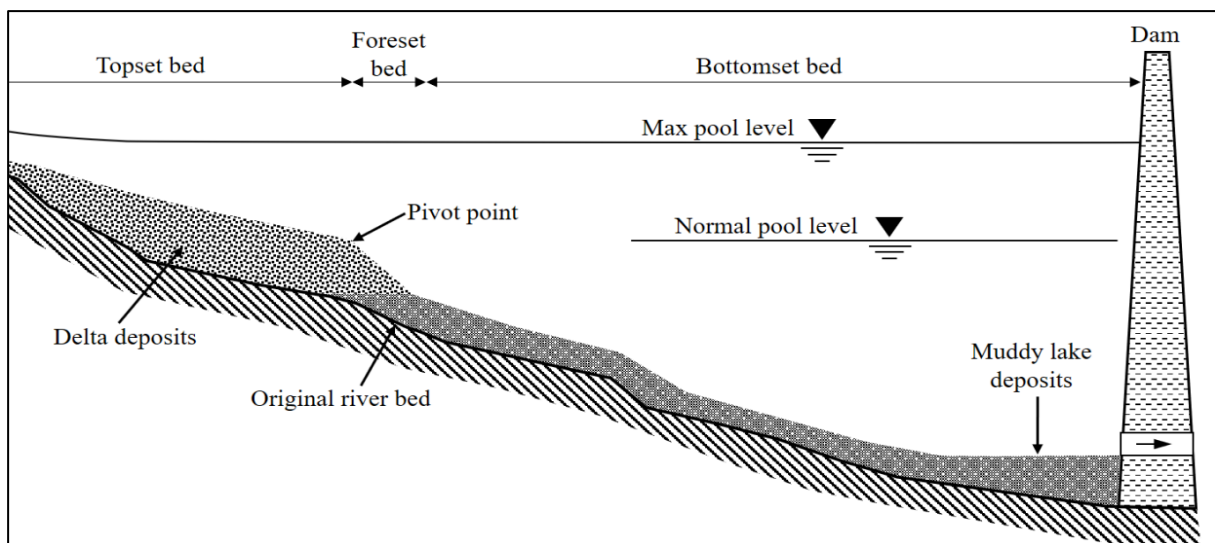


Figure 2.7. Reservoir deposition patterns (adapted from Shen, 1999)

2.2.5 Impacts of Reservoir Sedimentation

The impacts of reservoir sedimentation are not limited to the reservoir itself but extend upstream and downstream of the original design pool. The impacts are thus discussed separately for each zone.

2.2.5.1 Upstream Impacts

The main impacts upstream of the original design pool are due to deltaic deposition. The formation of a delta leads to backwater, increased depth and frequency of flooding, decreased navigational clearance at bridges and sedimentation at upstream water intakes. It also leads to bed aggradation above the normal pool level which increases groundwater levels and can cause soil waterlogging, salinization and destruction of ecological habitats (Morris *et al.*, 2008).

2.2.5.2 Within-Reservoir Impacts

The greatest impact within the reservoir is the loss of storage capacity which influences water supply, power generation and flood control. Reservoir storage is critical for ensuring a reliable supply of water, especially in semi-arid or arid regions where over-year storage is required. Reducing the storage capacity therefore greatly influences the yield which could impact potable water supply, agriculture and industry. Hydropower plants are affected in terms of power generation and abrasion of hydraulic machinery.

Okumura & Sumi (2012) investigated the impact of sedimentation on power generation in hydropower reservoirs in Japan and found that sedimentation has a detrimental effect on water use efficiency in both storage and run-of-river type facilities. They indicated that a direct relationship between the reduction of storage capacity and decrease in water use efficiency exists, but mentioned that climate change, maintenance and operating rules also play a key role.

Turbine abrasion is a major problem associated with reservoir sedimentation and is of specific interest in this study. It is discussed in detail in **Section 2.3.3**. Reduced storage capacity also reduces the benefits of flood peak attenuation, which could lead to flooding or even overtopping where attenuation is critical in reducing the peak discharge for which the spillways were designed (Annandale, 2005).

Sediments together with tree trunks and immersed debris can block low-level outlets, spillway tunnels or other conduits, influencing reservoir operation and preventing reservoir drawdown which could be a major safety risk (Fan, 1985).

Accumulated sediments could also impact the stability of the structure due to the extra pressures exerted on the dam as well as the chemical reactions within the deposits which could affect the concrete or surface lining (Fan, 1985; Schellenberg, Donnelly, Holder, Briand & Ahsan, 2017). Sedimentation can also negatively impact fishing or other recreational activities such as boating, swimming, water skiing etc.

2.2.5.3 Downstream Impacts

The trapping of sediment in a dam has a major impact on the downstream reaches of the river, because of the reduced sediment release compared to pre-reservoir conditions. River flow downstream of the dam becomes “sediment hungry”, implying it has a greater sediment transport capacity leading to streambed incision, accelerated bank erosion and possibly undermining of existing structures (Morris *et al.*, 2008).

The reduction in bed load reduces the amount of sand transported to the coast, thus contributing to coastal erosion (Annandale *et al.*, 2016). The reduction of fine sediment load reduces nutrient delivery to downstream ecosystems, affecting fish populations and the aquatic ecosystem. Additionally, it influences agriculture where plains are flooded with nutrient rich sediment seasonally (Fan, 1985). Sediment management strategies such as flushing, sluicing and sediment bypass also have considerable environmental effects downstream of the reservoir, often great enough to cause environmental authorities to prevent such events from taking place.

2.2.6 Reservoir Sedimentation in South Africa

Major dams in South Africa are typically designed with a storage capacity close to 100% of the mean annual runoff (MAR) to have over-year storage. Such large reservoirs are required for water resources management due to the predominantly low precipitation and high evaporation rate in the country. These reservoirs trap more than 95% of the incoming sediment load causing significant sedimentation problems (Braune & Looser, 1989).

According to the ICOLD Sedimentation Committee (2009) reservoir sedimentation in South Africa takes place at an average rate of 0.37% per year. This is considerably lower than the average for Africa, which Basson (2009) reported to be 0.85% (see Schleiss *et al.*, 2016). This can be ascribed to the fact that major reservoirs in South Africa are designed with dead storage for sedimentation so that the firm yield is not affected after 50 years of operation (ICOLD Sedimentation Committee, 2009). Even though the average sedimentation rate in South Africa is low, Msadala (2009) reports that nearly a quarter of South Africa's major reservoirs have lost more than 30% of their original storage capacity.

The Welbedacht Dam, a 32 m high concrete gravity dam on the Caledon River, is a prime example of how poor design, in combination with underestimation of the sediment yield, can lead to extreme sedimentation issues. The dam was commissioned in 1973 but lost 50% of its storage capacity within the first five years of operation. Currently at 95% storage loss, the dam is approaching its equilibrium state. Originally the dam was designed to facilitate drawdown flushing, but it has not been effective due to the poor design of the outlets.

The major design flaw with the outlets was the fact that they were placed 15 m above the original river bed, thus not allowing sufficient drawdown and scouring of deposited sediment. Another mistake was that the first flushing event was only implemented 20 years after commissioning. Operators should probably have attempted flushing at a much earlier stage to prevent the rapid sedimentation rate (ICOLD Sedimentation Committee, 2009).

2.3 Hydropower Reservoirs

2.3.1 Introduction

Hydropower plants (HPPs) use the hydraulic energy of water to produce electricity, contributing more than 16% of the global electricity supply (International Hydropower Association, 2017a). Many different types of HPPs can be distinguished as discussed in **Section 2.3.2**, but all share a few common components such as the reservoir, intake structure, penstock, turbine, generator and powerhouse. The general layout of a HPP with its different components is shown in **Figure 2.8**.

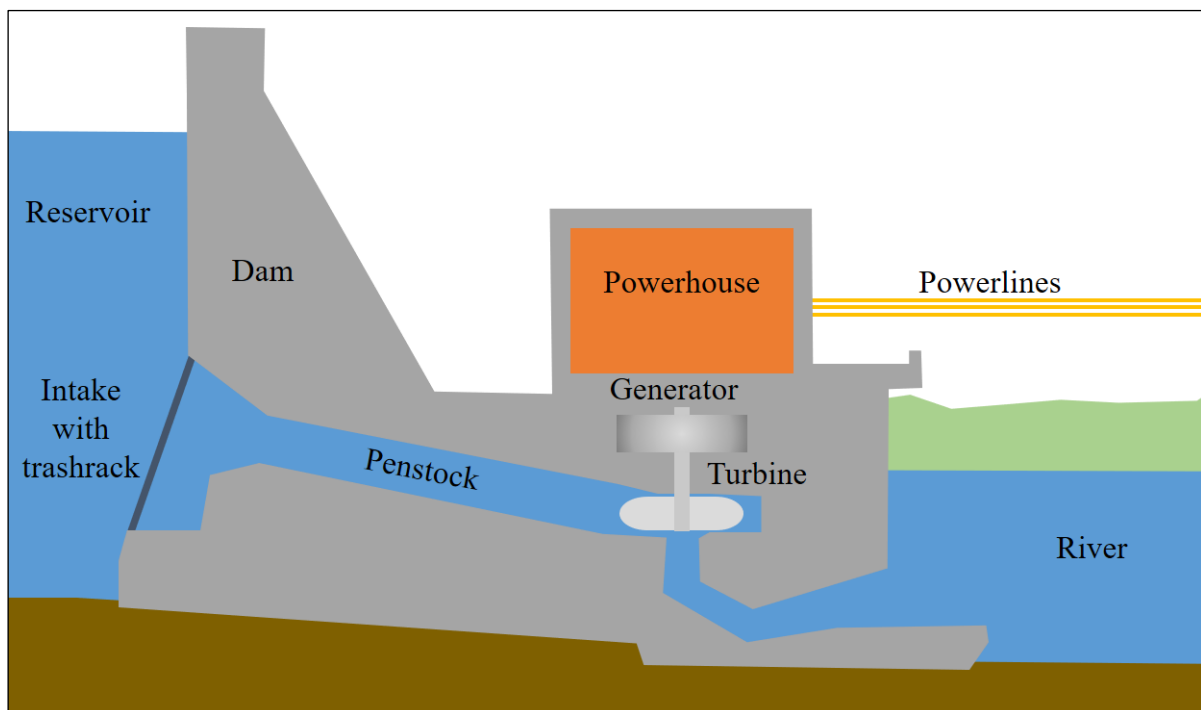


Figure 2.8 General HPP layout and its components (adapted from Daware, 2016)

2.3.2 Classification of Hydropower Plants

Hydropower plants can mainly be classified according to head size, installed capacity, operation, layout or type of turbines (Cleveland & Morris, 2014). This section provides a general overview of the main hydropower classification categories whilst the different types of turbines are discussed in **Section 2.3.3.1**.

2.3.2.1 Classification by Head Size

Classification by head size is not standardised and there is no international consensus on definitions of these categories (FMC AG, 2011; Kumar, Schei, Ahenkorah, Caceres Rodriguez,

Chapter 2: Literature Review

Devernay, Freitas, Hall, Killingtveit & Liu, 2011). The usual scales to separate high, medium and low head schemes are as follows (FMC AG, 2011; Gatte & Kadhim, 2012):

- High Head ($H > 100\text{ m}$): these are commonly storage type schemes located in mountainous areas, but could also be diversion schemes in steep terrain.
- Medium Head ($30\text{ m} < H < 100\text{ m}$): these schemes are also often of storage type and commonly found in mountainous terrain, but many run-of-river schemes belong to this category.
- Low Head ($H < 30\text{ m}$): these schemes are usually run-of-river plants with little or no pondage, located in wide valleys in lowland areas and requiring high flow rates to produce a useful amount of power.

2.3.2.2 Classification by Installed Capacity (P)

Similar to the classification by head, the categories for classification by installed capacity has no generally accepted definition (Egré & Milewski, 2002). However, it is the traditional means of classification and is of institutional and legislative importance. Due to the sustainability issues associated with large-scale hydropower projects, many governments use incentives to promote the development of small-scale hydropower. This can influence project financing and potentially act as a barrier to hydropower development as a whole. Therefore, as shown in **Table 2.2**, the definitions vary in different countries depending on local resource management and energy needs.

**Table 2.2 Definition of small hydropower as defined by various countries
(IRENA, 2012; Kumar et al., 2011)**

Country	Small hydropower defined by installed capacity (MW)
Brazil	≤ 30
Canada	< 50
China	≤ 50
European Union	≤ 20
UK	≤ 20
India	≤ 25
Norway	≤ 10
Sweden	≤ 1.5
USA	5-100

Chapter 2: Literature Review

The categories for installed capacity presented here are typical to describe hydropower project sizes and are based on the category bands presented by IRENA (2012):

- *Pico* hydropower projects ($P < 5 \text{ kW}$) are always run-of-river type installations only used in remote areas far from the grid.
- *Micro* hydropower projects ($5 \text{ kW} < P < 100 \text{ kW}$) are usually stand-alone run-of-river HPPs in rural areas that supply electricity to a local community or a remote industry. These are common in rural areas of developing countries where they provide people with a fuel independent energy source.
- *Mini* hydropower projects ($100 \text{ kW} < P < 1 \text{ MW}$) can be either stand-alone, connected to a mini grid or to the main grid depending on its location.
- *Small* hydropower projects ($0.1 \text{ MW} < P < 20 \text{ MW}$) tend to exploit much lower discharges than medium or large schemes and are mostly run-of-river HPPs connected to the grid.
- *Medium* hydropower projects ($20 \text{ MW} < P < 100 \text{ MW}$) can be either of run-of-river type or storage type and are almost always feeding into the grid.
- *Large* hydropower projects ($P > 100 \text{ MW}$) are also of run-of-river or storage type and are always connected to a large grid.

2.3.2.3 Classification by Operation (Campbell, 2010)

Hydropower plants are traditionally classified in three categories based on the plant operation and flow type, namely storage, run-of-river or pumped storage hydropower. A fourth category, in-stream technology, is a young and developing technology which has recently been included in some publications but is beyond the scope of this section.

2.3.2.3.1 Storage Schemes

Hydropower plants with a reservoir are called storage hydropower schemes, because they provide water storage for later power generation. Reservoirs are essentially a form of energy storage which can store water during periods of high flow, providing flood control, and use this stored water when the flow is low. These schemes are mostly large facilities that can store enough water to offset seasonal rainfall fluctuations and thereby reduce the dependency on a constant inflow. This allows for a constant electricity supply that can be controlled easily since the release of water can be adjusted to cater for base and peak load fluctuations. The powerhouse can be integrated inside the dam or placed downstream as shown in **Figure 2.9**.

Site characteristics and financial capability usually determine the size of the reservoir, which ultimately determines the level of flow regulation. The larger the reservoir the better the energy security, but also the greater the environmental impact and controversy (Egré & Milewski, 2002). Reservoirs used for hydropower generation often serve multiple purposes including water supply, irrigation, flood control and recreation (Campbell, 2010).

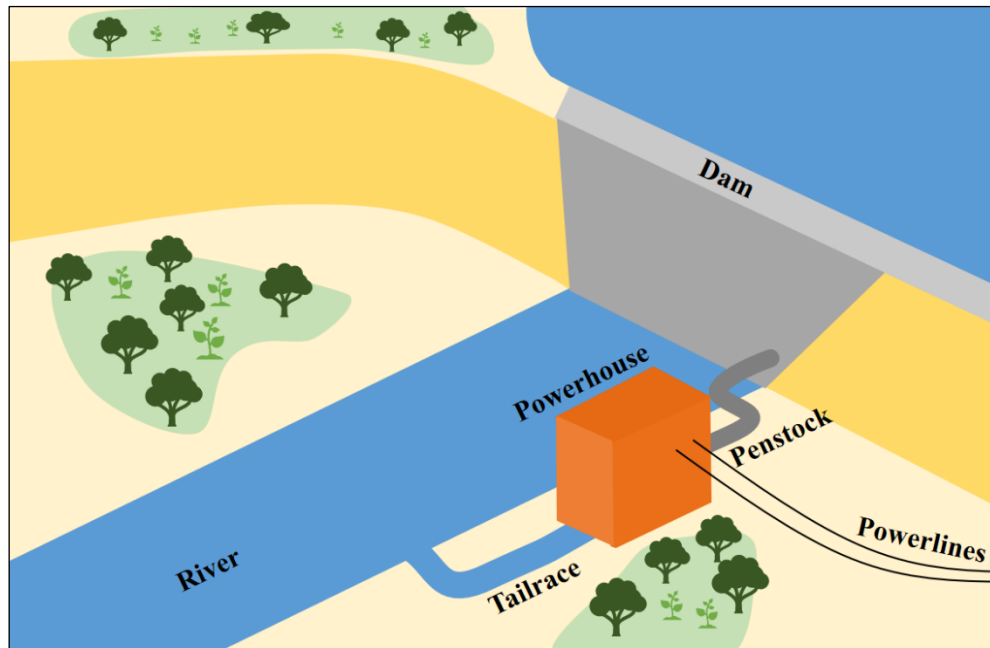


Figure 2.9 Typical storage scheme layout (adapted from Kumar *et al.*, 2011)

2.3.2.3.2 Run-Of-River Schemes

Run-of-river (RoR) hydropower schemes have traditionally been defined as HPPs that use the natural river flow without storage to generate electricity. Although, many hydropower plants with some degree of storage are nowadays still classified as RoR schemes. Countries define RoR schemes differently which has led to great confusion across the globe. The general definition has thus changed to accept HPPs with short-term storage as RoR. Run-of-river plants have thus been split into two sub-categories (Majumder & Ghosh, 2013):

1. Run-of-river plants *without pondage*: these plants do not have any storage and generation capacity is entirely dependent on the real-time flow of the river.
2. Run-of-river plants *with pondage*: these plants have pondage that stores water for a few hours to a few days, allowing operators to cope with fluctuations in river flow and electricity demand. These plants are much more useful than those without pondage. This type of RoR should importantly be distinguished from storage HPPs that provide over-year storage. Such a scheme layout is shown in **Figure 2.10**.

Chapter 2: Literature Review

It is generally accepted in the case of a run-of-river plant with pondage that the impoundment should keep the water level within the river's banks (Campbell, 2010). RoR plants are usually of diversion type, channelling some of the river's flow into a series of structures, often including a desilting facility, headrace and forebay, that lead to a penstock and powerhouse. Most pico, mini, micro and small hydropower plants are RoR, but plants with installed capacity over 1000 MW exist indicating the wide range of applications for RoR plants. For example, the Santo Antonio Dam in Brazil is a RoR scheme that has a capacity of 3580 MW (Reda, Viña, Alves & Ribeiro, 2016).

The lack of a large storage reservoir makes RoR schemes especially attractive due to their simplicity as well as their lower environmental and social impacts, but herein also lies their main weakness since the plant has to rely entirely on the river flow (Breeze, 2014). A large reservoir is often built upstream of several smaller RoR schemes to even out the flows and optimise the energy output (Egré & Milewski, 2002).

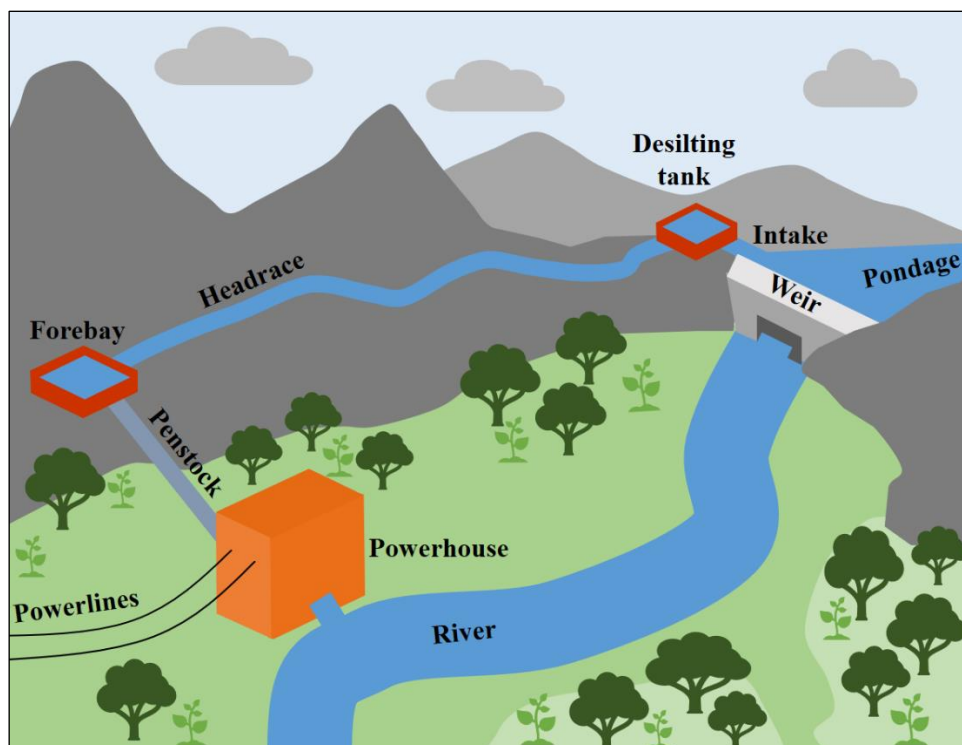


Figure 2.10 Typical run-of-river scheme with pondage (adapted from Kumar *et al.*, 2011)

2.3.2.3.3 Pumped Storage Schemes

Pumped storage HPPs utilise off-peak hours where the power demand is low to pump water from a lower reservoir or river to a higher reservoir using the surplus electricity. The water is then stored in the upper reservoir and released back to the lower reservoir during peak hours to

generate electricity by reversing the turbine operation. This process is a net energy consumer since it takes more power to pump than what is generated due to inefficiencies, but currently provides the largest form of grid storage worldwide (Kumar *et al.*, 2011). Technological advancements have made it possible to develop pump storage plants with efficiencies over 80% (FMC AG, 2011). A typical layout of such a scheme is shown in **Figure 2.11**.

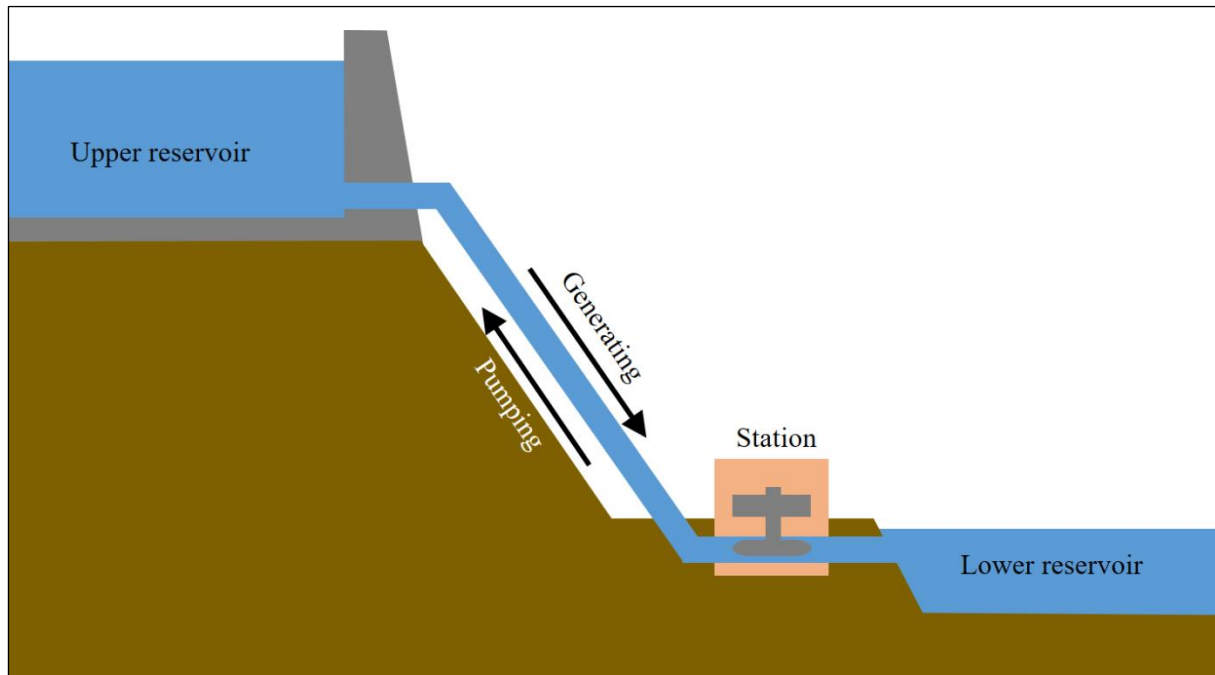


Figure 2.11 Layout of a pumped storage scheme (adapted from Kumar *et al.*, 2011)

2.3.2.4 Classification by Layout

Hydropower scheme layouts depend on several aspects such as the topography, geology, hydrology and environment. Each HPP must be designed to optimise the layout for the site-specific conditions. However, two general layouts of the position of the powerhouse with respect to the headworks exist, namely non-diversion schemes and diversion schemes.

2.3.2.4.1 Non-Diversion Schemes

These schemes have the powerhouse incorporated into the headworks and water that passes through the turbines is returned to the river immediately downstream. High and medium head non-diversion schemes consist of a reservoir used to generate the head, whereas such schemes with a low head have a weir with a powerhouse incorporated into it. Such schemes often experience major sedimentation issues and it is important to position the power intake in such a way that it limits sediment diversion. Positioning the intake correctly may not be sufficient for these schemes and other means of sediment control is often required. A typical non-diversion scheme layout is shown in **Figure 2.8** on page 22.

2.3.2.4.2 Diversion Schemes

These schemes consist of a diversion structure, typically a weir, that diverts water from the river into a pipe or tunnel which carries the water to the powerhouse located downstream, using the local topography to create the desired head. High and medium head schemes are characterised by a pressure tunnel whereas low head schemes have a canal diversion. Sediment in the diverted water is usually removed by settling basins before reaching the penstock. **Figure 2.10** on page 26 shows the general layout of a diversion scheme.

2.3.3 HPP Turbine Damage

Sedimentation in hydropower dams cause deposition near the intakes, which could lead to obstruction. However, in most cases obstruction does not occur, but coarse sediment enters the intakes and damages the turbines and other components as it passes through the power station. This sediment-induced wear causes changes in the turbine blade profile, increased vibration and fatigue damage (Padhy & Saini, 2008). Kumar *et al.* (2011) reported that the effect of turbine wear could include:

- reduced turbine efficiency,
- generation losses,
- reduced turbine life,
- irregular power generation, and
- increased repair and maintenance work.

All the above-mentioned effects have a negative financial impact and could lead to major problems at a HPP. The extent of turbine wear is largely dependent on the type of turbine.

2.3.3.1 Types of Turbines

Turbines are the most important mechanical components of a hydro power scheme, converting hydropower energy into rotating mechanical energy (Gatte & Kadhim, 2012). Historically, hydraulic turbines have been used by different civilisations across the world for centuries, with the earliest records indicating that the Chinese used wooden water wheels to grind grain. These early water wheels were placed in a stream and the flowing water against the radial tilted blades caused it to turn. This principle forms the basis for what are currently known as impulse turbines. In the 18th century it was discovered that more energy can be generated by pressurising the flow through damming and then directing a pressurised jet against the blades. This led to the development of the second branch of turbines, namely reaction turbines. The different working principles of impulse and reaction turbines are shown in **Figure 2.12**.

Chapter 2: Literature Review

Over the past few centuries turbine designs have improved to such an extent that efficiencies up to 95% can be achieved nowadays (Breeze, 2014). The choice of a turbine depends on the system characteristics including the net head, unit discharge and unit power (Cleveland & Morris, 2014).

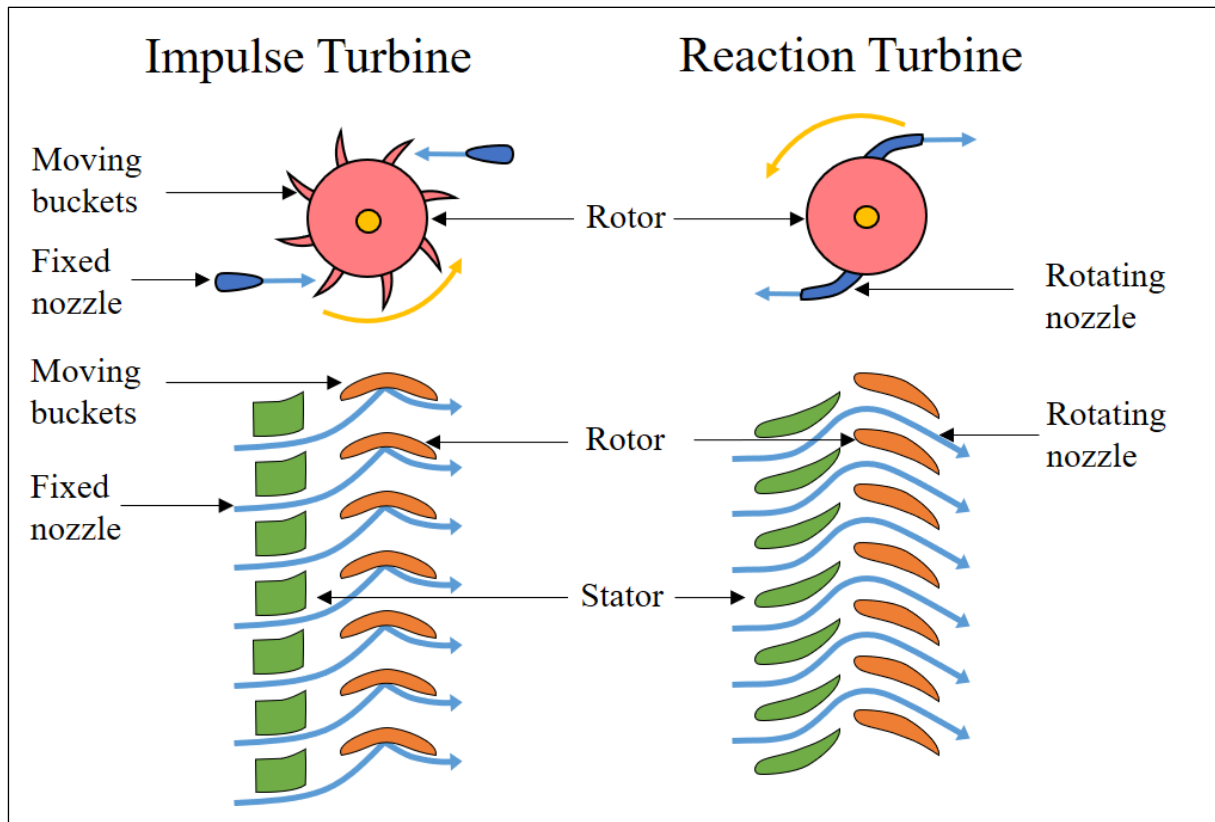


Figure 2.12 Comparison between impulse and reaction turbines (adapted from Rathore *et al.*, 2015)

2.3.3.1.1 Impulse Turbines

Impulse turbines consist of a fine nozzle through which water under pressure is released and directed onto a bucket shaped paddle on a wheel, causing it to turn. The key feature of these turbines is that they are not submerged and operate in free air, making them cheaper than reaction turbines because no pressure casing is needed and maintenance costs are lower (Gatte & Kadhim, 2012). Impulse turbines are not suitable for low heads due to their low specific speeds but are well suited for medium heads. The three main types of impulse turbines are:

i. Pelton turbines

The main type of impulse turbine used today is the Pelton turbine, which operates at high efficiencies when a high head (60 – 1000 m) and low flow rate (0.2 – 5 m³/s) are available (Breeze, 2014). A Pelton turbine is made up of a circular disc with a series of shaped buckets

Chapter 2: Literature Review

mounted on the periphery. The runner is spun by the impulse generated from the forced water jet on each of the buckets. The buckets are designed to deflect the water jet at the maximum angle (165°) possible without the return jet causing interference with the next jet (Gatte & Kadhim, 2012).

ii. Turgo turbines

Another type of impulse turbine is the Turgo turbine, which can handle higher flow rates than the Pelton turbine, but is more difficult to build. Turgo turbines are similar to Pelton turbines, but instead of the water jet being in the same plane as the wheel, the jet strikes the bucket on one side and flows out on the other side. Single or multiple nozzles can be used, with an increase in specific speed as the number of jets increase. These turbines have higher specific speeds and can handle greater flows than a Pelton turbine of the same diameter. The runner is also less expensive than a Pelton runner, reducing the installation cost. Turgo turbines are usually used for medium-head schemes with heads ranging from 30 to 200 *m*, producing between 100 and 6000 *kW* (Cleveland & Morris, 2014).

iii. Crossflow turbines

A crossflow turbine, also called a Michell-Banki turbine, lets water flow across the turbine blades and after passing the runner it leaves at the opposite end. The water has to pass over the runner twice to provide additional efficiency, with approximately $2/3^{\text{rd}}$ of the power being transferred on the first pass. The efficiency of a crossflow turbine is less than Pelton, Francis and Kaplan turbines, but has the added advantage that its efficiency curve is flat under varying load. While the flow and load varies from $1/6^{\text{th}}$ to its maximum, the turbine maintains its efficiency making it an attractive turbine option for small run-of-river schemes where the stream flow could vary greatly seasonally. These turbines are therefore mostly installed in mini and micro HPPs with heads less than 50 *m* and generating units between 2 and 15 *kW* (Cleveland & Morris, 2014). Due to their good performance under reduced flows, self-cleansing ability as the water leaves the runner, simple construction and easy maintenance these turbines are well-suited for stand-alone electricity generation where reliability is important (Gatte & Kadhim, 2012).

2.3.3.1.2 Reaction Turbines

Unlike impulse turbines, the runner of a reaction turbine is completely submerged and enclosed with a pressure spiral casing. The weight of the water against the surface of the runner blades creates a pressure difference which imposes lift forces causing the runner to rotate. With the

Chapter 2: Literature Review

same head and flow, reaction turbines rotate faster than impulse turbines, making it possible to be coupled directly to an alternator without the need for a speed-increasing drive system. This ensures design simplicity, easy maintenance and reduces costs. There are several different types of reaction turbines, namely Kaplan, propeller, bulb and most popular the Francis turbine.

i. Francis turbines

Named after James Bichens Francis, the Francis turbine is by far the most popular turbine in operation today, accounting for 80% of all hydraulic turbines (Breeze, 2014). The unique characteristic of these turbines is that water enters radially, changes direction and exits axially after interacting with the turbine blades. The guide vanes that direct the water onto the runner are adjustable to allow efficient operation for various conditions. The water changes pressure as it moves through the turbine, transferring energy to the runner, making these turbines suitable for dam sites where the source has a high pressure and the exit a low pressure (Gatte & Kadhim, 2012). Francis turbines can be used in almost any situation (head of 20-700 *m*), but for very low heads, the other reaction turbine types are preferred (Breeze, 2014).

ii. Propeller and bulb turbines

Propeller turbines are mostly used in low-head (typically less than 10 *m*) applications such as slow flowing, lowland rivers. The propeller turbine looks like the propeller of a ship, but with reverse operation where moving water drives the propeller to generate power. When the flow rate drops to less than 75% of its design flow, the efficiency drops significantly. In order to maintain optimum efficiency, designers often make use of multiple turbines in parallel so that some can be switched off when the flow drops. For extremely low heads, a variant of the propeller turbine, a bulb turbine is used. Bulb turbines are designed with a water-tight generator encapsulated and sealed within a bulb-shaped casing, called a nacelle. Bulb turbines can have fixed or adjustable blades and there is no change of flow direction through the turbine, also making it suitable for tidal power plants (Breeze, 2014).

iii. Kaplan turbines

The Kaplan turbine is a propeller turbine, developed on the design principles of the Francis turbine by Viktor Kaplan in 1913. It has adjustable blades allowing it to achieve efficiencies over 90%. Its main advantage compared to the Francis turbine is its suitability for use at low head sites with high flow. The Kaplan turbine is an inward flow reaction turbine, meaning that the fluid changes pressure as it moves through the turbine, transferring its

energy to the propeller shaped runner. Kaplan turbines have fewer runner blades due to their twists but are much more expensive to manufacture and install. They are thus only used where the head is low (2-20 *m*) and the flow rate is between 3 and 50 m^3/s . They generally have an output range of 5 to 200 *MW* (Cleveland & Morris, 2014).

Table 2.3 provides a summary of the different turbines and their typical application ranges.

Table 2.3 Summary of the application ranges of different turbines

Type	Turbine	Head (<i>m</i>)	Flow rate (m^3/s)	Power (<i>kW</i>)
Impulse	Pelton	60 – 1 000	0.2 – 5	200 – 15 000
	Turgo	30 – 200	0.1 – 10	100 – 6 000
	Crossflow	2 – 50	0.01 - 0.12	2 - 15
Reaction	Francis	10 – 700	0.7 – 20	100 – 20 000
	Propeller	1 – 10	0.5 – 20	50 – 5 000
	Kaplan	2 – 20	3 – 50	50 – 20 000

2.3.3.2 Hydro-Abrasive Erosion

Managing hydropower plants to achieve high efficiencies over the design life of the project is important in ensuring a reliable electricity supply, however turbine performance usually declines over time due to blade damage. This damage is mainly due to abrasion caused by coarse suspended sediment passing through the turbines (Padhy & Saini, 2008). The damage is not restricted to turbines, but also affects pumps, valves and gate seals (Morris & Fan, 1998).

The erosion of turbines due to solid particles has been challenging engineers since the major developments in turbine inventions in the 19th century. Solid particle erosion is also referred to as ‘silt erosion’, ‘sand erosion’ or ‘hydro-abrasive wear’ in literature but is termed ‘hydro-abrasive erosion’ in this study. According to Padhy & Saini (2008) hydro-abrasive erosion is the process of gradual removal of material from the surface of a mechanical component as a result of repeated deformation and cutting actions.

The erosive wear of turbine components in HPPs occurs mainly as a result of the high velocity impact of abrasive particles suspended in the water (Duan & Karelin, 2002). This type of wear breaks down the oxide layer on the surfaces of flow guiding components, leading to surface irregularities which may become the origin for cavitation. Even with major advances in turbine design and material development, hydro-abrasive erosion still remains the main cause of damage and performance loss in medium and high head HPPs (Felix, Albayrak, Abgottspon & Boes, 2016; Sangal, Singhal & Saini, 2018). Pelton and Francis turbines are mostly affected,

Chapter 2: Literature Review

because these are installed in medium- and high-head HPPs. The parts of these two turbines most susceptible to erosion are elaborated on.

In Pelton turbines the needle tips, nozzles, seal rings, deflectors and runner buckets are commonly affected by hydro-abrasive erosion (Dorji & Ghomashchi, 2014; Felix *et al.*, 2016; Kjølle, 2001; Padhy & Saini, 2008). Pelton turbines are normally designed for high heads and thus the velocity of the jets can be up to 150 *m/s* (Duan & Karelin, 2002). According to Padhy and Saini (2008) sediment with grain size less than 0.06 *mm* has led to severe damage of a Pelton turbine's nozzles and needles, with negligible erosion of the buckets. This could be explained by the strong turbulence in the high velocity jet causing particles to rotate and oscillate while colliding with the surface (Kjølle, 2001). Bouvard (1992) states that at very high heads (> 400 *m*) even 0.05 *mm* quartz particles will cause severe damage to a Pelton turbine. However, where coarse sand is present, the damage of the nozzles is less serious, but the buckets are severely eroded. This is due to the acceleration of particles in the buckets that could reach 100 000 *m/s*², depending on the bucket size and the scheme head (Kjølle, 2001).

Francis turbines suffer less severely from erosion damage than Pelton turbines, but their guide vanes, stay vanes, labyrinth rings, and runners are still often affected (Agrawal, Slade, Pottsmith & Dana, 2016; Dorji & Ghomashchi, 2014). The guide vanes and labyrinth rings are most susceptible to hydro-abrasive erosion and also have the greatest influence on the turbine's efficiency (Kjølle, 2001).

The erosive wear of turbine blades is mainly dependent on the sediment particles, the substrate and the blades. Bouvard (1992) states that the characteristics of the sediment particles which affect turbine wear include (1) size, (2) shape, (3) hardness and (4) concentration.

The sediment shape and size are considered the top contributing factors in turbine erosive wear (Poudel, Thapa, Shrestha, Thapa, Shrestha & Shrestha, 2012). The particle shape is an important characteristic, but the erosive effect it has is difficult to quantify (Padhy & Saini, 2008). Schellenberg *et al.* (2017) state that angular particles with a Mohs hardness greater than 5 (quartz, feldspar and tourmaline) are problematic. Ramos & Betâmio de Almeida (2000) state that particles with a median diameter (*d*₅₀) of 0.2 *mm* are considered acceptable for small turbines. Raudkivi (1993) suggests that particle sizes should be limited to 0.1 *mm* for heads exceeding 50 *m* and at heads exceeding 200 *m* even silts need to be excluded.

2.3.3.3 Cavitation

Cavitation is the formation of vapour cavities in a liquid due to forces acting on it and is based on the principle that if the pressure of a liquid falls, the boiling temperature also decreases. Thus, if the fall in pressure is great enough, it will induce boiling. It usually occurs when the liquid undergoes a rapid change in pressure that causes cavities to form. If the pressure is high enough the cavities can implode and release large amounts of energy in the form of a shock wave (Chadwick, Morfett & Borthwick, 2013).

The water entering a hydraulic turbine undergoes major pressure and velocity changes as it transfers energy to the runner. When the local pressure drops below the vapour pressure of the fluid it induces the formation of vapour cavities in the flow. This is the case for fluids flowing over the surface of turbine components where the dynamic pressure increases due to the flow velocity suppressing the static component.

Hydro-abrasive erosion can break down the oxide layer on turbine components and make the surfaces uneven which may be the origin of cavitation erosion. Cavitation could thus occur near the blades or at the exit of the turbine where the static and dynamic components of fluid pressure differ greatly (Dorji & Ghomashchi, 2014). Vapour cavity or bubble formation is governed by the static pressure but is also affected by the superimposed dynamic pressure of the flow, hydraulic conditions and the operating point. The repeated collapse of vapour cavities will eventually lead to erosion of several turbine components. The rate and extent of this erosion will depend on the energy and number of the vapour cavities, as well as the material's erosion resistance (Bourdon, Farhat, Mossoba & Lavigne, 1999).

The parts of a turbine susceptible to cavitation vary according to the type of turbine and its operating conditions. Francis, Kaplan and bulb turbines are most susceptible to cavitation of the runner blades and draft tubes. Pelton turbines generally experience cavitation where the bucket surface has been roughened by hydro-abrasive erosion (Dorji & Ghomashchi, 2014).

Cavitation prevention is mainly focused on improving hydraulic design, high quality manufacturing, using erosion resistant material and searching for operating conditions that minimise cavitation. Extensive research in new alloy steel qualities over the past few decades have significantly advanced the development of materials with high strength, wear resistance, corrosion resistance and reduction in brittleness (Kjølle, 2001). Kjølle (2001) and Singh, Tiwari & Mishra (2012) showed that the best weldable alloy steel to combat cavitation, is made of 13% Cr and 4% Ni or 16% Cr and 5% Ni.

Chapter 2: Literature Review

Continued research on the fluid flow through turbines, specifically over blade surfaces, is required using the latest Computational Fluid Dynamics (CFD) software to improve turbine geometry and thereby further minimise cavitation in new developments (Dorji & Ghomashchi, 2014).

2.3.4 Hydropower Intake Structure Design

The main function of hydropower intakes is to divert the required discharge into the power canal or penstock with minimum head loss (ESHA, 2004). According to Kumar & Singal (2013) an intake should more specifically:

- draw the required amount of water at minimum reservoir level
- draw the minimum amount of sediment
- check entry of trash and debris
- have hydraulically smooth passage so as to have minimum head loss
- be located so as to eliminate vortex formation.

According to the same authors, the following design details are necessary to perform the above-mentioned functions:

- The centre line of the intake and the size of inlet should be such that the intake could draw the required amount of water at minimum reservoir level without vortex formation and at a sufficiently low velocity.
- The sill of the intake should be kept at the highest possible level in order to reduce silt entry to a minimum extent.
- Looking from the river towards the bank, the intake, should be located on the concave side (outside of bend) if at all possible so as to reduce coarse sediment content.
- The inlet opening should be of bell mouth shape and transitions should be hydraulically streamlined.
- A trash rack structure should be provided at the entrance and the velocity through the trash racks should be kept low.

A number of different types of intakes exist, but for this study the only intake that is relevant is the horizontal reservoir type intake. A horizontal reservoir type intake is one where the trash rack is situated horizontally in the reservoir, normally at the dam.

Chapter 2: Literature Review

2.3.4.1 Entrance Shape and Transition Zone

The entrance of a hydropower intake is very important for the overall efficiency of the plant since head losses lead to lower power generation. According to the ASCE Hydropower Committee (1995) the area of the intake can be calculated as:

$$A_{inlet} = \frac{A_{penstock}}{(C_c \cdot \cos \varphi)} \quad 2-21$$

where:

C_c = Coefficient of contraction ($C_c = 0.6$ for high and medium heads & $C_c = 0.7$ for low heads)

φ = Angle of inclination of the centre line to horizontal

In order to minimise head losses and avoid cavitation, the entrance to the conduit needs to be streamlined to provide smooth flow. The Bureau of Indian Standards (1995) states that the entrance surface should take the form of the natural contraction curve and the conduit must be the size of the jet at maximum contraction. Bell mouth entrances are commonly used, but the entrance could be rectangular which narrows until it reaches the penstock (Bratko & Doko, 2013). Based on field studies and laboratory testing, the general equation for the bell mouth shape is (Bratko & Doko, 2013):

$$\frac{x_c^2}{(3K_x D)^2} + \frac{y_c^2}{(K_y D)^2} = 1 \quad 2-22$$

where:

x_c = coordinates whose x-x axis are parallel to and $0.65D$ from the conduit centreline

y_c = coordinates whose y-y axis are normal the conduit centreline and $0.5D$ downstream from the entrance face

D = diameter of the conduit at the end of the entrance transition

K_x, K_y = constants for different conditions as defined in **Table 2.4**

Table 2.4 Constants defining bell mouth shape of different inlets (Bratko & Doko, 2013)

Conditions	K_x	K_y
Circular entrance	0.167	0.15
Rectangular or square entrance	0.33	0.33
Suppressed bottom and side contractions	0.5	0.5
Suppressed one side only, for unsuppressed side	0.33	0.67

Chapter 2: Literature Review

The transitions from the rectangular opening to the circular section should be designed according to the following (Bureau of Indian Standards, 1995):

- i. Transitions should be made about the centre line and should be gradual.
- ii. Maximum side wall expansion of 5 degrees from centre line.
- iii. Gate slots should only operate beyond the transition zone.

The contraction and expansion transitions to and from the control sections of the conduit should be gradual, such that they do not exceed the relationships given in **Equation 2-23** and **Equation 2-24** for contractions and expansions respectively (USBR, 1987). Expansions need to be more gradual than contractions in order to prevent possible cavitation at sharp sidewall changes.

$$\tan \alpha = \frac{1}{U} \quad 2-23$$

$$\tan \alpha = \frac{1}{2U} \quad 2-24$$

where:

α = angle between conduit centreline and the wall surface

U = arbitrary parameter defined by $\frac{V}{\sqrt{gD}}$, where V and D are the average velocities and diameters between the start and end of the transition

2.3.4.2 Intake Centre Line and Submergence

In order to avoid air entering the intake, it is essential that the intake is submerged sufficiently, to prevent vortex formation and thus ensuring turbine efficiency (Ramos & Betâmio de Almeida, 2000). Several formulae for the minimum submergence (S) have been defined in the literature, with the most common being the Gordon, Knauss and Rohan formulae defined by **Equation 2-25**, **Equation 2-26** and **Equation 2-27** respectively (Bratko & Doko, 2013). **Figure 2.13** illustrates the definition of intake submergence.

$$S \geq C \cdot V_p \cdot \sqrt{D} \quad 2-25$$

$$S \geq D \cdot \left(1 + 2.3 \cdot \frac{V_p}{\sqrt{gD}} \right) \quad 2-26$$

$$S \geq C \cdot V_p \cdot \sqrt{D} \quad 2-27$$

where:

S = minimum submergence from the top of the intake (m)

V_p = velocity in the conduit or penstock (m/s)

C = 0.7245 (asymmetrical lateral approach conditions) or 0.5434 (symmetrical lateral approach conditions)

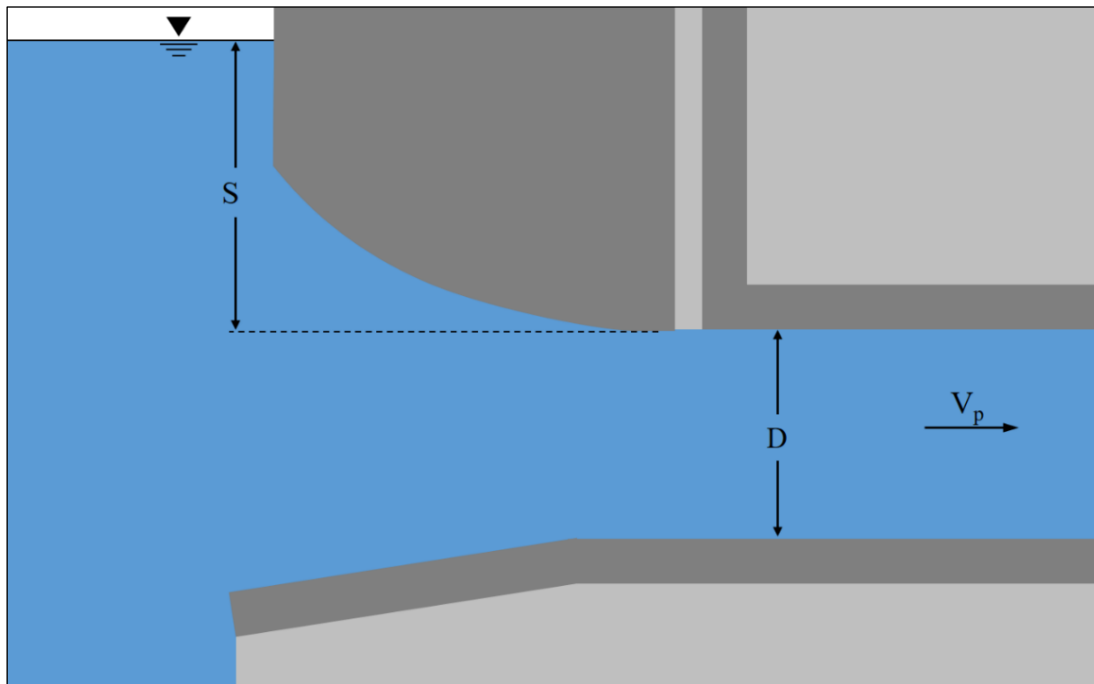


Figure 2.13 Definition sketch for intake submergence (Johnson, 1988)

Sarkardeh (2017) studied the differences between several submergence formulae and compared the results to physical experiments and numerical simulation. He concluded that the Gordon equation did not agree with some of the experimental data and that the Knauss equation was in good agreement but requires a rational safety factor.

More detail on submergence requirements and the prevention of vortex formation can be found in the detailed guidelines of the ASCE Hydropower Committee (1995) and in Walker (2016). Although empirical equations are helpful for design, physical modelling in parallel with numerical simulations are required for the optimisation of important structures.

2.3.4.3 Plan Location of the Intake

Water intakes should ideally be placed along a straight section of the stream where the following are present:

- Stable streambed
- Constant flow
- Bedrock
- Small gradient (longitudinal slope)

Chapter 2: Literature Review

River bends should generally be avoided because sediment tends to accumulate on the inner sides and on the outer banks erosion rates are high. If there is no straight section available, the outer side of the bend is preferred (FMC AG, 2011). The positioning of the intake structure is highly dependent on site-specific conditions and the type of hydropower plant and should be optimised for each project.

2.3.4.4 Trash rack and Intake Velocity

A trash rack must always be provided at the upstream end of the intake to prevent debris from flowing into the entrance (Kumar & Singal, 2013). The bar spacing of the trash rack is very important, because that determines what size particle can pass through the turbines. Bar spacing is specified by turbine manufacturers and can vary from 12 mm for high head Pelton turbines to 150 mm for large propeller turbines. Nielsen (2012) proposes that the trash rack is located at a 5 to 10 degree incline to the vertical to ease cleaning operation. ESHA (2004) states that the head loss over the trash rack can be calculated using **Equation 2-28** and **Figure 2.14**.

$$h_t = K_b \cdot t \cdot \left(\frac{t_b}{b_b}\right)^{\frac{4}{3}} \left(\frac{V_a^2}{2g}\right) \cdot \sin \varphi \quad 2-28$$

where:

- h_t = head loss (mm)
- K_b = coefficient for bar shape
- t_b = bar thickness (mm)
- b_b = width between bars (mm)
- V_a = approach velocity (m/s)
- φ = angle of inclination from horizontal (degrees)

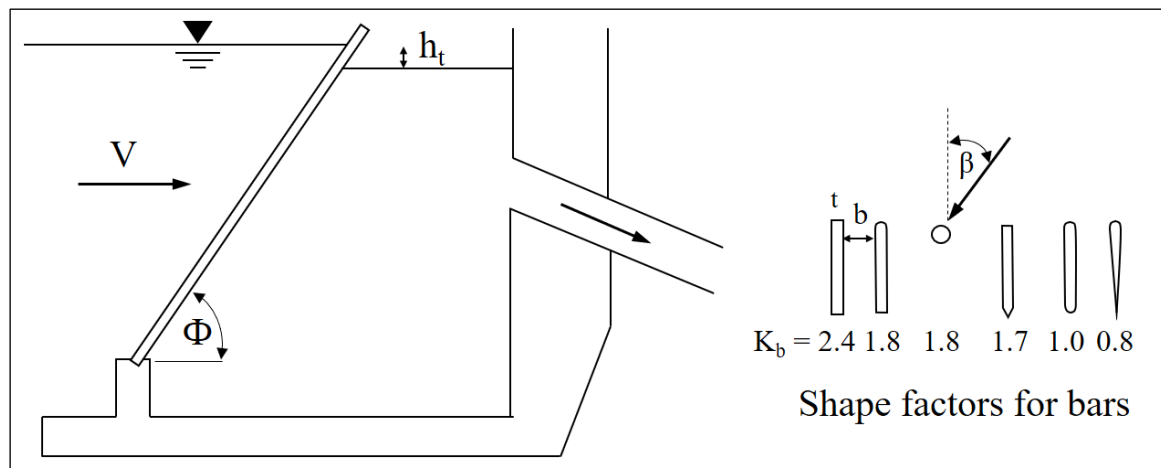


Figure 2.14. Trash rack parameters and bar shape factors (adapted from ESHA, 2004)

Equation 2-28 is only valid if the length of the bars are smaller than five times their diameter. If the flow is not perpendicular to the bars, but makes an angle of β , the result of **Equation 2-28** must be multiplied with a correction factor k as provided in **Table 2.5**.

Table 2.5 Correction factor k for flow at an angle to the bars (Bratko & Doko, 2013)

t/b	1	0.9	0.8	0.7	0.6	0.5	0.4	0.3	0.2
β									
0°	1	1	1	1	1	1	1	1	1
10°	1.06	1.07	1.08	1.09	1.1	1.11	1.12	1.14	1.5
20°	1.14	1.16	1.18	1.21	1.24	1.26	1.31	1.43	2.25
30°	1.25	1.28	1.31	1.35	1.44	1.5	1.64	1.9	3.6
40°	1.43	1.48	1.55	1.64	1.75	1.88	2.1	2.56	5.7
50°	1.75	1.85	1.96	2.1	2.3	2.6	3	3.8	-
60°	2.25	2.41	2.62	2.9	3.26	3.74	4.4	6.05	-

The flow velocity through the trash racks is important to minimise head loss, since head losses over a trash rack are a function of flow velocity and trash rack geometry (Rettedal & Nielsen, 2012). The recommended maximum velocity through the trash rack varies from 0.6 to 1.5 m/s (Bratko & Doko, 2013; Bureau of Indian Standards, 1995; ESHA, 2004; Johnson, 1988). The general consensus it that the velocity through the trash rack can be up to 0.75 m/s for units with hand raking and up to 1.5 m/s for units with mechanical raking. The velocity in the penstock is considerably higher, generally ranging between 2 and 5 m/s (ESHA, 2004).

2.4 Low-Level Outlet Design

As the number of possible dam locations worldwide decrease, the focus of dam design has shifted to more efficient and sustainable dam design. On some older dams, sedimentation was not a primary concern and was often underestimated. In South Africa reservoirs are sized large relative to the MAR with typically no excess flow available for flushing. This led to the design of dams without low-level outlets or with outlets that were too small. As these dams near their design life, sedimentation severely affects operation and low-level outlets, or intakes need to be reconstructed at high costs. New trends in dam design suggest that larger low-level outlets are being designed to preserve reservoir storage in the long term especially in cases where there is excess runoff available (Basson & Rooseboom, 1999). According to Fan (1985), low-level outlets are a critical part of modern dam design and must be optimised for the following events:

- Sluicing of floods
- Emptying of reservoirs
- Sediment control by flushing or sluicing

Chapter 2: Literature Review

Low-level outlets are common in concrete dams and less common in earthen dams due to the high occurrence of piping failure and accidents. Therefore, flushing of sediments through low-level outlets is commonly done in concrete dams (Srivastav & Nayak, 2015).

2.4.1 Criteria for Low-Level Outlet Design

Low-level outlets play an important role in dam safety and operation, and according to Amirsayafi (2015) they can have one or more of the following functions:

- Reservoir evacuation for maintenance, inspection or emergency reasons.
- Supporting the reservoir flood discharge system during construction, unexpected floods or floods larger than the design flood.
- Controlling the first impounding of the reservoir to allow inspection of the dam and prevent quick consolidation of the embankment or foundation.
- Providing water downstream of the dam for environmental, industrial, agricultural or drinking water demands.
- Flushing of sediments through the reservoir to regain lost storage capacity or to prevent sediment from affecting the intake works.

According to Amirsayafi (2015), the use of low-level outlets for flood discharging is generally not recommended for the following reasons:

- The high flow velocities in the low-level outlet conduit can cause abrasion and cavitation damage, as well as damage to gates.
- The high water pressure in low-level conduits cause a risk of failure of service gates.
- During flooding, spillway gates are generally more reliable than low-level outlet gates.
- The risk of low-level outlet blockage is higher during a flood due to the increased amount of sediment and debris.

Thus, the use of low-level outlets for flood discharge is only considered in special cases. In such cases the low-level outlet must be carefully designed, and frequent inspection and maintenance should follow after construction. Low-level outlets often experience erosion of the conduit due to the high sediment load. This in turn causes an increase in surface roughness which can lead to cavitation damage.

Chapter 2: Literature Review

Another major problem associated with low-level outlets is the malfunctioning of gates, leading to uncontrolled release of water. Damage to the downstream stilling basin due to the clash of debris and coarse sediment has also been reported (Amirsayafi, 2015).

2.4.2 Discharge Capacity

The discharge capacity of a low-level outlet is arguably its most important design consideration. Even if low-level outlets will mostly be used for pressure flushing, they must still be designed for full drawdown and free flow conditions (Morris & Fan, 1998). The high flows of the river must be analysed and it is suggested that a 1:5 to 1:10 year flood should be able to pass through without inundating the floodplains (Basson & Rooseboom, 1999; ICOLD Sedimentation Committee, 2009).

The discharge capacity of low-level outlets can be calculated using **Equation 2-29** for free surface flow and **Equation 2-30** for pressurised flow (Sayah, Calvo, Bonanni & Fenelli, 2015).

$$Q_o = n \cdot C_d \cdot b_g \cdot H_h \cdot \sqrt{2 \cdot g \cdot H_h} \quad 2-29$$

$$Q_o = n \cdot C_d \cdot b_g \cdot a_g \cdot \sqrt{2 \cdot g \cdot (H_h - \Delta H)} \quad 2-30$$

where:

- Q_o = discharge capacity (m^3/s)
- n = number of outlets
- C_d = flow coefficient, depending on the head and gate opening (ranges from 0.5 for sharp entrances to 0.96 for well-designed bell mouth entrances)
- a_g = gate height (m)
- b_g = gate width (m)
- H_h = hydraulic head of the reservoir, from the gate's horizontal axis (m)
- ΔH = head losses from intake to gate (m)

Several countries take different approaches to the design capacity due to local conditions. For Chinese reservoirs, Jiang (1980) provides the following simplified formula for the discharge capacity:

$$\frac{Q_m}{Q_d} \cdot \frac{S_n}{S_0} \geq 0.5 \quad 2-31$$

where:

- Q_m = maximum free discharge of the outlets without flood detention (m^3/s)

Chapter 2: Literature Review

Q_d = dominant discharge in the river (m^3/s)

S_n = slope of the line connecting the upstream end of the maximum pool level with the low-level outlets

S_0 = original gradient of the river

In Russia, drawdown flushing was optimal at three hydropower plants when the discharge was 2 to 4 times the mean annual discharge. This is substantiated by Pitt & Thompson (1984) who proposed a discharge capacity of at least 2 times the mean annual discharge.

In India, low-level outlets are designed to discharge the bankfull discharge of the inflowing stream (Brown, 1943).

In France, low-level outlets are designed with a capacity that can reduce the maximum water level in the reservoir to half in less than 8 days with no inflow in the reservoir (Srivastav & Nayak, 2015). This is given by **Equation 2-32**.

$$Q_o = 0.7 \cdot \left(\frac{V_R}{t} \right) \quad 2-32$$

where:

V_R = total volume of the reservoir (m^3)

t = time in seconds (8 days = 691 200 s)

Paul & Dhillon (1988) documented various examples of successful flushing operations all over the world (China, Russia, Venezuela, India, Taiwan and Iran) and propose an optimum outlet height of 1.5 to 2.5 m. The discharge capacity can be achieved by choosing the height and then altering the outlet width.

The above-mentioned low-level outlet discharge capacities have been obtained by field experience and should only be used as a guide. Detailed analytical or physical tests need to be carried out for each reservoir to determine the required low-level outlet capacity.

2.4.3 Shape and Geometry

Numerous geometric shapes and combinations have been developed for the design of intake shapes, where intake in this case refers to the entrance of the low-level outlet and not to the hydropower intake discussed in **Section 2.3.4**. The plan cross-section can be rectangular, circular or irregular and the elevation profile can be either tapered or uniform. Rectangular structures are more functional for low-head projects designed for large discharges whereas circular structures provide cost savings in high-head projects due to structural efficiency.

Chapter 2: Literature Review

Rectangular shapes are more easily constructible and also provide a more efficient layout for entrances, gates, openings and operating equipment (USACE, 2003).

Morris & Fan (1998) state that low-level outlets should generally be as wide as possible, suggesting that a rectangular shaped outlet will be more efficient in sediment removal than a circular shaped outlet.

Sayah *et al.* (2015) recommend that the low-level outlet intake geometry must be designed to:

- avoid cavitation;
- maintain positive pressure;
- minimise total head losses, progressively increasing along the flow path; and
- minimise the dimensions to keep the gates small, but should be of sufficient size to prevent debris blockage.

In the case of the Cerro del Águila Dam, the intake consists of a rectangular cross-section with elliptical transition curves on all four ends such that the width and height diminish along the flow direction and join the conduit tangentially (Sayah *et al.*, 2015). This is similar to the transitions described for hydropower intakes in **Section 2.3.4.1**.

2.4.4 Layout

According to Basson & Rooseboom (1999) the elevations of the low-level outlets are the most important consideration for the layout. Ideally the outlet should be placed at the original river bed level (Basson & Rooseboom, 1999; Brandt, 2000; Morris & Fan, 1998). Xu & Lu (1991) suggested that low-level outlets should be installed not higher than the relative water depth of 0.15 to 0.2 from the river bed. Placing the outlets at the original river bed will enable drawdown flushing and ensure retrogressive erosion. If the outlets are placed above the original river bed level, the region below it will be silted up, creating a dead storage region. For the maximum release of gravel load, Bouvard (1992) suggests that low-level outlets be positioned on the inner side of the bend, i.e. the opposite bank of a concave bend.

The low-level outlets must be located below the intakes to form local scour zones in order to reduce the amount of sediment entering the intakes. In cases where the intakes are not situated in the reservoir wall, the low-level outlets must be positioned to limit sedimentation at the intakes (Basson & Rooseboom, 1999). Morris & Fan (1998) propose that at least two low-level outlets should be used and that they should be at the same elevation. In contrast Brandt (2000)

suggests that outlets should be placed on different elevations to allow withdrawal from different levels. **Figure 2.15** shows the Gebidem Dam layout with low-level flushing outlets located below the power intakes.

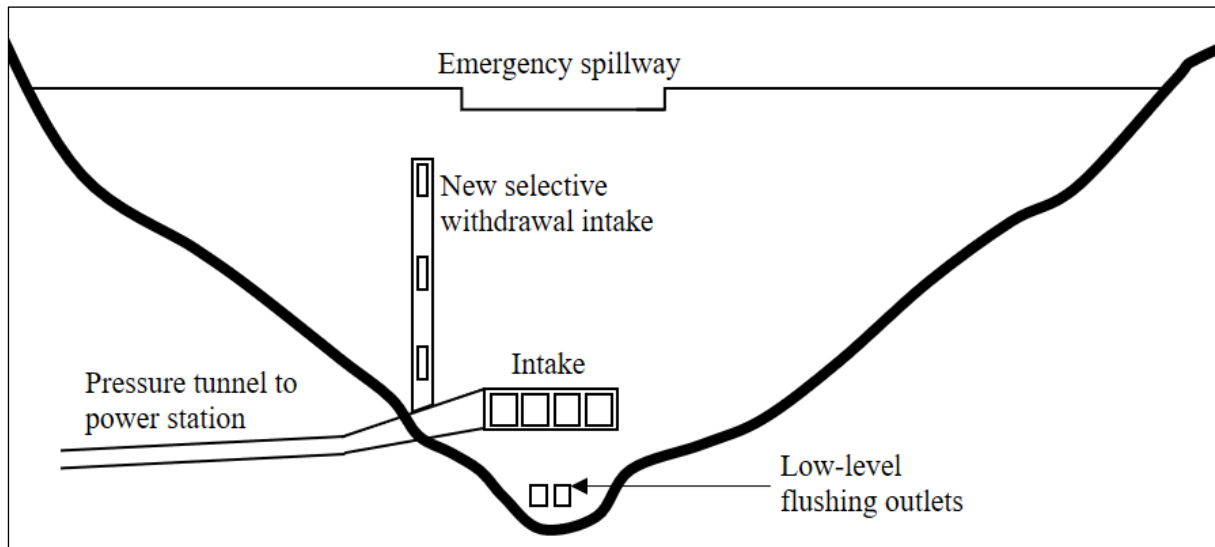


Figure 2.15. Low-level outlet and intake layout of Gebidem Dam (adapted from Morris & Fan, 1998)

2.4.5 Abrasion and Cavitation

According to Fan (1985) the velocity through low-level outlets can be greater than 40 *m/s*, inducing cavitation, vibration and abrasive action of sediment on the structures. This can affect the intake part of the outlet, conduit linings, gates and other structures exposed to the flowing water.

Due to the high sediment loads in low-level outlet flushing, abrasion resistant material is required for the outlet and conveyance structures. There are numerous abrasion resistant lining materials available for use in low-level outlets, but medium- to high-strength concrete linings are the most widely used (Boes, Müller-Hagmann, Albayrak, Müller, Caspescha, Flepp, Jacobs & Auel, 2018). Expensive options such as epoxy resin mortar and mounted rubber plates are not frequently used. Steel linings are frequently used in regions of high abrasive wear such as the section near the intake where acceleration takes place. Natural stone such as granite or cast basalt can also be used.

Compared to high-strength concrete (compressive strength about 110 *MPa*), granite has a higher abrasion-resistance and a much lower average abrasion rate (by a factor of 6 to 7) under severe abrasion conditions. The damage seen in granite-lined sediment bypass tunnels is concentrated at the joints between the plates, suggesting a jointless tight installation should be

Chapter 2: Literature Review

achieved with gaps filled with special highly resistant mortar. The availability and cost of natural stone should also be carefully considered, as well as the available skills of the construction team. Another problem of natural stone material is that it has a high abrasion resistance against the grinding action of particles, but due to their brittleness saltating sediments could lead to fracturing. Where saltating of large sediment particles are expected, steel or concrete are suggested, with the latter being the more economical alternative (Boes *et al.*, 2018).

Kriewitz, Gabl & Lazaro (2018) report serious damage to the lining of the Simmeweir low-level outlet where three different lining materials were used, namely steel, high strength steel fibre concrete and granite plates. The steel lining at the intake end showed very little damage, but the granite plating and concrete were destroyed during testing, thereby indicating the importance of choosing the correct lining material.

Cavitation of low-level outlets is based on the same principles as discussed for turbines in **Section 2.3.3.3**. In low-level outlets cavitation commonly takes place in the conduit and at the slots of gates. As the water flows over a slot it separates at the upstream edge of the slot and reattaches at the downstream side. The high velocity flow from the gate slot undergoes a pressure decrease and cavitation can occur in the slot or downstream thereof (Khosrojerdi & Ahmad-Abad, 2012).

Preventing cavitation can be done in three main ways: (1) increasing the allowable tension stresses in the wall by changing the material, (2) making the flow surface smoother or (3) flow aeration to increase local pressures. All three methods are practical, but for economic reasons engineers are motivated to use aeration (Abdolahpour & Roshan, 2014). More information on the need for aeration is discussed in **Section 2.4.9** and several formulae describing the air demand for different flow mixtures are described in Vischer & Hager (1998), as well as Sayah *et al.* (2015).

2.4.6 Gates and Operation

Low-level outlet gates are exposed to extreme sediment loads that could lead to erosion of the gate seals. Due to the sediment deposits against low-level outlet gates, the force required to open these gates increases by 16-33% (Basson & Rooseboom, 1999).

Morris & Fan (1998) recommend bottom opening flap gates and radial gates for low-level outlets, because they do not have guide slots or mechanical equipment in the low-level outlet canal. Radial gate seals face downstream and are thus not subjected to the sediment scour. Radial gates are preferable where the gate has to be able to control the discharge by changing

Chapter 2: Literature Review

the gate opening (Srivastav & Nayak, 2015). Flap gate seals are flush with the conduit and therefore not exposed to the sediment. These gates are operated by hydraulic actuators, allowing them to be used in high head conditions (Morris & Fan, 1998).

Another commonly used alternative is a sliding gate. According to Rollo, Bonnani, Sayah, Arboli & Braghini (2018) these gates are more compact, easier to install and impact less on dam stability. Sliding gates have been proven to be suitable in high-head low-level outlets for discharge control and silting prevention, and when properly designed allow good gate stability (avoiding pulsation and vibration) during partial openings (Rollo *et al.*, 2018).

Radial gates are typically used where the head is less than 120 *m* and the discharge high, however sliding gates are preferred where the head is greater and the discharge smaller (ICOLD, 2017). Sliding gates also require less space compared to radial gates and are thus preferred in many cases such as the Cerro del Águila Dam which has two sliding gates in each of its six low-level outlets.

Low-level outlets are normally designed with two gates that operate in series, with the downstream gate used for normal operations and the upstream gate serving as an emergency closure gate. The use of two gates is generally preferred, except in cases where operating characteristics or safety would significantly improve with the addition of a third gate (USACE, 2003). Providing sufficient spacing between gates is important to avoid simultaneous blockage by debris such as a tree trunk (Srivastav & Nayak, 2015). The location of control gates is also an important factor and provides a summary of the advantages and disadvantages of different locations.

Table 2.6 Comparison of the advantages and disadvantages of different control gate locations (USACE, 2003)

Position	Description	Advantages	Disadvantages
Upstream end	Gates, bulkheads and trash racks combined into a single structure on the upstream end of the outlet works	<ul style="list-style-type: none"> • Allows for inspection or maintenance of the entire conduit • Lower internal hydrostatic pressure in the conduit • Single structure is more economical 	<ul style="list-style-type: none"> • Extra cost of extending the structure above the pool and requires and access bridge
Near the dam axis	Gates placed in a chamber or shaft in the abutment	<ul style="list-style-type: none"> • Provides increased seismic protection • No extra cost of extending the structure above pool level 	<ul style="list-style-type: none"> • Separate bulkhead required to dewater upstream end of conduit for maintenance • Design required to withstand high earth loads in embankment dams • Conduit upstream of the gate chamber needs to be designed for full internal hydrostatic load
Downstream end	Control gates located downstream of the conduit	<ul style="list-style-type: none"> • Favourable in special conditions such as high-head projects with short outlet tunnels 	<ul style="list-style-type: none"> • Full internal hydrostatic pressure over entire conduit • Requires steel lining inside concrete lining for safety • Less economical • Upstream bulkhead closure required

2.4.7 Blockage by Sediment and Debris

Di Silvio (1990) examined obstruction of outlets in a physical model and came to the conclusion that the initial and final phases of flushing are most critical to prevent clogging by sediment. The outlets should be large in relation to the outlet tunnel length and depth of the sediment above the outlets. When the gates are opened, and the sediments are consolidated, there is a risk that a vacuum can form downstream of the sediment and upstream of the gates (Sayah *et al.*, 2015). In order to prevent blockage the sediment level should be monitored and short local scour periods should be applied (Basson & Rooseboom, 1999). Blocked low-level outlets should be closed and flushed again under pressure (Brandt, 2000).

In the case of the Cerro del Águila Dam, a syphon was placed in front of the low-level outlet entrance, as shown in **Figure 2.16**, to initiate the flushing process at the outlet. The syphon is oriented upstream and can deliver a water jet streaming out at 34 m/s, at normal operating level, which will hit the sediment and initiate the scouring process.

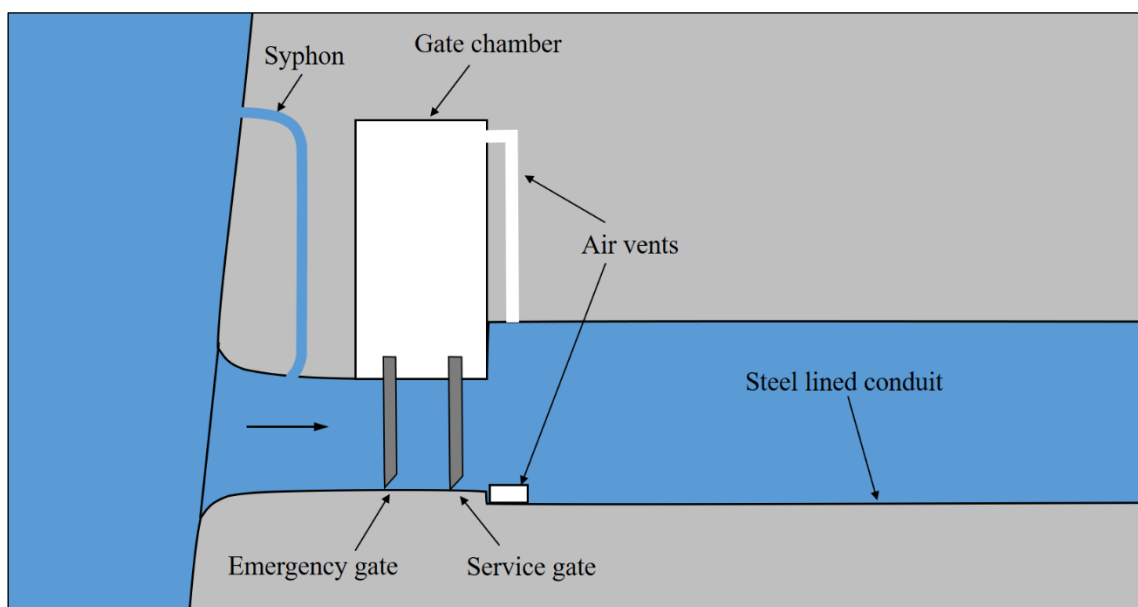


Figure 2.16 Low-level outlet configuration of the Cerro del Águila Dam showing the syphon structure to assist in sediment flushing (adapted from Sayah *et al.*, 2015)

Fan (1985) states that the blockage of low-level outlets can be worsened by entangled tree trunks and debris under free flow conditions. At the planning stage, the correct facilities should be designed in the right places to allow evacuation of floating objects. The low-level outlets should be straight, of sufficient size and the gates must allow free passage of flow. Fan (1985) further recommends the cutting of trees in the reservoir area before filling. In order to further minimise the influx of driftwood, all trees with a diameter greater than 80 mm within a tree

length from the upstream riverside should be felled (Darbre, Beckstein, de Goumoëns, Senn, Schlegel, Stahl, Klein, Walti & Muller, 2018).

2.4.8 Maintenance and Inspection

In order to ensure the satisfactory functioning of low-level outlets when required, Amirsayafi (2015) and Darbre *et al.* (2018) recommend that the following inspections and maintenance procedures are performed on an annual basis:

- Air vents should be inspected to ensure there is no blockage.
- The low-level outlet opening should be checked for blockage by debris or sediment.
- Conduit upstream and downstream of the service gates should be inspected to ensure a smooth, uniform surface to prevent cavitation arising from the high flow velocities.
- Mechanical equipment should be inspected and gates should be tested.

To allow optimal operation, inspection and maintenance it is important that designers ensure easy access to the low-level outlet both inside and outside the dam. Vischer & Hager (1998) summarise the technical requirements for a low-level outlet as follows:

- smooth flow when the structure is completely open,
- good performance for flows with partial opening,
- effective energy dissipation structures at the terminal outlet,
- no leakage of the structure,
- immediate and straight-forward application,
- access for servicing and maintenance,
- useful and economically efficient design, and
- long life.

2.4.9 Typical Design

Figure 2.17 shows a typical low-level outlet configuration. The flow is pressurised upstream of the gates and free-surface flow downstream of the gates. Low-level outlets should always be designed for free-surface flow to reduce gate vibration and cavitation. The gate on the upstream end is the emergency gate and the one on the downstream end is the service gate. Upstream of

the emergency gate, the tunnel contracts to a rectangular section and downstream of the service gate it expands both laterally and at the ceiling.

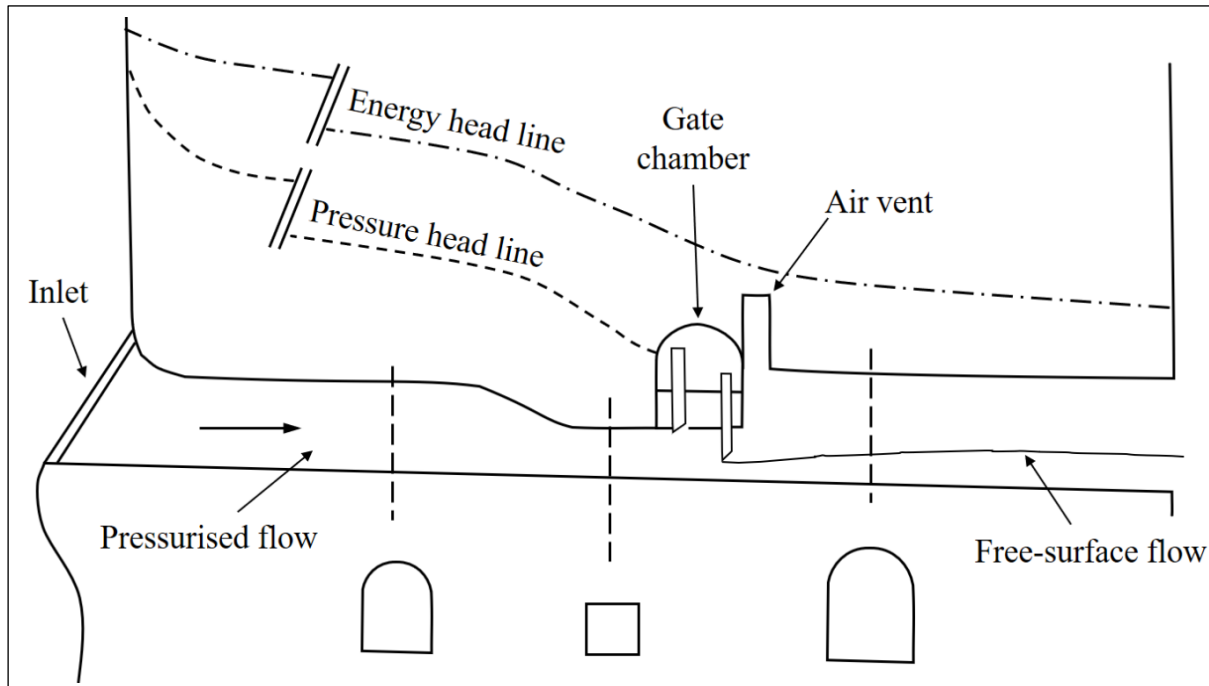


Figure 2.17 Typical low-level outlet arrangement (adapted from Vischer & Hager, 1998)

No additional aeration is required for short conduits, but for longer conduits a vertical aeration conduit discharging downstream of the gate chamber is required. Flow aeration can either originate from three different sources, namely (1) the tunnel outlet (2) an air supply conduit or (3) a bottom aerator.

2.4.10 Chinese Low-Level Outlets

China has been at the forefront of hydropower development over the last few years and added more hydropower than the rest of the world combined for the tenth consecutive year in 2017 (International Hydropower Association, 2017b). This has led to noticeable improvements in the field of hydraulic research in China, more specifically in the fields of energy dissipation, aeration, cavitation and discharge structures (Guo, 2012). A key trend observed when analysing Chinese dams is that their low-level outlet structures are mostly of rectangular shape, especially in dams currently being constructed or constructed in the past 20 years.

Table 2.7 shows the low-level outlet dimensions of thirteen major Chinese hydropower projects. It is interesting to note that the width to height ratios of the low-level outlets for twelve of the thirteen dams are lower than 1, indicating a rectangular outlet that is placed with the long

Chapter 2: Literature Review

edge positioned vertically. The low-level outlet width to height ratio for these projects range from 0.5 to 1.25, with a mean value of 0.76. The average outlet width is 5.3 m and the average outlet height 7 m. Eleven of the thirteen projects also have more than one low-level outlet to ensure the dam can be drawn down completely even if one of the outlets are obstructed.

More examples of dams with tunnel spillways and the different types are given in **Appendix A**. **Table A.1** shows that many countries adopt the horseshoe or circular shapes, but that rectangular tunnels are more common (18 out of 32 are rectangular shaped), especially in dams constructed more recently. When comparing the length to width ratios of the Chinese low-level outlets (in **Table 2.7**) and those of the rectangular tunnel spillways in **Table A.1**, similarities are seen between the width to height ratios of the outlets. **Figure 2.18** graphically presents the width to height ratios of 31 major dams, predominantly from China. A general trendline of the data is also plotted to describe the width to height ratio.

Table 2.7 Low-level outlets of Chinese hydropower projects (Guo, 2012)

Project Name	Country	Type of dam	Dam height (m)	No of	Width (m)	Height (m)	Width to height ratio
Three Gorges	China	PG	183	23	7	9	0.78
Ankang	China	PG	128	4	5	8	0.63
Wuqiangxi	China	PG	84.5	5	3.5	7	0.50
Longtan	China	RCC	216	2	5	8	0.63
Guangzhao	China	RCC	196	2	4	6	0.67
Dachaoshan	China	RCC	115	3	7.5	10	0.75
Longyangxia	China	PG/VA	178	1	5	7	0.71
Xiluodu	China	VA	273	7	5	6	0.83
Ertan	China	VA	240	4	3	5	0.60
Goupitan	China	VA	225	2	6	7	0.86
Dongjiang	China	VA	157	2	6	7	0.86
Shuibuya	China	CFRD	233	2	4	5	0.80
Gongboxia	China	CFRD	127	1	7.5	6	1.25

Note: PG = gravity dam, RCC = roller compacted concrete dam, VA = arch dam, CFRD = concrete faced rockfill dam

Chapter 2: Literature Review

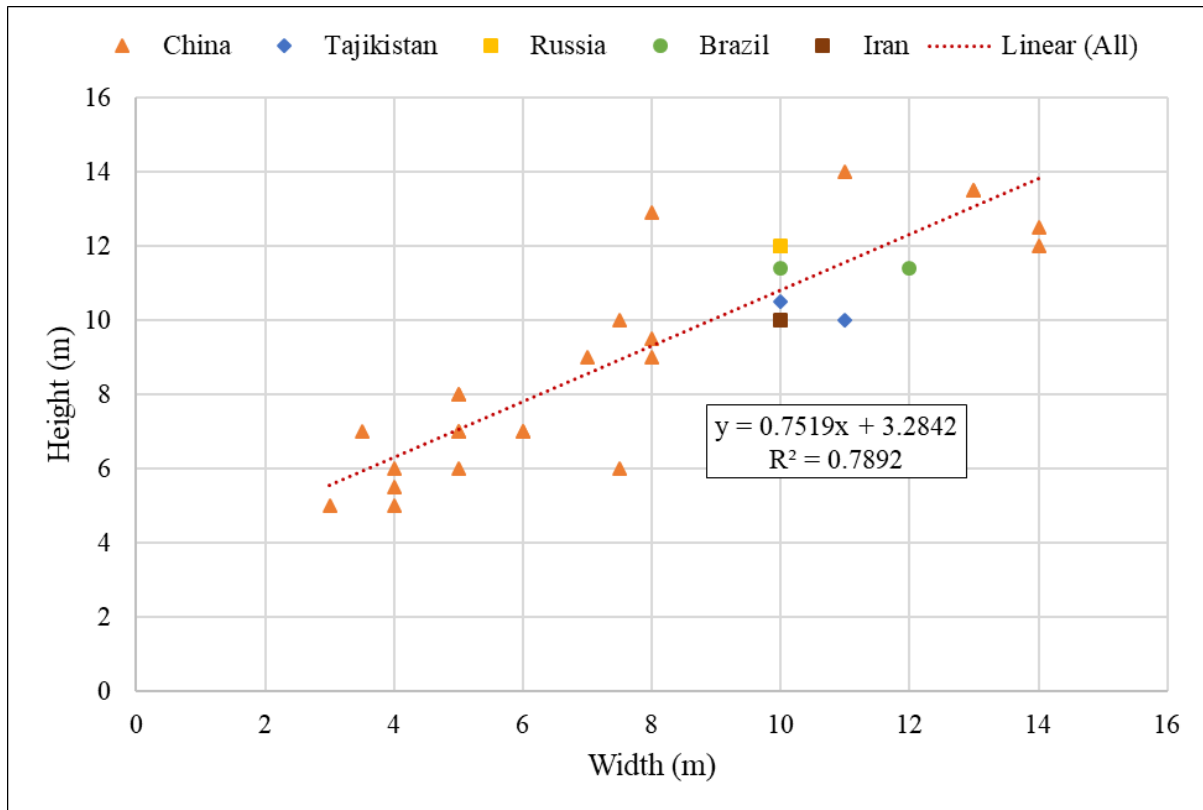


Figure 2.18 Graph showing the height versus width plots of for 31 major dams with rectangular shaped tunnel outlets

2.5 Sedimentation Management Strategies

Morris *et al.* (2008) describe three distinct stages of a reservoir's life:

1. Continuous sediment trapping: relatively rapid deposition of sediment in the reservoir during all inflow events.
2. Partial sediment balance: mixed regime of sediment deposition and removal through sediment management techniques such as sluicing and flushing; fine material reaches a balance, but the coarse material continues to accumulate.
3. Full sediment balance: a long-term sediment balance for all particle sizes where the entire inflowing sediment load can be transported beyond the dam or removed artificially.

The authors state that most of the world's reservoirs are currently in Stage 1 and were not designed to reach sediment balance due to poor design practices of the past. According to Basson & Rooseboom (2007), many reservoirs were designed with a dead storage capacity of about 50 years and with most dams built between 1950 and 1990, the effects of reservoir sedimentation are of growing concern. Proper sediment management can slow down the sedimentation process and reduce the effects thereof.

Implementing reservoir sedimentation management techniques is not only of great importance to prevent loss of storage capacity, but also to prevent abrasion of hydraulic machinery, sedimentation of intakes, clogging of low-level outlets, increased flooding, loss in water quality and damage to the structure (Basson & Rooseboom, 1999; Bruk & Zebidi, 1996; Fan & Morris, 1992b; Mahmood, 1987).

Sediment management is, however, often in conflict with reservoir management that requires high water levels for electricity generation, but in turn increases sediment deposition (Brandt, 2000). Therefore the economic aspects of sediment management strategies need to be analysed carefully to determine their feasibility (Brabben, 1988).

Several methods to control reservoir sedimentation have been studied and applied in reservoirs worldwide, each with its own limitations and impacts. The various methods for sediment control are generally divided into three "active" management categories (Basson & Rooseboom, 1999; Morris & Fan, 1998; Sumi & Kantoush, 2010) and Morris (2015) describes "adaptive" strategies, which do not manipulate sediment, as the fourth category to be included.

Chapter 2: Literature Review

The four categories for reservoir sedimentation management widely recognised today are:

- reduce sediment inflow from upstream
- route sediments to minimize deposition
- remove accumulated sediment deposits
- adapt to or compensate for reservoir sedimentation.

Figure 2.19 provides a summary of the sediment management control categories and the methods used in each of these categories.

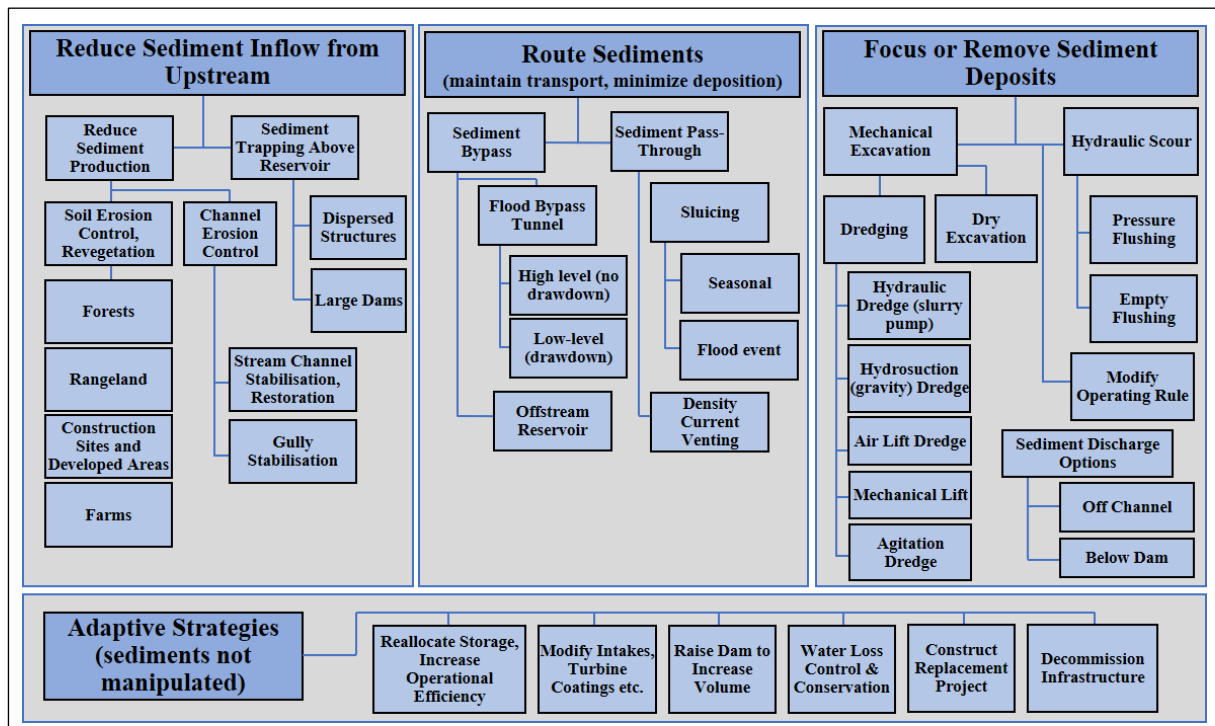


Figure 2.19. A summary of sediment control measures (adapted from Morris, 2015)

2.5.1 Reduce Sediment Inflow from Upstream

Morris & Fan (1998) described the following two strategies to reduce the sediment yield entering the reservoir from the upstream watershed: (1) soil and channel erosion control at the source or (2) trap sediment upstream of the reservoir.

2.5.2 Route Sediments to Minimize Deposition

Sediment routing is a group of techniques to either bypass sediment around the reservoir or to pass sediment through the impoundment. Bypass strategies include (1) selectively excluding sediment-laden flood flows and diverting clear water into the reservoir and (2) bypassing sediment-laden flood flows around an on-stream reservoir. Pass-through strategies include (1)

Chapter 2: Literature Review

sluicing, which is passing sediment-laden floods through the impoundment by reservoir drawdown and (2) turbid density current venting through a low-level outlet (Annandale *et al.*, 2016).

Sluicing is often used to allow the first floods of the season to pass through as these floods usually contain the highest sediment loads. Jiang & Fu (1998) report floods with high sediment loads in the northern parts of China where 90% of the annual sediment load is carried during the flood season, whereas only 60% of the annual runoff occurs in the corresponding period. By routing these floods through the reservoirs sedimentation rates have been greatly reduced. During the sluicing operation, velocities in the reservoir are high enough to keep sediment in suspension, ultimately preventing deposition.

Sluicing is often more efficient than flushing, because the velocities required to keep sediment suspended is lower than the velocities required to erode previously deposited sediment (Basson & Rooseboom, 1999). Fan & Morris (1992a) state that the effectiveness of sluicing is enhanced if the reservoir is already almost fully drawn down using large low-level outlets when the flooding starts, because sediment concentrations tend to be highest on the hydrograph's rising limb. If the reservoir water level is low, it reduces backwater effects and minimizes hydraulic detention time. After the flood season, the clear water can be impounded and the reservoir level raised for usage.

Sediment routing partially preserves the sediment transport properties of a river and is considered the most environmentally friendly benign sediment management strategy, compared to flushing which is potentially the most damaging. One major disadvantage of sediment routing is that large amounts of water is required to transport the sediments and can therefore not be impounded. Due to this restriction sediment routing is most applicable in small reservoirs where the water discharged during large floods is greater than the reservoir capacity (Morris & Fan, 1998).

Turbidity currents, as described in **Section 2.2.3.2**, are important in the transport and deposition of sediment in many reservoirs worldwide. However, it is often possible to allow the turbidity current to pass through the low-level outlets of the dam, referred to as turbidity current venting. Venting of turbidity currents is done by opening the low-level outlets as soon as the current reaches the dam which is often in a flood event. The loss of water is minimised in a turbidity current venting event, because the outflow is relatively small and the reservoir is not drawn down, making it suitable for arid regions where sluicing is not feasible (Chamoun *et al.*, 2016).

Chapter 2: Literature Review

Morris & Fan (1998) report dams that have been able to pass half the inflowing load by turbidity current venting, but this is only possible where the current has sufficient turbulence and velocity to keep particles in suspension and does not dissipate before reaching the dam. Facilities such as low-level outlets located near the original river-bed should be provided at all projects where turbidity currents are anticipated (Kondolf *et al.*, 2014). Designers must be aware that turbidity current venting will only help reduce sediment deposition of very fine particles (typically less than 30 μm). **Table 2.8** compares the two methods of sediment routing described.

Table 2.8 Comparison of sluicing and turbidity current venting (from Fan & Morris, 1992a)

Type of routing	Sediment discharge	Operating rule	Outlet type	Mode of action	Advantages and disadvantages
Sluicing or flood routing	Discharge < Inflow	Outlets opened to minimize storage during flood periods, stays seasonally low	Large capacity low-level outlets	Turbulent flow maintains sediment in suspension and some deposits are removed by retrogressive erosion	Utilizes excess water during floods; requires reservoir drawdown
Turbidity current venting	Discharge < Inflow	Outlets vent turbidity current when it reaches the dam site	Moderate capacity low-level outlets	Venting of a portion of the turbidity current containing fine particles	No drawdown required; efficiency not very high

2.5.3 Remove Accumulated Sediment Deposits

The two main methods to remove deposited sediment is (1) flushing or (2) mechanical removal. Flushing is the second oldest method used for sediment control in reservoirs and is discussed in more detail in **Section 2.6** (Brown, 1943). Mechanical removal of sediment is the oldest method used for reservoir silting control (Brown, 1943) and can take place as dry excavation, dredging or siphoning, where the latter refers to excavating sediments from beneath the water.

Dry excavation involves traditional earth moving equipment transporting excavated sediment to a suitable disposal area. This method requires reservoir drawdown which together with the transport costs make it very expensive (Tiğrek, Göbelez & Aras, 2009). Dry excavation is best suited for reservoirs which remain dry for long periods of time (Kondolf *et al.*, 2014). Dredging is the mechanical removal of accumulated sediment by pumping or by mechanical equipment without emptying the reservoir. Dredging is generally more economic than dry excavation, but is still considered an expensive method of restoring storage capacity and should only be done

Chapter 2: Literature Review

where alternatives are not possible (Basson & Rooseboom, 1999; Mahmood, 1987). Fan (1985) states that dredging is undertaken where:

- flushing is not successful,
- construction of a bypass is not possible,
- reservoir drawdown is not allowed for the sake of saving water,
- the dam is not replaceable and cannot be raised, or
- drawdown flushing is uneconomical

Siphoning is similar to hydraulic dredging but exploits the hydraulic head difference between the upstream and downstream levels of the dam. It is also referred to as the Hydrosuction Removal System (HSRS) in the United States. Since potential energy is used and no external pumping is required, this method's operating costs are much lower. Siphoning is typically limited to short reservoirs where flushing is not feasible (Kondolf *et al.*, 2014).

2.5.4 Sediment Management for Different Types of Dams

Sediment management strategies vary depending on several factors including the catchment and reservoir characteristics, climate, reservoir use and water supply needs. A perfectly sustainable solution for every scenario therefore does not exist, but management strategies can be optimised for the particular reservoir. In regions where high sediment loads occur predictably and often, sediment management methods such as sediment bypass, sluicing and turbidity current venting can be most effective. Sediment removal methods such as flushing and dredging are often used to reclaim storage in cases where the reservoir design was non-sustainable (Healy, Cox, Hanes & Chambers, 2014). However, the applicability of most of these methods (including sediment routing, sluicing, flushing, turbidity current venting, dredging and siphoning) depend on the availability of excess water, making it less applicable in semi-arid and arid regions where dams tend to have a storage capacity close to 100% of the MAR (ICOLD Sedimentation Committee, 2009).

2.6 Reservoir Desiltation by Means of Flushing

The term 'flushing' has been used in different contexts over the years, to describe what is currently differentiated as sluicing and drawdown flushing. Brown (1943) used the phrase 'flood sluicing' to describe the removal of deposits through large sluice gates at the base of the dam by utilizing the scour action caused by the sudden release of water under a high head

Chapter 2: Literature Review

(known as pressure flushing) or from incoming flood flows (known as sluicing). He used the phrase ‘draining and flushing’ to refer to the process of slowly releasing all the stored water in the reservoir through gates or valves located near the bottom of the dam and then allowing the normal stream flow to scour out a channel in the sediment deposits (known as drawdown flushing).

The oldest known method of flushing was referred to by D’Rohan, who described the operation of Spanish undersluices in the 16th century to release sediment from reservoirs (Brown, 1943). Flushing is defined as the method of hydraulically clearing deposited sediment in a dam through a low-level outlet (Mahmood, 1987). Often when referring to flushing, water level drawdown in the reservoir is insinuated, because that is the more common flushing method being used and is what most previous flushing studies have focused on. However, flushing can be more generally distinguished as drawdown, also known as empty or free-flow flushing, or pressure flushing, also known as local flushing (Fan, 1985; Lai & Shen, 1996; Shen, 1999).

Figure 2.20 illustrates the differences between the two types. Over the years the increasing need for sediment management has changed the outlook of many engineers and researchers about flushing as an effective method for reservoir desilting.

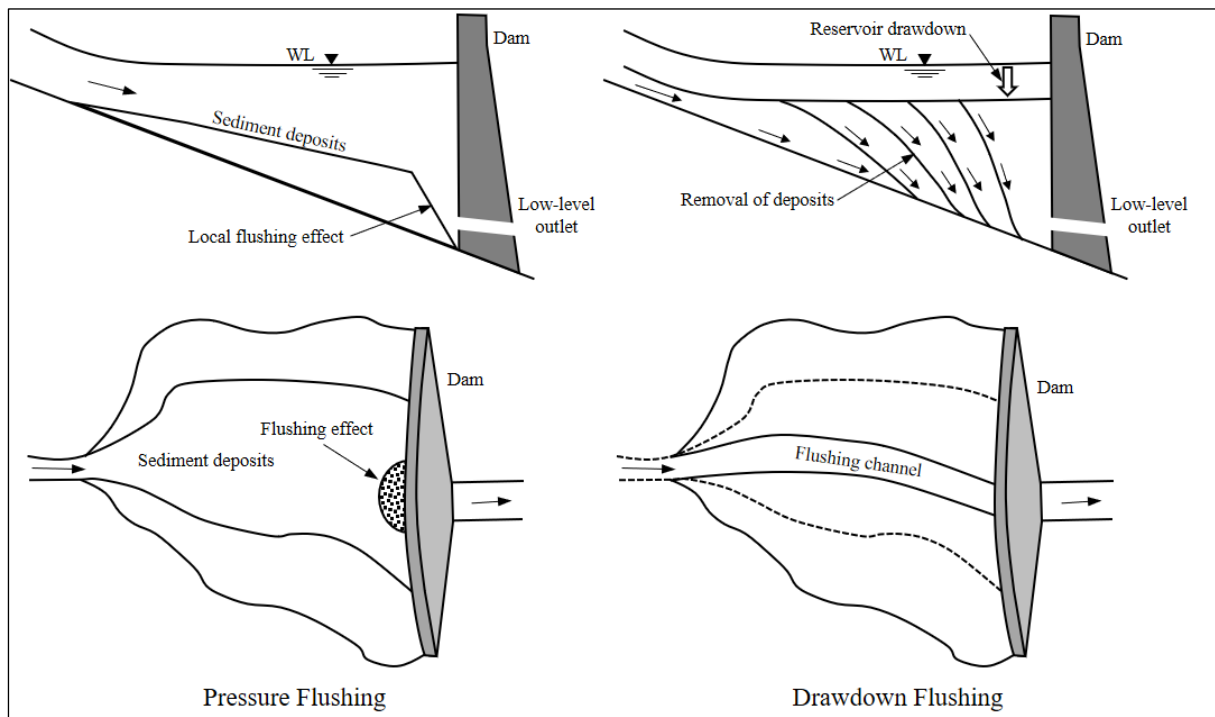


Figure 2.20 Comparison of pressure and drawdown flushing (adapted from Shen, 1999)

The main objective of flushing is to erode previously deposited sediment from the reservoir. Boeriu, Roelvink, Mulatu, Thilakasiri, Moldovanu & Margaritescu (2011) distinguish between

Chapter 2: Literature Review

two modes of erosion which can occur during flushing, namely retrogressive and progressive erosion:

- *Retrogressive erosion* is the process of erosion that propagates upstream by cutting a flushing channel into the deposited sediment. Retrogressive erosion is characterised by a zone of steep slope and rapid erosion which moves upstream along a channel with a lower slope. This type of erosion results from the hydraulic energy change caused by the discontinuous longitudinal profile. It continues to erode until a unified slope is achieved whereafter the erosional process becomes progressive erosion (Morris & Fan, 1998).
- *Progressive erosion* happens due to the flow of water entering the reservoir eroding the channel uniformly along the entire length. Progressive erosion takes place during the final stage of drawdown flushing and is dependent on the sediment carrying capacity and bed erosion rate. The rate of erosion is higher upstream and reduces downstream as the erosional and transport capacity for additional sediment decreases.

2.6.1 Drawdown Flushing

According to Morris & Fan (1998) drawdown flushing involves lowering the reservoir water level by opening a low-level outlet to temporarily establish riverine flow along the impounded reach. First time flushing results in a channel that forms in the deposited material and during the next flushing period this channel will be maintained. Free-flow flushing is done by emptying the reservoir and routing the sediment under natural riverine conditions through the low-level outlets. White (2001) states that this method of flushing is the only realistic option for removing significant quantities of previously deposited sediments. In order to reach free flow conditions the water level must be drawn down all the way to the top elevation of the low-level outlets (Shen, 1999). Although this is considered an effective technique to restore storage capacity in many scenarios, power generation during the process, which can last months, is greatly decreased or inhibited completely due to the low water level (Basson & Rooseboom, 1999).

2.6.2 Pressure Flushing

Pressure flushing is a variant of drawdown flushing which has received increased attention from engineers and researchers since the start of the 21st century. This technique involves the release of deposited sediment through a low-level outlet while the water level is high (Morris, 2015). This is not a commonly used method for sediment removal from reservoirs, due to the fact that

Chapter 2: Literature Review

it only creates a localised scour zone and has no effect on sediment deposits upstream of the scour cone (Mahmood, 1987; Shen, 1999). When flushing is attempted without reservoir drawdown, the high flow velocities at the outlets are only localised and the impact is very small (White & Bettess, 1984). However, if the goal is to keep the intakes free of sediment, this method is definitely an option for reservoirs that have low-level outlets located beneath the intakes since it uses much less water than drawdown flushing (Kondolf *et al.*, 2014; Lai & Shen, 1996; Morris, 2015).

Qian (1982) stated that this method of flushing is only an option for reservoirs with large capacity sluice gates and a small reservoir capacity to inflow ratio. Pressure flushing is thus of particular importance for hydropower dams in arid and semi-arid countries where over-year storage is a necessity.

Although the volume of water released is much less compared to drawdown flushing, it is regarded as an ineffective flushing technique to restore reservoir active capacity (Shen, 1999; Morris & Fan, 1998).

Table 2.9 Comparison of pressure and drawdown flushing (from Fan & Morris, 1992a)

Type of routing	Sediment discharge	Operating rule	Outlet type	Mode of action	Advantages and disadvantages
Drawdown flushing	Sediment outflow load > Inflow load	Outlets opened to drawdown reservoir completely and create rapid free-surface flow	Large capacity low-level outlets capable of discharging high sediment loads	Turbulent flow maintains sediment in suspension and can remobilise deposits by progressive and retrogressive erosion	Can remove large amounts of deposited sediment; Total power plant shutdown
Pressure flushing	Sediment outflow load > Inflow load	Outlets opened for a short period of time without significant drawdown	Large capacity low-level outlets	Pressurised flow creates high velocities near the outlet, creating a scour cone in a short period of time	Keeps the power intakes free of sediment; Does not recover large amounts of active storage

2.6.3 Applications and Limitations

Flushing as a periodic sediment removal method has been carried out successfully in many reservoirs worldwide and remains one of the most widely practiced sediment management options. However, the downstream environmental impact of flushing is a major concern and should be investigated before initiating flushing. Flushing causes sediments to be released from the reservoir at a higher concentration than normal river conditions, which can lead to serious problems downstream such as channel aggradation, flooding, clogging of water intake structures or diversion channels, fish kills and habitat destruction (Baoligao, Xu, Chen, Wang & Chen, 2016; Brandt, 2000; Espa, Castelli, Crosa & Gentili, 2013; Morris & Fan, 1998). Sediment deposition along the downstream watercourse can also greatly alter the riverbed and fill pools, thus changing river habitats (Quadroni, Brignoli, Crosa, Gentili, Salmaso, Zaccara & Espa, 2016). Besides the site-specific conditions, the concentration of sediments during flushing is the most important parameter in determining the total impact of the flushing event and should be carefully monitored to lower the environmental impact (Espa, Brignoli, Crosa, Gentili & Quadroni, 2016). Therefore, the more effective the flushing process, in terms of sediment removal, the greater the downstream effects (Brandt, 2000).

Yin, Yang, Petts & Kondolf (2014) describe specific operating rules and conditions to minimise the downstream effect of flushing and protect the riverine ecosystem. In some dams, mid-level outlets have been installed together with low-level outlets to regulate the downstream water quality during flushing. The downstream impacts of pressure flushing have not been extensively studied, but if the flushing event is short to conserve water, the evacuated deposits may simply deposit just downstream of the dam. Flushing will always negatively impact on the downstream river reach but to minimise the impact, each reservoir should have flushing rules adapted for the site-specific conditions.

2.7 Low-Level Outlet Flushing Under Pressure

2.7.1 Orifice Flow Theory

Orifices are commonly used hydraulic structures consisting of an opening in a wall through which flow occurs. Orifices are often used as flow measuring devices but can also be used to flush deposited sediments from a reservoir. Thus, low-level outlets in dams essentially act as orifices during pressure flushing. The top of the orifice must be well below the upstream water level, such that air entrainment does not occur (Hussain, Ahmad & Ojha, 2016). In general, the true orifice condition is established when the head above the centre of the orifice becomes 2 to

Chapter 2: Literature Review

2.2 times the orifice depth (Hussain, Ahmad & Asawa, 2010). Orifices are classified based on the following characteristics:

- **Size:** Based on the size and fluid head, orifices can be classified as either small or large. A small orifice is one in which the head of fluid above the centre of the orifice is more than five times the depth of the orifice. If the head is less than 5 times the orifice depth, it is classified as a large orifice.
- **Shape:** Orifices can be classified as circular, square, rectangular or triangular.
- **Nature of discharge:** Orifices can be classified as free-discharging, fully submerged or partially submerged.
- **Nature of upstream edge:** Based on the upstream edge, orifices can be classified as sharp-edged or bell mouthed orifices.

The discharge through an orifice can be calculated by applying the Bernoulli equation between a point upstream of the plate (1) and the vena-contracta point downstream of the plate (2) as shown in **Figure 2.21** (Chadwick *et al.*, 2013).

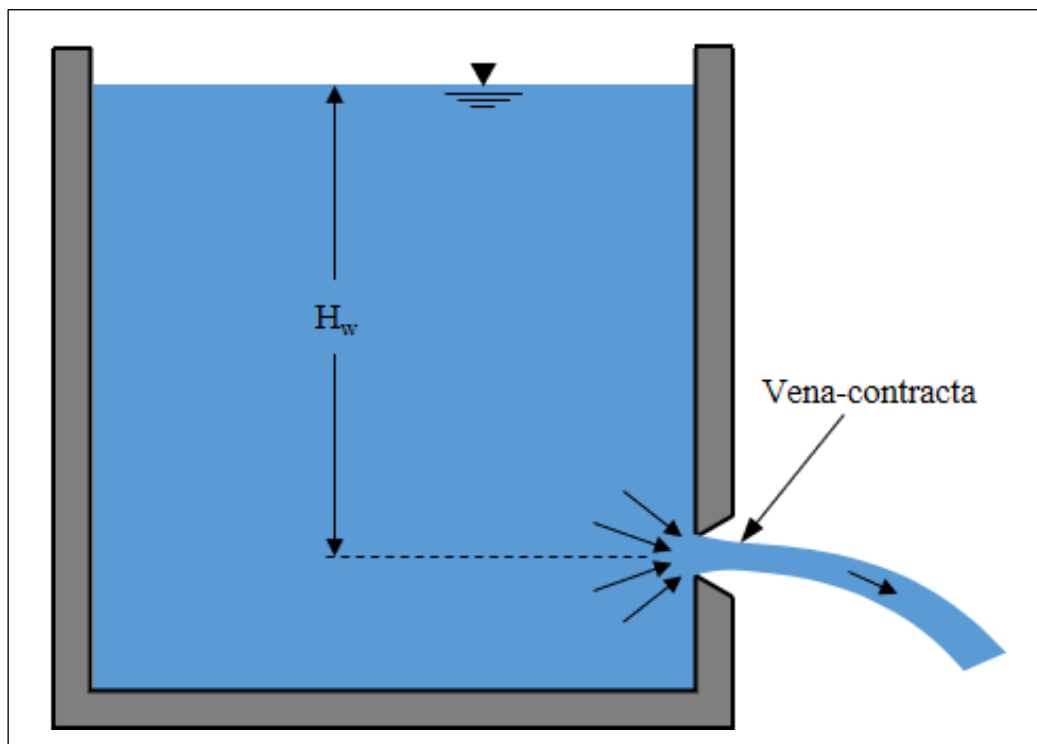


Figure 2.21 Flow through an orifice (Chadwick *et al.*, 2013)

$$\frac{p_1}{\rho g} + \frac{V_1^2}{2g} + z_1 = \frac{p_2}{\rho g} + \frac{V_2^2}{2g} + z_2 \quad 2-33$$

Chapter 2: Literature Review

where:

$p_{1,2}$ = pressure at specified point (Pa)

$V_{1,2}$ = velocity at specified point (m/s)

$z_{1,2}$ = elevation of the specified point above the datum (m)

But the following assumptions hold:

$$z_1 = z_2$$

$$\frac{p_1}{\rho g} = H_w$$

$$\frac{p_2}{\rho g} = 0$$

V_1 is very small in comparison to V_2 since the reservoir is very large compared to the area of the jet. The simplification yields:

$$H_w + 0 = 0 + \frac{v_2^2}{2g} \quad 2-34$$

$$V_2 = \sqrt{2gH_w} \quad 2-35$$

This represents the theoretical velocity and can be expressed in terms of the flow rate and orifice area. The actual flow rate (Q) is influenced by the discharge coefficient (C_d) and is given as:

$$Q = C_d A \sqrt{2gH_w} \quad 2-36$$

The discharge coefficient generally varies between 0.59 and 0.65 depending on the characteristics of the orifice plate, such as the thickness.

2.7.2 Pressure Flushing Process

White & Bettess (1984) describe two effects that discharging water through low-level outlets to flush sediment has: (1) a local effect of the low-level outlets and (2) a general movement in the bulk of the reservoir. During pressure flushing, only the local effect of the low-level outlets removes sediment from the reservoir. The distance which this local effect acts on the deposited sediment is, however, very limited and cannot contribute to sediment flushing from the bulk of the reservoir. As the low-level outlet is opened, sediment in the immediate area of influence is scoured out by the high approach velocities close to the outlet.

This scour at the opening forms a funnel-shaped crater, called the flushing cone (also called the scour cone, flushing half-cone, semi-cone hole, local half-cone, scour hole or scour funnel),

Chapter 2: Literature Review

within a very short period of time whereafter the water flowing through the outlet is clear (Emamgholizadeh *et al.*, 2006). That implies that a relatively stable cone has formed and that no sediment will be removed unless the water level is reduced drastically (Di Silvio, 1990).

2.7.3 Scour Cone Geometry

The geometry of the scour cone which forms during pressurized flushing is specifically of importance where the flushing event is aimed at removing accumulated sediment around the entrance of an intake and preventing abrasion of hydraulic structures. The effect of the scour cone is restricted to the zone near the flushing outlet but plays a key role in preventing sediment from entering the power intakes and blocking the trash racks. Thus, when designing a sediment flushing outlet, it is crucial to understand the geometric features of the scour cone which will form under pressure flushing (Fang & Cao, 1996). A generalised reservoir configuration with a scour cone formed by pressure flushing is shown in **Figure 2.22**.

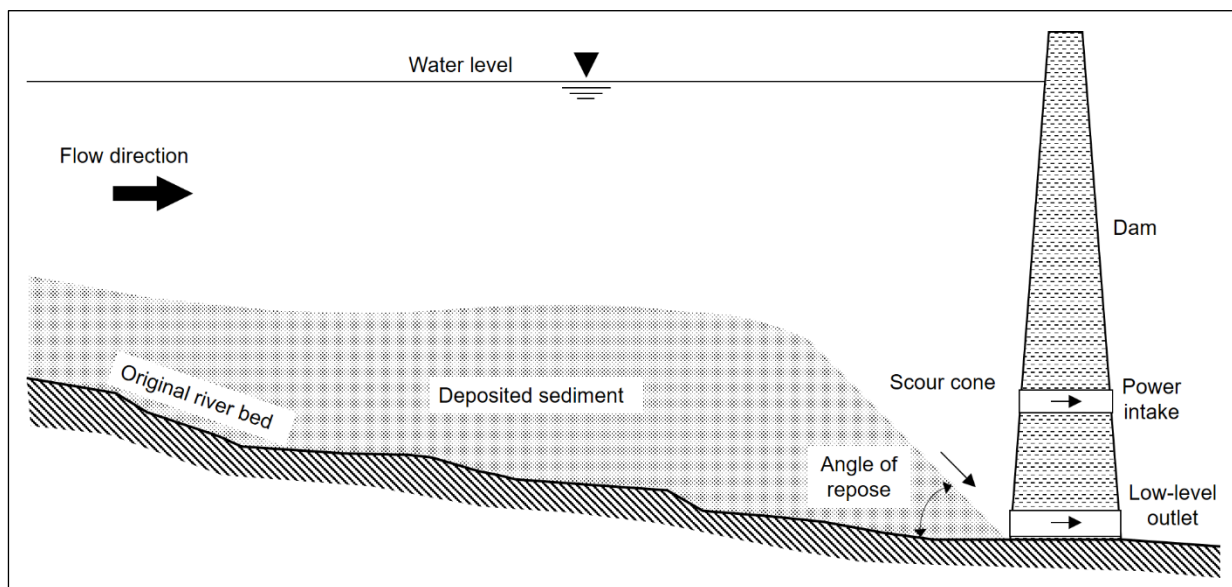


Figure 2.22 Scour cone formed by pressure flushing (Lai & Shen, 1996)

The scour cone geometry indicates the area in front of an intake which can be cleared of sediment and also influences the time it will take to refill with incoming sediment. Knowing the rate of sediment deposition near the dam wall, an estimate can then be made on how often flushing should be done.

2.7.3.1 Predicting the Scour Cone Geometry

According to Fang & Cao (1996) the scour cone's geometric characteristics depend on three main factors:

Chapter 2: Literature Review

1. Hydraulic conditions in front of the outlet – water depth, discharge, flow velocity, outlet shape, etc.
2. Properties of the deposited sediment – median diameter, mineral composition, submerged angle of repose, viscosity, etc.
3. Operating conditions of the reservoir – flushing duration, flushing frequency, etc.

Theoretical estimation of the scour cone's geometry is however rather difficult, because the flushing process is a complicated three-dimensional turbulent flow problem with a combination of variables and random effects that are difficult to predict (Scheuerlein, Tritthart & Nuñez Gonzalez, 2004). Several empirical and numerical models have been developed for estimating the scour cone's dimensions with varying accuracy and application.

White & Bettess (1984) provided a diagram (shown in **Figure 2.23**) which indicated the scour limit in static water for different discharges and depths. Their results showed that for a given discharge, lowering the water level increases the developing rate of the scouring cone.

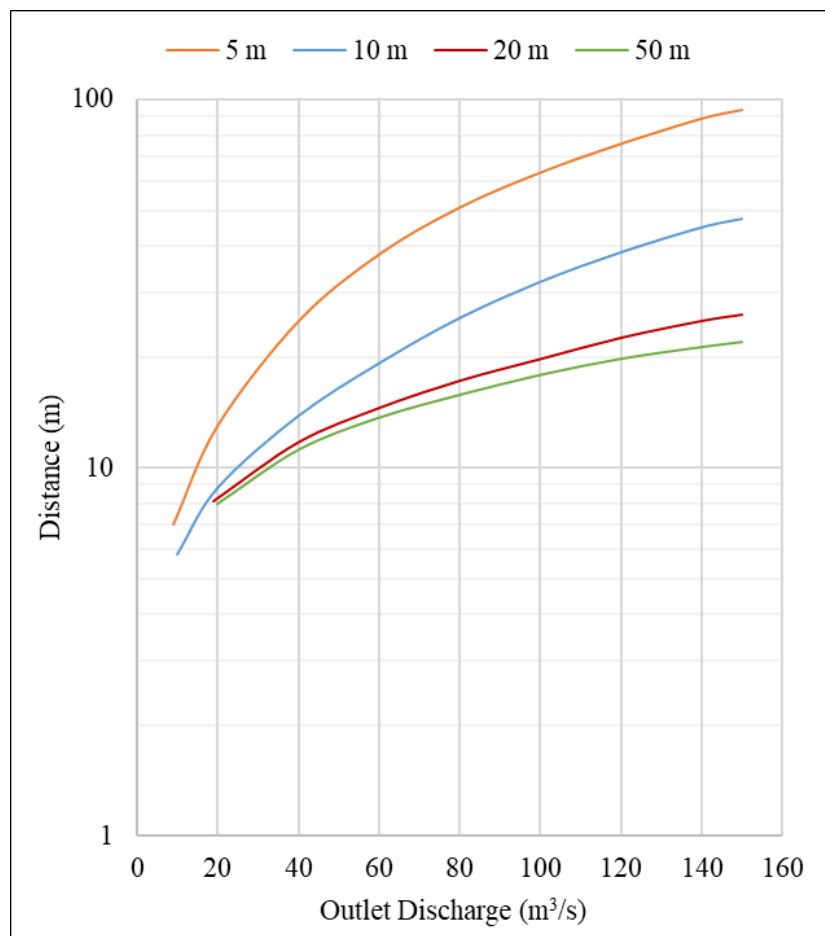


Figure 2.23 Scour limit in static water for different outlets (adapted from White & Bettess, 1984)

Chapter 2: Literature Review

Scheuerlein (1993) presented a simplified analytical approach to identify the flushing process' governing parameters. The approach is based on a combination of basic hydraulic principles applied to a grid of three-dimensional streamlines and isotachs, and stability criteria of sediment deposits against eroding forces of water flow. **Figure 2.24** shows the simplified flow pattern at a low-level outlet used to derive **Equation 2-37**.

$$\frac{r}{D} = \frac{1}{2} \sqrt{\frac{\mu_G \sqrt{2gH_w}}{V_r}} \quad 2-37$$

where:

- r = radial distance of a sphere-shaped isotach from the low-level outlet (m)
- μ_G = coefficient summarizing all the losses at the outlet
- V_r = flow velocity at a distance r from the outlet (m/s)

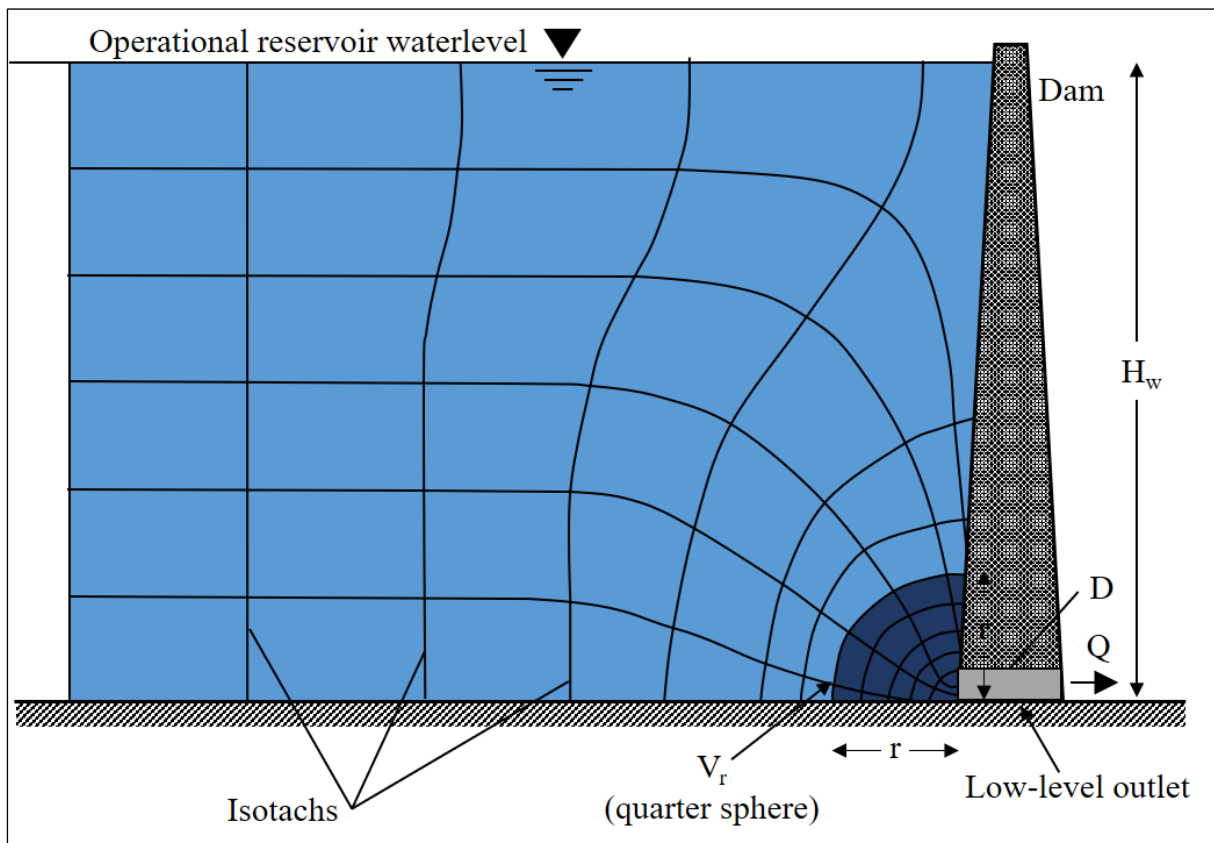


Figure 2.24 Simplified flow pattern at a low-level outlet (adapted from Scheuerlein, 1993)

The flow velocity is indirectly proportional to the distance from the outlet r , thus the velocity v_r decreases with increasing distance. Sediment particles in front of the outlet can only be

Chapter 2: Literature Review

remobilized if the induced forces exceed the particles' resistance to movement. Therefore, the critical distance r_c at which a particle of grain size d_s can be remobilized depends on the threshold velocity V_h of the sediment.

During the first stage of flushing without water level drawdown the scour cone theoretically stabilizes at a distance r_c with the front slope approximately at the submerged angle of repose β of the deposits. When this stage is reached, no further scouring of the deposits will occur until the water level is drawn down. Lowering the water level will not immediately cause further scouring, because r_c is proportional to H_0 . Scheuerlein (1993) states that in order to initiate the second stage of flushing, the water level must be drawn down to the “effective flushing water level”, H_{EF} , as defined by the simplified approach presented in **Equation 2-38** and explained by **Figure 2.25**.

$$H_{EF} = H_S + \frac{1}{2} \left(\frac{KD^2}{V_h} \right)^2 + \frac{KD^2}{V_h} \sqrt{H_S + \frac{1}{4} \left(\frac{KD^2}{V_h} \right)^2} \quad 2-38$$

where:

$$K = \frac{\mu_G \sqrt{2g}}{4 \left(\frac{H_S}{\tan \beta} + r_c \right)} \quad 2-39$$

- H_S = horizontal sediment level above outlet invert (*m*)
- V_h = threshold velocity, equal to approach flow velocity V_a (*m/s*)
- β = submerged angle of repose of deposits (*degrees*)
- r_c = distance of flushing cone without drawdown from **Equation 2-37** (*m*)

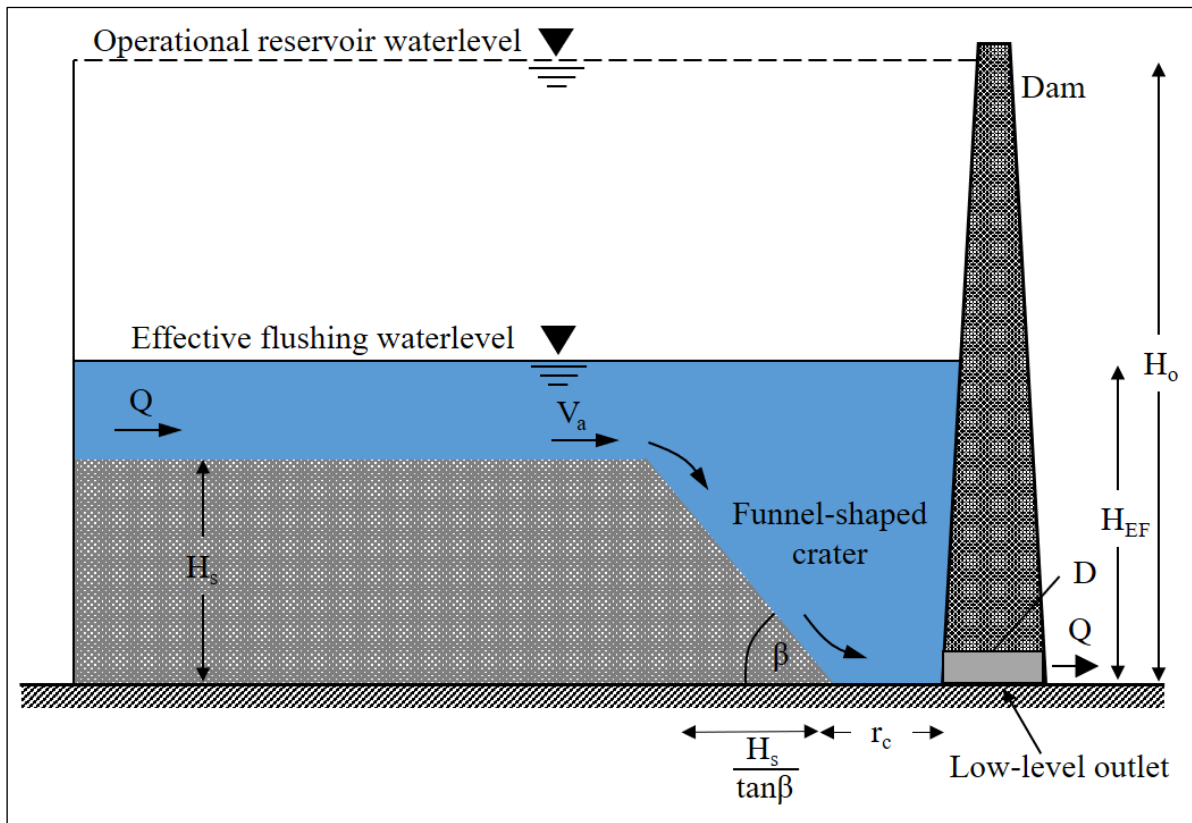


Figure 2.25. Flushing actions at water level drawdown (adapted from Scheuerlein *et al.*, 2004)

The results from a physical model study by Scheuerlein *et al.* (2004) showed that the simplified approach contains some deficiencies and did not agree satisfactorily for flushing with water level drawdown. Samto Atmodjo & Suripin (2012) developed an equation for determining the effective water depth for pressure flushing from laboratory experiments. They stated that the flushing efficiency is less when the water level is above or below this level. The focus of this study is, however, on the formation of a scour cone without water level drawdown and it was found that the simplified approach was generally confirmed by the physical model and the slope of the cone was equivalent to the sediment's submerged angle of repose. The assumption that the streamlines and isotachs are sphere-shaped, was not perfectly accurate and an ellipsoidal pattern is suggested. A study by Shammaa, Zhu & Rajaratnam (2005) confirmed that the velocity pattern close to the orifice is semi-ellipsoidal, becoming hemispherical further away and uniform far upstream.

The formation of the scour cone is unfortunately not as simple as presented by Scheuerlein *et al.* (2004) and according to a physical model study by Powell (2007), the size of the scour cone primarily depends on the vortex structure which develops below the outlet.

Chapter 2: Literature Review

Meshkati *et al.* (2009) studied the evolution of the scour cone over time and presented equations for the length, width and depth as a function of time and the final scour hole geometry.

The formation of a stable cone could take place in a very short period of time as reported in field observations at the Dez Dam and Sanmexia Dam where flushing cones formed in ten to twenty minutes (Emamgholizadeh *et al.*, 2006). Several equations for predicting the scour cone geometry are presented in **Section 2.7.4**.

2.7.3.2 Scour Cone Slope Angles

The bed slopes of the scour hole have also been studied extensively and several comparisons have been made between the slope angles of the longitudinal and transverse axes. The general consensus is that for non-cohesive sediment the scour cone slopes would be approximately the same as the submerged angle of repose of the deposits. Jin (1992) noted that the transverse bed slope is slightly steeper than the longitudinal bed slope, an observation which is supported by Fang & Cao (1996) and Morris & Fan (1998). Fang & Cao (1996) state that the difference between these two slopes will increase in a range of 4-11% if the sediment size and outlet discharge are increased. Jin (1992) mentioned that the transverse slope sometimes does not develop freely due to the effects of adjacent sluice gates or the river banks. Furthermore, he also stated that the longitudinal slope can be especially steep when the water level is high and the flow velocities are low.

Field measurements of the slope angles at several Chinese reservoirs, shown in **Table 2.10**, are much smaller than the angles measured in laboratory studies which are typically around 30 degrees. The field data was, however, influenced by reservoir drawdown and thus presents the actions of progressive erosion, not pure flushing under pressure.

**Table 2.10 Field data of scour cone slope angles in Chinese reservoirs
(Fang & Cao, 1996)**

Reservoir	Annual sediment load ($10^6 m^3$)	Storage capacity ($10^6 m^3$)	Scour cone angle (<i>degrees</i>)	
			Longitudinal	Transverse
Kongzhue	33.7	357	6	-
Bikou	18.9	512	3.4-5.4	8-17
Qington Gorge	139.2	606	4-7	9-14
Fen He	17.8	702	9.5-11	13-17
Yan Gou Gorge	58.5	216	7-9	11-15

2.7.4 Previous Hydraulic Model Studies

Fang & Cao (1996) conducted laboratory experiments on a 1:100 undistorted model of the Zippingpu Reservoir in China to investigate whether the designed flushing outlet could ensure a sediment free zone, thereby preventing coarse sediment from passing through the turbines, in front of the power intake which is located approximately 20 m above the outlet. The results showed that the scour cone formed by the flushing outlet is restricted but would be able to maintain a sediment free condition in front of the power intake. Water samples were collected during testing and indicated that no sediment passed through the power intake. The scour cone slopes were also measured, indicating that the angles were approximately the same as the submerged angle of repose of the sediment (31.5°) for flushing under pressure, but significantly lower (9.5° and 18° for the longitudinal and transverse slopes respectively) when the water was drawn down.

Emamgholizadeh *et al.* (2006) investigated the effect of low-level outlet discharge, water depth and sediment size on the pressure flushing process. A total of 45 laboratory experiments were conducted on a physical model with a circular outlet of 50.8 mm diameter and 0.42 m thick sediment bed. Three non-cohesive sediment sizes (ranges 2-0.595 mm, 0.595-0.25 mm and <0.25 mm), three water depths (0.52, 0.90 and 0.12 m) and five discharges (1, 3, 4.5, 6 and 8 l/s) were used. The experiment time was set to one hour whereafter the scour cone was measured with a point gauge and the scour cone volume calculated. From the results, the authors developed an equation for the scour cone volume which is presented in **Equation 2-40**. The authors concluded that a decrease in water depth for a specific discharge or an increase in low-level outlet discharge at a specific water depth increased the volume of sediments flushed. They also concluded that a decrease in sediment size increased the scour cone volume under the same flow conditions. They suggested that as a general rule for improving sediment flushing, pressure flushing should be carried out when the reservoir is at the minimum operating level and the low-level outlets should operate at their maximum operational capacities.

$$\frac{V_c}{H_w^3} = 0.6139 \cdot \left(\frac{U_o}{\sqrt{(g \cdot H_w)}} \right)^{0.0062} \left(\frac{H_s}{d_s} \right)^{0.05} \left(\frac{H_s}{H_w} \right)^{0.0036} \quad 2-40$$

where:

V_c = scour cone volume (m^3)

H_w = available head above outlet centreline (m)

H_s = sediment level above outlet centreline (m)

Chapter 2: Literature Review

U_o = velocity through the outlet (m/s)

d_{50} = median sediment diameter (m)

Powell (2007) investigated the flow field as well as the sediment scour upstream of an orifice in a physical model study. The effect of sediment size and water depth on the scour cone dimensions were tested by using gravitational flow which means the discharge was a function of the available head. The experimental setup used a 152.4 mm circular orifice as the reservoir low-level outlet and a movable sediment bed levelled with the outlet invert. Three non-cohesive uniform sediment sizes with d_{50} of 0.29 mm , 0.73 mm and 0.89 mm were each tested at water depths of 0.46 m , 0.61 m and 0.76 m above the outlet. Experiments were run until equilibrium was reached, which was defined as less than 2 mm movement in 24 hours. Powell (2007) found that the initial stage of sediment motion was governed by high shear stress, but a complex vortex system below the outlet governed the equilibrium size of the scour cone. Using the scour measurements, he derived the following non-dimensional equations by linear regression for the scour depth, length and width:

$$D_c = \frac{18576 \cdot \left(\frac{H_w}{D}\right) + 33273}{\frac{\rho \cdot U_o}{\mu} \cdot \left(\frac{d_{50}}{H_w}\right)^{0.1}} \quad 2-41$$

$$L_c = \frac{72017 \cdot \left(\frac{H_w}{D}\right) + 45656}{\frac{\rho \cdot U_o}{\mu} \cdot \left(\frac{d_{50}}{H_w}\right)^{0.1}} \quad 2-42$$

$$W_c = \frac{55789 \cdot \left(\frac{H_w}{D}\right) + 144557}{\frac{\rho \cdot U_o}{\mu} \cdot \left(\frac{d_{50}}{H_w}\right)^{0.1}} \quad 2-43$$

where:

D_c = scour cone depth (m)

L_c = scour cone length (m)

W_c = scour cone width (m)

Meshkati *et al.*, (2009) investigated the temporal development of the scour cone formed by pressure flushing through a low-level outlet. This was achieved through laboratory experiments where the pressure flushing tests were stopped at different intervals and the scour cone measured. The physical model had a uniform silica bed with median sediment size of 1 mm

Chapter 2: Literature Review

levelled to 0.4 m above the 25.4 mm circular outlet. Three water depths (0.5, 0.8 and 1.1 m) and three discharges (0.25, 0.5 and 0.75 l/s) were tested. By regression analysis, the authors derived equations for the time development of the scour cone dimensions as functions of the equilibrium dimensions, time to reach equilibrium and Froude number of the outlet.

In a study with a similar laboratory setup, Meshkati Shahmirzadi, Dehghani, Sumi, Naser, *et al.* (2010) studied the effect of the low-level outlet diameter on the scour cone dimensions. Four outlet diameters (25.4, 38.1, 50.8 and 76.2 mm) were tested at three different water depths (0.36, 0.66 and 0.96 m relative to the outlet centre) and five discharges ranging from 0.15 to 15 l/s. Non-cohesive silica particles with median diameter of 1 mm were used for the sediment bed which was packed to 0.16 m above the outlet centre. The tests were run for 45 minutes and after draining the flume the scour cone was measured with a point gauge. The authors found that the outlet area is the main parameter influencing the scour cone volume. Thus, they concluded that increasing the discharge and lowering the water level increased the scour cone dimensions. Through multiple linear regression they developed non-dimensional relationships for the scour width and volume:

$$\frac{V_c}{H_w^3} = 4.6 \cdot \left(\frac{U_o}{\sqrt{(g \cdot (G_s - 1) \cdot d_{50})}} \right)^{0.21} \left(\frac{H_s}{H_w} \right)^{2.2} \left(\frac{D}{H_w} \right)^{0.89} \quad 2-44$$

$$\frac{W_c}{H_w} = 0.02 \cdot \left(\frac{U_o}{\sqrt{(g \cdot (G_s - 1) \cdot d_{50})}} \right)^{0.1} \left(\frac{H_s}{H_w} \right)^{0.75} \left(\frac{D}{H_w} \right)^{0.34} \quad 2-45$$

A further study on the same setup was conducted by Meshkati Shahmirzadi *et al.* (2010) with the same outlets, water depths and discharges, but the sediment level was 0.30 m above the outlet instead of 0.16 m. Similar results were found, but the regression analysis was performed with slightly different terms and included an equation for scour length. However, the equations for scour width and length are the same, which is questionable since no other authors have found these to be exactly the same. The following equations were developed in this particular study:

$$\frac{V_c}{H_w^3} = 0.042 \cdot (Fr)^{0.149} \left(\frac{H_s}{H_w} \right)^{3.082} \left(\frac{A_o}{H_w^2} \right)^{0.174} \quad 2-46$$

$$\frac{L_c}{H_w} = 0.031 \cdot (Fr)^{0.104} \left(\frac{H_s}{H_w} \right)^{0.733} \left(\frac{A_o}{H_w^2} \right)^{0.146} \quad 2-47$$

Chapter 2: Literature Review

$$\frac{W_c}{H_w} = 0.031 \cdot (Fr)^{0.104} \left(\frac{H_s}{H_w}\right)^{0.733} \left(\frac{A_o}{H_w^2}\right)^{0.146} \quad 2-48$$

where:

Fr = Froude number of the outlet (dimensionless)

A_o = outlet cross-sectional area (m^2)

Similar to Emamgholizadeh *et al.* (2006), Fathi-Moghadam, Emamgholizadeh, Bina & Ghomeshi (2010b) investigated the effect of the discharge, water depth and sediment size on the scour cone dimensions. A physical model with a 50.8 mm circular outlet and a 0.42 m thick sediment bed was used for the investigation. Three sediment sizes with d_{50} of 0.27, 0.42 and 1.2 mm were tested at water depths of 0.52, 0.90 and 1.20 m. The five different discharges that were tested were 1, 3, 4.5, 6 and 8 l/s.

The authors found that the pressure effect from the water depth is the significant parameter for initial scour cone formation, but the suction effect of the flow velocity is the most significant parameter in final cone development. This implies that the water depth has a minor effect on the cone equilibrium but has a significant effect on the initial cone formation, confirming that the pulling effect arising from the outflowing water is greater than the pushing effect from the high water level. The sediment size had a great effect on the cone size, with finer grains forming larger cones due to a higher buoyancy effect and a lower angle of repose. Based on their results, the authors proposed dimensionless equations for estimating the volume and length of the cone.

$$\frac{V_c}{D^3} = 5.28 \cdot \left(\frac{U_o}{\sqrt{(g \cdot (G_s - 1) \cdot d_{50})}}\right)^{0.1} \left(\frac{H_s}{H_w}\right)^{-0.046} \quad 2-49$$

$$\frac{L_c}{D} = 8.19 \cdot \left(\frac{U_o}{\sqrt{(g \cdot (G_s - 1) \cdot d_{50})}}\right)^{0.1} \left(\frac{H_s}{H_w}\right)^{-0.033} \quad 2-50$$

As part of a Bachelor's project, Kistner (2013) carried out a physical model study to test the effect of sediment height and outlet discharge on the scouring process. He used a 90 mm circular orifice to conduct nine pressure flushing tests on sediment with a median size of 0.7 mm. Three sediment levels (0, 140 and 280 mm) and three discharge rates (12.6, 25.3 and 38.0 l/s) were tested at a constant water depth of 805 mm. The author formulated equations for the scouring dimensions by regression analysis, but states that their applicability should be tested due to the small number of tests as well as the estimations and extrapolations made in the analysis.

Chapter 2: Literature Review

$$\frac{L_c}{H_w} = -0.297 + 0.073 \cdot \ln\left(\frac{U_o^2}{g \cdot (G_s - 1) \cdot d_{50}}\right) + 1.34 \cdot \ln\left(\frac{H_w}{H_w - H_s}\right) \quad 2-51$$

$$\frac{W_c}{H_w} = -0.72 + 0.149 \cdot \ln\left(\frac{U_o^2}{g \cdot (G_s - 1) \cdot d_{50}}\right) + 2.22 \cdot \ln\left(\frac{H_w}{H_w - H_s}\right) + \frac{173.34}{H_w} \quad 2-52$$

$$\frac{D_c}{H_w} = 0.029 \cdot \left(\frac{U_o^2}{g \cdot (G_s - 1) \cdot d_{50}}\right)^{0.18} \cdot \left(\frac{H_w}{H_w - H_s}\right)^{0.29} \quad 2-53$$

$$\frac{H_c}{H_w} = -0.107 + 0.029 \cdot \ln\left(\frac{U_o^2}{g \cdot (G_s - 1) \cdot d_{50}}\right) + 0.86 \cdot \ln\left(\frac{H_w}{H_w - H_s}\right) \quad 2-54$$

$$V_c = -3.38 \cdot 10^{-9} \cdot M^2 + 1.43 \cdot M - 2.9 \cdot 10^6 \quad 2-55$$

where

$$M = H^3 \cdot \left[0.00039 \cdot \left(\frac{U_o^2}{g \cdot (G_s - 1) \cdot d_{50}}\right)^{0.44} \cdot \left(\frac{H_w}{H_w - H_s}\right)^{6.3} \right]$$

where:

H_c = scour height, distance from top of sediment bed to lowest point (m)

Dodaran *et al.* (2012) experimentally investigated the effect of local vibrations in the sediment layers on the dimensions of the flushing cone. The experiments were done with silica particles with a median diameter of $d_{50} = 1 \text{ mm}$ which were levelled to 400 mm above the centre of the outlet. Two low-level outlets (25.4 and 50.8 mm), three vibrator frequencies (20, 35 and 50 Hz), three vibrator positions and one water depth (800 mm) were tested for 45 minutes at discharges ranging from 0.15-6.11 l/s.

Since a larger low-level outlet and greater vibration frequency led to an increase in the scour hole size, the authors concluded that the low-level outlet cross-sectional area and the vibration frequency are the main parameters responsible for the dimensions of the scour cone. It was also found that the optimal vibrator configuration for pressure flushing requires two vibrators which should be positioned a specific distance from the outlet. Based on the results of the case without vibrators, one should be located a distance equal to the maximum flushing length and the other located at the maximum flushing width from the outlet.

Emamgholizadeh & Fathi-Moghadam (2014) conducted laboratory experiments to investigate the scour cone formation of cohesive sediments under a range of flow parameters. Cohesive sediment samples were taken from the Dez Dam reservoir in Iran and five classes with wet bulk

Chapter 2: Literature Review

densities ranging from 1230 to 1405 kg/m^3 were prepared for the tests. The sediment samples were levelled 0.42 m above the circular outlet with a diameter of 50.8 mm . Each sample was tested at three flow depths (0.52, 0.90 and 1.20 m) and four discharges (1, 3, 6 and 8 l/s).

The authors found that the sediment bulk density, which indicates degree of compaction and grain size, is the most effective parameter in the scour cone's development. Equations for the length and volume of the scour cone were developed by statistical analysis of the results. The equations were verified with field measurements taken at flushing events of the Dez Reservoir and predicted the cone volume and length with tolerable accuracy (<27%).

$$\frac{V_c}{D^3} = 0.99 \cdot \left(\frac{H_s}{H_w}\right)^{0.59} \cdot \left(\frac{\rho_{wb} - \rho}{\rho_s}\right)^{-2.85} \quad 2-56$$

$$\frac{L_c}{D} = 0.33 \cdot \left(\frac{H_s}{H_w}\right)^{0.40} \cdot \left(\frac{\rho_{wb} - \rho}{\rho_s}\right)^{-1.44} \quad 2-57$$

Madadi, Rahimpour & Qaderi (2016) experimentally tested a structure made of a semi-circular group of vertical piles with a horizontal confining plate upstream of the low-level outlet. The aim of their study was to investigate the pile structure's effect on sediment flushing efficiency due to the increased orifice flow power and vortices arising from the constricted spacing between the piles. The effect of the pile diameter, pile spacing and distance from the outlet were investigated at a constant water depth and two discharges (10 and 14.5 l/s). Non-cohesive sediment with $d_{50} = 0.36$ mm was levelled with the invert of the 95 mm circular orifice and the tests were run for 6 hours. The scour cone was measured after each test and compared to the reference tests without the pile structure. The authors found that the constrictions caused by the piles, established a flow with higher velocity, turbulence and shear forces which removed bed material in greater quantities and at a faster rate compared to the reference tests. Furthermore, they found that the sediment removal efficiency was best when the pile diameter and pile spacing was equal. The authors also observed an increase in the amount of sediment scoured as the distance of the piles from the orifice increased. They concluded that the semi-confined pile structure increased the volume of sediments flushed by up to 250% compared to the reference test.

A further study by the same authors (Madadi *et al.*, 2017) was carried out to test the effect of a proposed new configuration, called the "projecting semi-circular structure" (PSC structure), on pressurized flushing efficiency. The PSC structure is connected to the dam body at the low-level outlet and is fixed to columns which rest on piles driven into the reservoir bed. According

Chapter 2: Literature Review

to Madadi *et al.* (2017) the PSC structure changes the vertical vortices described by Powell (2007) into horizontal vortices, increasing their strength and extent, leading to an increase in sediment removal. Furthermore, the arch shape of the PSC structure transfers the stresses induced by the hydrostatic force to the columns and also prevents the build-up of suspended sediment.

The same sediment and experimental setup was used as Madadi *et al.* (2016), but the water depth was 0.6 m and discharge rates 10, 12.5 and 14 l/s. Four different lengths (0.15, 0.25, 0.4 and 0.5 m) and four diameters (0.11, 0.125, 0.15 and 0.16 m) of the PSC structure were tested to investigate the effect of these parameters on the flushing cone. The authors observed the maximum scour cone dimensions with the PSC structure to orifice ratios of $L_{sc}/D_o = 5.26$ and $D_{sc}/D_o = 1.32$. In addition, they found that this configuration was able to increase the scour cone volume by up to 4.5 times that of the reference test without the structure. From their results, they obtained a dimensionless equation for estimating the scour cone volume with the PSC structure.

$$\frac{V_c}{D^3} = 0.31 \cdot \left(\frac{Q_o}{\sqrt{g \cdot D^5}} \right)^{0.53} \cdot \left(\frac{D_{sc}}{D} \right)^{0.58} \cdot \left(\frac{L_{sc}}{D} \right)^{0.91} \quad 2-58$$

where:

D_{sc} = diameter of PSC structure (m)

L_{sc} = length of PSC structure (m)

Hajikandi, Vosoughi & Jamali (2017) experimentally investigated the effect of the orifice shape on sediment scouring and the velocity profile near the orifice. The sediment scour upstream of a square (62 x 62 mm) and a circular (70 mm) orifice was compared for fixed and mobile bed tests. Both orifices were classified as “small” orifices and had equal opening areas of 3845 mm². Four water depths (0.45, 0.60, 0.75 and 0.90 m) and two sediment types (d_{50} of 0.28 mm and 0.87 mm) were used for both fixed and mobile bed tests which were all run for 2.5 days to ensure equilibrium of the cone. The fixed-bed tests indicated that the scour zone upstream of the square orifice is on average 1.46 times greater than that of the circular orifice for the same water depths. From the mobile-bed tests the authors showed that the scour depth, width and length were greater for the square orifice, with the scour width being the most sensitive to the orifice shape.

In addition, they described three phases of vortex formation during the scouring process and observed that the vortices upstream of square orifices are more random in shape and location.

Chapter 2: Literature Review

Furthermore, the authors observed an increase in scour cone geometry with a decrease in sediment size, confirming the findings of other researchers (Emamgholizadeh *et al.*, 2006; Emamgholizadeh & Fathi-Moghadam, 2014; Fathi-Moghadam *et al.*, 2010b; Powell, 2007). It was also found that an increase in water depth led to a greater scour cone, due to the higher outflowing discharge, but different discharges were not tested at the same water depths, because the laboratory setup was purely gravitational, and no pump was attached to the orifice.

Similarly, Mohammad, Daham & Bilal (2017) conducted a laboratory study to investigate the effect of the internal offset of the low-level outlet on the scour cone geometry. Two non-cohesive sediments with median diameter of 1.44 mm and 0.84 mm were tested at three different sediment heights of 74.6, 204.6 and 274.6 mm. Two internal offset lengths (20 and 80 mm) were tested at six different water depths (325.4, 425.4, 525.4, 575.4, 625.4, 675.4 mm).

The authors observed that the increase in internal outlet offset from 20 to 80 mm was associated with an 80% increase in scour cone volume. Furthermore, they found that the maximum scour cone volume was achieved when the water depth to sediment height ratio (H_w/H_s) was between 2.06 and 2.26. Similar to other studies, they also found that a greater amount of sediment was scoured when the sediment height increased, or the sediment size decreased. From the results four dimensionless equations, with different variables, for the scour cone volume were developed. Analysis of the developed equations showed that the uniformity coefficient of the sediment, $C_u = d_{60}/d_{10}$, can be used to estimate scour volume instead of d_{50} . Mohammad *et al.* (2017) stated that the effective flushing time in the models was less than 70 seconds and concluded that the outflow discharge should be set to an optimum value to maximize pressure flushing.

In a 1:55 scale hydraulic model study of the Chamera II Hydroelectric Project Stage II run-of-river project, Kamble, Kunjeer, B & Isaac (2017) investigated the effect of water depth, discharge and sediment height on the dimensions of the pressure flushing cone. Three sediment levels, two discharges and several water depths were tested with fine river sand ($d_{50} = 0.25$ mm) as the bed material. They found that the ratio of water depth to sediment height is an important parameter influencing the scour cone dimensions. In terms of the effect of discharge and water depth, the results from their study were in agreement with the findings of Emamgholizadeh *et al.* (2006). In terms of the effect of the outlet area their results confirmed the findings of Meshkati Shahmirzadi *et al.* (2010). Non-linear multiple regression analysis of the results yielded equations for the length and depth of the scour cone as follows:

$$\frac{L_c}{H_w} = e^{1.0675} \cdot \left(\frac{H_s}{H_w}\right)^{0.5089} \cdot \left(\frac{A_o}{H_w^2}\right)^{0.31162} (Fr)^{-0.4411} \quad 2-59$$

$$\frac{D_c}{H_w} = e^{-0.0706} \cdot \left(\frac{H_s}{H_w}\right)^{0.9859} \cdot \left(\frac{A_o}{H_w^2}\right)^{0.2309} (Fr)^{0.5719} \quad 2-60$$

2.8 Laws of Hydraulic Similarity for Physical Models

A physical hydraulic model is usually a scaled representation of a prototype (full scale structure) that commonly assists designers with optimising the structure during the design phase. To get accurate results the boundary conditions, flow field and upstream flow conditions must be scaled in the correct manner. A physical scale model involves no scale effects and is completely similar to its prototype if it satisfies the following three mechanical similarity criteria (Heller, 2011):

- geometric similarity;
- kinematic similarity; and
- dynamic similarity.

Geometric similarity refers to similarity in shape, i.e. all model length dimensions are λ times shorter than the prototype as shown in **Equation 2-61**. Model areas and volumes therefore scale with λ^2 and λ^3 respectively.

$$\lambda = \frac{L_p}{L_m} \quad 2-61$$

where:

λ = scale between prototype and model

L = characteristic linear dimension

p = prototype

m = model

Kinematic similarity refers to the similarity of motion, thus requiring constant ratios of time, velocity, acceleration and discharge between homologous points in the model and prototype. Since boundaries affect the model flow patterns, geometric similarity is a prerequisite for kinematic similarity.

Chapter 2: Literature Review

Dynamic similarity refers to the similarity of forces, which requires that forces at specific points in the model and prototype have the same ratio and act in the same direction. Since the flow patterns are governed by forces, both geometric and kinematic similarity must be achieved before dynamic similarity can be obtained.

2.8.1 Similarity Laws

Hydraulic similarity between the model and the prototype can be achieved by a number of similarity laws. The phenomenon of fluid compressibility is excluded from the discussion of similarity laws due to its insignificant effect (Heller, 2011).

2.8.1.1 Froude Law

The Froude law represents dynamic similarity conditions for flow in the model and the prototype that is governed by gravity exclusively. This law states that inertial and gravitational forces acting on the fluid are the same in the model and the prototype wherever a free surface gradient exists. According to Webber (1971) the Froude law is defined by:

$$Fr = \frac{V}{\sqrt{gL}} \quad 2-62$$

where:

V = velocity (m/s)

L = characteristic linear dimension

To comply with **Equation 2-62**, the corresponding model and prototype velocities must be related as indicated by **Equation 2-63**.

$$\frac{V_p}{V_m} = \frac{(gL_p)^{\frac{1}{2}}}{(gL_m)^{\frac{1}{2}}} = \lambda^{\frac{1}{2}} \quad 2-63$$

Table 2.11 defines the scalar relationships for physical modelling with the Froude Law.

Table 2.11 Scalar relationships for Froude Law similarity (adapted from Webber, 1971)

Quantity	Dimensions	Natural scale (1: λ)
Geometric		
Length	l	λ
Area	l^2	λ^2
Volume	l^3	λ^3
Kinematic		
Time	T	$\lambda^{1/2}$
Velocity	l/T	$\lambda^{1/2}$
Acceleration	l/T^2	1
Discharge	l^3/T	$\lambda^{5/2}$
Dynamic		
Pressure	M/IT^2	$\rho_r \lambda$
Force	MI/T^2	$\rho_r \lambda^3$
Energy	MI^2/T^2	$\rho_r \lambda^4$
Power	MI^2/T^3	$\rho_r \lambda^{7/2}$

*where $\rho_r = \rho_p/\rho_m$, M is mass and T is time

2.8.1.2 Reynolds Law

The Reynolds Law expresses dynamic similarity of the motion of two incompressible viscous fluids under the exclusive effect of internal friction (Novák & Cabelka, 1981). This law should be considered in models where viscous inertia and shear drag forces are present such as flow around spheres (Heller, 2011). Another example is found in fully enclosed systems that operate in the transition zone, where the pressure losses are basically related to the Reynolds number, Re , defined by **Equation 2-64**.

$$Re = \frac{VL}{\nu} \quad 2-64$$

where:

$$Re = \text{Reynolds number}$$

Compliance with **Equation 2-64** in terms of velocities is demonstrated by (Webber, 1971):

$$\frac{V_p}{V_m} = \frac{v_p L_m}{v_m L_p} = \frac{v_p}{v_m} \frac{1}{\lambda} \quad 2-65$$

2.8.1.3 Weber Law

The Weber law represents the condition of dynamic similarity for the prevailing effect of capillary forces that cause surface tension. Physical model studies that are influenced

Chapter 2: Literature Review

significantly by surface tension such as spray, air entrainment or low weir heads should consider the use of the Weber Law for similarity. This law is governed by:

$$We = \frac{V}{\sqrt{\frac{\sigma_t}{L\rho}}} \quad 2-66$$

where:

We = Weber number

σ_t = surface tension (N/m)

Equation 2-67 expresses equality of the Weber number for model and prototype velocities. This relation shows that if the model and prototype fluid are the same, model velocities must be scaled to $\lambda^{1/2}$ times the prototype velocities for compliance with the Weber Law (Novák & Cabelka, 1981).

$$\frac{V_p}{V_m} = \frac{\sigma_p^{1/2} \rho_m^{1/2} L_m^{1/2}}{\sigma_m^{1/2} \rho_p^{1/2} L_p^{1/2}} = \frac{\sigma_p^{1/2} \rho_m^{1/2}}{\sigma_m^{1/2} \rho_p^{1/2}} \frac{1}{\lambda^{1/2}} \quad 2-67$$

2.8.1.4 Euler Law

The Euler law can be applied for enclosed systems where the viscous forces are insignificant compared to the inertial forces, and gravity forces and surface tension are absent. Fluid flow problems do not usually comply with these requirements and the Euler law is thus mostly used for scale models using air rather than water (Chanson, 1999).

The Euler law is governed by the Euler number, defined in **Equation 2-68**. For compliance of the Euler law, the model velocities are related to the prototype velocities by the scalar relationship described by **Equation 2-69**.

$$E = \frac{V}{\sqrt{\frac{2\Delta p}{\rho}}} \quad 2-68$$

$$\frac{V_p}{V_m} = \frac{\rho_p g h_{pi_p} \rho_m^{1/2}}{\rho_m g h_{pi_m} \rho_p^{1/2}} = \lambda^{1/2} \quad 2-69$$

where:

E = Euler number

Δp = change in pressure (kN/m^2)

h_{pi} = piezometric head (m)

2.8.2 Scaling of Sediment

Scaling of movable-bed hydraulic models is a complex process that often yields unsatisfactory results. The primary difficulty is accurately scaling both the fluid motion and the sediment movement simultaneously. Sediment transport in movable bed models can be described by various relationships, with the best known and most widely used being the Shields relationship (Cao, Pender & Meng, 2006). The Shields relationship is based on a unique dimensionless shear value at which the incipient motion state exists for a specific Reynolds number. Incipient motion is the threshold condition for either mobilisation or deposition (Gill & Pugh, 2009). For a specific set of sediment and fluid parameters, the critical bed shear stress required for the Shields relationship can only be found by trial and error or iteration, making its application in hydraulic engineering rather difficult (Cao *et al.*, 2006).

It has been argued that the particle size is not a representative or unique measure of sediment transportability. Rooseboom, Basson, Loots, Wiggett & Bosman (1983) recommends using the settling velocity of particles as representative of sediment transportability. This so-called stream power approach led to the development of the Modified Liu Diagram, shown in **Figure 2.26**, which expresses the boundary between sediment movement and no movement.

Sediment movement in this approach is explained in terms of a plot of the shear Reynolds number against the ratio of shear velocity and settling velocity (referred to as the Movability number). The ratio between shear velocity and settling velocity is constant for turbulent boundary conditions as shown in **Equation 2-70**. For laminar boundary conditions the critical condition is given by **Equation 2-71**.

For turbulent flow:

$$\frac{V_{*c}}{V_{SS}} = 0.12 \quad 2-70$$

For laminar flow:

$$\frac{V_{*c}}{V_{SS}} = \frac{0.16}{\frac{V_* d_{50}}{\nu}} \quad 2-71$$

where:

$$V_* = \sqrt{gD\bar{S}}$$

2-72

V_{*C} = critical shear velocity (m/s)

V_{SS} = sediment settling velocity (m/s)

Sediment scaling can be done using **Figure 2.26**, by plotting model and prototype values and ensuring they align at the same position on the vertical axis, thus having the same ratio of shear velocity to settling velocity.

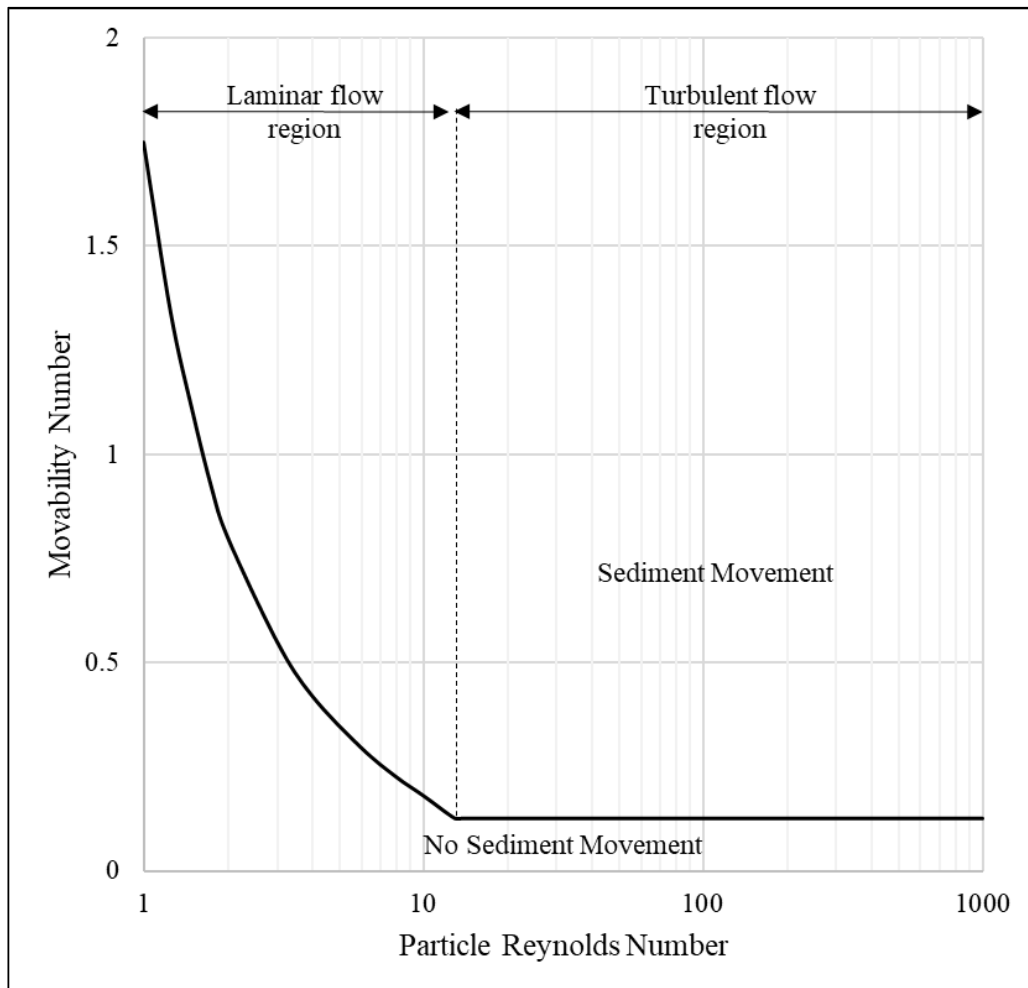


Figure 2.26 Modified Liu Diagram (adapted from SANRAL, 2013)

3 EXPERIMENTAL SETUP

3.1 Objectives

Physical hydraulic models are essential for hydraulic engineering research due to the large number of variables and complicated boundary conditions involved (Pugh, 2008). Numerical modelling of sediment transport, deposition and erosion is especially difficult and even with great advances in technology and years of research in the field, physical modelling is still the preferred method for accurate prediction of these processes. With the major cost and effort involved in remedial measures to counter sedimentation problems, engineers are encouraged to take great care when using mathematical models for dam design (Basson & Rooseboom, 2007). Thus, the difficulty of modelling the scouring process at a low-level outlet under several different conditions meant that a physical model was required.

For this study, a physical model of a reservoir with a low-level outlet was designed, constructed and tested in a controlled laboratory environment. The physical model is not based on any specific existing reservoirs, but rather a representation of the general problem of deposited sediment near any dam wall. The physical model was thus not designed to a specific scale, but as large as possible so that results could be scaled up to different prototype scenarios. Reservoir conditions were simulated by pressure flushing sediment through different low-level outlets in a large flume filled with water and a sediment bed. The physical model was designed and tested to provide insight on the scour cone formation associated with different low-level outlet shapes, sediment levels and water depths.

The main objective of the experiments was to determine the optimal low-level outlet shape for pressure flushing of hydropower reservoirs, such as to minimise sediment build up in front of the intakes. The scour cone dimensions were the most important parameters for determining the optimal low-level outlet shape, since the dimensions indicated the size of the area that could be cleared as well as the flushing efficiency.

3.2 Dimensional Analysis

Dimensional analysis is a commonly used method in the field of physical sciences to reduce the complexity of the fundamental equations that describe the behaviour of a system. According to Albrecht, Nachtsheim, Albrecht & Cook (2013) there are two major advantages of using dimensional analysis, namely:

Chapter 3: Experimental Setup

1. It allows the experiment designer to reduce the number of independent variables in a standard experiment, leading to time and cost savings in the experimental phase.
2. It allows the scaling of results, because each factor in the dimensional analysis is dimensionless.

It was therefore advantageous to use dimensional analysis in this study to simplify the experiments by reducing the number of independent variables as well as to allow for scalability, which was crucial. The dimensional analysis was conducted to eliminate variables which have the smallest influence on the scour cone geometry and then designing the experiment. The dimensional analysis also aided in the development of equations that represent the different geometrical parameters of the scour cone.

Albrecht *et al.* (2013) distinguish four steps in the dimensional analysis process, namely:

1. Identifying the independent and dependent variables
2. Identifying a complete dimensionally independent subset
3. Identifying the dimensionless forms of the variables not in the subset
4. Applying Buckingham's π theorem to obtain a dimensional analysis model

In order to consider the effect of the outlet shape on the scour cone geometry, several shape related parameters were identified for the dimensional analysis. All the geometrical parameters (length, width, height, depth and volume) can be represented by the same variables and volume is simply used as an example.

Step 1

The set of n variables appropriate for determining the volume of the cone can be represented in functional form as:

$$f(V_c, U_o, A_o, H_w, H_s, d_{50}, g, \rho, \rho_s, \mu, b_{oc}, h_{oc}, b_{oe}, h_{oe}, P_o, R_o) = 0 \quad 3-1$$

where:

- V_c = scour cone volume (m^3)
- U_o = velocity through the outlet (m/s)
- A_o = outlet area (m^2)
- H_w = available head above outlet invert (m)
- H_s = height of sediment above outlet invert (m)
- d_{50} = median diameter of sediment (mm)
- g = gravitational acceleration constant ($9.81 m/s^2$)

Chapter 3: Experimental Setup

- ρ = density of water (kg/m^3)
 ρ_s = density of sediment (kg/m^3)
 μ = fluid dynamic viscosity ($kg/(m.s)$)
 b_{oc} = outlet width over centreline (m)
 h_{oc} = outlet height over centreline (m)
 b_{oe} = outlet width at the edge (m)
 h_{oe} = outlet height at the edge (m)
 P_o = outlet perimeter (m)
 R_o = hydraulic radius of the outlet (m)

where f denotes “function of”. The volume of the scour cone can be therefore be represented as a function of the following variables:

$$V_c = f(A_o, U_o, H_w, H_s, d_{50}, g, \rho_w, \rho_s, \mu, b_{oc}, h_{oc}, b_{oe}, h_{oe}, P_o, R_o) \quad 3-2$$

Step 2

In the above set with $n = 16$, there are $k = 3$ base dimensions involved, namely mass (m), length (L) and time (T). Step 2 requires that a complete dimensionally independent subset with k variables should be identified. A subset is ‘complete’ if the dimensions of any of the variables can be written as products of powers of the dimensions contained in the subset variables. The subset is ‘dimensionally independent’ if none of the dimensions of the basis variables can be written as a product of powers of the other (Albrecht *et al.*, 2013). The subset, also called the basis set, of repeating variables was identified as:

$$\{U_o, H_w, \rho_w\} \quad 3-3$$

One can see that $[U_o] = LT^{-1}$, $[H_w] = L$ and $[\rho_w] = ML^{-3}$ are a complete, independent subset of independent variables.

Step 3

The variables not contained in the basis set are thus:

$$\{A_o, H_s, d_{50}, g, \rho_s, \mu, b_{oc}, h_{oc}, b_{oe}, h_{oe}, P_o, R_o\} \quad 3-4$$

By using the Buckingham π theorem, the variables not in the basis set can be written in dimensionless forms as follows:

$$\pi_1 = \frac{A_o}{H_w^2}; \quad \pi_2 = \frac{H_s}{H_w}; \quad \pi_3 = \frac{d_{50}}{H_w}; \quad \pi_4 = \frac{gH_w}{U_o^2} \rightarrow \frac{U_o}{\sqrt{gH_w}} = Fr_o; \quad \pi_5 = \frac{\rho_s}{\rho_w};$$

Chapter 3: Experimental Setup

$$\pi_6 = \frac{\mu}{\rho_w U_o H_w}; \quad \pi_7 = \frac{b_{oc}}{H_w}; \quad \pi_8 = \frac{h_{oc}}{H_w}; \quad \pi_9 = \frac{b_{oe}}{H_w}; \quad \pi_{10} = \frac{h_{oe}}{H_w}; \quad \pi_{11} = \frac{P_o}{H_w};$$

$$\pi_{12} = \frac{R_o}{H_w};$$

The functional relationship describing the dimensionless flushing cone volume is then:

$$\frac{V_c}{H_w^3} = f \left(\frac{A_o}{H_w^2}, \frac{H_s}{H_w}, \frac{d_{50}}{H_w}, \frac{U_o}{\sqrt{gH_w}}, \frac{\rho_s}{\rho_w}, \frac{\mu}{\rho_w U_o H_w}, \frac{b_{oc}}{H_w}, \frac{h_{oc}}{H_w}, \frac{b_{oe}}{H_w}, \frac{h_{oe}}{H_w}, \frac{P_o}{H_w}, \frac{R_o}{H_w} \right) \quad 3-5$$

Step 4 is only applicable where terms cannot be expressed in dimensionless form. It is thus not applicable in this dimensional analysis.

3.3 Experiment Design

In order to consider the shape of the outlet on the scour cone geometry, different outlet shapes had to be tested for different scenarios. These scenarios had to be determined by analysis of the functional relationship shown in **Equation 3-5**. To simplify this relationship, certain parameters had to be kept constant for the tests and others had to be varied to determine their influence on the results.

Varying the outlet shape influences terms 7 to 12 of **Equation 3-5**, since they are all related to the outlet geometry. Term 4 as indicated was derived as the Froude number of the outlet, which is an important dimensionless parameter influencing the scour cone. The influence of term 4 can therefore be assessed by varying the water depth which also influences the outlet velocity. Assessing the influence of term 2 would require the sediment height to be varied.

The influence of sediment size on the scour cone geometry was studied by other authors and clear conclusions about its effect on the scour cone geometry are described in **Section 2.7.4** (Emamgholizadeh *et al.*, 2006; Emamgholizadeh & Fathi-Moghadam, 2014; Fathi-Moghadam *et al.*, 2010b; Hajikandi *et al.*, 2017; Mohammad *et al.*, 2017; Powell, 2007). Therefore, only one sediment size was tested to reduce the number of experiments required, eliminating term 3 and 5 from the analysis. For further simplification, the Reynolds-type term 6 was discarded from the analysis, because the water quality was constant for all tests (thus ρ_w and μ constant) and the effect of the other variables (H_w , U_o) contained in the term are represented in other terms of the analysis.

Four different outlet shapes were designed to all have the same outlet area ($A = 0.05 \text{ m}^2$), thus removing term 1 from the set of variables. Three water depths (1.75, 1.125 and 0.5 m) and three

Chapter 3: Experimental Setup

sediment levels were tested (0, 0.1 and 0.2 *m*). The flow rate corresponding to each water depth was measured by a flow meter as described in **Section 3.6.2**. The simplifications yielded:

$$\frac{V_c}{H_w^3} = f \left(\frac{H_s}{H_w}, \frac{U_o}{\sqrt{gH_w}}, \frac{b_{oc}}{H_w}, \frac{h_{oc}}{H_w}, \frac{b_{oe}}{H_w}, \frac{h_{oe}}{H_w}, \frac{P_o}{H_w}, \frac{R_o}{H_w} \right) \quad 3-6$$

The mean approach velocity upstream of the plate over the sediment bed ranged from 0.005 *m/s* (for the highest water level with lowest sediment bed level) to 0.023 *m/s* (for the lowest water level with highest sediment bed level), which can be considered to have had negligible influence on the scour cone. Varying the outlet shape, water depth and sediment level as described meant a total of 36 tests were required, as summarised in **Table 3.1**.

Table 3.1 Range of tests conducted

Test no	Test ID	Q (m ³ /s)	H _w (m)	H _s (m)	Test no	Test ID	Q (m ³ /s)	H _w (m)	H _s (m)
1	RoHs1Hw1	0.0174	1.75	0	19	FrHs2Hw1	0.0175	1.75	0.1
2	RoHs1Hw2	0.01395	1.125	0	20	FrHs2Hw2	0.01406	1.125	0.1
3	RoHs1Hw3	0.0089	0.5	0	21	FrHs2Hw3	0.00904	0.5	0.1
4	SqHs1Hw1	0.0175	1.75	0	22	UrHs2Hw1	0.01725	1.75	0.1
5	SqHs1Hw2	0.0141	1.125	0	23	UrHs2Hw2	0.0139	1.125	0.1
6	SqHs1Hw3	0.00901	0.5	0	24	UrHs2Hw3	0.008865	0.5	0.1
7	FrHs1Hw1	0.01705	1.75	0	25	SqHs3Hw1	0.01755	1.75	0.2
8	FrHs1Hw2	0.01305	1.125	0	26	SqHs3Hw2	0.01418	1.125	0.2
9	FrHs1Hw3	0.00835	0.5	0	27	SqHs3Hw3	0.00905	0.5	0.2
10	UrHs1Hw1	0.01725	1.75	0	28	FrHs3Hw1	0.0175	1.75	0.2
11	UrHs1Hw2	0.0139	1.125	0	29	FrHs3Hw2	0.01415	1.125	0.2
12	UrHs1Hw3	0.008865	0.5	0	30	FrHs3Hw3	0.00907	0.5	0.2
13	RoHs2Hw1	0.0174	1.75	0.1	31	UrHs3Hw1	0.0172	1.75	0.2
14	RoHs2Hw2	0.01395	1.125	0.1	32	UrHs3Hw2	0.01385	1.125	0.2
15	RoHs2Hw3	0.0089	0.5	0.1	33	UrHs3Hw3	0.00886	0.5	0.2
16	SqHs2Hw1	0.01755	1.75	0.1	34	RoHs3Hw1	0.01725	1.75	0.2
17	SqHs2Hw2	0.01412	1.125	0.1	35	RoHs3Hw2	0.0139	1.125	0.2
18	SqHs2Hw3	0.00896	0.5	0.1	36	RoHs3Hw3	0.0089	0.5	0.2
Key:									
Sq	=	Square orifice			Q	=	Flow rate (m ³ /s)		
Fr	=	Flat rectangular orifice			H _s	=	Sediment height above invert (m)		
Ro	=	Round orifice			H _w	=	Water depth above invert (m)		
Ur	=	Upright rectangular orifice							

3.4 Physical Model Design

The experimental investigation was conducted in the Hydraulic Laboratory of the Civil Engineering Department of Stellenbosch University. The physical model consisted of three main parts, namely the inflow control system, main reservoir and downstream control system. All three parts were constructed in a large rectangular concrete flume of 60 m long, 2 m wide and 2 m high. A schematic drawing of the experimental layout is shown in **Figure 3.1**.

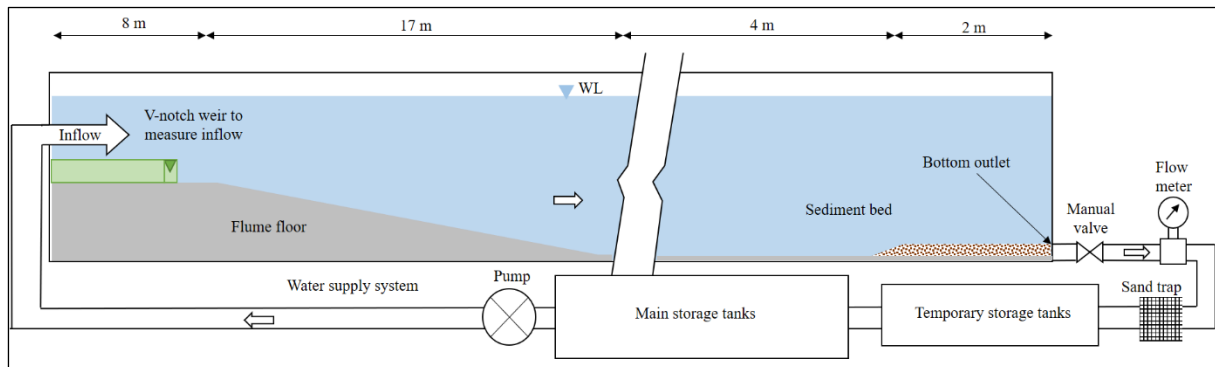


Figure 3.1 Schematic drawing of the experimental setup

A 5 mm thick steel plate that had 50 mm bent edges for extra torsional resistance was mounted in the flume to simulate the dam. The plate was supported at the downstream end by 10 mm thick steel L-angles mounted into the flume sidewalls and floor with 12 mm thick chemical anchors. The connections between the supporting angle irons, plate and flume were sealed using close-cell silicone strips combined with silicone adhesive sealant. Three 10 mm thick steel L-angles were used as reinforcing lateral braces to ensure the strength of the installation and thereby the safety of the operators. The steel plate installation is shown in **Figure 3.2**.

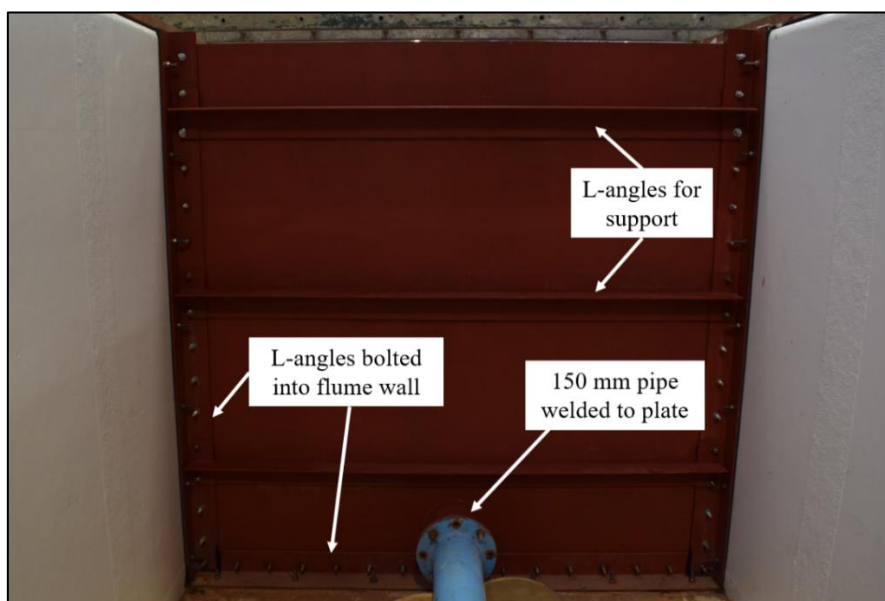


Figure 3.2 View from downstream of steel plate installation with supports

Chapter 3: Experimental Setup

A 180 mm diameter hole was made 110 mm above the bottom of the plate. At the downstream end of the hole, a short 150 mm diameter pipe with flange was welded to the plate. Four 5 mm thick steel discs with a diameter of 175 mm and different shaped outlets were cut out of plate as shown in **Figure 3.3**.

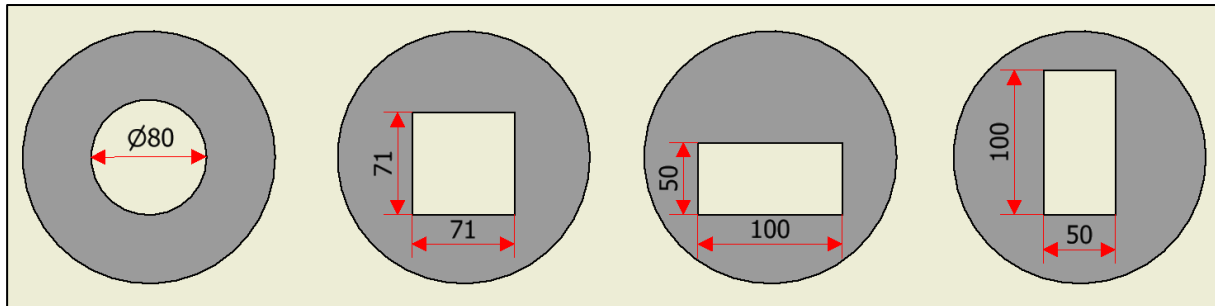


Figure 3.3 Steel discs with different shaped outlets

Determining the size of the outlets was based on the recommendations by Novák & Cabelka (1981). They state that gravity is the decisive force for flow through orifices and that the Froude law should be the criterion of similarity. However, to prevent the roughness of the upstream face from influencing the flow, certain minimum limits are suggested for the orifice. Novák & Cabelka (1981) state that for diameters less than 70 mm, viscosity and surface tension influence the discharge coefficient, but for diameters greater than 70 mm it is constant. The circular orifice was thus used as the benchmark and was selected to be 80 mm in diameter. This leads to an outlet area of $A_o = 0.005 \text{ m}^2$, which was used to size the other three outlets. For the rectangular outlets it was decided to create one with the width twice the height (100 x 50 mm) and the other with the height twice the width (50 x 100 mm). The square outlet's sides were 71 mm in length.

The outlets acted as small sharp-edged orifices since the water depth to orifice depth ratio was more than 5 as mentioned in **Section 2.7.1**. The invert level of all four outlets was set to 0.158 m above the flume floor to allow deep scour below without bottom influence. Setting the invert level for all four outlets the same also allowed for comparison of scouring results. Although the outlets are not hydraulically identical due to the different positions of their centrelines and edges, the discharge was measured for results comparison. One disc at a time was inserted into the hole in the plate from the upstream end and pressed against the flange of the pipe at the downstream end. The disc was sealed around the edges using silicone sealant and could be removed and replaced once the tests for that shape were completed.

At the downstream end, a 1 m long pipe with a diameter of 150 mm was connected to the pipe welded on the plate. This pipe was followed by a butterfly valve and a 150 to 110 mm reducer, as shown in **Figure 3.4**. A 1.5 m long pipe with a SAFMAG electromagnetic flow meter was

Chapter 3: Experimental Setup

installed behind the reducer. Downstream of the flow meter another 2.5 m long pipe with a diameter of 110 mm was connected to ensure full pipe flow and accurate flow meter readings. The connections on the downstream side are shown in **Figure 3.4**. To collect the scoured-out sediment, a sediment trap was constructed from a geotextile fabric connected to a steel frame and placed over the temporary storage tanks, as shown in **Figure B.5**.

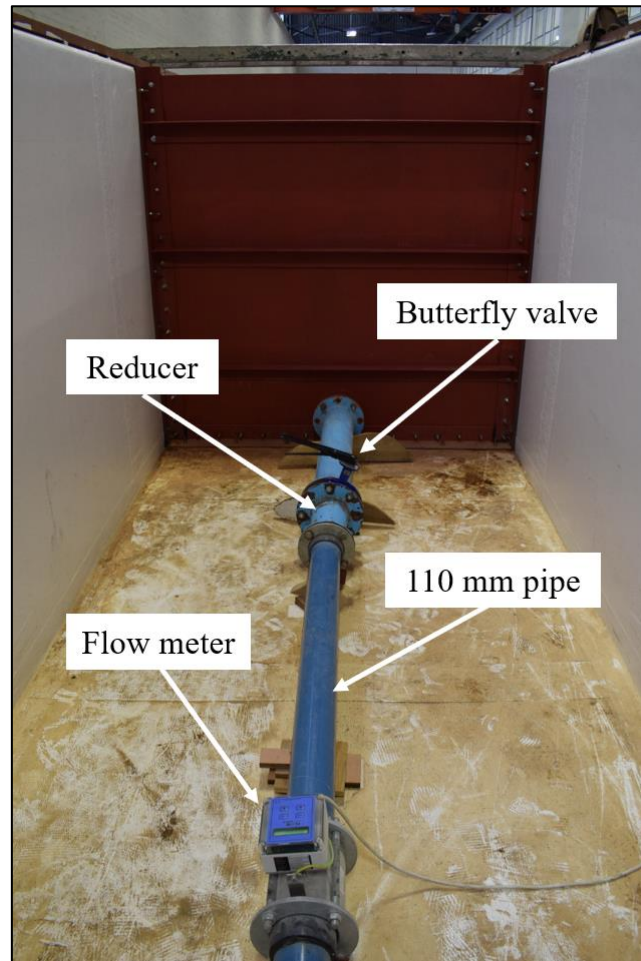


Figure 3.4 Connections at the downstream end of the plate

At the upstream end of the plate, the bolt nuts were welded onto the plate to form a seal and prevent any leakages. A 2 m long sediment bed was levelled to the required height in front of the outlet, as shown in **Figure 3.5**, and large concrete blocks were placed 6 m from the plate to act as flow straighteners as shown in **Figure B.1**. A 20 mm PVC pipe with numerous holes in it and covered with geotextile fabric was installed through the right side of the plate. This pipe extended 3 m upstream of the plate and on the downstream end of the plate a small gate valve was installed to allow for draining of the flume.

On the inflow end, a 110 mm pipe supplied water from the main laboratory supply, controlled by a gate valve. This pipe was placed inside a 6 m long basin with flow straighteners and a

Chapter 3: Experimental Setup

polystyrene float to smooth the inflow, as shown in Figure 3.9. A V-notch weir at the downstream end of this basin was used to measure the inflow, so that the water depth in the main reservoir could be kept constant. More photos of the experimental setup are shown in **Appendix B**.

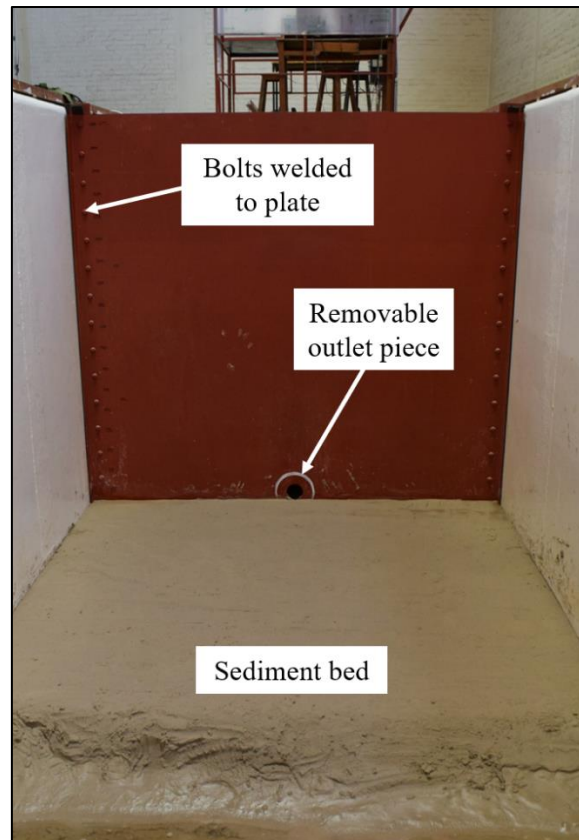


Figure 3.5 Sediment bed and plate viewed from upstream

3.5 Sediment

A movable sediment bed was packed and levelled at different heights for the experimental investigation. The sand used was No. 2 Foundry sand consisting of 99.45% silica. The sand had a dry bulk density of 1461 kg/m^3 as indicated by the specification sheet (shown in **Appendix C**) provided by the supplier. Sediment armouring was one of the concerns in this study as it could cause variations in scour hole development. However, rather than using a well- or gap-graded sediment, a uniform sediment was used, ensuring that hiding and exposure effects did not modify the sediment's critical shear stress. The grain size distribution curve is shown in **Figure 3.6** based on a sieve analysis. The sediment used in the experiments was non-cohesive fine sand with a median diameter of $d_{50} = 0.095 \text{ mm}$.

Sediment size distributions often only approximate a normal distribution and could be skewed, instead of being centred on the median size. To determine whether this was the case, the

Chapter 3: Experimental Setup

gradation coefficient (Gr) and standard deviation (σ) were calculated using **Equation 2-1** and **Equation 2-2** respectively. A value of 1.415 was found for Gr , indicating a highly uniform size distribution. The standard deviation for the sediment was calculated to be $\sigma = 1.414$. To better represent the size of the sediment it is also recommended to calculate the effective diameter. This was calculated by dividing the grain size distribution into 5 bands (of 20% each) and identifying the median sediment size for each band, as shown in **Figure 3.6**.

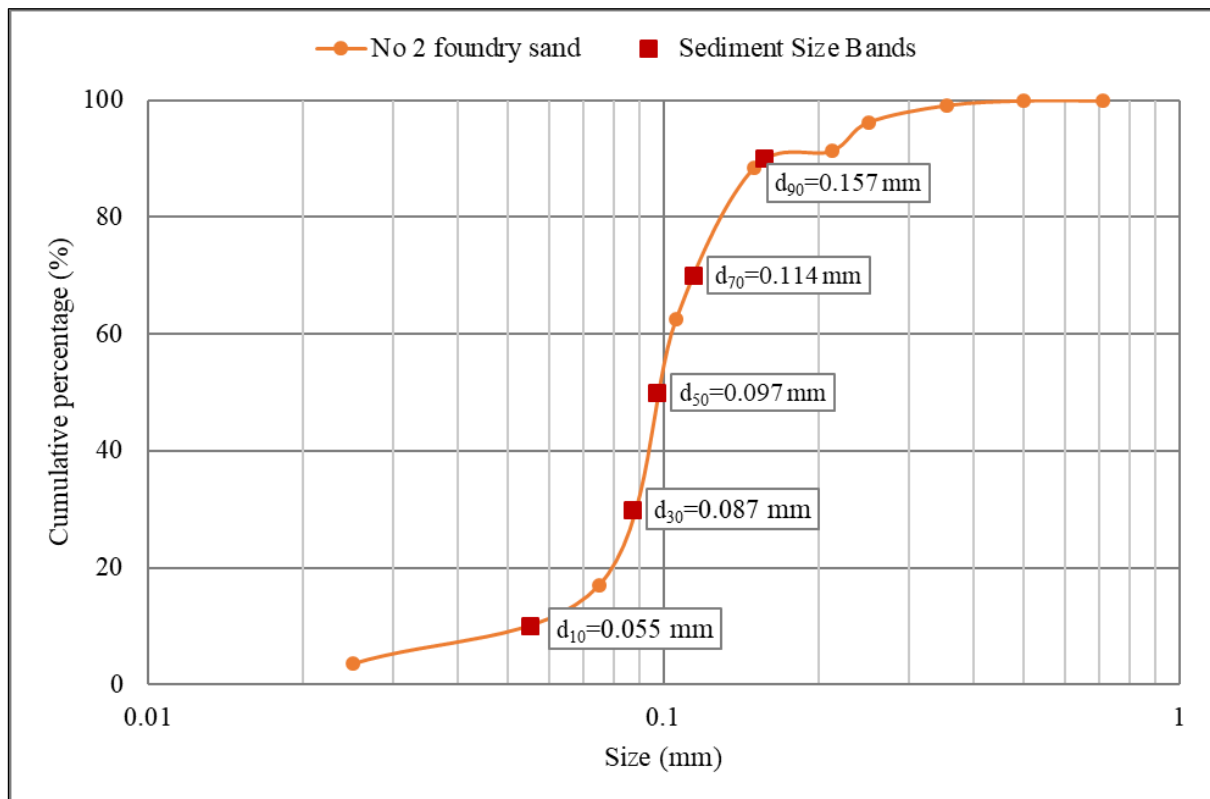


Figure 3.6 Grain size distribution curve with five percentage bands

The settling velocity for each band, shown in **Table 3.2** was calculated using **Equation 2-18** and **Equation 2-19**.

Table 3.2 Parameters for calculating weighted settling velocity

Percentage band	Median size for band	Size (mm)	Settling velocity (m/s)
0-20	d_{10}	0.055	0.0024
20-40	d_{30}	0.087	0.0060
40-60	d_{50}	0.097	0.0075
60-80	d_{70}	0.114	0.0089
80-100	d_{90}	0.157	0.0159

Chapter 3: Experimental Setup

Thereafter, the effective settling velocity ($\bar{\omega} = 0.0065 \text{ m/s}$) was calculated using:

$$\bar{\omega} = 0.2 \cdot \omega_{10} + 0.2 \cdot \omega_{30} + 0.2 \cdot \omega_{50} + 0.2 \cdot \omega_{70} + 0.2 \cdot \omega_{90} \quad 3-7$$

where:

$\bar{\omega}$ = effective settling velocity (m/s)

ω_n = settling velocity of associated diameter (m/s)

Finally, the effective diameter $d_{\text{eff}} = 0.090 \text{ mm}$ was determined from a backwards calculation using **Equation 2-18**. A summary of the sediment characteristics is shown in **Table 3.3**.

Table 3.3 Sediment characteristics

Parameter	Value
Name	No. 2 Foundry Sand
Composition	99.45% SiO ₂
Specific gravity, G_s	2.65
Bulk density, ρ_b	1461 kg/m^3
Median diameter, d_{50}	0.095 mm
Effective diameter, d_{eff}	0.090 mm
Gradation coefficient, Gr	1.415
Standard deviation, σ	1.414
Effective settling velocity, $\bar{\omega}$	0.0065 m/s

3.6 Measurement Techniques

3.6.1 Scour Measurements

Scour hole measurements were taken using a DPI-8 handheld three-dimensional (3D) scanner shown in **Figure 3.7**. This scanner instantly creates a coloured 3D model with a point density of $<1.7 \text{ mm}$ at 1 m distance (DotProduct, 2017). More scanner specifications are given in **Appendix D**. The scanner consists of an Android tablet with PrimeSense Carmine 1.082 sensor fixed to the back. A point cloud is developed by traversing over the area of interest with steady movements. More traverses over an area give a higher level of detail which is indicated by green areas on the display.



Figure 3.7 DPI-8 handheld three-dimensional (3D) scanner

3.6.1.1 Measurement Accuracy

Using the recommended methods of the product manual (DotProduct, 2017), initially a large area was scanned (including the model plate and sides of the flume) and the required detail of the scour cone was filled in by moving closer and traversing over the area several times. The scanner was held orthogonally (normal to the surface being scanned) as much as possible, since this improved data quality. Three scanner targets, called AprilTags, were placed on the plate to further improve scene accuracy and tracking stability. The data accuracy of the DPI scanner is shown in **Table 3.4**. The percentage values are with regard to the measuring distance, e.g. at a distance of 1 m an accuracy of 0.5% means approximately 5 mm error. The scanner was held at the minimum distance of 0.6 m when scanning the scour cone for all tests. This implies a typical data accuracy of $0.6\text{ m} \times 0.2\% = 0.0012\text{ m}$ or 1.2 mm. The minimum accuracy was determined to be 2.4 mm.

Table 3.4 Data accuracy of the DPI-8 handheld scanner

Range	Typical Accuracy (RMSE)	Minimum Accuracy
< 1 m	0.2%	0.4%
1 – 2 m	0.5%	0.8%
2 – 3.3 m	0.8%	1.2%
> 3.3 m	Not specified	Not specified

Chapter 3: Experimental Setup

The point cloud data generated from these 3D scans is more extensive than point gauge measurements due to the dense point cloud which is generated. The measuring process is also much less time-consuming than noting down hundreds of point gauge readings. The point cloud was used to measure the scour dimensions and to calculate an accurate volume of the scour cone as described in **Section 4.1**.

3.6.1.2 Coordinate System

Figure 3.8 shows the coordinate system of the experimental setup, which was also used for defining the scour cone geometry. It must be noted that the scour depth (D_c) was measured from the invert of the orifice to the lowest scouring point whereas the scour height (H_c) was measured from the top of the sediment bed to the lowest scoured point. The scour height therefore takes into account the initial sediment height (H_s).

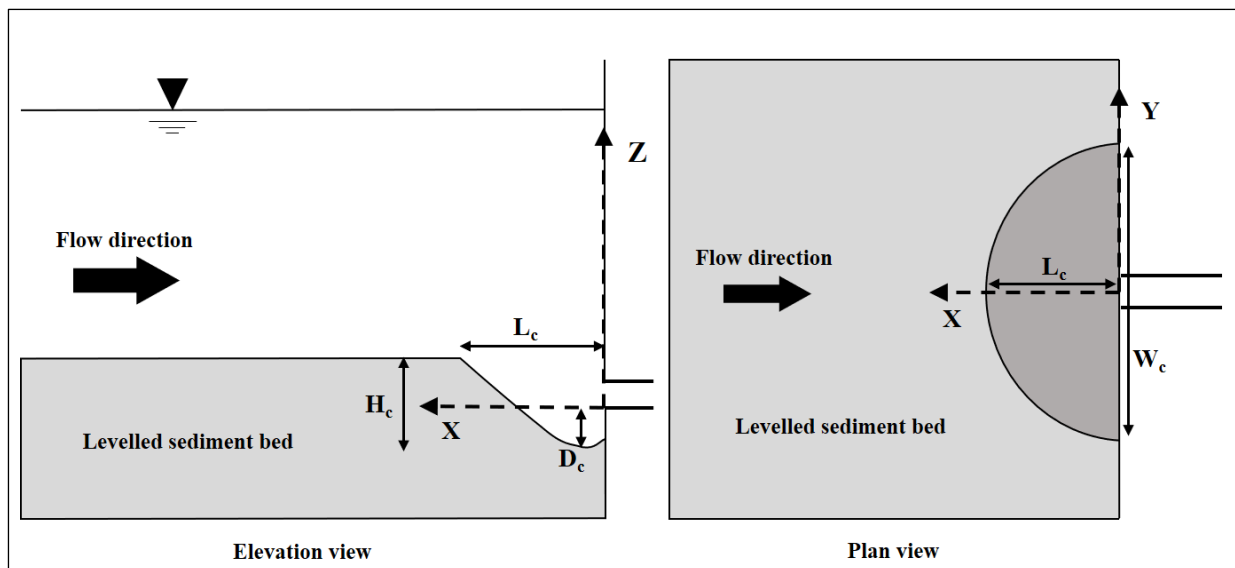


Figure 3.8 Coordinate system of the experimental setup

3.6.2 Discharge Measurement

The discharge through the low-level outlet had to be determined for each test and was measured separately for the inflow and outflow. To keep the water depth constant during the tests it was crucial to keep the inflow and outflow the same.

3.6.2.1 Inflow Measurement with V-notch Weir

V-notch weirs permit discharge measurement for low discharges that is more accurate than horizontally-crested weirs (Brater, King, Lindell & Wei, 1996). On the inflow side of the flume, a sharp-crested V-notch weir capable of measuring flows up to 40 l/s was used to measure the inflow (less than 20 l/s). Flow straighteners and a polystyrene float were used to stabilise the

Chapter 3: Experimental Setup

flow in the channel approaching the V-notch. The inflow setup is shown in **Figure 3.6**. **Equation 3-8** was used to determine the inflowing discharge over the V-notch weir.

$$Q = \frac{8}{15} C_d \sqrt{2g} \tan\left(\frac{\theta}{2}\right) h_1^{\frac{5}{2}} \quad 3-8$$

where:

- C_d = discharge coefficient (typically 0.59 for a 90° V-notch)
- θ = angle of V-notch (*degrees*)
- h_1 = head upstream of V-notch crest, measured 5 h_1 upstream (*m*)

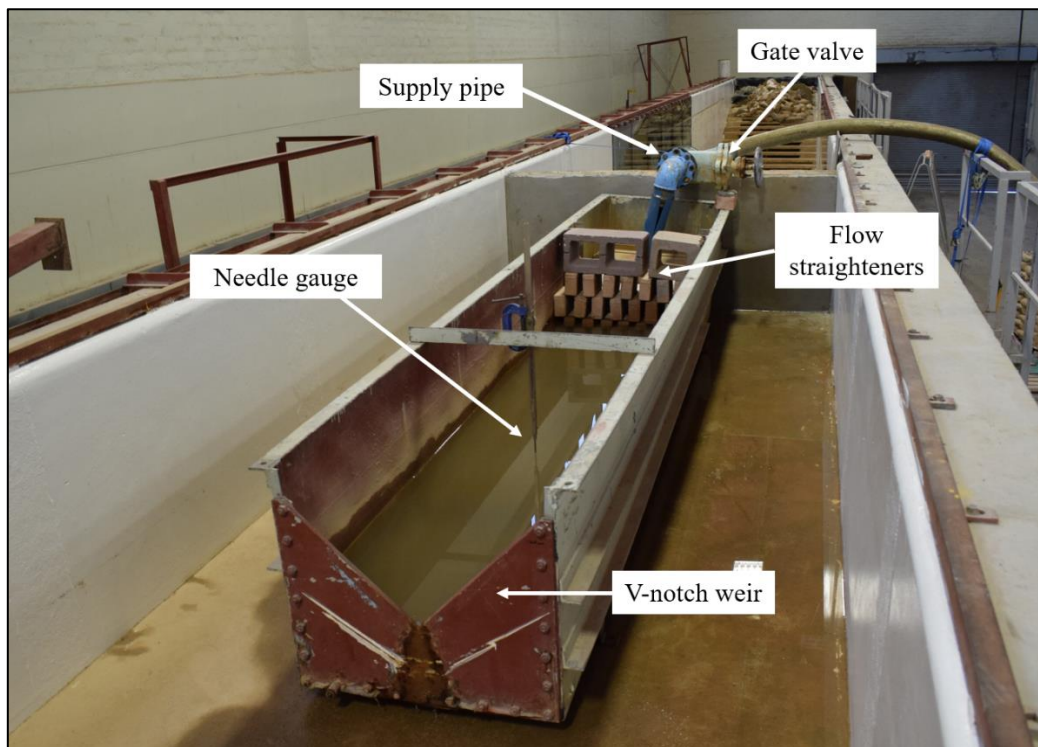


Figure 3.9 Upstream inflow control setup

3.6.2.2 Outflow Measurement with Flow Meter

At the downstream end of the outlet a SAFMAG Electromagnetic flow meter was used to measure the discharge through the low-level outlet. The flow meter was installed on the 110 mm pipe downstream of the butterfly valve and reducer as shown in **Figure 3.4**. To ensure that the butterfly valve and reducer did not influence the flow measurement, a 1.5 m long approach pipe was installed before the flow meter, thereby ensuring stable full pipe flow. After opening the butterfly valve, the flow meter readings varied due to the high sediment concentration at the start of the test. After about 5 minutes the flow stabilised, and the flow measurements were manually recorded from the flow meter's display. The flow meter is capable of measuring high

Chapter 3: Experimental Setup

velocities (up to 10 m/s), has a repeatability of $\pm 0.1\%$ and an accuracy of $\pm 0.5\%$ of the rate. This corresponds to a maximum error ± 0.0878 l/s at the maximum discharge of 17.55 l/s . The stage-discharge relationships for the outlets were determined from the outflow measurements. **Figure 3.10** shows the stage-discharge curve for the round outlet. The other three outlets had very similar plots.

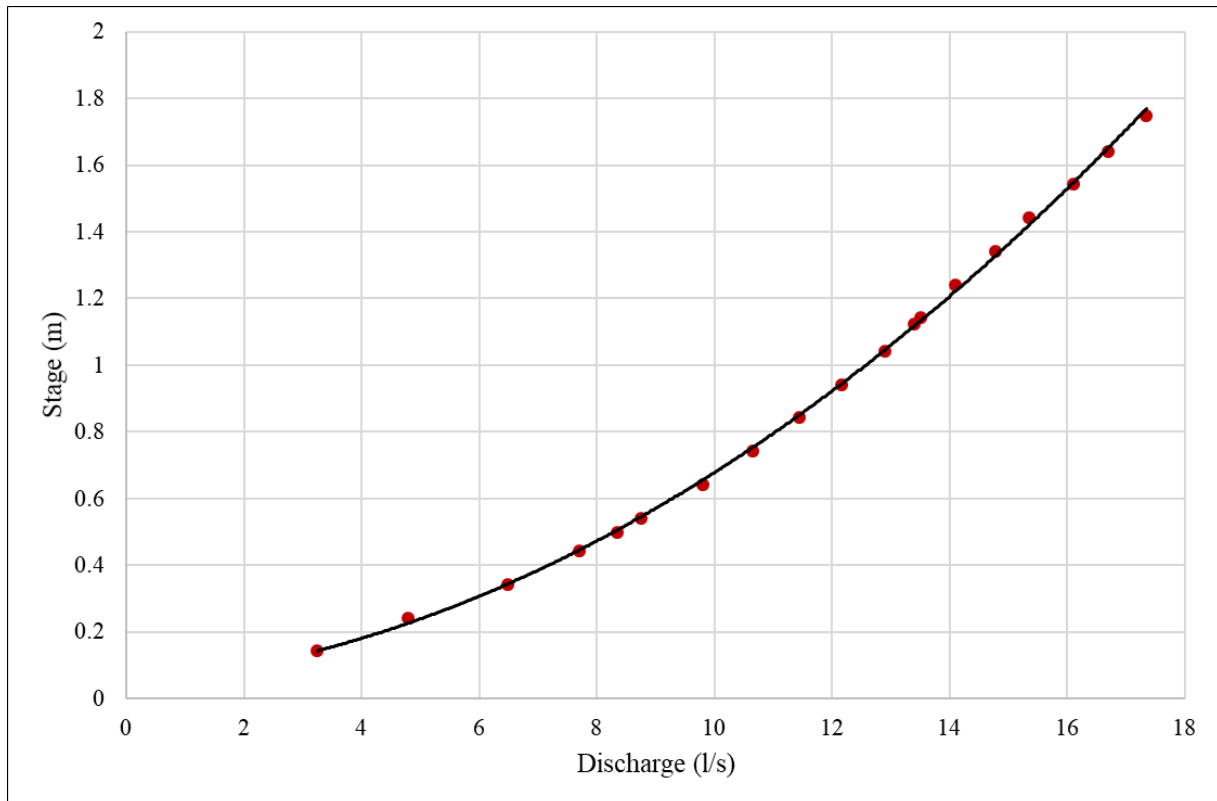


Figure 3.10 Stage-discharge relationship for the round outlet

3.6.3 Water Level Measurement

On the plate, water level markings were made so that the water depth could be monitored by constant observation. If the water depth seemed to change slightly, the inflow was immediately adjusted slightly by turning the valve on the inflow end.

3.7 Experimental Procedure

The appropriate outlet shape was installed and sealed, and all downstream valves were closed. Before the start of each test, the surface of the sediment bed in the flume was levelled to the required elevation for the specific test. The flume was initially filled slowly to prevent any disturbances to the surface of the packed sediment bed. When the water level was high enough above the sediment bed, the inflow was steadily increased to fill the flume quicker. Since the capacity of the main reservoir in the flume was more than 80 000 l , this was a time-consuming

Chapter 3: Experimental Setup

process. The discharge through the low-level outlet at each specific water depth was tested separately before placing the sediment in the flume. The discharge was noted and the required water level at the V-notch weir was calculated. When the water level was just below the required water level, the inflow was set equal to the predetermined outflow. Upon reaching the correct water level, the butterfly valve was immediately opened completely, initialising the pressure flushing process.

The time from the start to the end of the flushing process was kept constant at one hour as determined by the procedure described in **Section 3.8**. After an hour the downstream valve was closed, and the inflow was switched off. A submersible pump with a 50 mm diameter pipe was placed in the flume 6 m from the plate. The submersible pump was then switched on and the flume was drained slowly overnight to preserve the scour pattern. By opening the small gate valve downstream of the plate, the small pipe was used for draining the water left in the flume which the submersible pump could not pump. After draining the flume, the scour cone geometry was carefully surveyed using the 3D scanner. The process was repeated for all the tests, a total of 36.

3.8 Determining Experimental Time

The experimental time required for the formation of a stable scour cone had to be determined before commencing with the experiments. The scour cone formation for pressure flushing in physical models is relatively fast as described by several authors (Dodaran *et al.*, 2012; Fathi-Moghadam *et al.*, 2010a). Powell (2007) defined the equilibrium state as the time when the scour cone did not change more than 2 mm in a 24 hour period. In this study, the laboratory water was turbid and deep, so there was no way to monitor the scour cone formation over time. The purpose of pressure flushing is to create a scour cone in as short a time period as possible, ensuring that the flushing efficiency is as high as possible and minimizing water loss. Thus, running the experiments for many hours was not the purpose of this study and the time was fixed for all tests to allow comparison of the different outlet shapes.

Three tests were conducted to determine the approximate time required to form a stable cone by taking water samples from the outflow every 5 minutes. The suspended sediment was allowed to settle in clear bottles for several minutes. By visual inspection of the sample bottles (shown in **Figure 3.11**), it was determined whether there was still major cone formation taking place. The sediment samples taken in the first 10 minutes of the tests contained a large volume of sediment, steadily decreasing over time. After about 30 minutes the volume of sediment had

Chapter 3: Experimental Setup

decreased significantly and after approximately 50 minutes only a few individual sediment particles were observed in the samples. Based on these observations, the experimental time was set to 1 hour which is similar to studies by Emamgholizadeh *et al.* (2006), Meshkati Shahmirzadi *et al.* (2010), Dodaran *et al.* (2012) and Shahraki *et al.* (2014).

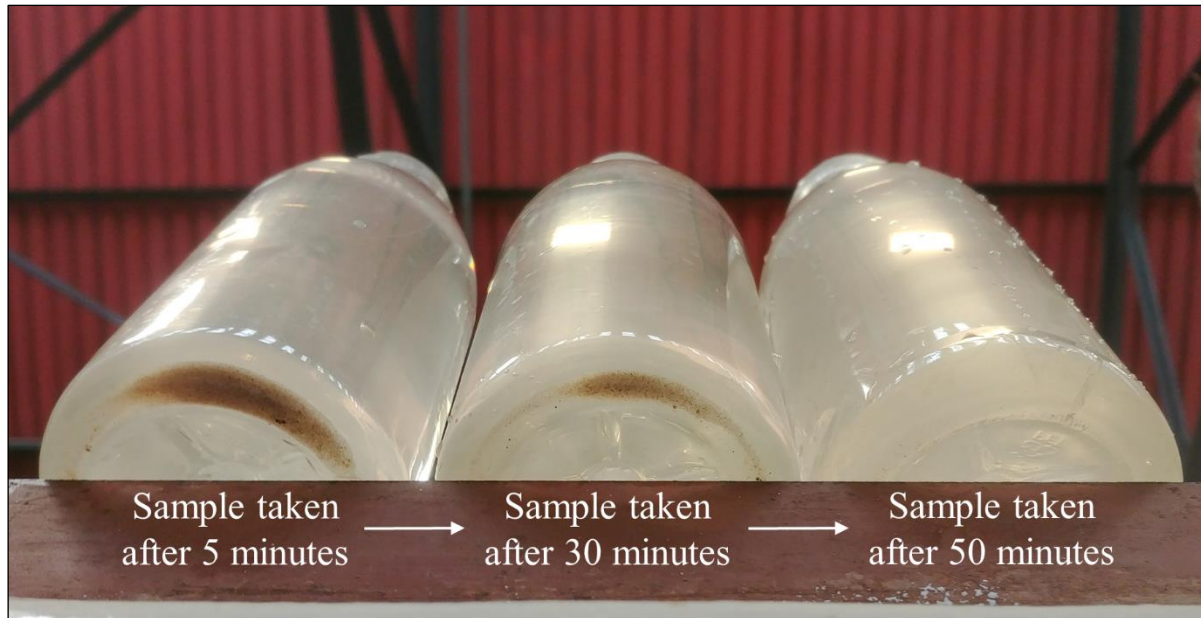


Figure 3.11 Sediment in water samples taken at different times during the test

3.9 Improvements from Previous Pressure Flushing Physical Models

The physical model design was based on previous pressure flushing physical model studies, taking into account the recommendations made by other authors and the aspects of pressure flushing which have not been extensively studied. A brief discussion of how the experimental setup compares with previous studies follows and is to the author's knowledge up to date.

Most authors who studied pressure flushing with physical models only considered circular low-level outlets and did not test other outlet shapes (Dodaran, Park & Mardashti, 2014; Emamgholizadeh *et al.*, 2006; Emamgholizadeh & Fathi-Moghadam, 2014; Fathi-Moghadam *et al.*, 2010a; Kistner, 2013; Madadi *et al.*, 2016; Meshkati *et al.*, 2009; Meshkati Shahmirzadi, Dehghani, Sumi, Mosaedi, *et al.*, 2010; Meshkati Shahmirzadi, Dehghani, Sumi, Naser, *et al.*, 2010; Mohammad *et al.*, 2017; Sawadogo, 2015; Shahraki *et al.*, 2014).

Hajikandi *et al.* (2017) studied the scour pattern upstream of square and circular orifices with the same opening areas. They concluded that the scour cone dimensions and volume are significantly larger for the square orifice, but more studies are required with rectangular shaped outlets. The same authors mentioned that in order to compare the scour geometry upstream of different orifices, a shape factor parameter needs to be added to the dimensional analysis, which

Chapter 3: Experimental Setup

was not possible in the case of their study because it required more experiments with more orifice shapes. This study addresses this issue by testing four different outlet shapes and comparing the scour cones.

To the author's knowledge, most other authors who conducted pressure flushing physical modelling used a pump to generate the required outflowing discharge (Dodaran *et al.*, 2014; Emamgholizadeh *et al.*, 2006; Emamgholizadeh & Fathi-Moghadam, 2014; Fathi-Moghadam *et al.*, 2010a; Hajikandi *et al.*, 2017; Kistner, 2013; Madadi *et al.*, 2016, 2017; Meshkati *et al.*, 2009; Meshkati Shahmirzadi, Dehghani, Sumi, Mosaedi, *et al.*, 2010; Meshkati Shahmirzadi, Dehghani, Sumi, Naser, *et al.*, 2010; Sawadogo, 2015; Shahraki *et al.*, 2014). In some of the studies the discharges which were tested were greater than would be physically attainable even with $C_d = 1$.

Under normal pressure flushing conditions, the water depth above the low-level outlet together with the discharge coefficient determines the maximum possible discharge through the dam. Pumping allows the experimental designer to investigate different discharges at the same water depth. However, the effect of varying discharge at a constant water depth has been extensively studied as discussed in the literature review. In this study no pumping was used to generate the outflowing discharge, instead the water depths were used to determine the outflow, similar to the study done by Powell (2007).

A 2 m deep flume was used to ensure that relatively high discharges (± 17 l/s) could be obtained without pumping. To the author's knowledge the high water depths (up to 1.75 m above the invert level) tested in this study are also greater than the highest used by other authors, namely 1.2 m (Emamgholizadeh & Fathi-Moghadam, 2014; Fathi-Moghadam *et al.*, 2010a). The head to outlet area ratio is, however, of more importance, as this indicates the relative water depth above the outlet.

This study also used different sediment levels to test the scouring pattern, unlike many authors who only studied one sediment level (Dodaran *et al.*, 2014; Dodaran, Park, Mardashti, Noshadi & Afsari, 2013; Emamgholizadeh *et al.*, 2006; Emamgholizadeh & Fathi-Moghadam, 2014; Fathi-Moghadam *et al.*, 2010a; Kistner, 2013; Madadi *et al.*, 2016, 2017; Meshkati *et al.*, 2009; Meshkati Shahmirzadi, Dehghani, Sumi, Mosaedi, *et al.*, 2010; Sawadogo, 2015; Shahraki *et al.*, 2014).

Chapter 3: Experimental Setup

To the author's best knowledge, apart from the cohesive sediment study by Emamgholizadeh & Fathi-Moghadam (2014), the sediment used in this study was the finest non-cohesive sediment ($d_{50} = 0.095 \text{ mm}$) used in a pressure flushing physical model to date.

The scour cone measurements in this study were done by using a 3D laser scanner, which accurately maps the scour cone. This method is much faster and more elaborate than using a point gauge, due to its ease of use, time saving and improved accuracy. **Table 3.5** provides a summary of the improvements made to the physical model compared to the way in which previous authors did their experiments.

Table 3.5 Improvements made in this study compared to other physical model studies

This study	Previous studies
Different outlet shapes	Mostly circular
No pumping used at outlet	Pump used to create discharge required
Greater water depth (1.75 m)	Maximum water depth of 1.2 m
Different sediment levels	Mostly tested one sediment level only
Very fine non-cohesive sand	Less fine non-cohesive sand
Laser scanner used to measure scour	Point gauge used to measure scour

3.10 Visual Observations

For the tests with the sediment level above the soffit of the outlet, the outlet was initially blocked, and the outflow took between 5 and 15 seconds to start. This blockage could be of a more permanent nature if the sediment level is even higher and consolidated over time.

Due to the fact that the laboratory water was too turbid to observe the scouring action under water, water samples were taken at the outflow end to monitor the scouring process. The change in sediment concentration over time was not part of the scope of this study, but visual inspection of the water samples provided a good idea of how much scouring was taking place at a specific time in the tests.

3.11 Limitations

The research output was limited by several factors beyond the author's control. The biggest constraint was time, because conducting laboratory tests on a pressure flushing model is a time-consuming process. The design and construction of the model took several months to complete and was further delayed by flume maintenance issues. Each test took more than a day to

Chapter 3: Experimental Setup

complete since filling up and draining a flume with a capacity of 80 000 *l* was no quick task. Removing the outlet and installing the next one was also time-consuming due to the silicone which had to dry overnight each time. Resetting the sediment level after each test was also time-consuming.

In order to reduce the number of experiments, certain variables had to be kept constant. Only one sediment size was tested, because it was not the most important parameter for determining the most suitable outlet shape. In addition, only one discharge was tested for each water depth. Removing those two variables from the tests significantly reduced experiment time, without significant effect on the final results.

Due to the severity of the drought conditions in the Western Cape region, the Hydraulics Laboratory was unable to fill the tanks with clean water for more than a year. The water was thus murky and not clear enough to see through, not allowing visual observations during the scouring process. Visually observing the scour hole formation would have allowed the author to develop time dependent equations as well as describe the vortex formation of the different outlet shapes.

Velocity measurements on the upstream side of the plate could also not be taken because the Acoustic Doppler Velocimeter (ADV) in the laboratory has a restricted depth (less than 0.5 *m*) to which it could measure. Velocity measurements upstream of the low-level outlet would provide information on the flow field upstream of different orifice shapes, which could substantiate the differences in scour cone geometry results for different outlets. Velocity measurements close to the orifice could also provide insight to vortex structure development near the outlet and inside the scour cone.

4 EXPERIMENTAL RESULTS

4.1 Data Processing and Analysis

After conducting each laboratory test and finalising the scour cone measurements, the acquired data had to be processed. Processing the scour cone data was time-consuming due to the large point cloud files that had to be converted, aligned, edited, analysed and finally exported from AutoCAD Civil 3D. The scan file for each test's scour cone was transferred to a computer from the scanning device and then opened using Autodesk Recap. Recap was used to remove areas of the scan that were not of interest and then convert the scan file into a point cloud file. The point cloud file was then opened in Civil 3D and correctly orientated to the axis system using the aligning tools of the software. Thereafter, a surface object was made from the point cloud and the points were extracted from the surface. Finally, all points (more than 200 000 for some scans) were then converted into AutoCAD points which were extracted to a .csv file in XYZ coordinates.

Using the XYZ data exported from Civil 3D, two-dimensional contour plots of each scour cone were prepared in Surfer 13.0. Measurements of the scour cone length and width were done on the contour plots and the volume was also calculated in Surfer. The volume calculation was done by taking the volumetric difference between the original sediment surface and the surface of the scour cone. The scour depth was simply determined by taking the lowest Z-value from the XYZ data and verifying its position. The profile tool in Surfer was used to export longitudinal and transverse profile data to Microsoft Excel where it was processed and plotted further.

4.2 Outlet Comparison

The four outlets used in the experiments had different shapes and thus were not hydraulically identical. Even though the cross-sectional areas of the outlets were the same, the centre of each outlet was at a slightly different position. Since the centre of the outlet is used for calculating the water depth above the outlet, the theoretical discharge through the outlets is slightly different. In order to compare the results of the outlets, it was necessary to calculate the discharge coefficient (C_d) for each outlet from the measured discharge. A comparison of the average discharge coefficients of the four outlets is given in **Table 4.1**, where the average discharge coefficient was calculated from all nine tests conducted with that outlet. The discharge coefficients are all very close to or equal to 0.6, which is a commonly used value in

Chapter 4: Experimental Results

practice. The actual discharge of the square outlet was the highest and the upright rectangular outlet the lowest. The largest difference in discharge observed was however only 2.33%, indicating that the scour cone results of all the outlets are comparable.

Table 4.1 Observed average discharge coefficient for different outlets

Outlet	C_d
Square	0.604
Flat rectangular	0.600
Round	0.599
Upright rectangular	0.599

4.3 Scour Cone Results

As described in **Section 3.3**, a total of 36 tests were completed for varying outlet shapes, water levels and sediment heights. Photos of the scour cones are given in **Appendix E**. The 2D scour cone plots are presented in this section and are separated into three subsections according to sediment height. This is simply to allow visual comparison of the results between the different outlet shapes, since the tests with the same sediment level can be plotted with the same colour scale and grid size.

4.3.1 Tests 1 to 12 with $H_s = 0$ m

The first set of tests was completed with the sediment levelled to the outlet invert levels ($H_s = 0$ m). A relatively small scour cone formed below the outlets as shown in **Figure 4.1**. The scour cones were not all perfectly symmetrical, with the deepest point of scour often located slightly towards one side of the cone. This can be ascribed to vertical vortices that form below the outlet and move around inside the cone as described by Powell (2007).



Figure 4.1 Photo showing the scour cone of Test 6

Chapter 4: Experimental Results

The contour plots for the square outlet are shown in **Figure 4.2** and the plots for the other outlets are given in **Appendix F**. A significant increase in scour cone size with increase in discharge is observed. When comparing the results of Test 4 and 6, it is further observed that at higher discharges the flat area in the immediate vicinity of the outlet is much larger and deeper. The contour plot of Test 6 also shows how the base of the scour cone is almost rectangular due to the square shape of the outlet influencing the cone geometry.

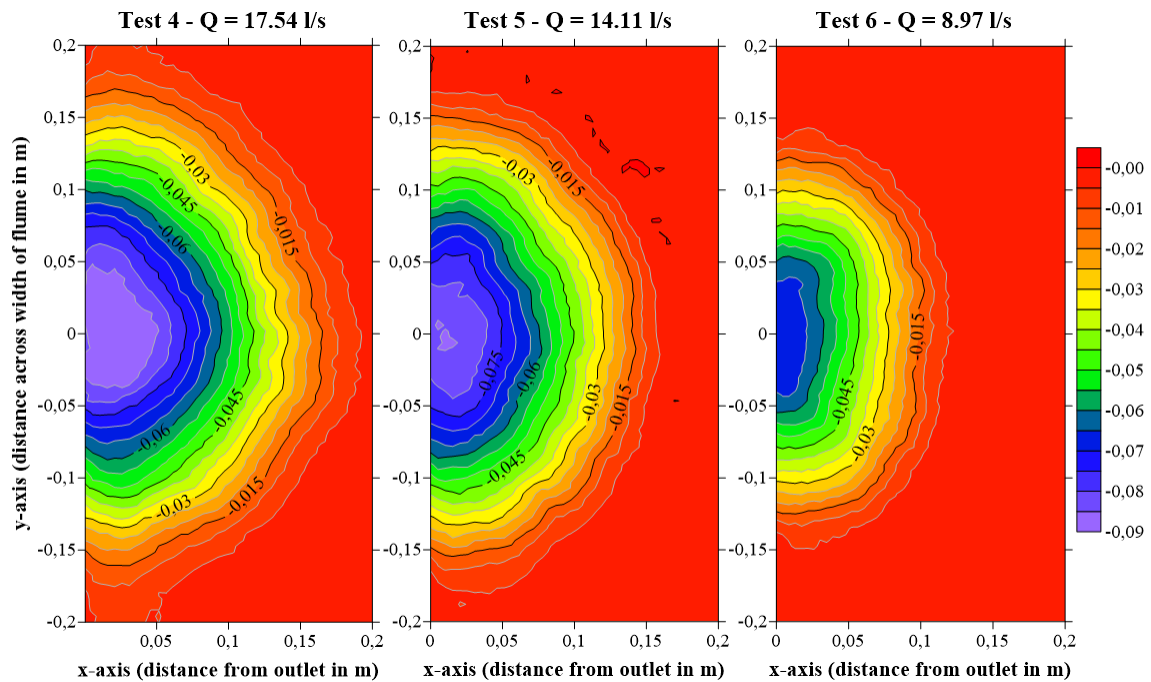
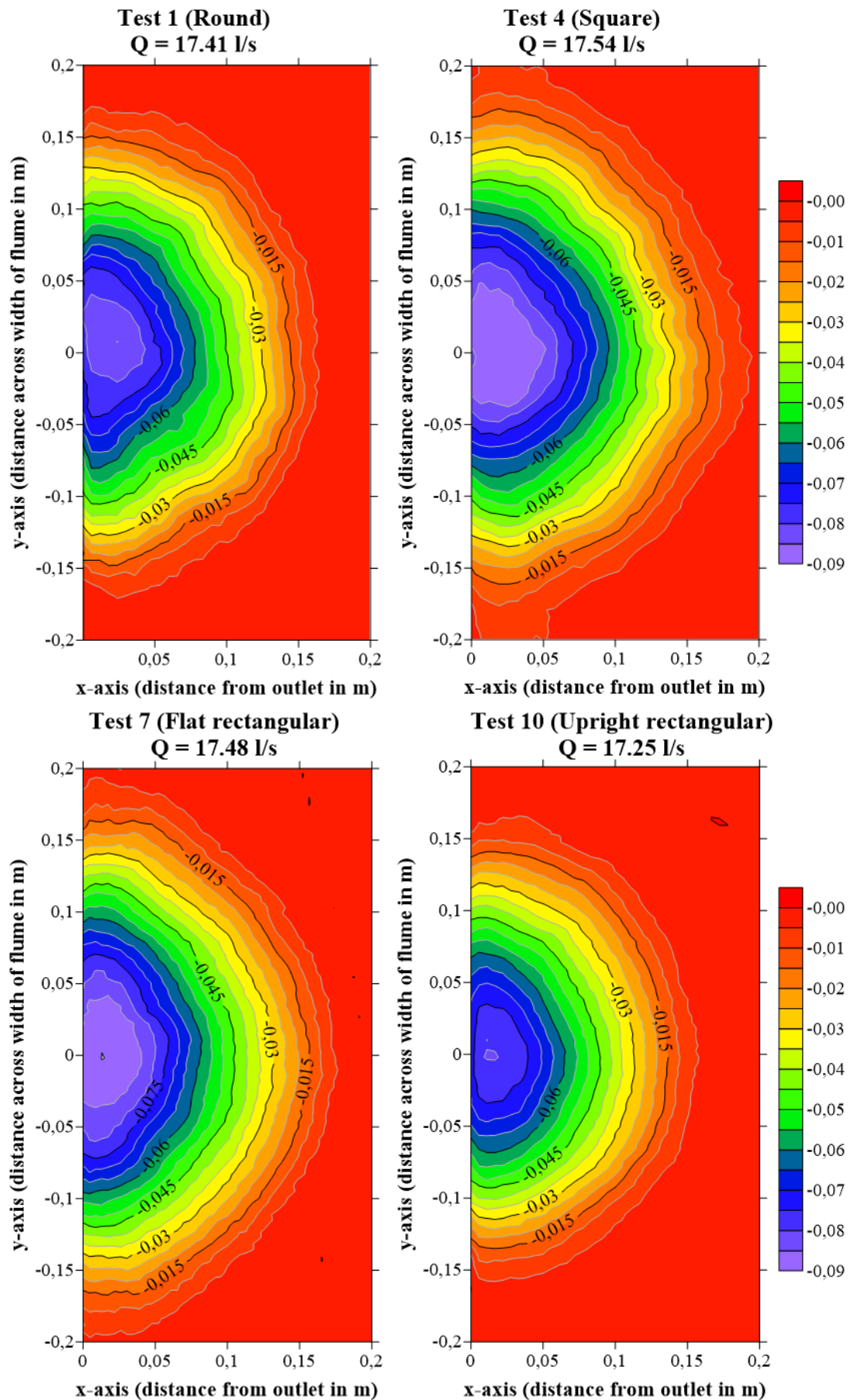


Figure 4.2 Scour cone contour plots of the square outlet for $H_s = 0$ m

Figure 4.3 compares the scour cone contour plots of the four outlets for the maximum water depth ($H_w = 1.75$ m). Major differences in the scour cone size are observed between the outlets in both longitudinal and transverse directions. The square and flat rectangular outlets have much larger scour cones, implying that a greater volume of sediment was removed and thus that a higher flushing efficiency was achieved. The scour cone of Test 10 (the upright rectangular outlet) is observed to be the narrowest at $x = 0$ m and is also less deep than the other three. As could be expected the base of the scour cone against the plate is widest for the flat rectangular outlet.

Chapter 4: Experimental Results

Figure 4.3 Scour cone contour plots for different outlets at $H_w = 1.75$ m and $H_s = 0$ m

Chapter 4: Experimental Results

4.3.2 Tests 13 to 24 with $H_s = 0.1$ m

After raising the sediment level to 0.1 m above the invert level, the second set of tests was completed and scour cone contour plots generated. **Figure 4.4** shows the scour cone of Test 19 which was conducted at $H_w = 0$ m. Several ridges and troughs are present along the scour cone edge as indicated. As the scour cone develops in the region close to the outlet (the critical shear area), the slopes of the cone become unstable resulting in slope failure. The unstable sediment on the slopes then flow down the into the critical shear area where it is scoured out by the dominant vortices in the region. Test 19 also shows the presence of a circular shaped ridge near the outlet caused by the central vortex forming right below the outlet as shown in **Figure 4.4**.

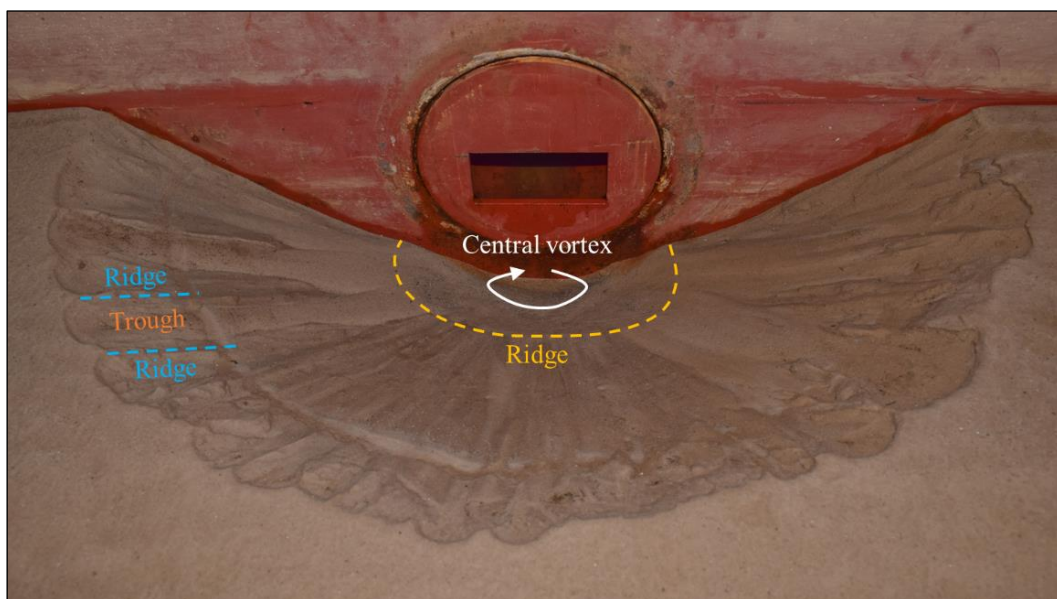


Figure 4.4 Photo showing the scour cone of Test 19 with different scour cone features

Figure 4.5 shows the contour plots for the flat rectangular outlet, which performed best in terms of creating the largest scour cone for the intermediate sediment level. The contour plots for the other outlets are shown in **Appendix F**. Note must be taken that the contour plot grid is larger than for the first set of tests. The scour cone length (>250 mm) and width (>500 mm) are clearly greater than for the first set of tests where the sediment was levelled to the invert.

Chapter 4: Experimental Results

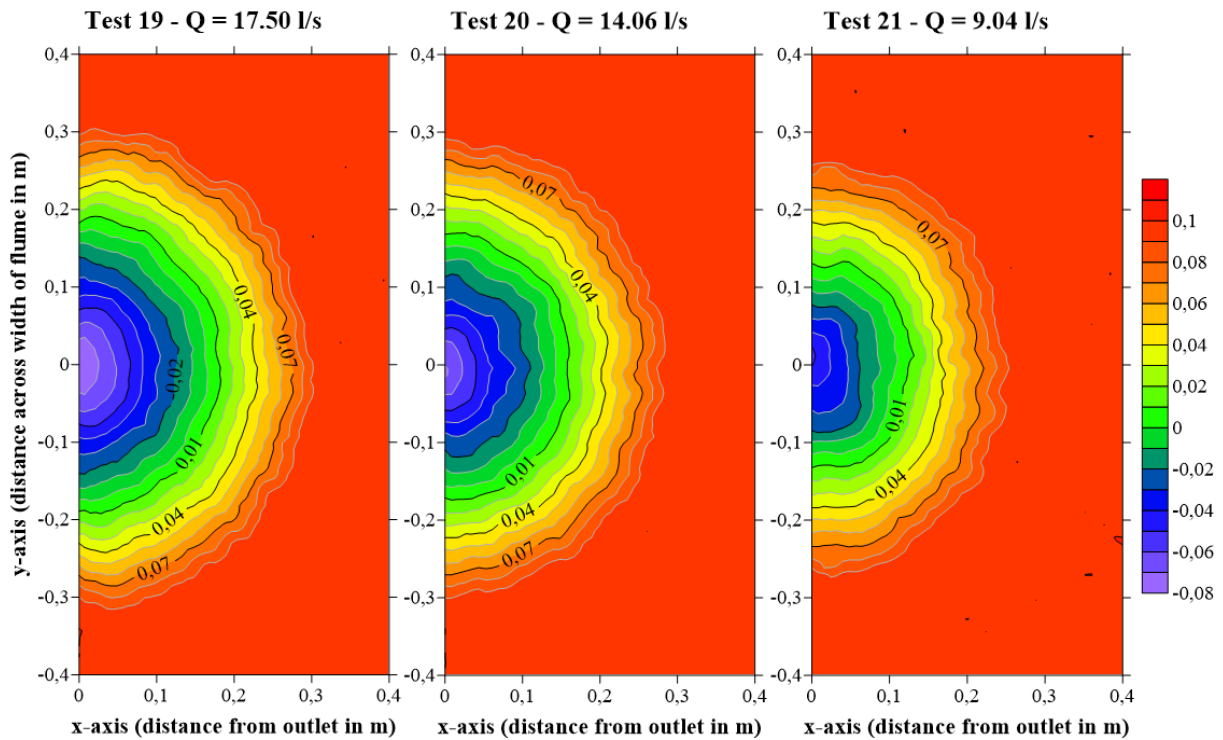


Figure 4.5 Scour cone contour plots of the flat rectangular outlet for $H_s = 0.1$ m

4.3.3 Tests 25 to 36 with $H_s = 0.2$ m

The final set of tests was conducted with the sediment level 0.2 m above the outlet invert and the scour cones measured. **Figure 4.6** shows the scour cone of Test 36 which was conducted with the lowest water depth ($H_w = 0.5$ m). It is clear from the figure that the existence of ridges and troughs is less prominent than shown in **Figure 4.4** and the slopes are more uniform.



Figure 4.6 Scour cone of Test 36

Chapter 4: Experimental Results

The scour cone contour plots of the flat rectangular outlet are shown in **Figure 4.7** and those of the other outlets are shown in **Appendix F**. It can be observed that the scour cones are much more uniform than for the first two sets of tests. Furthermore, the difference in scour cone size for different discharges is less than for the first two sets of tests. The effect of discharge thus decreases with an increase in sediment level. The contour plots do not provide the optimal comparison between tests, so the scour cone geometry results are given in **Section 4.3.4**. To fully investigate the effect of outlet shape, water depth and sediment level on the scour cone geometry a more thorough analysis of the scour cone geometry is given in **Section 5.1**.

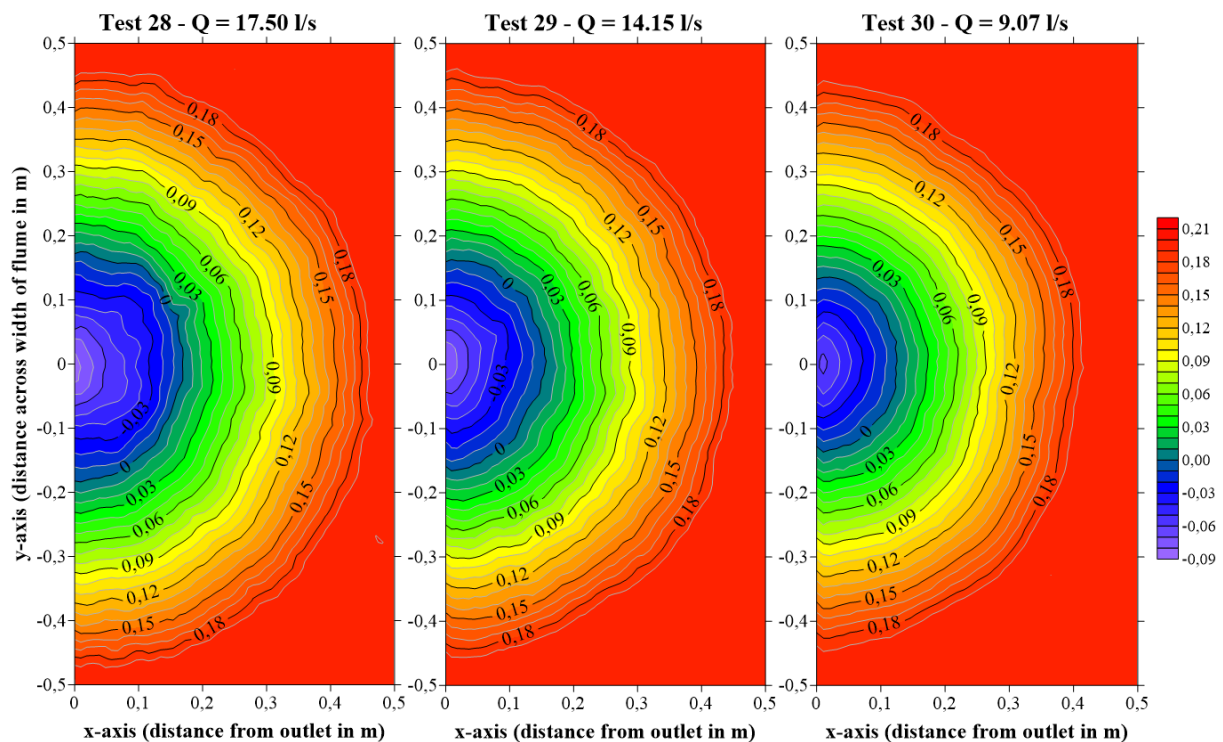


Figure 4.7 Scour cone contour plots of the flat rectangular outlet for $H_s = 0.2$ m

4.3.4 Scour Cone Geometry Results

The scour cone for each test was measured using the 3D scanner as explained in **Section 3.6.1** and from the scan results the scour cone geometry was determined as described in **Section 4.1**. The scour cone geometry is vitally important since it provides a way to compare the performance of the different shaped outlets. The scour cone geometry results of all the experiments are tabulated in **Table 4.2** according to the coordinate system used for the measurements as presented in **Section 3.6.1.2**. In **Section 5.1** an in-depth analysis of the geometry of the scour cone is done for different outlet shapes, water depths and sediment heights.

Chapter 4: Experimental Results

Table 4.2 Scour cone geometry results for all tests

Test setup parameters						Scour hole geometry					
Test no	Test ID	Q (l/s)	U (m/s)	H _w (m)	H _s (m)	L (mm)	W (mm)	H (mm)	D (mm)	V (10 ⁻³ m ³)	
Sediment level 1 – H_s = 0 m											
1	RoH _{s1} H _w	17.41	3.462	1.75	0	178	368	83	83	1.719	
2	RoH _{s1} H _w	13.94	2.775	1.125	0	155	320	68	68	1.178	
3	RoH _{s1} H _w	8.92	1.771	0.5	0	118	280	64	64	0.702	
4	SqH _{s1} H _{w1}	17.54	3.472	1.75	0	196	400	88	88	2.148	
5	SqH _{s1} H _{w2}	14.11	2.797	1.125	0	171	378	85	85	1.717	
6	SqH _{s1} H _{w3}	8.97	1.787	0.5	0	138	298	67	67	0.975	
7	FrH _{s1} H _{w1}	17.48	3.41	1.75	0	188	392	90	90	1.997	
8	FrH _{s1} H _{w2}	14.08	2.61	1.125	0	162	362	79	79	1.654	
9	FrH _{s1} H _{w3}	9.02	1.67	0.5	0	142	296	67	67	1.074	
10	UrH _{s1} H _{w1}	17.25	3.45	1.75	0	179	336	80	80	1.425	
11	UrH _{s1} H _{w2}	13.9	2.78	1.125	0	149	288	68	68	0.998	
12	UrH _{s1} H _{w3}	8.87	1.773	0.5	0	109	268	57	57	0.642	
Sediment level 2 – H_s = 0.1 m											
13	RoH _{s2} H _w	17.4	3.462	1.75	0.1	288	619	165	65	8.509	
14	RoH _{s2} H _w	13.95	2.775	1.125	0.1	270	552	160	60	7.031	
15	RoH _{s2} H _w	8.9	1.771	0.5	0.1	244	515	143	43	5.657	
16	SqH _{s2} H _{w1}	17.55	3.481	1.75	0.1	306	624	173	73	10.597	
17	SqH _{s2} H _{w2}	14.12	2.801	1.125	0.1	284	588	164	64	9.101	
18	SqH _{s2} H _{w3}	8.96	1.777	0.5	0.1	240	536	155	55	6.477	
19	FrH _{s2} H _{w1}	17.5	3.5	1.75	0.1	318	644	177	77	11.206	
20	FrH _{s2} H _{w2}	14.06	2.812	1.125	0.1	290	616	169	69	9.500	
21	FrH _{s2} H _{w3}	9.04	1.808	0.5	0.1	270	544	149	49	6.823	
22	UrH _{s2} H _{w1}	17.25	3.45	1.75	0.1	296	592	167	67	8.822	
23	UrH _{s2} H _{w2}	13.9	2.78	1.125	0.1	272	580	157	57	7.561	
24	UrH _{s2} H _{w3}	8.87	1.773	0.5	0.1	232	508	143	43	5.668	
Sediment level 3 – H_s = 0.2 m											
25	SqH _{s3} H _{w1}	17.55	3.481	1.75	0.2	468	935	270	70	35.038	
26	SqH _{s3} H _{w2}	14.18	2.813	1.125	0.2	455	920	272	72	33.031	
27	SqH _{s3} H _{w3}	9.05	1.795	0.5	0.2	433	860	256	56	27.009	
28	FrH _{s3} H _{w1}	17.5	3.5	1.75	0.2	476	940	282	82	37.823	
29	FrH _{s3} H _{w2}	14.15	2.83	1.125	0.2	460	925	272	72	34.986	
30	FrH _{s3} H _{w3}	9.07	1.814	0.5	0.2	435	905	259	59	29.537	
31	UrH _{s3} H _{w1}	17.2	3.44	1.75	0.2	451	905	267	67	33.116	
32	UrH _{s3} H _{w2}	13.85	2.77	1.125	0.2	442	860	260	60	29.534	
33	UrH _{s3} H _{w3}	8.86	1.772	0.5	0.2	415	805	245	45	24.693	
34	RoH _{s3} H _w	17.25	3.432	1.75	0.2	453	905	269	69	34.554	
35	RoH _{s3} H _w	13.9	2.765	1.125	0.2	443	875	260	60	30.326	
36	RoH _{s3} H _w	8.9	1.771	0.5	0.2	420	845	246	46	25.604	
Key:											
Sq	=	Square outlet				H _s	=	sediment level (m)			
Fr	=	Flat rectangular outlet				H _w	=	water depth (m)			
Ro	=	Round outlet				Q	=	flow rate (l/s)			
Ur	=	Upright rectangular outlet				U _o	=	velocity through outlet (m/s)			

4.4 Repeatability

The repeatability of the experiments was investigated to eliminate variability in the measurements and results. Typically, 10% of experiments are repeated to ensure that the results are reproduced with acceptable accuracy. Four of the thirty-six tests were repeated independently, and the scour cone geometry was measured and compared with the original results. **Table 4.3** provides a comparison of the scour cone results between the original and repeated tests. The comparison indicates good repeatability of the tests, with differences between original and repeated tests less than 5% for the scour cone length, width and height, and less than 7% for the volume. The scour cone depth for the repeat of test 28 was the only outlier, being nearly 15% less than that of the initial test. This was due to the minor sliding of sediment into the bottom of the scour cone during draining of the flume.

Table 4.3 Results of repeated tests

Test no	L (mm)	W (mm)	H (mm)	D (mm)	V ($10^{-3} m^3$)
1	178	368	83	83	1.719
1 repeat	175	359	82	82	1.653
Difference	1.69%	2.45%	1.20%	1.20%	3.84%
3	118	280	64	64	0.702
3 repeat	116	285	61	61	0.748
Difference	1.69%	1.79%	4.69%	4.69%	6.55%
28	476	940	282	82	37.823
28 repeat	478	949	270	70	38.476
Difference	0.42%	0.96%	4.26%	14.63%	1.73%
30	435	905	259	59	29.537
30 repeat	432	899	262	62	30.298
Difference	0.69%	0.66%	1.16%	5.08%	2.58%

5 ANALYSIS AND DISCUSSION OF RESULTS

5.1 Analysis of Scour Cone Geometry

5.1.1 Cone Length

The scour cone length gives an indication of how far upstream the orifice flow has an influence on the sediment. The length is however directly related to the sediment height and the angle of repose of the sediment. **Figure 5.1** shows the cone length versus water depth and discharge for different outlet shapes and sediment levels. The cone length versus discharge curves show a near-linear trend for all outlet shapes at $H_s = 0\text{ m}$ and $H_s = 0.1\text{ m}$.

5.1.1.1 Outlet Shape Effect

A longer cone length is associated with a larger scour cone which implies better outlet performance. Analysing the performance of the four different outlet shapes is done by comparing the scour cone lengths for the same water depth and sediment level. Since most previous pressure flushing studies have been conducted with round outlets, the scour cone lengths of the other three outlet shapes were compared to that of the round outlet as presented in **Table 5.1**.

Table 5.1 Cone length comparison of different outlet shapes compared to round outlet

H_s (m)	H_w (m)	Discharge		Length (mm) and % difference from round outlet						
		Range (l/s)	% Increase	Round	Square		Flat rectangular		Upright rectangular	
0	1.75	17.25-17.54	94-95%	178	196	10%	188	6%	179	1%
	1.125	13.9-14.11	56-58%	155	171	10%	162	5%	149	-4%
	0.5	8.87-9.02	0%	118	138	17%	142	20%	109	-8%
0.1	1.75	17.25-17.55	93-96%	288	306	6%	318	10%	296	3%
	1.125	13.9-14.12	55-58%	270	284	5%	290	7%	272	1%
	0.5	8.87-9.02	0%	244	240	-2%	270	11%	232	-5%
0.2	1.75	17.2-17.55	93-95%	453	468	3%	476	5%	451	0%
	1.125	13.9-14.11	56-57%	443	455	3%	460	4%	442	0%
	0.5	8.86-9.07	0%	420	433	3%	435	4%	415	-1%

With reference to **Table 5.1**, it is clear that the outlet shape effect is greatest at the lower sediment levels, decreasing with an increase in sediment level. The square outlet performed slightly better when the sediment level was at the invert, but the flat rectangular outlet performed best with sediment levels above the invert.

Chapter 5: Analysis and Discussion of Results

It is interesting to note that the performance of the round and upright rectangular outlets is closely related and follow similar trends. The upright rectangular outlet performed worse than the round outlet, possibly due to the way the flow enters the vertically orientated outlet, but the results closely matched those of the round outlet. It is clear that the outlet shape greatly influences the length of the scour cone at all sediment levels.

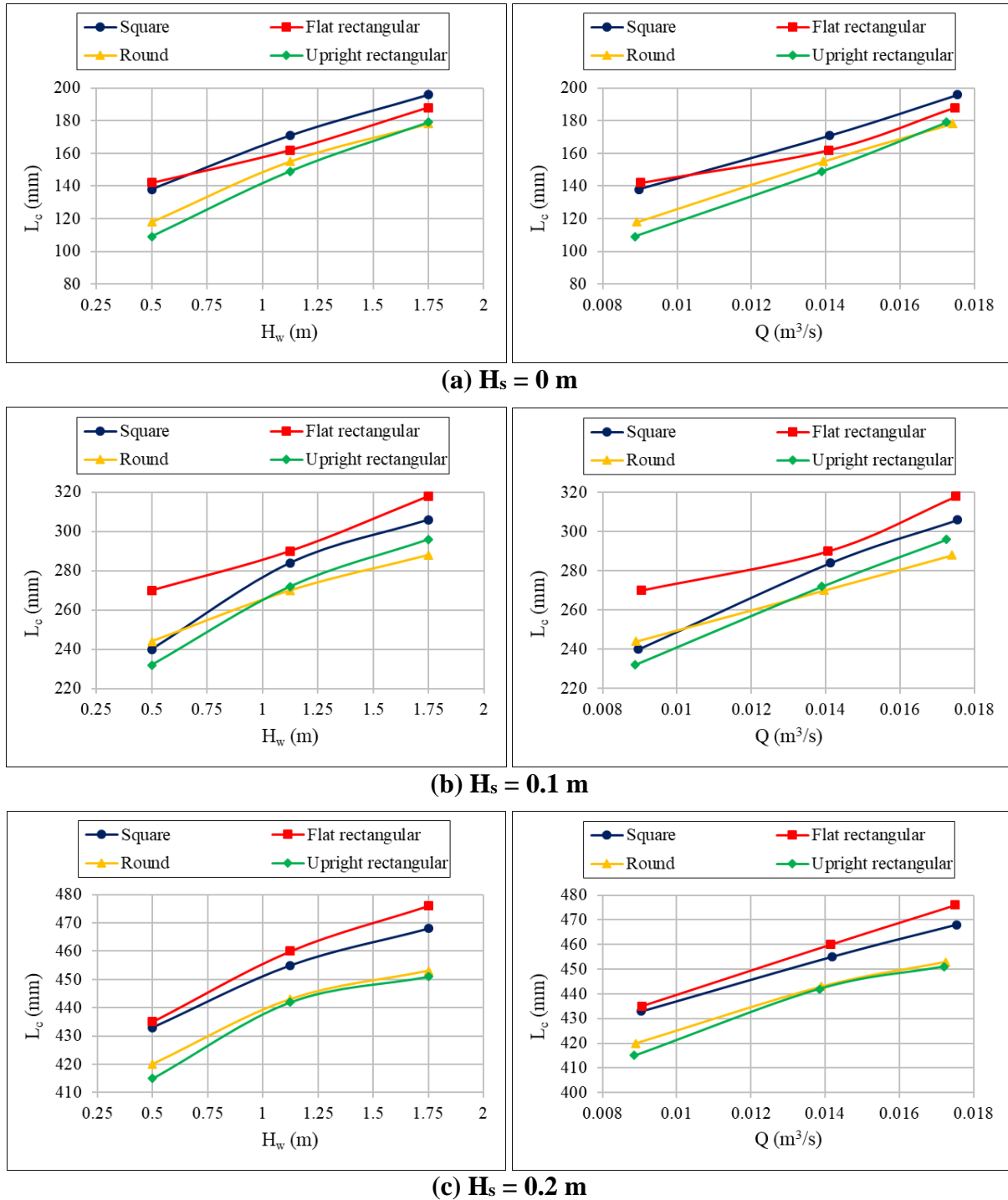


Figure 5.1 Cone length comparison for different outlet shapes and sediment levels

Chapter 5: Analysis and Discussion of Results

5.1.1.2 Discharge and Water Level Effect

The effect of water depth and discharge are discussed interchangeably since these are directly linked through the orifice discharge equation mentioned in **Section 2.4.2**. The results in **Figure 5.2** and **Table 5.2** show that an increase in discharge clearly leads to an increase in scour cone length for all outlet shapes. An increase in discharge through the outlet increases the orifice flow, leading to higher velocities over the bed which extend further upstream, causing scour further from the outlet. The discharge versus cone length curves reveal a near linear relationship, but for the water depth versus cone length curves the trend closer resembles a logarithmic function.

Table 5.2 Comparison of the cone length increase with increasing discharge

H_s (m)	H_w (m)	Discharge		Length (mm) and % increase from lowest discharge							
		Range (l/s)	% Increase	Square	Flat rectangular		Round		Upright rectangular		
0	1.75	17.25-17.54	94-95%	196	42%	188	32%	178	51%	179	64%
	1.125	13.9-14.11	56-58%	171	24%	162	14%	155	31%	149	37%
	0.5	8.87-9.02	0%	138	0%	142	0%	118	0%	109	0%
0.1	1.75	17.25-17.55	93-96%	306	28%	318	18%	288	18%	296	28%
	1.125	13.9-14.12	55-58%	284	18%	290	7%	270	11%	272	17%
	0.5	8.87-9.02	0%	240	0%	270	0%	244	0%	232	0%
0.2	1.75	17.2-17.55	93-95%	468	8%	476	9%	453	8%	451	9%
	1.125	13.9-14.11	56-57%	455	5%	460	6%	443	5%	442	7%
	0.5	8.86-9.07	0%	433	0%	435	0%	420	0%	415	0%

Table 5.2 shows that the influence of the discharge on the cone length is greatest at $H_s = 0$ m and decreases with increasing sediment height. Furthermore, **Figure 5.2** illustrates that the lower the sediment level, the greater the difference in cone length at different discharges for the square outlet. However, for the flat rectangular shape the difference in cone length (in mm) remains similar at different discharges.

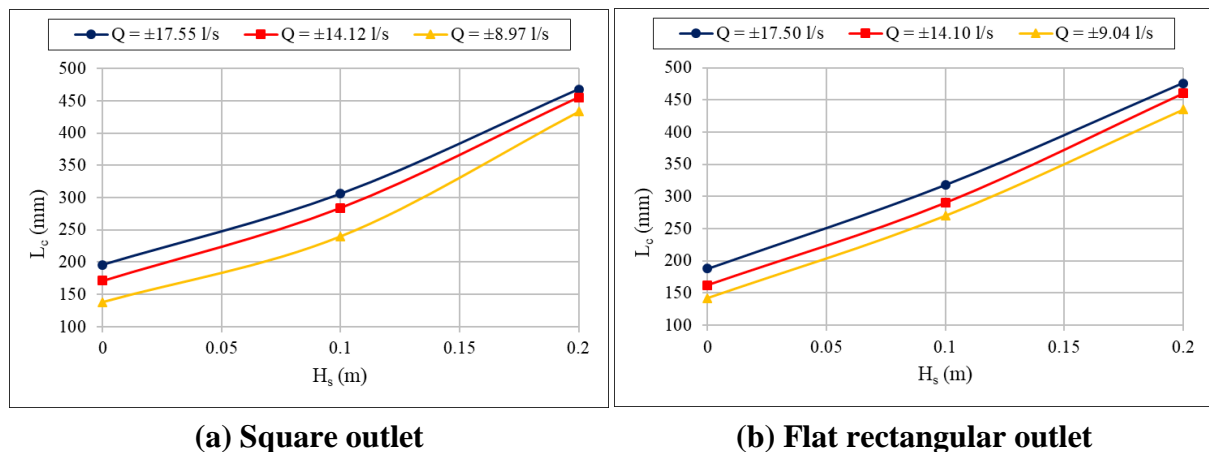


Figure 5.2 Discharge effect on cone length

Chapter 5: Analysis and Discussion of Results

5.1.1.3 Sediment Level Effect

In order to investigate the effects of sediment level on the scour cone length, a comparison was made between the scour cone lengths of different sediment levels as shown in **Table 5.3**. It is shown that the percentage increase in length is greatest at the lowest discharge/water depth, e.g. for the square outlet, when the sediment level is raised from 0 m to 0.2 m at a constant discharge of 17.55 l/s, the cone length increases by 140%, but when the same sediment level change is done at 9.02 l/s, the cone length increases by 237%. Increasing the sediment level had the greatest effect on cone lengths of the upright rectangular outlet and the smallest effect on the square outlet. The cone length increases greatly with an increase in sediment height, as illustrated in **Figure 5.2**.

Table 5.3 Comparison of the cone length increase with increasing sediment level

Discharge (l/s)	H _w (m)	H _s (m)	Length (mm) and % increase from lowest sediment level							
			Square		Flat rectangular		Round		Upright rectangular	
17.2-17.55	1.75	0	196	0%	188	0%	178	0%	179	0%
		0.1	306	56%	318	69%	288	62%	296	65%
		0.2	468	139%	476	153%	453	154%	451	152%
13.9-14.12	1.125	0	171	0%	162	0%	155	0%	149	0%
		0.1	284	66%	290	79%	270	74%	272	83%
		0.2	455	166%	460	184%	443	186%	442	197%
8.86-9.07	0.5	0	138	0%	142	0%	118	0%	109	0%
		0.1	240	74%	270	90%	244	107%	232	113%
		0.2	433	214%	435	206%	420	256%	415	281%

5.1.2 Cone Width

The width of the scour cone is of particular importance, since it indicates the size of the area against the dam that can be cleared and thus provides an indication of how many power intakes may be kept sediment free by pressure flushing through a single outlet. **Figure 5.3** shows the cone width versus water depth and discharge for different outlet shapes and sediment levels.

Similar to what is observed for cone length, the round and upright rectangular shapes showed similar performance trends but performed significantly worse than the other two outlets. At the lowest sediment level, the scour cone width for the square outlet was very similar to that of the flat rectangular shape, only 8-9 mm less. Where the sediment level was above the invert of the outlet, however, this difference was much greater, ranging from 17-44 mm.

Chapter 5: Analysis and Discussion of Results

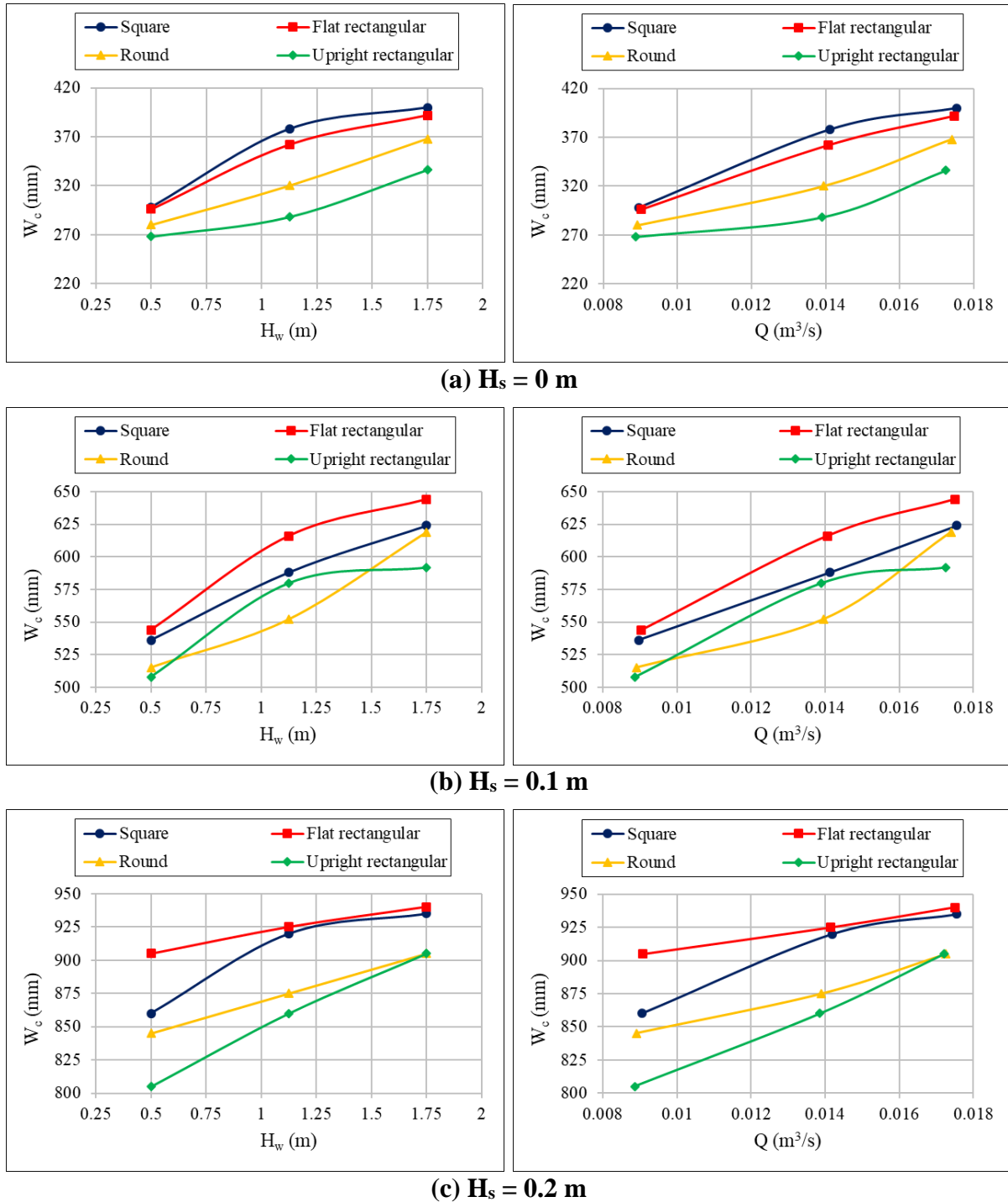


Figure 5.3 Cone width comparison for different outlet shapes and sediment levels

5.1.2.1 Outlet Shape Effect

Investigating the outlet shape effect on the scour width was done in the same way as for the cone length, by comparing the results of the other three outlets to the round outlet. **Table 5.4** shows that the outlet shape effect decreases with an increase in sediment level. As expected, the widest outlet (the flat rectangular shape) formed the widest scour cone and the narrowest outlet (the upright rectangular shape) formed the narrowest cone for all sediment levels.

Chapter 5: Analysis and Discussion of Results

Therefore, it is concluded that the shape of the outlet (more specifically the width) greatly influences the width of the final scour cone.

Table 5.4 Cone width comparison of different outlet shapes compared to round outlet

H_s (m)	H_w (m)	Discharge		Width (mm) and % difference from round outlet						
		Range (l/s)	% Increase	Round	Square		Flat rectangular		Upright rectangular	
0	1.75	17.25-17.54	94-95%	368	400	9%	392	7%	336	-9%
	1.125	13.9-14.11	56-58%	320	378	18%	362	13%	288	-10%
	0.5	8.87-9.02	0%	280	298	6%	296	6%	268	-4%
0.1	1.75	17.25-17.55	93-96%	619	624	1%	644	4%	592	-4%
	1.125	13.9-14.12	55-58%	552	588	7%	616	12%	580	5%
	0.5	8.87-9.02	0%	515	536	4%	544	6%	508	-1%
0.2	1.75	17.2-17.55	93-95%	905	935	3%	940	4%	905	0%
	1.125	13.9-14.11	56-57%	875	920	5%	925	6%	860	-2%
	0.5	8.86-9.07	0%	845	860	2%	905	7%	805	-5%

In terms of the most effective outlet shape for forming a wide scour cone, the flat rectangular outlet far outperformed the others by a significant margin. The upright rectangular outlet performed the worst in nearly all conditions.

5.1.2.2 Discharge and Water Level Effect

A comparison of the cone width results for changes in discharge is provided in **Table 5.5**. It is clear that the cone width increases for all increases in discharge. Furthermore, it is observed that the effect of discharge reduces with an increase in sediment level. The greatest effect is an approximately 30% increase in cone width for all outlet shapes with a 95% increase in discharge with the sediment level at the invert.

When the sediment level is 0.2 m above the invert, the same discharge increase only leads to a cone width increase of less than 12%. At the lowest sediment level, the effect of a 95% increase in discharge on the cone width was less (30-32%) than the effect on the cone length (43-61%). At the highest sediment level, the effects were in a similar range, 5-12% and 9-12% for the width and length respectively.

Table 5.5 Comparison of the cone width increase with increasing discharge

H_s (m)	H_w (m)	Discharge		Width (mm) and % increase from lowest discharge							
		Range (l/s)	% Increase	Square		Flat rectangular		Round		Upright rectangular	
0	1.75	17.25-17.54	94-95%	400	34%	392	32%	368	31%	336	25%
	1.125	13.9-14.11	56-58%	378	27%	362	22%	320	14%	288	7%
	0.5	8.87-9.02	0%	298	0%	296	0%	280	0%	268	0%
0.1	1.75	17.25-17.55	93-96%	624	16%	644	18%	619	20%	592	17%
	1.125	13.9-14.12	55-58%	588	10%	616	13%	552	7%	580	14%
	0.5	8.87-9.02	0%	536	0%	544	0%	515	0%	508	0%
0.2	1.75	17.2-17.55	93-95%	935	9%	940	4%	905	7%	905	12%
	1.125	13.9-14.11	56-57%	920	7%	925	2%	875	4%	860	7%
	0.5	8.86-9.07	0%	860	0%	905	0%	845	0%	805	0%

5.1.2.3 Sediment Level Effect

Table 5.6 provides a comparison of the cone widths for different sediment levels at the same discharge. The effect of the sediment level on the cone width was similar to that of the cone length, i.e. an increase in sediment level greatly increased the cone width and was more sensitive on the lower discharges. The square and flat rectangular outlets experienced almost exactly the same percentage increase in cone width with increasing sediment level. As indicated, the upright rectangular outlet was most sensitive to the sediment level.

Table 5.6 Comparison of the cone width increase with increasing sediment level

Discharge (l/s)	H_w (m)	H_s (m)	Width (mm) and % increase from lowest sediment level							
			Square		Flat rectangular		Round		Upright rectangular	
17.2-17.55	1.75	0	400	0%	392	0%	368	0%	336	0%
		0.1	624	56%	644	64%	619	68%	592	76%
		0.2	935	134%	940	140%	905	146%	905	169%
13.9-14.12	1.125	0	378	0%	362	0%	320	0%	288	0%
		0.1	588	56%	616	70%	552	73%	580	101%
		0.2	920	143%	925	156%	875	173%	860	199%
8.86-9.07	0.5	0	298	0%	296	0%	280	0%	268	0%
		0.1	536	80%	544	84%	515	84%	508	90%
		0.2	860	189%	905	206%	845	202%	805	200%

5.1.3 Cone Height

The scour cone height represents the sediment level together with the depth of scouring below the outlet invert. It is thus of particular importance where low-level outlets are to be placed at a certain height above the original river-bed level. The low-level outlet should preferably not be placed exactly on the original river-bed level, but rather a few meters above the river bed to prevent blockage by boulders. The depth to which scouring is expected can be used to

Chapter 5: Analysis and Discussion of Results

approximate the distance above the original river-bed level at which the outlet should be placed. Designers must however keep in mind that the scouring induced by pressure flushing is only local and that any storage below the low-level outlet will become dead storage and fill up with sediment. **Figure 5.4** shows the scour cone height results plotted against water depth and discharge at different sediment levels. The trends are fairly similar to those of the scour length and width where the flat rectangular and square outlets performed best.

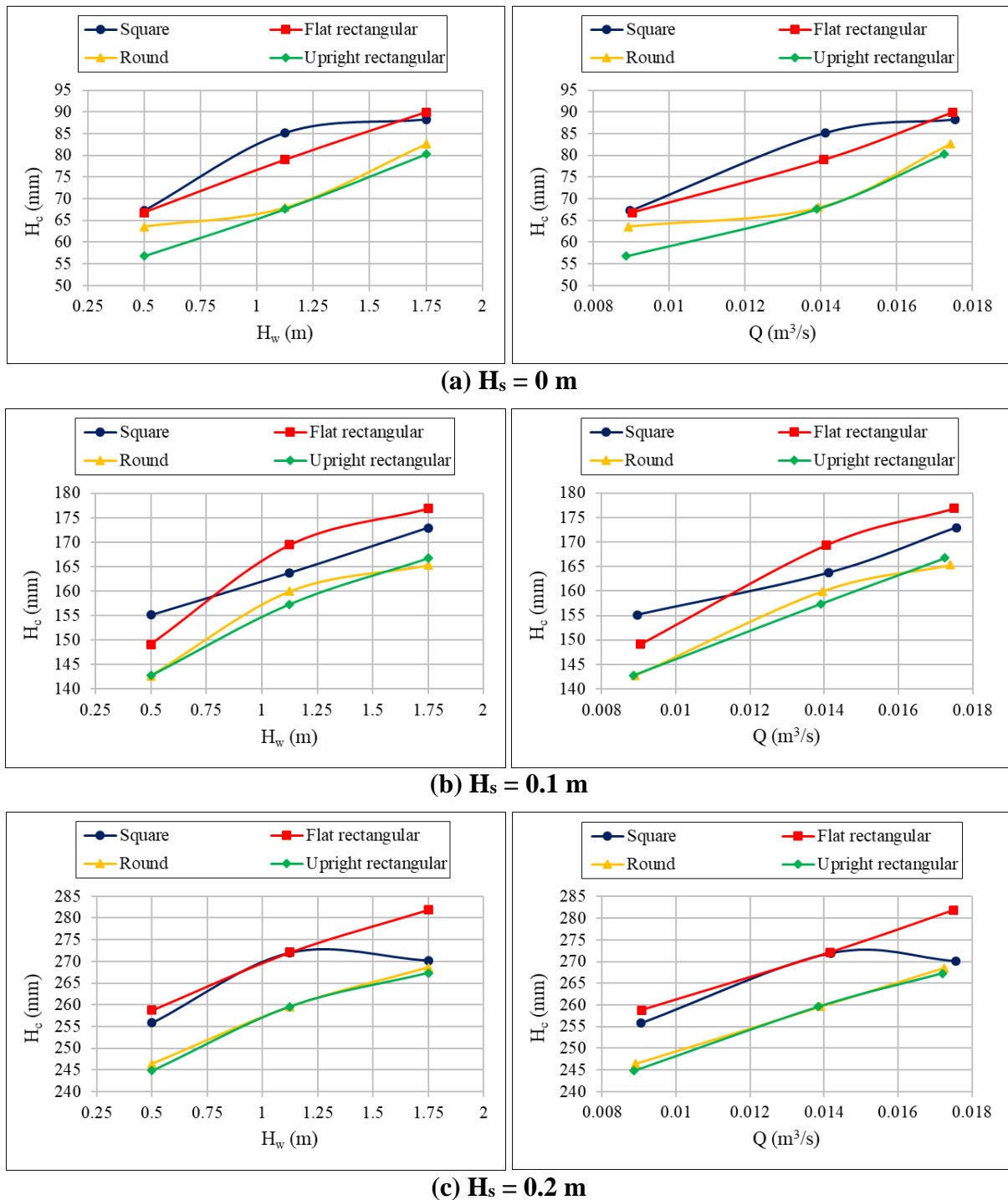


Figure 5.4 Cone height comparison for different outlet shapes and sediment levels

Chapter 5: Analysis and Discussion of Results

5.1.3.1 Outlet Shape Effect

The performance of the three other outlets was compared to that of the round outlet and the results are shown in **Table 5.7**. Although there are differences between the shapes, these differences are not as significant as for the length and width as presented in **Table 5.4**. One exception was observed with $H_w = 1.125\text{ m}$ and $H_s = 0\text{ m}$, where the round outlet performed significantly worse than the square and flat rectangular shapes. The outlet shape seems to reduce slightly with increasing sediment level. The flat rectangular outlet was overall the best performing outlet in terms of scour cone height, with the exception of a few tests where the square outlet was better.

Table 5.7 Cone height comparison of different outlet shapes compared to round outlet

H_s (m)	H_w (m)	Discharge		Height (mm) and % difference from round outlet						
		Range (l/s)	% Increase	Round	Square		Flat rectangular		Upright rectangular	
0	1.75	17.25-17.54	94-95%	83	88	7%	90	9%	80	-3%
	1.125	13.9-14.11	56-58%	68	85	25%	79	16%	68	0%
	0.5	8.87-9.02	0%	64	67	6%	67	5%	57	-11%
0.1	1.75	17.25-17.55	93-96%	165	173	5%	177	7%	167	1%
	1.125	13.9-14.12	55-58%	160	164	2%	169	6%	157	-2%
	0.5	8.87-9.02	0%	143	155	9%	149	5%	143	0%
0.2	1.75	17.2-17.55	93-95%	269	270	1%	282	5%	267	0%
	1.125	13.9-14.11	56-57%	260	272	5%	272	5%	260	0%
	0.5	8.86-9.07	0%	246	256	4%	259	5%	245	-1%

5.1.3.2 Discharge and Water Depth Effect

A comparison of the cone height at different discharges is presented in **Table 5.8**. As shown, the discharge effect is greatest at the lowest sediment level and decreases with increasing sediment levels. The effect of discharge on scour cone height was very similar to the effect of discharge on cone width shown in **Table 5.5**. The effect of discharge on cone height also seems similar for all outlet shapes.

Table 5.8 Comparison of the cone height increase with increasing discharge

H_s (m)	H_w (m)	Discharge		Height (mm) and % increase from lowest discharge							
		Range (l/s)	% Increase	Square		Flat rectangular		Round		Upright rectangular	
0	1.75	17.25-17.54	94-95%	88	31%	90	35%	83	30%	80	41%
	1.125	13.9-14.11	56-58%	85	27%	79	18%	68	7%	68	19%
	0.5	8.87-9.02	0%	67	0%	67	0%	64	0%	57	0%
0.1	1.75	17.25-17.55	93-96%	173	11%	177	19%	165	16%	167	17%
	1.125	13.9-14.12	55-58%	164	6%	169	14%	160	12%	157	10%
	0.5	8.87-9.02	0%	155	0%	149	0%	143	0%	143	0%
0.2	1.75	17.2-17.55	93-95%	270	6%	282	9%	269	9%	267	9%
	1.125	13.9-14.11	56-57%	272	6%	272	5%	260	5%	260	6%
	0.5	8.86-9.07	0%	256	0%	259	0%	246	0%	245	0%

5.1.3.3 Sediment Level Effect

Since the cone height was directly related to the sediment level, a significant increase was observed with increasing sediment level. As was the case for cone length and width, the height was also more sensitive to increasing sediment levels at lower discharges/water depths. The upright rectangular outlet was most sensitive to sediment level variation at all discharges, as can be seen in **Table 5.9**.

Table 5.9 Comparison of the cone height increase with increasing sediment level

Discharge (l/s)	H_w (m)	H_s (m)	Height (mm) and % increase from lowest sediment level							
			Square		Flat rectangular		Round		Upright rectangular	
17.2-17.55	1.75	0	88	0%	90	0%	83	0%	80	0%
		0.1	173	96%	177	97%	165	100%	167	108%
		0.2	270	206%	282	213%	269	225%	267	233%
13.9-14.12	1.125	0	85	0%	79	0%	68	0%	68	0%
		0.1	164	92%	169	115%	160	135%	157	133%
		0.2	272	219%	272	245%	260	282%	260	284%
8.86-9.07	0.5	0	67	0%	67	0%	64	0%	57	0%
		0.1	155	131%	149	123%	143	125%	143	151%
		0.2	256	281%	259	287%	246	288%	245	331%

5.1.4 Cone Depth

The cone depth was the depth of scour below the invert level and is partially discussed in **Section 5.1.3** as part of the cone height analysis.

5.1.4.1 Outlet Shape Effect

The effect of the outlet shape on the cone depth was determined by comparing the three other outlets to the round shape as shown in **Table 5.10**. The results were very similar to those of the

Chapter 5: Analysis and Discussion of Results

cone height analysis due to the way the two dimensions are linked. In general, the flat rectangular outlet created the deepest scour cones and the upright rectangular outlet the least deep scour cones, with a few exceptions. Unlike the results of cone length, width and height, the outlet shape effect did not decrease with an increase in sediment level.

Table 5.10 Cone depth comparison of different outlet shapes compared to round outlet

H_s (m)	H_w (m)	Discharge		Depth (mm) and % difference from round outlet						
		Range (l/s)	% Increase	Round	Square		Flat rectangular		Upright rectangular	
0	1.75	17.25-17.54	94-95%	83	88	7%	90	9%	80	-3%
	1.125	13.9-14.11	56-58%	68	85	25%	79	16%	68	0%
	0.5	8.87-9.02	0%	64	67	6%	67	5%	57	-11%
0.1	1.75	17.25-17.55	93-96%	65	73	12%	77	18%	67	2%
	1.125	13.9-14.12	55-58%	60	64	6%	69	16%	57	-4%
	0.5	8.87-9.02	0%	43	55	29%	49	15%	43	0%
0.2	1.75	17.2-17.55	93-95%	69	70	2%	82	19%	67	-2%
	1.125	13.9-14.11	56-57%	60	72	21%	72	21%	60	0%
	0.5	8.86-9.07	0%	46	56	20%	59	27%	45	-3%

5.1.4.2 Discharge and Water Depth Effect

The effect of discharge on the cone depth is shown in **Table 5.11**. The effect of discharge seems to be relatively constant for all sediment levels, which was not the case for the cone length, width and height where the discharge effect reduced with an increase in sediment level. The increase in discharge however, had a slightly greater effect on the cone depth at the medium sediment level $H_s = 0.1$ m, with the exception of the square outlet.

Table 5.11 Comparison of the cone depth increase with increasing discharge

H_s (m)	H_w (m)	Discharge		Depth (mm) and % increase from lowest discharge							
		Range (l/s)	% Increase	Square		Flat rectangular		Round		Upright rectangular	
0	1.75	17.25-17.54	94-95%	88	31%	90	35%	83	30%	80	41%
	1.125	13.9-14.11	56-58%	85	27%	79	18%	68	7%	68	19%
	0.5	8.87-9.02	0%	67	0%	67	0%	64	0%	57	0%
0.1	1.75	17.25-17.55	93-96%	73	32%	77	56%	65	53%	67	56%
	1.125	13.9-14.12	55-58%	64	16%	69	41%	60	40%	57	34%
	0.5	8.87-9.02	0%	55	0%	49	0%	43	0%	43	0%
0.2	1.75	17.2-17.55	93-95%	70	26%	82	39%	69	48%	67	50%
	1.125	13.9-14.11	56-57%	72	29%	72	23%	60	28%	60	33%
	0.5	8.86-9.07	0%	56	0%	59	0%	46	0%	45	0%

5.1.4.3 Sediment Level Effect

The analysis of the sediment level effect on the cone depth is shown in **Table 5.12**. This analysis yielded interesting results, indicating that the difference in scour depth was greater between H_s

Chapter 5: Analysis and Discussion of Results

= 0 m and $H_s = 0.1$ m, than between $H_s = 0$ m and $H_s = 0.2$ m. Only two exceptions to this was observed, namely for the square and flat rectangular outlets at $H_w = 1.75$ m, where the cone depth was very similar between $H_s = 0.1$ and $H_s = 0.2$ m.

Table 5.12 Comparison of the cone depth decrease with increasing sediment level

Discharge (l/s)	H_w (m)	H_s (m)	Depth (mm) and % decrease from lowest sediment level							
			Square		Flat rectangular		Round		Upright rectangular	
17.2-17.55	1.75	0	88	0%	90	0%	83	0%	80	0%
		0.1	73	-17%	77	-15%	65	-21%	67	-17%
		0.2	70	-20%	82	-9%	69	-17%	67	-16%
13.9-14.12	1.125	0	85	0%	79	0%	68	0%	68	0%
		0.1	64	-25%	69	-12%	60	-12%	57	-15%
		0.2	72	-15%	72	-9%	60	-12%	60	-12%
8.86-9.07	0.5	0	67	0%	67	0%	64	0%	57	0%
		0.1	55	-18%	49	-26%	43	-33%	43	-25%
		0.2	56	-17%	59	-12%	46	-27%	45	-21%

Figure 5.5 illustrates the scour cone depth plotted against the sediment level, further showing that the cone depth initially decreased when the sediment level was raised to $H_s = 0.1$ m and then increased again when the sediment level was raised further to $H_s = 0.2$ m. This could be ascribed to a different vortex formation and increased turbulence at the higher sediment level, leading to a deeper cone. Taking velocity measurements upstream of the outlet was outside the scope of this study but could in future provide an idea of the flow pattern inside the cone and thus better explain this observation.

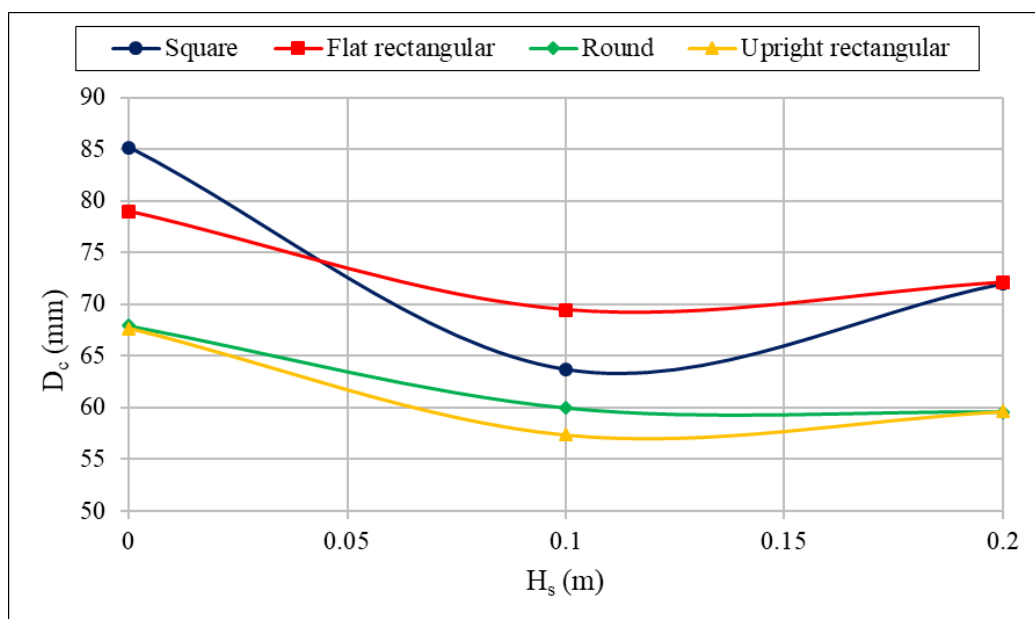


Figure 5.5 Scour depth versus sediment level plot for $H_w = 1.125$ m

Chapter 5: Analysis and Discussion of Results

5.1.5 Cone Volume

The scour cone volume provides an important insight into the amount of sediment that can be removed in a pressure flushing event and is also used to calculate the flushing efficiency. The volume of the scour cone is related to the combination of cone length, width and height and was computed for each test as explained in **Section 4.1**. **Figure 5.6** shows the cone volume versus water depth and discharge for different outlet shapes and sediment levels.

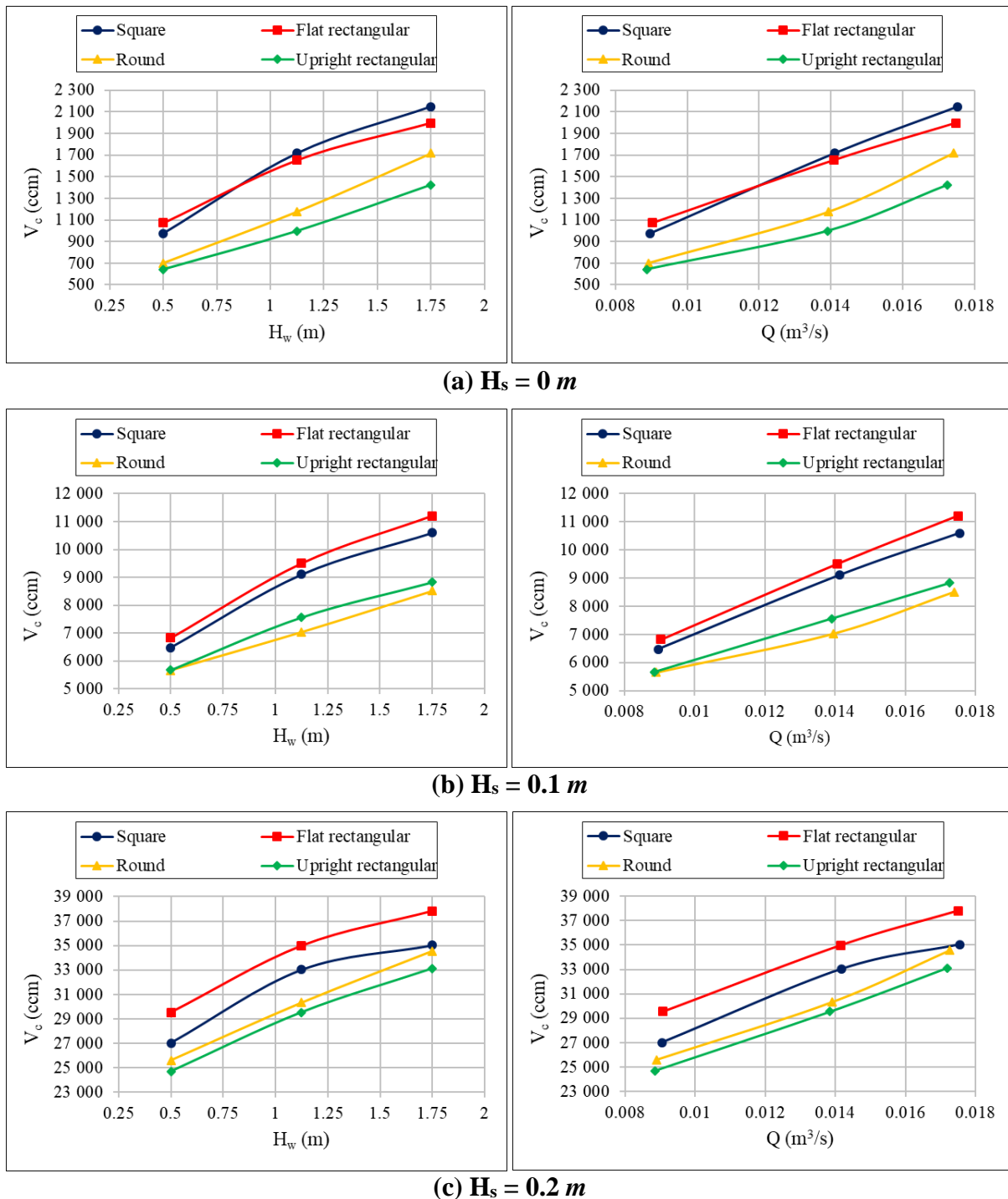


Figure 5.6 Cone volume comparison for different outlet shapes and sediment levels

Chapter 5: Analysis and Discussion of Results

5.1.5.1 Outlet Shape Effect

Table 5.13 compares the cone volume results of the different outlets with the round outlet. The square and flat rectangular outlets performed significantly better than the round outlet, specifically at $H_s = 0\text{ m}$ and $H_s = 0.1\text{ m}$. At $H_s = 0\text{ m}$, the upright rectangular outlet performed significantly worse than all others, but was better than the round outlet with $H_s = 0.1\text{ m}$. It is also observed that the outlet shape effect generally reduces with an increase in sediment level.

Table 5.13 Cone volume comparison of different outlet shapes compared to round outlet

H_s (m)	H_w (m)	Discharge		Volume (10^{-3} m^3) and % difference from round outlet						
		Range (l/s)	% Increase	Round	Square		Flat rectangular		Upright rectangular	
0	1.75	17.25-17.54	94-95%	1.719	2.148	25%	1.997	16%	1.425	-17%
	1.125	13.9-14.11	56-58%	1.178	1.717	46%	1.654	40%	0.998	-15%
	0.5	8.87-9.02	0%	0.702	0.975	39%	1.074	53%	0.642	-9%
0.1	1.75	17.25-17.55	93-96%	8.509	10.597	25%	11.206	32%	8.822	4%
	1.125	13.9-14.12	55-58%	7.031	9.101	29%	9.500	35%	7.561	8%
	0.5	8.87-9.02	0%	5.657	6.477	14%	6.823	21%	5.668	0%
0.2	1.75	17.2-17.55	93-95%	34.554	35.038	1%	37.823	9%	33.116	-4%
	1.125	13.9-14.11	56-57%	30.326	33.031	9%	34.986	15%	29.534	-3%
	0.5	8.86-9.07	0%	25.604	27.009	5%	29.537	15%	24.693	-4%

5.1.5.2 Discharge and Water Depth Effect

As mentioned, the cone volume is directly related to the discharge through the outlet. A comparison is shown in **Table 5.14**. The results indicate that the sensitivity to discharge reduces with an increase in the sediment level for all outlet shapes. At the lowest sediment level, the cone volume of the flat rectangular outlet is least affected by an increase in discharge, but at the highest sediment level the outlets were all similarly influenced (in % increase in volume) by discharge changes.

Table 5.14 Comparison of the cone volume increase with increasing discharge

H_s (m)	H_w (m)	Discharge		Volume (10^{-3} m^3) and % increase from lowest discharge							
		Range (l/s)	% Increase	Square		Flat rectangular		Round		Upright rectangular	
0	1.75	17.25-17.54	94-95%	2.148	120%	1.997	86%	1.719	145%	1.425	122%
	1.125	13.9-14.11	56-58%	1.717	76%	1.654	54%	1.178	68%	0.998	55%
	0.5	8.87-9.02	0%	0.975	0%	1.074	0%	0.702	0%	0.642	0%
0.1	1.75	17.25-17.55	93-96%	10.597	64%	11.206	64%	8.509	50%	8.822	56%
	1.125	13.9-14.12	55-58%	9.101	41%	9.500	39%	7.031	24%	7.561	33%
	0.5	8.87-9.02	0%	6.477	0%	6.823	0%	5.657	0%	5.668	0%
0.2	1.75	17.2-17.55	93-95%	35.038	30%	37.823	28%	34.554	35%	33.116	34%
	1.125	13.9-14.11	56-57%	33.031	22%	34.986	18%	30.326	18%	29.534	20%
	0.5	8.86-9.07	0%	27.009	0%	29.537	0%	25.604	0%	24.693	0%

Chapter 5: Analysis and Discussion of Results

5.1.5.3 Sediment Level Effect

As expected (when comparing the cone volumes at different sediment levels shown in **Table 5.15**) it is clear that there is a major increase in volume with an increase in sediment level. The effect of increasing the sediment level is greatest at lower discharges where the water depth is also less. Increasing the sediment level by 0.1 m when the water is only 0.5 m, greatly reduces the water depth above the sediment bed and thus simulates conditions similar to drawdown of the water level which leads to greater scour.

Table 5.15 Comparison of the cone volume increase with increasing sediment level

Discharge (<i>l/s</i>)	H_w (m)	H_s (m)	Volume ($10^{-3} m^3$) and % increase from lowest sediment level							
			Square		Flat rectangular		Round		Upright rectangular	
17.2-17.55	1.75	0	2.148	0%	1.997	0%	1.719	0%	1.425	0%
		0.1	10.597	393%	11.206	461%	8.509	395%	8.822	519%
		0.2	35.038	1531%	37.823	1794%	34.554	1910%	33.116	2224%
13.9-14.12	1.125	0	1.717	0%	1.654	0%	1.178	0%	0.998	0%
		0.1	9.101	430%	9.500	474%	7.031	497%	7.561	658%
		0.2	33.031	1824%	34.986	2015%	30.326	2474%	29.534	2859%
8.86-9.07	0.5	0	0.975	0%	1.074	0%	0.702	0%	0.642	0%
		0.1	6.477	564%	6.823	535%	5.657	706%	5.668	783%
		0.2	27.009	2670%	29.537	2650%	25.604	3547%	24.693	3746%

5.1.6 Summary

In summary, the general findings from the scour cone geometry analysis are as follows:

- the scour cone dimensions are significantly influenced by the outlet shape,
- the flat rectangular outlet was the overall best performer in terms of sediment removal and flushing efficiency,
- the square and flat rectangular outlets generally performed similarly, whilst the round and upright rectangular outlets followed similar trends,
- an increase in water depth led to an increase in scour cone dimensions (length, width, height and volume), and
- an increase in sediment level led to a dramatic increase in scour cone dimensions (length, width, height and volume).

5.2 Comparison with Literature

The scour cone geometry results were compared to the predictions of other authors' equations. It was found that most equations used the outlet diameter for scour cone prediction, which meant that they could only be applied to one of the four outlets. Another problem was that most equations were developed for sediment heights above the outlet and did thus not apply for $H_s = 0\text{ m}$ which represents a third of the tests. Several equations from many different authors were tested, but most did not correlate well with the results from this study. This was due to the fact that many authors only tested one outlet shape, sediment size and sediment level, had completely different laboratory conditions or the equations cannot be applied for the range of parameters in this study.

Figure 5.7 shows the cone length and width from the experimental results plotted against the predictions of Meshkati Shahmirzadi *et al.* (2010) which were presented as **Equation 2-47** and **Equation 2-48**. The predicted and measured data correlate well, but it is clear that the predicted values all fall within a small range and do not take into account the outlet shape.

In general the results correlate well with those of Meshkati Shahmirzadi *et al.* (2010), showing that for an increase in sediment level, there is an associated large increase in scour dimensions. However, when the water depth was reduced, the equations predicted an increase in scour cone length and width, which was not the case in the experiments.

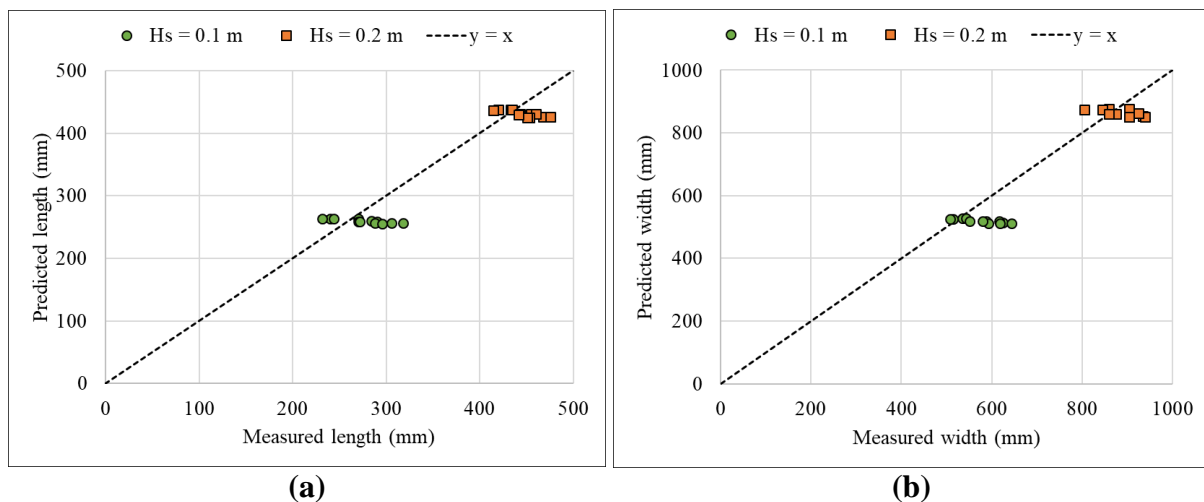


Figure 5.7 Comparison of measured and predicted results by Meshkati Shahmirzadi *et al.* (2010) for (a) cone length and (b) cone width

Chapter 5: Analysis and Discussion of Results

Emamgholizadeh (2006) developed an equation that describes the scour cone volume as shown in **Equation 2-40**. The predicted values from this equation are plotted against the measured data in **Figure 5.8**. Similar to the length and width predictions described, the predicted volume falls within a much smaller range than the range of the experimental results. The equation also underpredicts scour cone volume at $H_s = 0.1\text{ m}$, but overpredicts the cone volume for $H_s = 0.2\text{ m}$. Apart from the deviations by the equation, the general trend of increasing scour dimensions with an increase in sediment level or water depth was still observed.

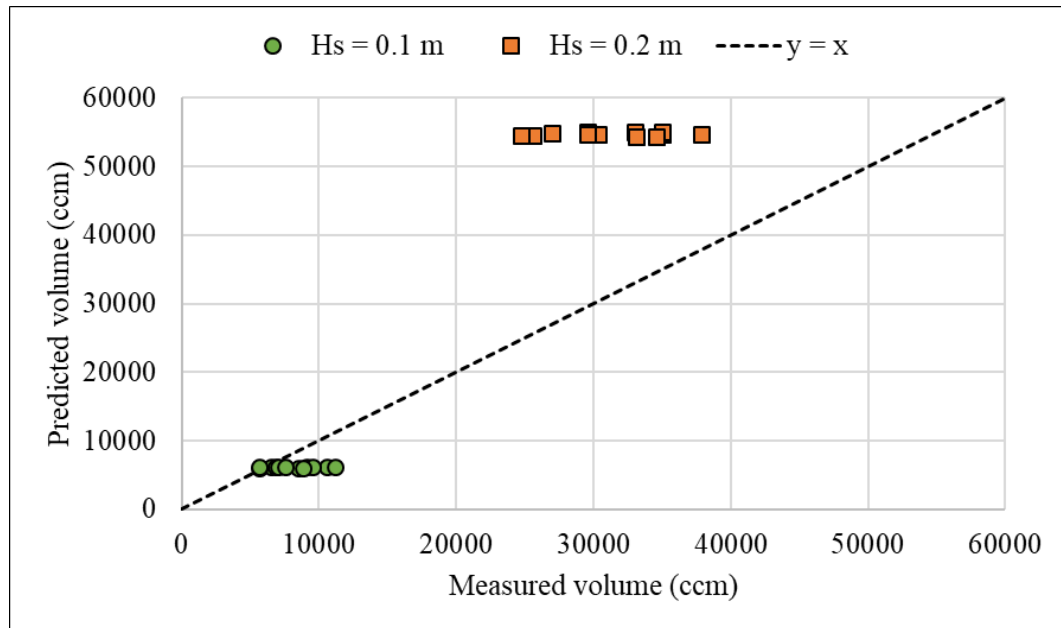


Figure 5.8 Measured versus predicted cone volume from Emamgholizadeh *et al.* (2006)

More scour cone geometry predictions from other studies are compared to the results of this study in **Appendix G**. These predictions by equations of other authors demonstrate how sensitive these equations are to certain parameters and show why they should only be applied within the range of parameters for which they were developed. **Appendix G** shows that some equations greatly over- or underpredict the scour cone geometry and that care should be taken when applying these in real-life scenarios.

5.3 Regression Analysis

Multi-linear regression analysis was done on the results of this study to find non-dimensional equations that define the scour cone geometry. **Table 5.16** gives the range of the different parameters involved in the regression analysis.

Table 5.16 Range of parameters in regression analysis

Parameter	Symbol	Range
Scour cone length (<i>m</i>)	L_c	0.109 – 0.476
Scour cone width (<i>m</i>)	W_c	0.268 – 0.940
Scour cone height (<i>m</i>)	H_c	0.0568 – 0.282
Scour cone depth (<i>m</i>)	D_c	0.0427 – 0.0899
Scour cone volume (m^3)	V_c	0.00064 – 0.03782
Water depth (<i>m</i>)	H_w	0.5 – 1.75
Sediment level (<i>m</i>)	H_s	0 – 0.2
Outlet velocity (<i>m/s</i>)	U_o	1.67 – 3.50
Outlet centreline width (<i>m</i>)	b_{oc}	0.05 – 0.10
Outlet edge width (<i>m</i>)	b_{oe}	0 – 0.1

5.3.1 Simplification Process

The $\frac{H_s}{H_w}$ term had to be changed since the sediment level was set to zero ($H_s = 0$ m) for some of the tests and thus the term would lead to problems in the regression analysis. The term was therefore changed to:

$$\pi_1 = \frac{H_w}{H_w - H_s} \quad 5-1$$

To further simplify the regression analysis, terms 7 and 9, as well as 8 and 10 of **Equation 3-5**, were combined. The following dimensionless parameters were used to define the scour geometry:

$$\left\{ \frac{H_w}{H_w - H_s}, \frac{U_o}{\sqrt{gH_w}}, \frac{b_{oc} + b_{oe}}{H_w}, \frac{h_{oc} + h_{oe}}{H_w}, \frac{P_o}{H_w}, \frac{R_o}{H_w} \right\} \quad 5-2$$

To simplify the parameters contained in **Equation 5-2**, initially a sensitivity analysis with all six terms was conducted to determine the sensitivity of the scour cone geometry to each of the terms. The sensitivity analysis was started by performing a regression analysis with all terms and then excluding terms with the least effect (p-value > 0.05, see discussion of statistical parameters in **Section 5.3.2**) one by one, also referred to as “reducing the model”. From the

Chapter 5: Analysis and Discussion of Results

sensitivity analysis, it was found that $\frac{P_o}{H_w}$ and $\frac{R_o}{H_w}$ had little influence on the results and a good correlation could not be found with any of the three models. Thus, these two terms were also eliminated since they were already represented in the other terms (outlet area and dimensions). The $\frac{h_{oc}+h_{oe}}{H_w}$ term also had no significant influence on the regression analysis (p-value > 0.05). The final parameters were thus:

$$\left\{ \frac{H_w}{H_w - H_s}, \frac{U_o}{\sqrt{gH_w}}, \frac{b_{oc} + b_{oe}}{H_w} \right\} \quad 5-3$$

These three terms incorporated all the independent variables which were varied in the experiments while also accounting for the shape of the outlet. **Table 5.17** shows the range of each of the terms in the experiments.

Table 5.17 Range of dimensionless parameters

Label	Term	Range
Q_1	$\frac{H_w}{H_w - H_s}$	1 – 1.667
Q_2	$\frac{U_o}{\sqrt{gH_w}}$	0.799 – 0.852
Q_3	$\frac{b_{oc} + b_{oe}}{H_w}$	0.046 – 0.4

5.3.2 Models

The dimensional analysis in **Section 3.2** and simplification in **Section 5.3.1** indicated that the experiments were a function of three variables and can be written as:

$$Q_0 = f(Q_1, Q_2, Q_3) \quad 5-4$$

where:

Q_0 = dependent variable

$Q_{1,2,3}$ = independent variables

The three terms in **Equation 5-3** can then be written as:

$$Q_1 = \frac{H_w}{H_w - H_s} \quad 5-5$$

$$Q_2 = \frac{U_o}{\sqrt{gH_w}} \quad 5-6$$

Chapter 5: Analysis and Discussion of Results

$$Q_3 = \frac{b_{oc} + b_{oe}}{H_w} \quad 5-7$$

This presents a complex problem which required multi-linear regression analysis. The regression analysis was done in Microsoft Excel. Three regression models were each analysed for length, width, height, depth and volume of scour. The regression models analysed were Linear, Logarithmic Transformed and Linear Logarithmic.

Linear:

$$Q_0 = k + a \cdot Q_1 + b \cdot Q_2 + c \cdot Q_3 \quad 5-8$$

where:

k = intercept value (constant)

a, b, c = coefficients

Logarithmic Transformed:

$$\ln(Q_0) = \ln(k) + a \cdot \ln(Q_1) + b \cdot \ln(Q_2) + c \cdot \ln(Q_3) \quad 5-9$$

which is transformed by a natural log-transformation to exponential form:

$$Q_0 = k \cdot Q_1^a \cdot Q_2^b \cdot Q_3^c \quad 5-10$$

Linear-Logarithmic:

$$Q_0 = k + a \cdot \ln(Q_1) + b \cdot \ln(Q_2) + c \cdot \ln(Q_3) \quad 5-11$$

From the regression analysis it was observed that adding the intercept to the model increased the average error and decreased the coefficient of determination for all the models. The intercept represents Q_0 when all other parameters are zero, but when the other parameters are zero, Q_0 must also be zero since no scour can take place. The intercept was therefore removed from the regression analysis by forcing it to be zero.

Distinguishing between the models was possible by analysing several statistical parameters of each model. The following statistical parameters (formulae given in **Appendix H**) were analysed:

- The coefficient of determination, R^2 , is commonly used to analyse how differences in one variable can be explained by the difference in a second variable. In other words, it gives an idea of how many data points fall within the results of the line formed by the regression equation. The R^2 value ranges from 0 to 1, with higher values indicating a

Chapter 5: Analysis and Discussion of Results

better goodness of fit for the observations. One problem with R^2 is that it increases each time a data point is added and can thus be misleading.

- Adjusted R^2 is an adjustment of the R^2 that accounts for the number of variables in the data set. The adjusted R^2 only increases if a new data point improves the regression more than you would expect by chance.
- The p-value or probability value for a term tests the null hypothesis that the coefficient is equal to zero. A low p-value (typically < 0.05) indicates that the null hypothesis can be rejected, since the term makes a meaningful contribution to the model. High p-values on the other hand imply that changes in the predictor are not associated with changes in the response.
- Mean absolute error (MAE) measures the average magnitude of the errors in a set of predictions, without considering the error direction. The MAE is a linear score since all individual differences are weighted equally in the average. It measures accuracy for continuous variables.
- Root mean squared error (RMSE) is the standard deviation of the prediction errors. It is a measure of how spread out the residuals are, in other words how concentrated the data is around the line of best fit.

5.3.3 Scour Cone Length

The scour cone length could be written in functional form as:

$$\frac{L_c}{H_w} = f\left(\frac{H_w}{H_w - H_s}, \frac{U_o}{\sqrt{gH_w}}, \frac{b_{oc} + b_{oe}}{H_w}\right) \quad 5-12$$

A summary of the analysis of the three regression models is given in **Table 5.18**. The Linear Logarithmic Model produced the most accurate prediction of the scour cone length with an average error of 5.84% and $R^2 = 0.998$.

Table 5.18 Regression analysis summary for scour cone length

Regression Model	R^2	Avg Error (%)	Max error (%)	a	b	c
Linear	0.996	8.34%	35.86%	0.948	-1.003	0.387
Log Transformed	0.971	21.10%	76.48%	3.085	4.557	0.410
Linear Logarithmic	0.998	5.84%	22.65%	1.206	-1.459	0.054

Chapter 5: Analysis and Discussion of Results

The equation to predict the cone length is given by:

$$\frac{L_c}{H_w} = 1.2060 \cdot \ln\left(\frac{H_w}{H_w - H_s}\right) - 1.4594 \cdot \ln\left(\frac{U_o}{\sqrt{gH_w}}\right) + 0.0536 \cdot \ln\left(\frac{b_{oc} + b_{oe}}{H_w}\right) \quad 5-13$$

Figure 5.9 compares the predicted values from **Equation 5-13** and the observed values from the experiments. The plots indicate that the equation provides a good estimate for scour cone length at all discharges, water depths and different outlet shapes and that there are no apparent outliers. Statistical parameters for the scour cone length regression analysis are given in **Appendix I**.

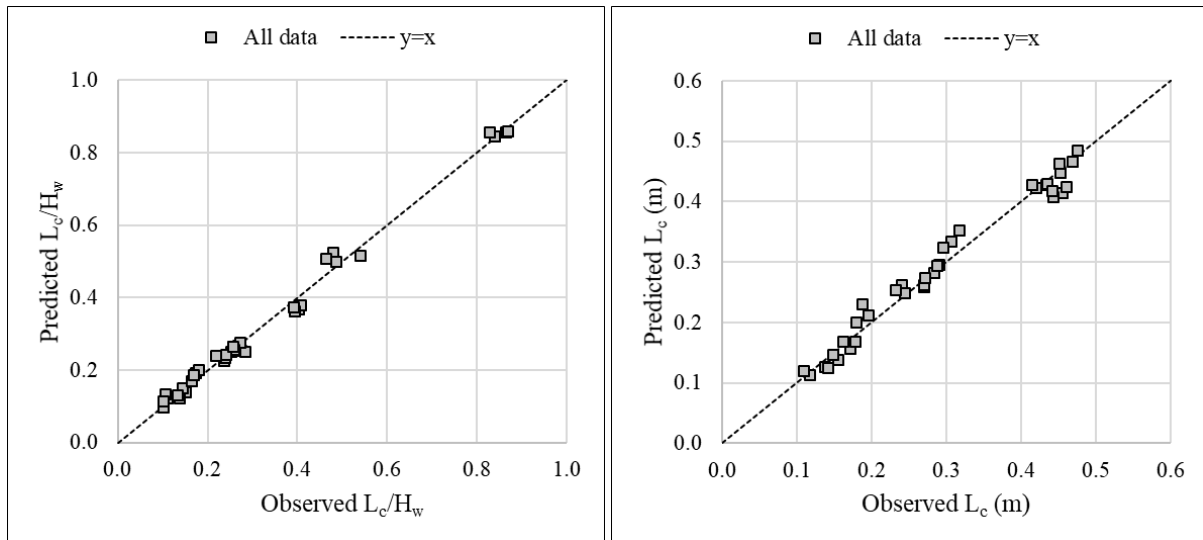


Figure 5.9 Scatter plots comparing observed and predicted values for the cone length

5.3.4 Scour Cone Width

The scour cone width could be written in functional form as:

$$\frac{W_c}{H_w} = f\left(\frac{H_w}{H_w - H_s}, \frac{U_o}{\sqrt{gH_w}}, \frac{b_{oc} + b_{oe}}{H_w}\right) \quad 5-14$$

A summary of the analysis of the three regression models is given in **Table 5.19**. Similar to the regression analysis of the cone length, the Linear Logarithmic Model produced the most accurate prediction of the scour cone width with an average error of 6.14% and $R^2 = 0.995$.

Table 5.19 Regression analysis summary for scour cone width

Regression Model	R ²	Avg Error (%)	Max error (%)	a	b	c
Linear	0.995	10.23%	45.92%	1.846	-1.947	0.963
Log Transformed	0.927	19.66%	68.65%	2.829	0.833	0.384
Linear Logarithmic	0.998	6.14%	27.71%	2.306	-3.420	0.136

Chapter 5: Analysis and Discussion of Results

The equation to predict the cone width is given by:

$$\frac{W_c}{H_w} = 2.3065 \cdot \ln\left(\frac{H_w}{H_w - H_s}\right) - 3.4197 \cdot \ln\left(\frac{U_o}{\sqrt{gH_w}}\right) + 0.1360 \cdot \ln\left(\frac{b_{oc} + b_{oe}}{H_w}\right) \quad 5-15$$

Figure 5.10 compares the predicted values from **Equation 5-15** and the observed values from the experiments. The plots indicate that the equation provides a good estimate for scour cone width for all the tests conducted and that no major outliers are present. Statistical parameters for the scour cone width regression analysis are given in **Appendix I**.

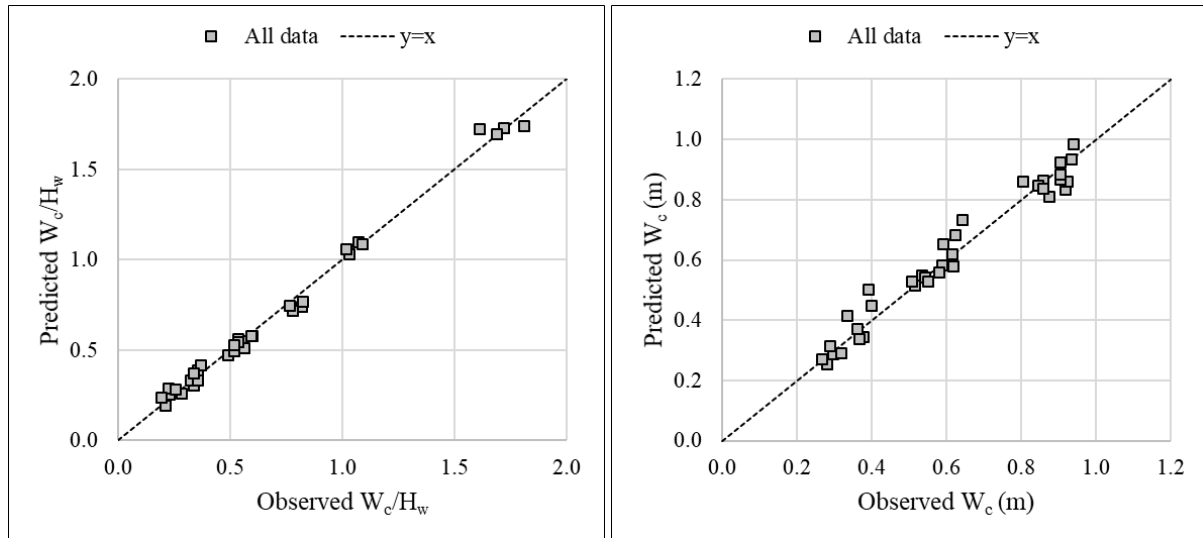


Figure 5.10 Scatter plots comparing observed and predicted values for the cone width

5.3.5 Scour Cone Height

The scour cone height could be written in functional form as:

$$\frac{H_c}{H_w} = f\left(\frac{H_w}{H_w - H_s}, \frac{U_o}{\sqrt{gH_w}}, \frac{b_{oc} + b_{oe}}{H_w}\right) \quad 5-16$$

A summary of the analysis of the three regression models is given in **Table 5.20**. Similar to the regression analysis of the cone length and width, the Linear Logarithmic Model produced the most accurate prediction of the scour cone height with an average error of 6.29% and $R^2 = 0.998$.

Table 5.20 Regression analysis summary for scour cone height

Regression Model	R^2	Avg Error (%)	Max error (%)	a	b	c
Linear	0.994	12.90%	57.52%	0.593	-0.639	0.183
Log Transformed	0.974	29.16%	100.07%	3.588	7.589	0.454
Linear Logarithmic	0.998	6.29%	31.25%	0.761	-0.752	0.028

Chapter 5: Analysis and Discussion of Results

The equation to predict the cone height is given by:

$$\frac{H_c}{H_w} = 0.7615 \cdot \ln\left(\frac{H_w}{H_w - H_s}\right) - 0.7519 \cdot \ln\left(\frac{U_o}{\sqrt{gH_w}}\right) + 0.0278 \cdot \ln\left(\frac{b_{oc} + b_{oe}}{H_w}\right) \quad 5-17$$

Figure 5.11 compares the predicted values from **Equation 5-17** and the observed values from the experiments. The plots indicate that the equation provides a good estimate for scour cone height for all 36 tests conducted. Statistical parameters for the scour cone height regression analysis are given in **Appendix I**.

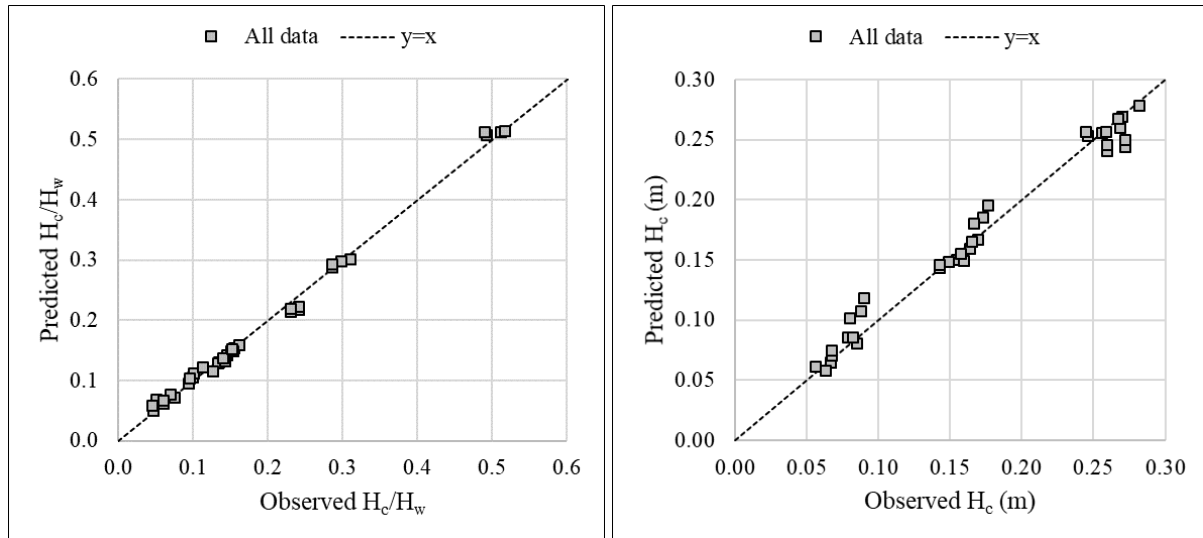


Figure 5.11 Scatter plots comparing observed and predicted values for the cone height

5.3.6 Scour Cone Depth

The scour cone depth could be written in functional form as:

$$\frac{D_c}{H_w} = f\left(\frac{H_w}{H_w - H_s}, \frac{U_o}{\sqrt{gH_w}}, \frac{b_{oc} + b_{oe}}{H_w}\right) \quad 5-18$$

A summary of the analysis of the three regression models is given in **Table 5.21**. Similar to the regression analysis of the other scour cone geometries, the Linear Logarithmic Model produced the most accurate prediction of the scour cone depth with an average error of 10.97% and $R^2 = 0.985$.

Table 5.21 Regression analysis summary for scour cone depth

Regression Model	R^2	Avg Error (%)	Max error (%)	a	b	c
Linear	0.956	16.10%	43.72%	0.003	0.035	0.255
Log Transformed	0.990	24.01%	63.14%	-0.214	5.588	0.778
Linear Logarithmic	0.985	10.97%	26.96%	-0.039	-0.751	0.032

Chapter 5: Analysis and Discussion of Results

The equation to predict the cone depth is given by:

$$\frac{D_c}{H_w} = -0.0386 \cdot \ln\left(\frac{H_w}{H_w - H_s}\right) - 0.7511 \cdot \ln\left(\frac{U_o}{\sqrt{gH_w}}\right) + 0.0317 \cdot \ln\left(\frac{b_{oc} + b_{oe}}{H_w}\right) \quad 5-19$$

Figure 5.12 compares the predicted values from **Equation 5-19** and the observed values from the experiments. The plots indicate that the equation provides a relatively good estimate of the scour depth. The percentage error increases slightly as the depth increases. Statistical parameters for the scour cone depth regression analysis are given in **Appendix I**.

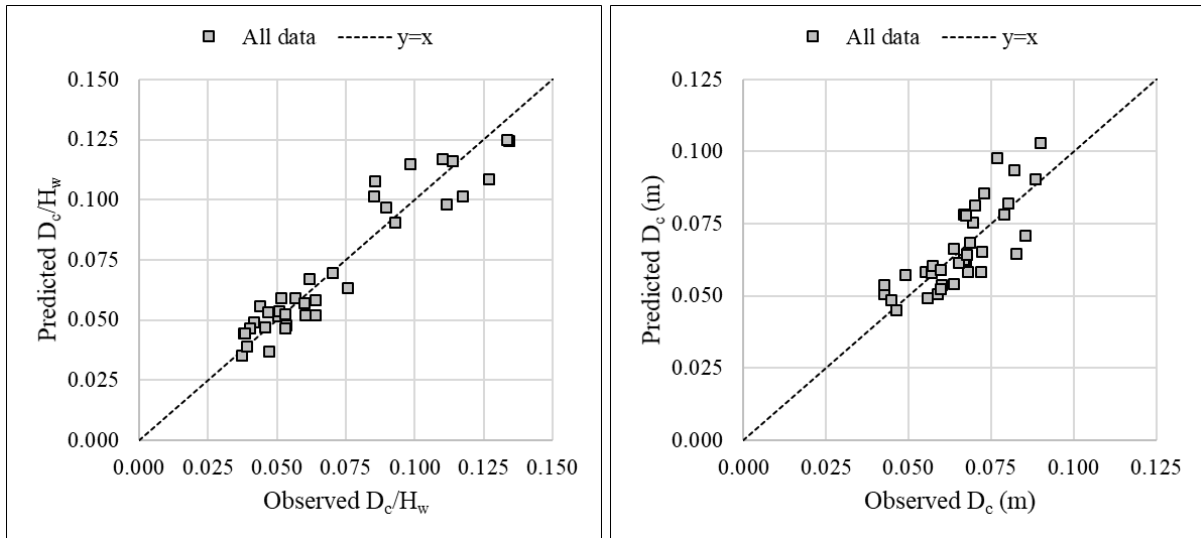


Figure 5.12 Scatter plots comparing observed and predicted values for the cone depth

It is important to note that the scour depth is directly related to the scour height and the sediment level, thus it is preferable to calculate the scour depth by subtracting the sediment level from the scour height as shown in **Equation 5-20**. Since the scour height equation has a better coefficient of determination ($R^2 = 0.998$), this method is preferable and would most likely yield more accurate results when applied.

$$D_c = H_c - H_s \quad 5-20$$

5.3.7 Scour Cone Volume

The scour cone volume could be written in functional form as:

$$\frac{V_c}{H_w^3} = f\left(\frac{H_w}{H_w - H_s}, \frac{U_o}{\sqrt{gH_w}}, \frac{b_{oc} + b_{oe}}{H_w}\right) \quad 5-21$$

A summary of the analysis of the three regression models is given in **Table 5.22**. Finding a good prediction for the volume of the scour cone was more difficult with the chosen parameters. Even though the R^2 -values are relatively high, indicating a good correlation between predicted

Chapter 5: Analysis and Discussion of Results

and observed $\ln\left(\frac{V_c}{H_w^3}\right)$, the average error on the final volume prediction is very high since the error becomes exponential when converting $\ln\left(\frac{V_c}{H_w^3}\right)$ into V_c . The best regression model for prediction of the scour cone volume using the parameters in **Equation 5-21** was the Log Transformed Model.

Table 5.22 Regression analysis summary for scour cone volume

Regression Model	R ²	Avg Error (%)	Max error (%)	a	b	c
Linear	0.946	943.29%	6896.56%	0.286	-0.369	0.059
Log Transformed	0.974	94.72%	598.98%	9.137	16.815	1.426
Linear Logarithmic	0.911	1151.72%	9772.51%	0.364	-0.083	0.014

The equation to predict the cone volume is given by:

$$\frac{V_c}{H_w^3} = \left(\frac{H_w}{H_w - H_s}\right)^{9.1372} \cdot \left(\frac{U_o}{\sqrt{gH_w}}\right)^{16.8151} \cdot \left(\frac{b_{oc} + b_{oe}}{H_w}\right)^{1.4263} \quad 5-22$$

Figure 5.13 compares the predicted values from **Equation 5-23** and the observed values from the experiments. The plots indicate that the equation does not predict the scour cone volume accurately and that the error increases significantly for larger cones.

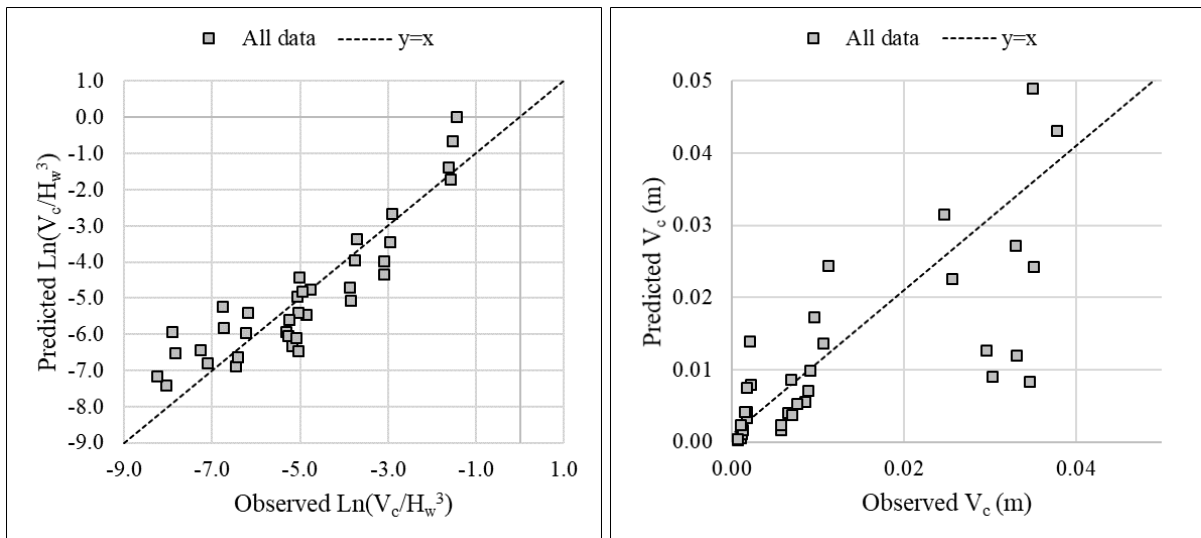


Figure 5.13 Scatter plots comparing observed and predicted values for the cone volume

Since the scour cone volume is directly related to the cone geometry, namely length, width and height, a better volume prediction was expected when writing the volume in the following functional form:

$$\frac{V_c}{H_w^3} = f\left(\frac{L_c}{H_w}, \frac{W_c}{H_w}, \frac{H_c}{H_w}\right) \quad 5-23$$

Chapter 5: Analysis and Discussion of Results

Since length, width and height could all be estimated using the developed equations which included a shape parameter, the volume prediction also indirectly includes that parameter, thus taking into account the outlet shape. **Table 5.23** provides a summary of the regression analysis using the new parameters. Since volume is three-dimensional, it is expected that the linear models would not provide a good prediction, as was the case for the regression analysis shown in **Table 5.22**.

Table 5.23 Regression summary for improved volume prediction

Regression Model	R ²	Avg Error (%)	Max error (%)	a	b	c
Linear	0.783	460.08%	2523.63%	0.224	-0.345	1.095
Log Transformed	0.999	10.98%	35.49%	1.953	-0.379	1.366
Linear Logarithmic	0.760	1312.79%	10496.36%	0.381	0.023	-0.285

However, the Log Transformed Model provided a very good prediction for the volume with an R² -value of 0.999 and an average error of 10.98%. **Equation 5-24** and **5-25** represent the Log Transformed Regression Model. Statistical parameters for the scour cone volume regression analysis are given in **Appendix I**.

$$\frac{V_c}{H_w^3} = \left(\frac{L_c}{H_w}\right)^{1.9529} \cdot \left(\frac{W_c}{H_w}\right)^{-0.3787} \cdot \left(\frac{H_c}{H_w}\right)^{1.3663} \quad 5-24$$

simplified to:

$$V_c = L_c^{1.9529} \cdot W_c^{-0.3787} \cdot H_c^{1.3663} \cdot H_w^{0.0595} \quad 5-25$$

Figure 5.14 shows the predicted versus observed cone volume for the new equation. The new equation provides a more accurate prediction for the cone volume than **Equation 5-22**. In **Figure 5.14** (b) it can be observed that the volume is slightly overestimated where $V_c > 0.02 \text{ m}^3$ which corresponds to the tests where $H_s = 0.2 \text{ m}$.

Chapter 5: Analysis and Discussion of Results

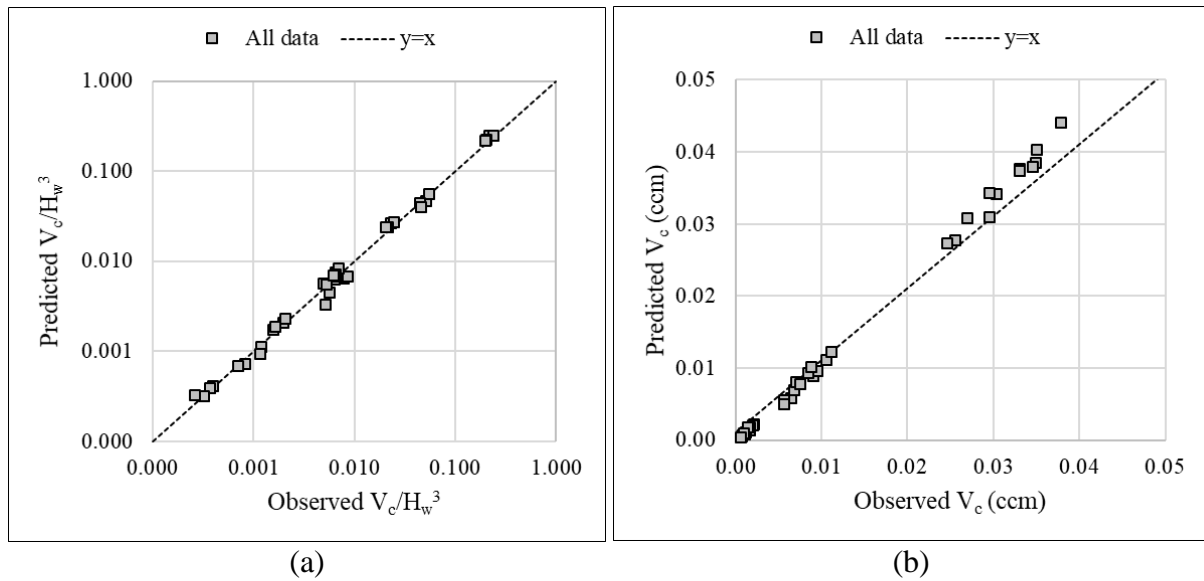


Figure 5.14 Scatter plots comparing observed and predicted values for the improved cone volume regression

In order to compensate for the slight overestimation for higher sediment levels, the observed versus predicted cone volume was plotted and a curve fitted through the data as shown in **Figure 5.15**.

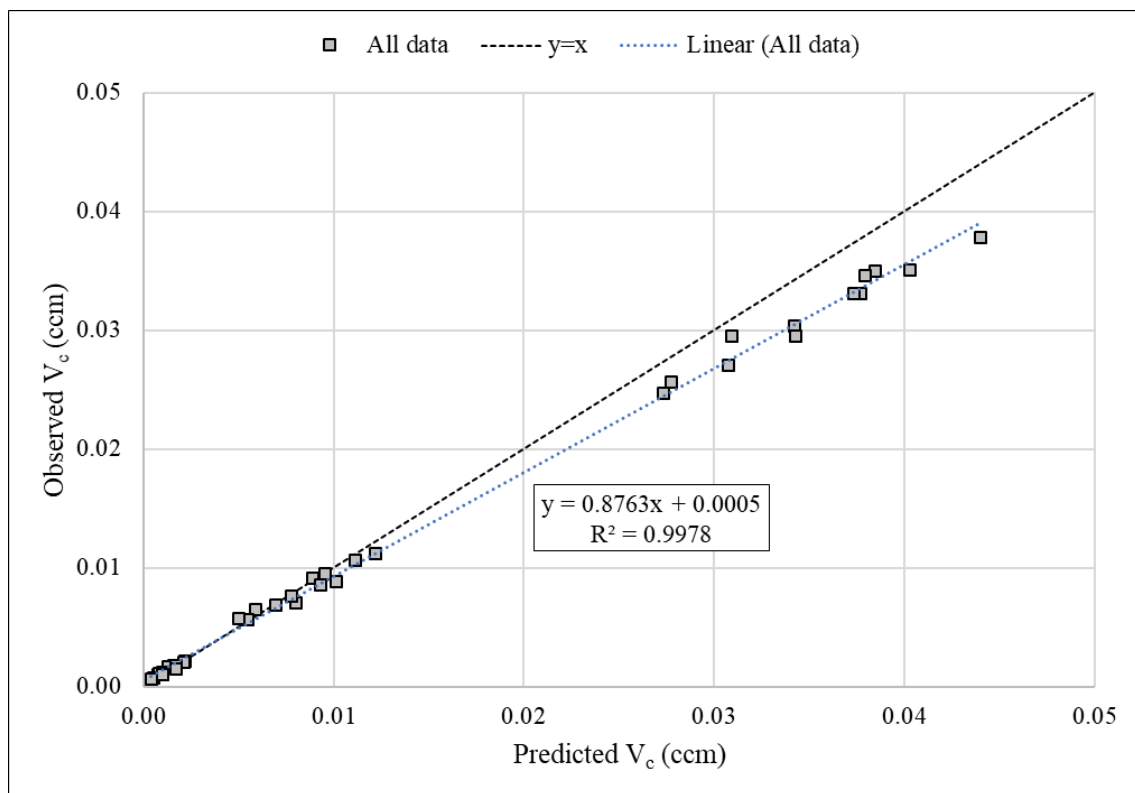


Figure 5.15 Observed versus predicted cone volume

Chapter 5: Analysis and Discussion of Results

Equation 5-25 was adjusted for $V_c > 0.008 \text{ m}^3$ using the linear equation which was fitted through the data. The new calibrated function for cone volume where $H_s > 0.1 \text{ m}$ is:

$$V_c = 0.8763 \cdot (L_c^{1.9529} \cdot W_c^{-0.3787} \cdot H_c^{1.3663} \cdot H_w^{0.0595}) + 0.0005 \quad 5-26$$

The new equation fits the data slightly better as shown in **Figure 5.16** and reduced the average error from 10.98% to 7.75%. It is however suggested that for practical application **Equation 5-25** be used since the calibration was not possible on the non-dimensional equation and is thus specific to the experimental setup.

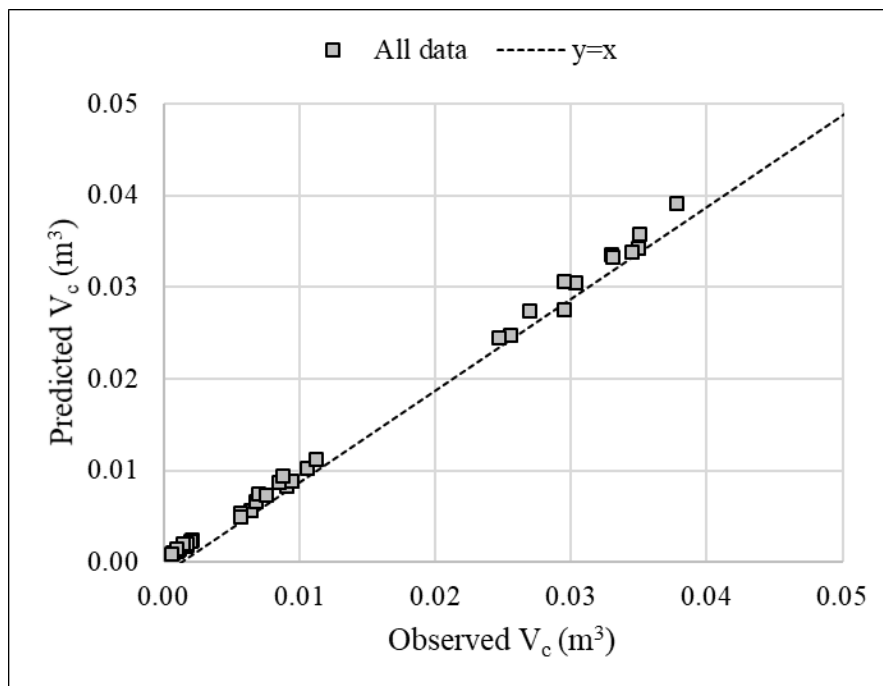


Figure 5.16 Calibrated cone volume prediction

5.3.8 Sensitivity Analysis

Sensitivity analysis was conducted to determine the significance of each of the independent parameters (shown in **Table 5.17** on page 132) on the scour cone length, width, height and depth. **Table 5.24** shows the comparison of the regression analysis with one of the independent parameters removed in each case. The results show that when the regression model is run without Q_1 the coefficient of determination (R^2) is much lower and the root mean squared error (RMSE) is much higher for the length, width and height than when the model is run without Q_2 or Q_3 . However, for the depth the R^2 value is lowest and RMSE highest when Q_2 is removed from the analysis. Therefore, Q_1 has the most significant effect on the scour cone length, width and height and Q_2 has the most significant effect on scour depth. For the cone length, width and height, the sensitivity can be ranked (highest to lowest) in the order Q_1 , Q_2 and Q_3 . Sensitivity

Chapter 5: Analysis and Discussion of Results

analysis of the scour cone volume equation (**Equation 5-24**) indicated that all three parameters had almost the same significance.

Table 5.24 Sensitivity analysis of the parameters used in the regression analysis

Analysis method	Length		Width		Height		Depth	
	R ²	RMSE	R ²	RMSE	R ²	RMSE	R ²	RMSE
Analysis with all parameters	0.998	0.019	0.998	0.043	0.998	0.012	0.985	0.009
Analysis without $Q_1 = \frac{H_w}{H_w - H_s}$	0.826	0.125	0.848	0.243	0.798	0.080	0.980	0.009
Analysis without $Q_2 = \frac{U_o}{\sqrt{gH_w}}$	0.960	0.063	0.949	0.145	0.969	0.032	0.725	0.033
Analysis without $Q_3 = \frac{b_{oc} + b_{oe}}{H_w}$	0.989	0.046	0.984	0.114	0.991	0.025	0.903	0.027

5.3.9 Regression Analysis for Each Outlet Shape

The proposed equations estimate the scour cone dimensions with reasonable accuracy, but since the regression analysis was done for four different outlet shapes, some parameters may be inaccurately estimated for one outlet shape and accurately for the others. **Table 5.25** shows the maximum and minimum errors associated with the equations for different outlets. The only clear pattern observed is that the maximum error on the scour cone length, width and height of the round outlet is much smaller than the others, implying that these parameters are generally slightly underestimated. In order to provide a slightly better prediction of the scour cone dimensions for each outlet shape, a regression analysis was undertaken to develop scour cone equations that are outlet shape specific.

Table 5.25 Maximum and minimum errors of proposed equations for different outlets

Outlet shape	L		W		H		D		V	
	Max	Min	Max	Min	Max	Min	Max	Min	Max	Min
Square	9.9	-8.2	11.9	-9.6	21.9	-10.4	17.4	-19.0	14.9	-18.6
Flat rectangular	22.7	-11.9	27.7	-7.0	31.2	-8.4	27.0	-13.9	16.4	-22.4
Round	2.1	-11.5	0.3	-9.3	3.8	-9.0	18.8	-21.9	13.7	-21.0
Upright rectangular	11.4	-5.4	23.5	-4.0	26.8	-5.3	25.7	-4.9	21.3	-35.5

The Linear Logarithmic Model was used for the scour cone dimensions and the Logarithmic Transformed Model used for the scour cone volume, as found to fit best according to the initial regression analysis. **Equation 5-27** represents the equation for the scour cone length, width, height and depth where L_c is replaced by the respective symbols for each. **Equation 5-28** represents the equation for the scour cone volume.

Chapter 5: Analysis and Discussion of Results

$$\frac{L_c}{H_w} = a \cdot \ln\left(\frac{H_w}{H_w - H_s}\right) + b \cdot \ln\left(\frac{U_o}{\sqrt{gH_w}}\right) + c \cdot \ln\left(\frac{b_{oc} + b_{oe}}{H_w}\right) \quad 5-27$$

$$\frac{V_c}{H_w^3} = \left(\frac{L_c}{H_w}\right)^a \cdot \left(\frac{W_c}{H_w}\right)^b \cdot \left(\frac{H_c}{H_w}\right)^c \quad 5-28$$

Separate regression analyses for each outlet shape yielded the coefficients a, b and c which are given in **Table 5.26**. The statistical parameters for each new equation are given in **Appendix J**. The equations for each outlet had lower average errors, with the exception of the length and width of the square outlet and the height of the round outlet which had slightly higher average errors. The equations for the flat rectangular outlet improved the most with an average decrease in average error of 2.52%. The average error range for the flat rectangular outlet is also much better; with the original equations having an average range of 37.7% and the new equations 27%. Since the average errors are slightly less with the outlet-specific equations, it is recommended to use these where the shape is exactly as in the experiments. For other cases the general equations presented in **Section 5.3.3** to **5.3.7** are recommended.

Table 5.26 Coefficients for the separate regression equations

Parameter	Coefficient	Square	Flat rectangular	Round	Upright rectangular
L_c	a	1.2149	1.2044	1.1914	1.2162
	b	-1.4297	-1.6830	-1.4495	-1.2224
	c	0.0503	0.0755	0.0496	0.0390
W_c	a	2.3170	2.4650	2.2358	2.1732
	b	-3.4061	-3.5208	-3.5718	-3.3141
	c	0.1332	0.1607	0.1351	0.1306
H_c	a	0.7710	0.7843	0.7345	0.7552
	b	-0.7848	-0.7605	-0.7766	-0.6778
	c	0.0300	0.0306	0.0272	0.0236
D_c	a	-0.0303	-0.0179	-0.0664	-0.0466
	b	-0.7906	-0.7628	-0.7896	-0.6915
	c	0.0347	0.0359	0.0315	0.0283
V_c	a	1.9405	4.1214	2.5188	0.6789
	b	-0.4151	-1.2774	-0.6290	0.1250
	c	1.3871	0.1575	1.0567	2.0861

Chapter 5: Analysis and Discussion of Results

5.3.10 Summary

Equations for the scour length, width, height, depth and volume were developed and presented in **Section 5.3.3 to 5.3.7** and are given in explicit form in **Table 5.27**. The equations all have a generally high value for the coefficient of determination (R^2) and the maximum error observed was below 36% which is very good considering the variables which were tested for different outlet shapes.

The sensitivity analysis indicated that the $\frac{H_w}{H_w - H_s}$ -term had the most significant effect on the cone length, width and height. Outlet shape-specific equations were also developed and are recommended in cases where the shape is exactly as in the experiments. For other cases where the shape is for example between the square and flat rectangular shape, it is recommended to use the equations in **Table 5.27**.

Table 5.27 Explicit equations for scour cone geometry prediction

	Equation	R^2
Length Eq. 5-13	$L_c = H_w \cdot \left[1.2060 \cdot \ln\left(\frac{H_w}{H_w - H_s}\right) - 1.4594 \cdot \ln\left(\frac{U_o}{\sqrt{gH_w}}\right) + 0.0536 \cdot \ln\left(\frac{b_{oc} + b_{oe}}{H_w}\right) \right]$	0.998
Width Eq. 5-15	$W_c = H_w \cdot \left[2.3065 \cdot \ln\left(\frac{H_w}{H_w - H_s}\right) - 3.4197 \cdot \ln\left(\frac{U_o}{\sqrt{gH_w}}\right) + 0.1360 \cdot \ln\left(\frac{b_{oc} + b_{oe}}{H_w}\right) \right]$	0.998
Height Eq. 5-17	$H_c = H_w \cdot \left[0.7615 \cdot \ln\left(\frac{H_w}{H_w - H_s}\right) - 0.7519 \cdot \ln\left(\frac{U_o}{\sqrt{gH_w}}\right) + 0.0278 \cdot \ln\left(\frac{b_{oc} + b_{oe}}{H_w}\right) \right]$	0.998
Depth Eq. 5-19	$D_c = H_w \cdot \left[-0.0386 \cdot \ln\left(\frac{H_w}{H_w - H_s}\right) - 0.7511 \cdot \ln\left(\frac{U_o}{\sqrt{gH_w}}\right) + 0.0317 \cdot \ln\left(\frac{b_{oc} + b_{oe}}{H_w}\right) \right]$	0.985
Volume Eq. 5-24	$V_c = H_w^3 \cdot \left(\frac{L_c}{H_w}\right)^{1.9529} \cdot \left(\frac{W_c}{H_w}\right)^{-0.3787} \cdot \left(\frac{H_c}{H_w}\right)^{1.3663}$	0.999

5.4 Centreline Bed Profiles

The centreline bed profile was taken along the x-axis upstream of the outlet and was determined from the scan data for each test. The centreline profiles for Tests 1 to 12 where the sand was levelled with the invert appear to be slightly S-curved, but where the sediment bed was above the invert level (Tests 13 to 36), the bed is generally more linear in shape. **Figure 5.17** shows

Chapter 5: Analysis and Discussion of Results

the centreline bed profiles for the flat rectangular outlet at $H_s = 0 \text{ m}$ for different water depths. A significant increase in scour cone depth and length is observed for increasing water depths. The centreline profiles for all tests can be seen in **Appendix K**.

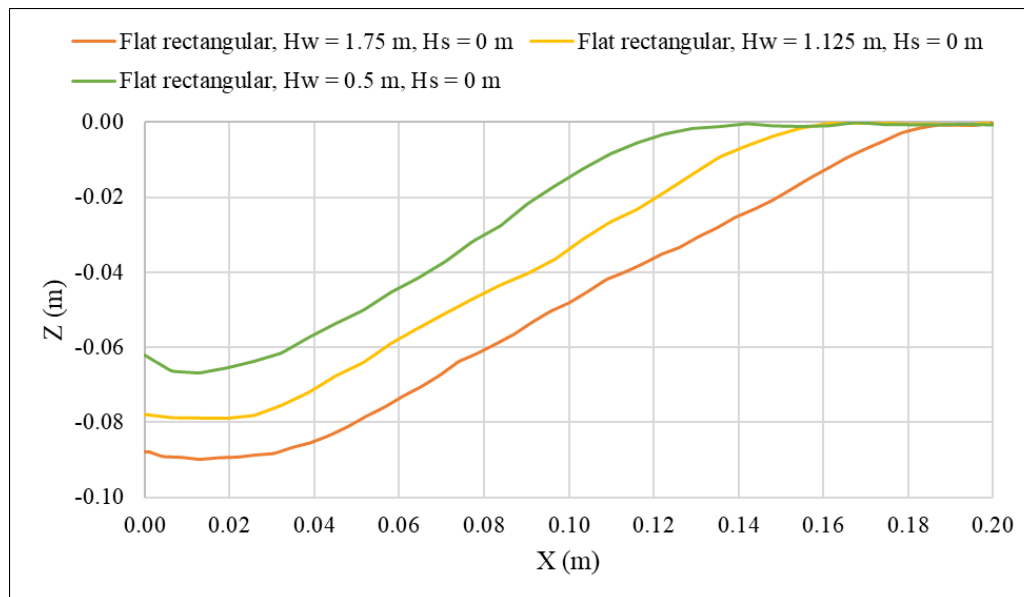


Figure 5.17 Centreline bed profiles for flat rectangular outlet at $H_s = 0 \text{ m}$

The centreline bed profiles for different outlet shapes at the same water and sediment level were also analysed as shown in **Figure 5.18**. For the conditions shown, the centreline bed profiles indicate that the square outlet had the greatest cone length and the flat rectangular outlet the deepest cone. The longitudinal slope angle is similar for all four outlets and the slight S-curve shape is observed.

To optimally visualize the centreline bed profile shape for the condition where $H_s = 0 \text{ m}$, the data for Test 1 to 12 was combined and made non-dimensional by dividing the x- and z-values by the cone length (L_c) and the maximum centreline depth (Z_{CL-max}) respectively. The non-dimensional profiles along with the best fit curve and the centreline bed profile shape suggested by Powell (2007) are shown in **Figure 5.19**. The position of maximum scour depth is generally located slightly away (up to $\frac{x}{L_c} = 0.117$) from the outlet for $H_s = 0 \text{ m}$, but for $H_s > 0$ it is most often observed right below the outlet at $\frac{x}{L_c} = 0$.

Chapter 5: Analysis and Discussion of Results

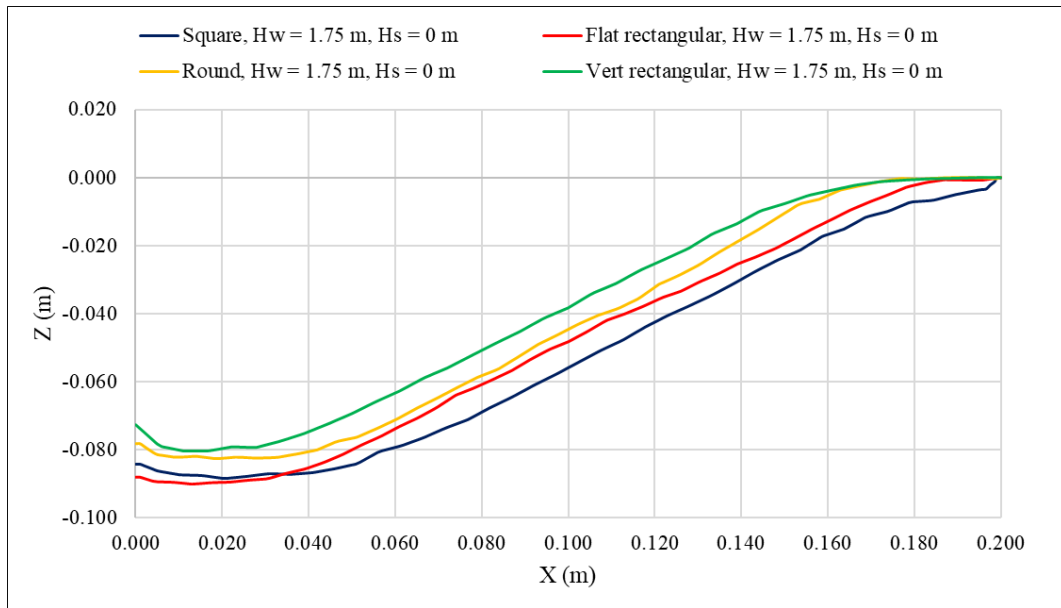


Figure 5.18 Comparison of centreline profiles for $H_s = 0 \text{ m}$ and $H_w = 1.75 \text{ m}$

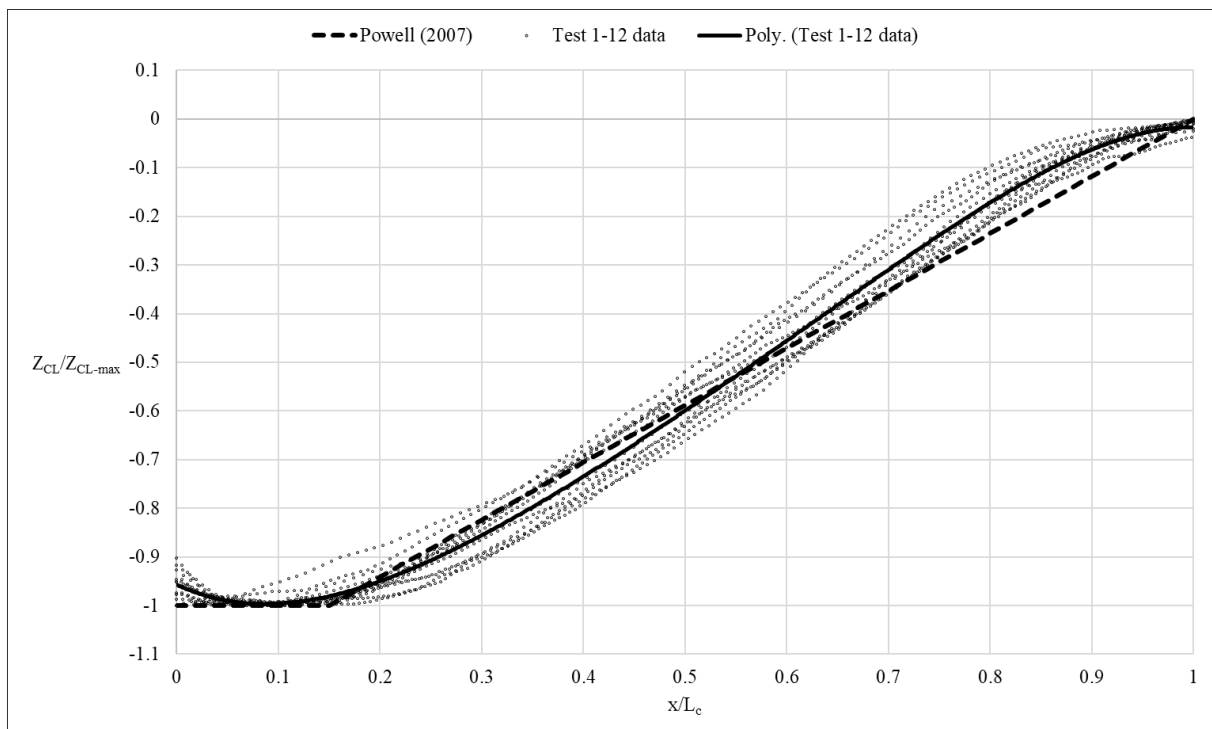


Figure 5.19 Centreline bed profile data for Test 1 to 12 ($H_s = 0 \text{ m}$)

It can be seen that the profile suggested by Powell (2007) slightly underestimates the scour length between $0.2 < \frac{x}{L_c} < 0.5$ and slightly overestimates the scour length between $0.6 < \frac{x}{L_c} < 0.95$. This might be caused by a lower submerged angle of repose for the sediment used in his

Chapter 5: Analysis and Discussion of Results

experiments. The equation that best fits the data ($R^2 = 0.99$) for the condition where the sediment is levelled to the invert is:

$$\frac{Z_{CL}}{Z_{CL-max}} = -4.119 \left(\frac{x}{L_c}\right)^5 + 10.438 \left(\frac{x}{L_c}\right)^4 - 11.406 \left(\frac{x}{L_c}\right)^3 + 7.015 \left(\frac{x}{L_c}\right)^2 - 0.988 \left(\frac{x}{L_c}\right) - 0.957 \quad 5-29$$

where:

$$\begin{aligned} Z_{CL} &= \text{centreline scour depth of profile (m)} \\ Z_{CL-max} &= \text{maximum centreline depth (m)} \\ x &= \text{distance from outlet along centreline (m)} \end{aligned}$$

The centreline profile data from the tests where the sediment level was above the invert level (Tests 13 to 36) showed strong correlation and are non-dimensionally presented in **Figure 5.20**. The centreline profile shape for these tests was more linear in shape than for Tests 1 to 12 which followed a slight S-curve. From **Figure 5.20** it is clear that Powell's equation significantly overpredicts scour in the longitudinal direction when the sediment level is above the invert. **Equation 5-30** represents the centreline bed profile for this condition.

$$\frac{Z_{CL}}{Z_{CL-max}} = 0.193 \left(\frac{x}{L_c}\right)^2 + 0.828 \left(\frac{x}{L_c}\right) - 1.014 \quad 5-30$$

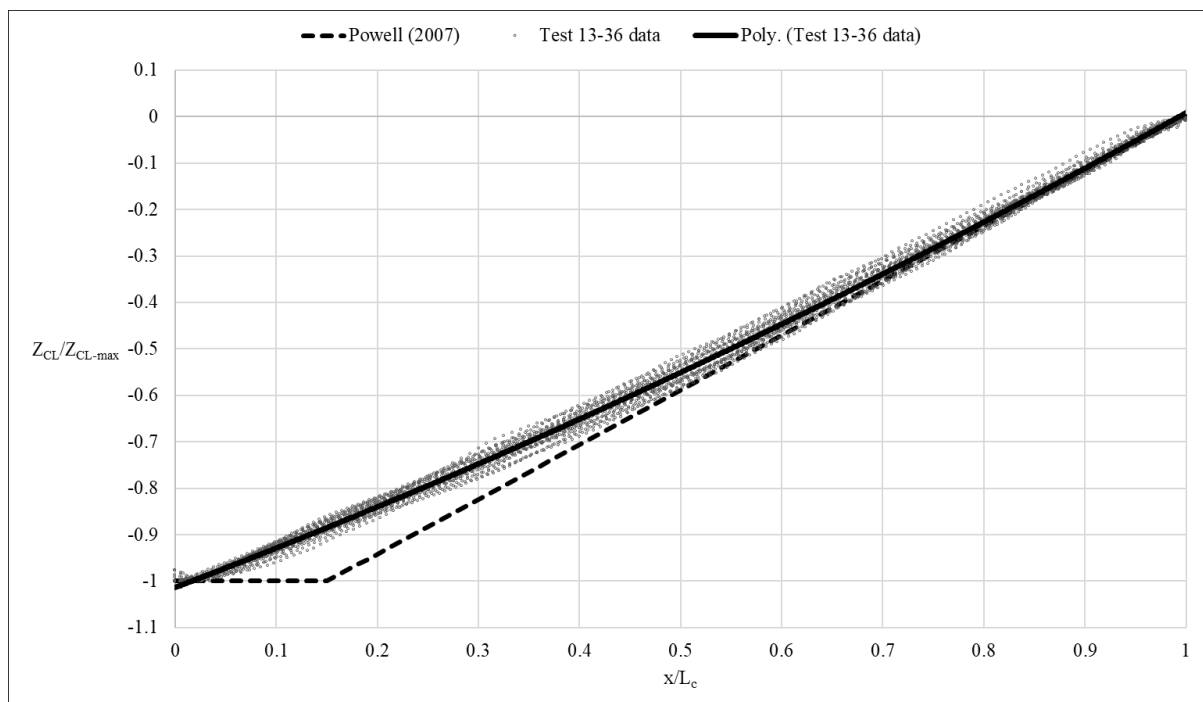


Figure 5.20 Centreline bed profile data for Test 13 to 36 ($H_s = 0.1$ & 0.2 m)

Chapter 5: Analysis and Discussion of Results

Using **Equation 5-29** and **Equation 5-30**, the centreline profile of the scour can be predicted if the cone length and maximum depth are known. Predicting the scour cone dimensions can be done using the equations developed in the regression analysis as discussed in **Section 5.3**.

From the centreline bed profile data, the longitudinal slope angle of the scour cone from each test was measured and is presented in **Table 5.28**. The longitudinal angle varies greatly between the different tests (it ranges from 29.5° to 35.7°) and some tests can be considered outliers, thus the average longitudinal angles for specific conditions were calculated to find the general trends. Analysis of the results shows that the average longitudinal angle generally decreases with an increase in sediment level. The trend is similar for the water depth; an increase in water depth generally decreases the longitudinal angle. In terms of outlet shape, the square and round outlets had the same average longitudinal slope of 31.7°, the flat rectangular outlet had the lowest average slope of 31.3° and the upright rectangular outlet the steepest average slope of 32.4°.

Table 5.28 Longitudinal slope angle comparison for all tests

H_w	H_s	Square	Flat rectangular	Round	Upright rectangular	Average
1.75	0	32.0	31.2	33.3	31.7	32.9
1.125	0	32.7	32.7	33.2	32.4	
0.5	0	33.8	34.9	32.2	34.9	
1.75	0.1	31.1	30.0	30.7	31.7	31.4
1.125	0.1	30.2	30.4	31.8	35.7	
0.5	0.1	33.4	29.5	30.6	32.3	
1.75	0.2	31.4	30.9	32.0	31.4	31.0
1.125	0.2	30.9	31.3	30.8	30.6	
0.5	0.2	30.1	30.5	30.9	30.9	
Average		31.7	31.3	31.7	32.4	

5.5 Cross-Sectional Bed Profiles

The lateral variation of the scoured area was studied by investigating the cross-sectional profiles of each test. The cross-sectional profiles for each test were plotted at various distances from the outlet, thus showing the change in scour width and depth as a function of the distance from the outlet, as shown in **Figure 5.21** which represents Test 7. The cross-sectional profiles at $x = 0$ m (against the outlet) for all tests are given in **Appendix L**. Note must be taken that the cross-sectional profiles at the outlet do not always show the point of deepest or widest scour since these points are in some cases located a distance from the outlet.

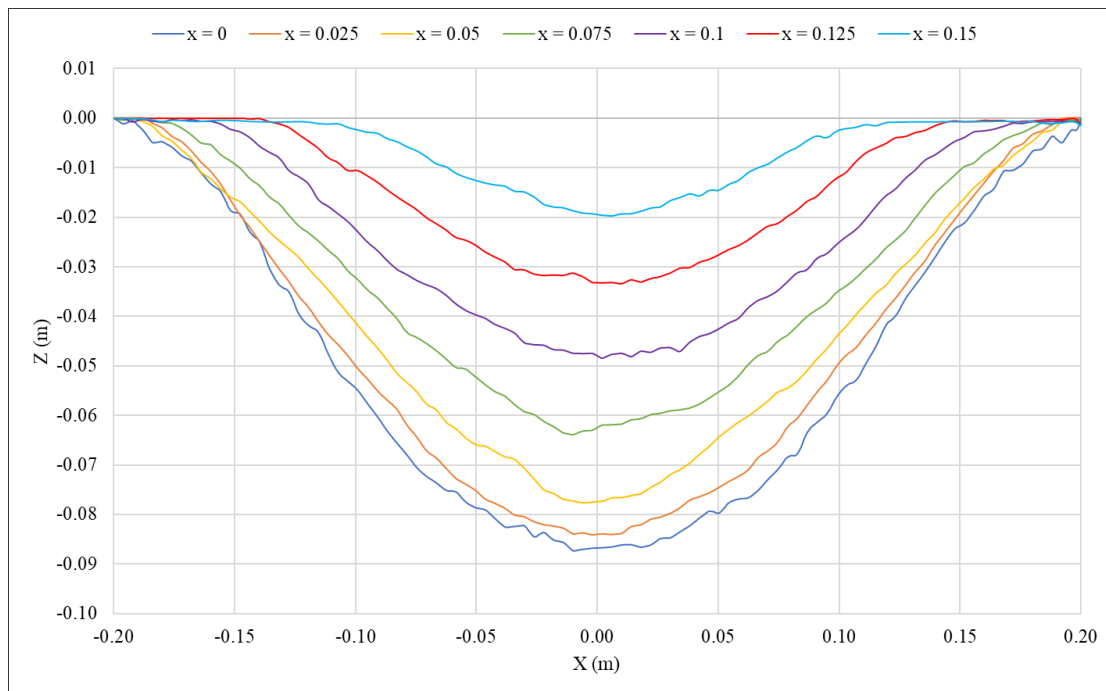


Figure 5.21 Cross-sectional profiles for Test 7–Flat rectangular outlet, $H_s=0\text{m}$, $H_w=1.75\text{m}$

As expected, the cross-sectional profiles were not exactly symmetrical and often had peaks and valleys on either side of the centreline that formed due to vortex development inside the cone as well as to sliding. In some tests the existence of a central ridge was evident as shown in **Figure 4.4**. The cross-sectional profiles further from the outlet were generally more asymmetrical and had less steep side slopes.

Non-dimensional cross-sectional profiles were plotted to determine generic equations for the shape of the profile at any distance from the outlet. The centreline scour depth for each profile (Z_{CL}) and scour half-width (w) at the location was used as scaling parameters. The centreline scour depth was a better scaling parameter than the maximum scour depth, because of the ridges and troughs present in some of the profiles.

Similar to the centreline profiles, the tests with the sediment level above the invert were analysed separately from those with the sediment level at the invert, due to the slight difference in non-dimensional profile shape. The non-dimensional cross-sectional profiles for Test 1 to 12 are plotted in **Figure 5.22** and for Test 13 to 36 in **Figure 5.23**. The even-ordered polynomial equation suggested by Powell (2007) is plotted in both figures as comparison and correlates well with the data from this study.

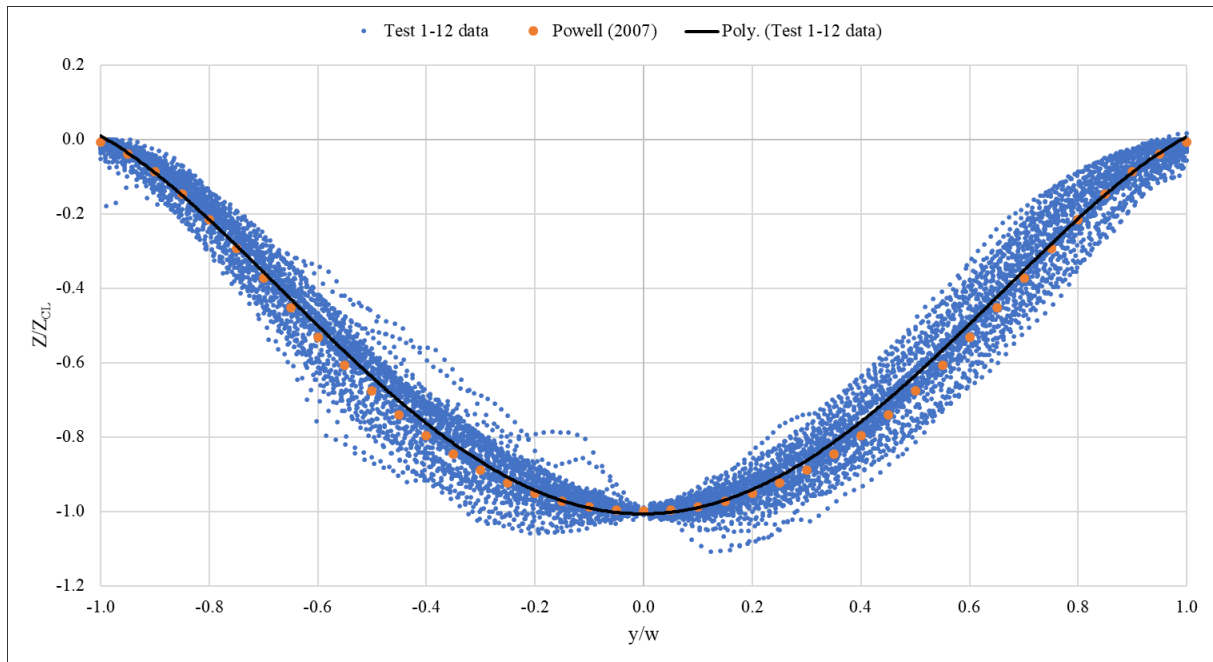
Chapter 5: Analysis and Discussion of Results

Figure 5.22 Non-dimensional transverse scour cone profiles for Test 1 to 12 ($H_s = 0$ m)

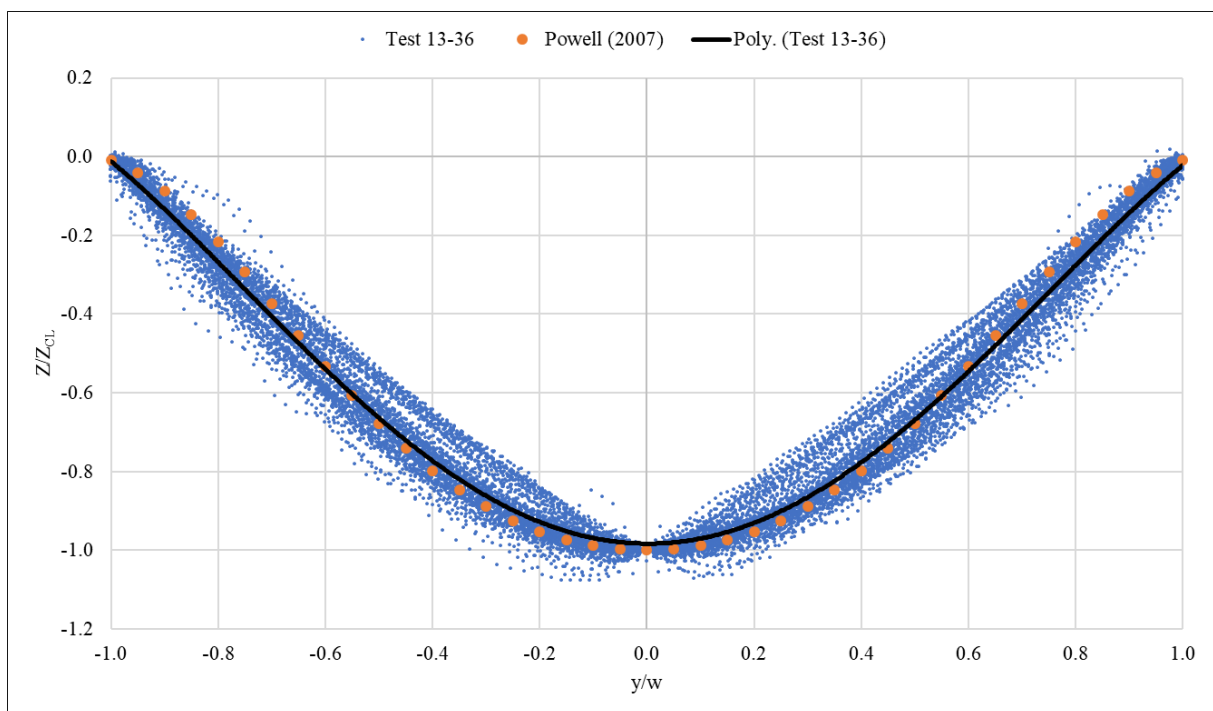


Figure 5.23 Non-dimensional transverse scour cone profiles for Test 13 to 36 ($H_s > 0$ m)

Non-dimensional polynomial equations were used to fit the data with good correlation ($R^2 = 0.97$). **Equation 5-31** is applicable to the case where the sediment is levelled with the invert and **Equation 5-32** for the case where the sediment is above the invert level.

Chapter 5: Analysis and Discussion of Results

For $H_s = 0$:

$$\frac{Z}{Z_{CL}} = -0.62 \left(\frac{y}{w}\right)^4 - 0.0075 \left(\frac{y}{w}\right)^3 + 1.6353 \left(\frac{y}{w}\right)^2 - 0.0066 \left(\frac{y}{w}\right) - 1.007 \quad 5-31$$

For $H_s > 0$:

$$\frac{Z}{Z_{CL}} = -0.4019 \left(\frac{y}{w}\right)^4 + 0.0002 \left(\frac{y}{w}\right)^3 + 1.3685 \left(\frac{y}{w}\right)^2 - 0.0052 \left(\frac{y}{w}\right) - 0.9831 \quad 5-32$$

for $-1 < \frac{y}{w} < 1$

where:

- Z = depth at position along profile (m)
- y = position along profile (m)
- w = half-width of profile (m)

The transverse scour cone slopes for each test were determined and are presented in **Table 5.29**. The transverse slopes were measured near the outlet where $\frac{x}{L_c} < 0.25$ and ranged from 28° to 33.3° . Analysis of the average transverse slope between tests with different water depths indicated no difference, with an average slope of 31.4° for all three water depths.

For tests with different sediment levels, the difference in average transverse slope was slight, with the medium sediment level ($H_s = 0 \text{ m}$) having slightly less steep slopes than the other two sediment levels. The results indicate that the round outlet had on average the steepest transverse slopes (31.94°), approximately one degree more than the flat rectangular outlet which had the least steep slopes (30.97°).

Table 5.29 Transverse slope angle comparison for all tests

H_w	H_s	Square	Flat rectangular	Round	Upright rectangular	Average
1.75	0	30.7	30.7	33.3	32.0	31.6
1.125	0	31.2	30.4	31.4	32.8	
0.5	0	32.0	31.9	30.7	32.5	
1.75	0.1	28.0	30.3	32.3	30.7	31.0
1.125	0.1	32.0	29.4	31.3	31.6	
0.5	0.1	32.5	30.6	33.1	30.1	
1.75	0.2	32.1	32.6	32.8	31.8	31.6
1.125	0.2	31.0	32.3	31.9	31.3	
0.5	0.2	31.0	30.5	30.6	31.4	
Average		31.2	31.0	31.9	31.6	

Chapter 5: Analysis and Discussion of Results

When comparing the longitudinal slopes to the transverse slope it can be observed that:

- The longitudinal slope is 4.12% steeper when the sediment is at the invert level and the transverse slope is 2% steeper when the sediment is 0.2 m above the invert level.
- The average difference decreases with increasing sediment level and increasing water depth.
- The average difference is greatest for the upright rectangular outlet and lowest for the round outlet.

To fully describe the scour cone shape in the transverse direction, an analysis was done to define the scour width at any x-location. The width (W) of the cone at each $\frac{x}{L_c}$ location was normalized with the maximum scour width (W_m) and plotted in **Figure 5.24** along with the equation defined by Powell (2007). A curve was fitted through the data and provided a good fit to the data with $R^2 = 0.986$.

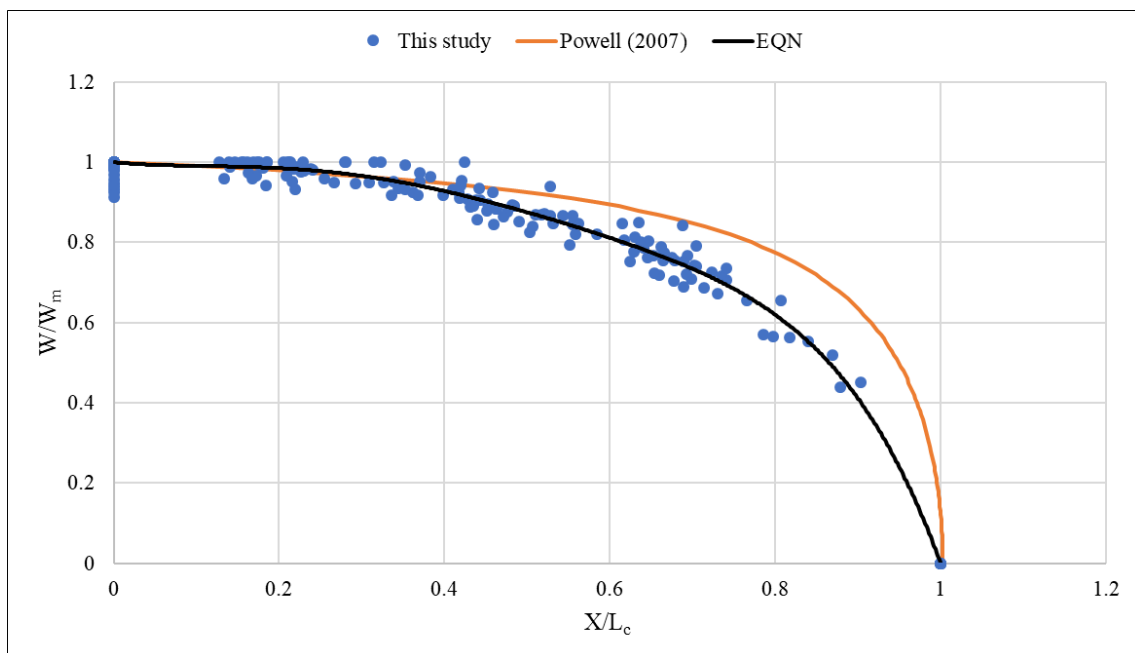


Figure 5.24 Non-dimensional shape of top of scour hole

The equation describing the curve is given in **Equation 5-33**. Powell's equation provides a reasonable estimate to the data of this study close to the outlet, but overpredicts the cone width for $\frac{x}{L_c} > 0.4$. The shape of the top of the scour cone is symmetrical across the longitudinal (x) axis.

$$\frac{x}{L_c} = -3.6072 \left(\frac{W}{W_m}\right)^6 + 1.9869 \left(\frac{W}{W_m}\right)^5 + 5.4559 \left(\frac{W}{W_m}\right)^4 - 6.3017 \left(\frac{W}{W_m}\right)^3 + 1.6687 \left(\frac{W}{W_m}\right)^2 - 0.2018 \left(\frac{W}{W_m}\right) + 1 \quad 5-33$$

where:

W = width at specific location (m)

W_m = maximum width of scour hole (m)

5.6 Scour Cone Aspect Ratio Analysis

The aspect ratio of a scour cone is the ratio of its length (L_c) to half-width ($w_c = \frac{W_c}{2}$) and is generally close to but below 1, representing a semi-ellipsoidal scour cone shape (Powell & Khan, 2012). The length and half-width are generally directly related to each other and were analysed to observe the trends associated with different outlet shapes, water depths and sediment levels. Powell (2007) states that the aspect ratio should approach 1 at higher discharges and water depths. **Figure 5.25** shows the plot of the length to half-width ratios of the experiments conducted, indicating that the ratios are mostly just below 1.

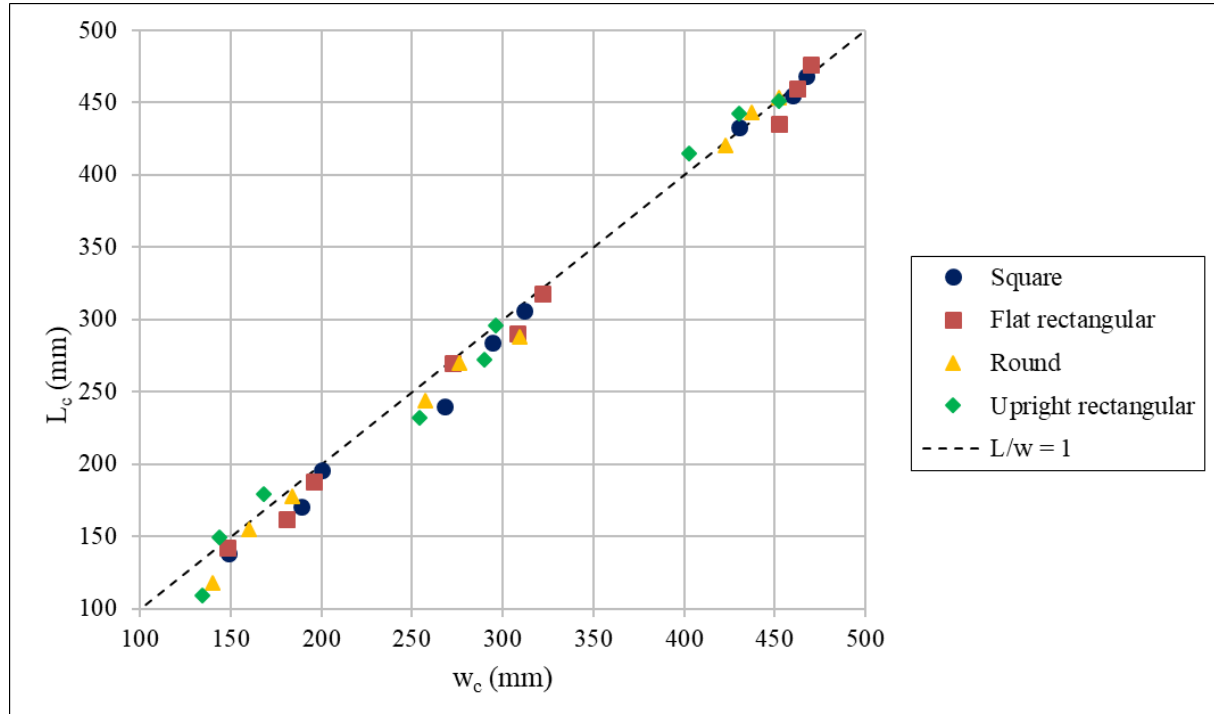


Figure 5.25 Graph showing the length to half-width of all tests

The aspect ratios of all the tests conducted are presented in **Table 5.30**. From the results it is clear that the tests for $H_s = 0$ m and $H_w = 0.5$ m yielded the lowest aspect ratios for the round

Chapter 5: Analysis and Discussion of Results

and flat rectangular outlet shapes, implying that the cone width was significantly more than the cone length. The greatest aspect ratios were observed for the upright rectangular outlet at the highest sediment level and the lowest aspect ratios were observed for the square and circular outlets. This can be explained by the fact that the upright rectangular outlet had the narrowest cross-section and thus the smallest influence in the transverse direction (width is less).

Table 5.30 Aspect ratios for all tests conducted

H_s	H_w	Square	Flat rectangular	Round	Upright rectangular
0	1.75	0.98	0.96	0.97	1.07
	1.125	0.90	0.90	0.97	1.03
	0.5	0.93	0.96	0.84	0.81
0.1	1.75	0.98	0.99	0.93	1.00
	1.125	0.97	0.94	0.98	0.94
	0.5	0.90	0.99	0.95	0.91
0.2	1.75	1.00	1.01	1.00	1.00
	1.125	0.99	0.99	1.01	1.03
	0.5	1.01	0.96	0.99	1.03
Average		0.95	0.96	0.97	0.96

Shammaa *et al.* (2005) studied the flow field upstream of different shaped orifices and plotted the isovels of the radial velocity (shown in **Figure 5.26**). Since the scour cone dimensions are strongly dependent on the flow upstream of the outlet, the findings of the flow field ratio should be similar to the scour cone aspect ratio. The flow field ratio is the distance from the outlet on the y-axis (length) divided by the distance on the x-axis where the same velocity is observed. The authors showed that the ratio for a rectangular shape with height four times its width is 0.98. For a rectangular shape with width four times its height the ratio was significantly lower at 0.67. The results from this study show that the flat rectangular outlet had an average aspect ratio, similar to those of the round and square outlets.

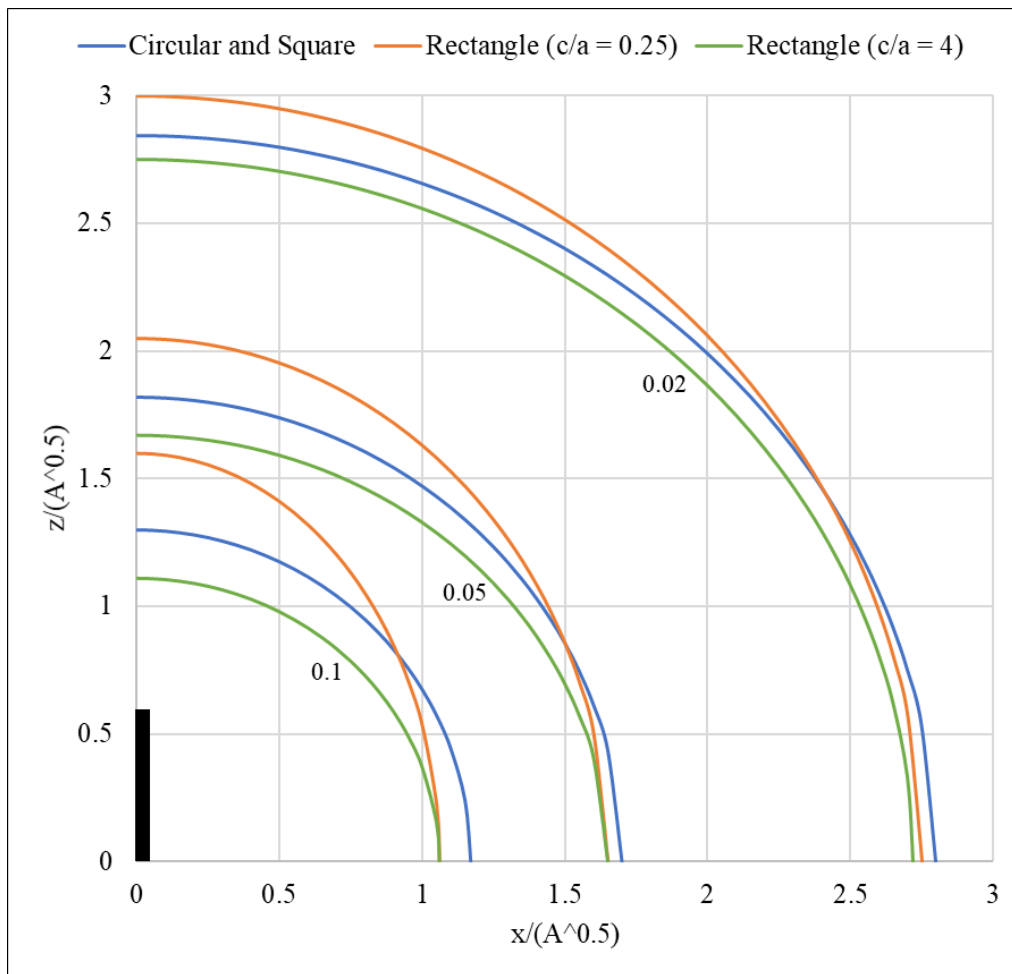


**Figure 5.26 Isovelocity contours upstream of different shaped orifices
(adapted from Shammaa *et al.*, 2005)**

Furthermore, the results of experiments by Shammaa *et al.* (2005) showed that the velocity distortion due to the corners of the square orifice was limited to the orifice edges and thus the semi-ellipsoidal isovels for the square and circular orifice coincide. This is consistent with the results of this study that showed an average aspect ratio of 0.96 for both square and circular outlets. The experimental results of Hajikandi *et al.* (2017) were however different, indicating that the aspect ratio of the square outlet had a lower aspect ratio (0.76) than that of the circular outlet (0.86).

As suggested by Powell (2007), Powell & Khan (2012) and Hajikandi *et al.* (2017), the aspect ratio generally decreases with an increase in discharge/water depth as substantiated by the results of this study shown in **Table 5.31**. Furthermore, it is shown that the aspect ratio tends to increase with increasing sediment level, similar to experimental results of Kistner (2013) which showed that the higher sediment level was associated with an increase in aspect ratio from 0.77 to 0.93 and 0.77 to 1.00 for different discharges in his experimental setup.

Powell & Khan (2012) found the average aspect ratio of 0.89 for their tests with the sediment bed at the invert level which is similar to the results of this study. The same authors also showed that the sediment type did not greatly influence the aspect ratio and showed that the aspect ratio for fixed bed tests is lower than for movable bed tests.

Table 5.31 Average aspect ratios for the sediment levels and water depths

Sediment level (m)	Average L_c/w_c	Water depth (m)	Average L_c/w_c
0	0.943	0.5	0.990
0.1	0.956	1.125	0.971
0.2	1.002	1.75	0.940

5.7 Flushing Efficiency

Flushing efficiency (E_f) was defined by Qian (1982) as the ratio of the volume of removed sediment (V_c) to the volume of water (V_w) used:

$$E_f = \frac{V_c}{V_w} \quad 5-34$$

Morris & Fan (1998) state that the efficiency of flushing is extremely dependent on the flushing method, i.e. drawdown or pressure flushing. Partial drawdown events have reported flushing efficiencies between 0.00017 and 0.012, whereas empty flushing efficiency ranges from 0.04 to 0.13 (Morris & Fan, 1998). Emamgholizadeh *et al.* (2014) reported an average flushing efficiency of 0.00343 for an experimental model simulating pressure flushing of cohesive sediments. With reference to drawdown flushing, Brown (1943) listed several factors that lead to increased flushing efficiency including:

- reduction in water depth
- increased outlet discharge
- increased outlet dimensions
- lower location of outlet
- longer time of flushing event

However, in a pressure flushing event, the initial sediment scouring takes place very fast and most sediment is removed in the first few minutes. Thus, increasing the time of a pressure flushing event beyond the initial scouring will decrease the flushing efficiency. The experimental results for this study showed an average flushing efficiency of 0.000291 and a range between 0.00002 to 0.000905 as shown in **Table 5.32**.

Table 5.32 Flushing efficiency for all tests (10^{-3})

H_s	H_w	Square	Flat rectangular	Round	Upright rectangular
0	1.75	0.034	0.032	0.027	0.023
	1.125	0.034	0.033	0.023	0.020
	0.5	0.030	0.033	0.022	0.020
0.1	1.75	0.168	0.178	0.136	0.142
	1.125	0.179	0.188	0.140	0.151
	0.5	0.201	0.210	0.177	0.178
0.2	1.75	0.555	0.600	0.556	0.535
	1.125	0.647	0.687	0.606	0.592
	0.5	0.829	0.905	0.799	0.774
Average		0.30	0.32	0.28	0.27

Although these values seem very low, it is relevant to note that most of the scour cone formation took place within the first 5-10 minutes, but the test time was set to one hour for all tests. This implies that if the tests were for example only run for 10 minutes, the flushing efficiency would be significantly more, possibly even 10 times more. The flushing efficiency was not the main interest of this study, which compared different outlet shapes, water depths and sediment levels. In summary the experimental results show that:

- the flushing efficiency increases with an increase in sediment level,
- the flushing efficiency increases with a decrease in water depth,
- the effect of the water depth becomes greater at higher sediment levels, and
- the flat rectangular outlet shape was most efficient.

5.8 Practical Application of Results

The practical application of the experimental results is important for future HPP designs. The proposed scour cone equations can be scaled up to prototype values and used for the prediction of the scour cone in real-life pressure flushing scenarios.

5.8.1 Scaled Results for Application

Since the tests were not conducted for a specific site and therefore did not have a defined scale, the results can be scaled to suit different scenarios. Since the physical model had free-surface flow, gravitational forces were dominant and thus prototype-model similarity is achieved by the Froude law as defined in **Section 2.8.1**. Heller (2011) suggested a scale of between 1:50 and 1:100 for reservoir low-level outlets due to their large prototype size. The general rule is

Chapter 5: Analysis and Discussion of Results

that the greater the scale of the model, the better the results reflect in the prototype. For illustrational purposes the results are scaled between 1:10 and 1:100, but the applicability of the results at a small scale should be investigated independently due to the use of sediment in the experiments.

The sediment used in the experiments was scaled up using the method described in **Section 2.8**. **Table 5.33** shows the prototype sediment sizes for different scales and **Figure 5.27** shows an example of sediment scaling for a 1:50 scale. In the figure it is shown that the model sand plots to the left in the graph where laminar sublayer conditions could affect the flow patterns. As the best approximation available for scaling of natural sediment, the prototype values for different scales were found by following the shape of the Modified Liu curve as indicated by the dashed lines. The d_{50} and d_{90} values of the model and the prototype must be similar on the vertical axis (y-axis) of **Figure 5.27** to conform to similarity.

Table 5.33 Prototype sediment sizes for different scales

Scale (1:)	Prototype d_{50} (mm)	Prototype d_{90} (mm)
10	0.188	0.380
20	0.237	0.535
30	0.275	0.700
40	0.308	0.861
50	0.340	0.995
60	0.370	1.005
70	0.398	1.040
80	0.425	1.150
90	0.455	1.300
100	0.480	1.480

The equations can be applied for different scales, other outlet shapes, water and sediment levels. However, it is recommended to stay within the range of parameters used in the experiments, since these were the conditions for which the equations were developed. **Table 5.34** shows the prototype range values within which the equations should be applied for different scales. In order to best illustrate the scaling of results, an example of the best performing outlet shape at a scale of 1:50 is used. This implies a 100 m high dam with a flat rectangular shaped low-level outlet. The outlet has dimensions 5 x 2.5 m (B x H) and is located near the original river-bed level. Pressure flushing is performed with the water depth at 87.5 m above the outlet invert, implying an outlet discharge of 309 m^3/s if the discharge coefficient is taken as 0.6. At a scale of 1:50 the median sediment diameter is $d_{50} = 0.34$ mm as shown in **Table 5.33**.

Chapter 5: Analysis and Discussion of Results

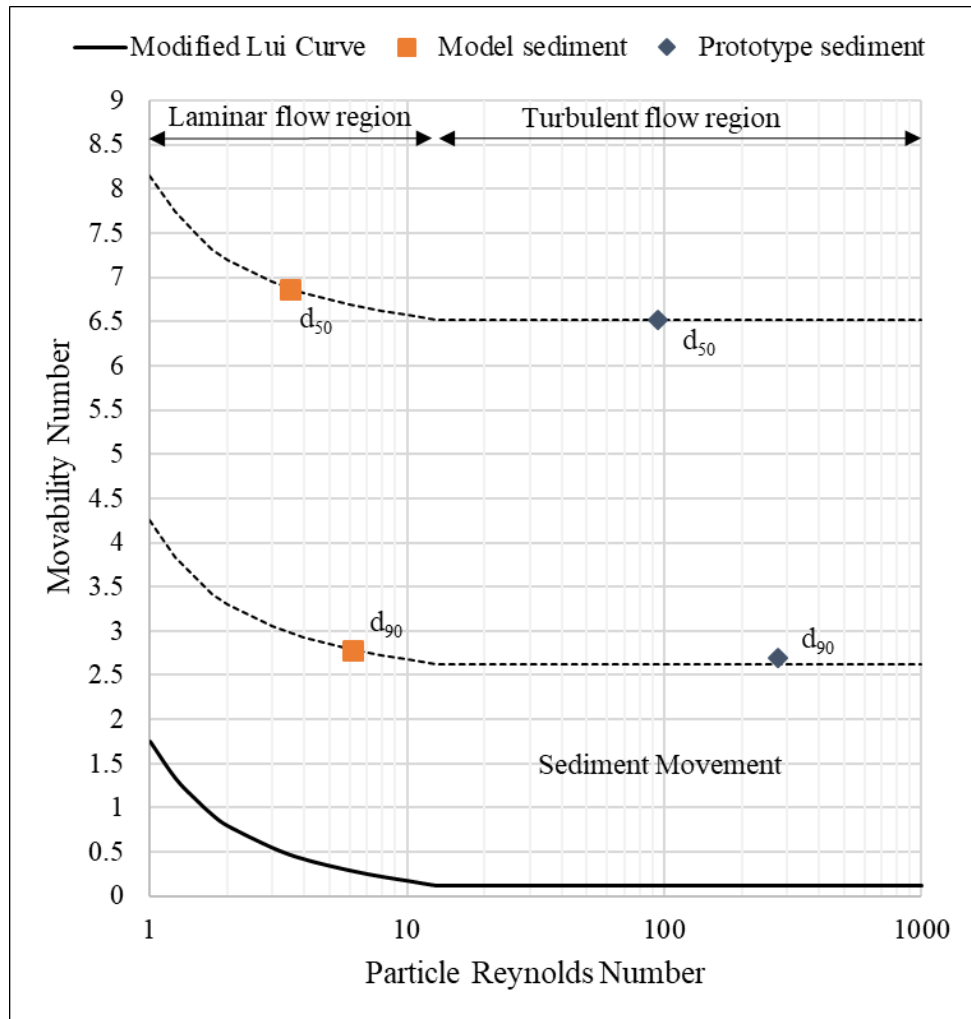


Figure 5.27 Sediment scaling for a 1:50 scale using the modified Liu diagram

Table 5.34 Range of parameters for different scales

Scale	H_w^*		H_s^{**}	
	Min (m)	Max (m)	Min (m)	Max (m)
10	5.0	17.5	0.0	2.0
20	10.0	35.0	0.0	4.0
30	15.0	52.5	0.0	6.0
40	20.0	70.0	0.0	8.0
50	25.0	87.5	0.0	10.0
60	30.0	105.0	0.0	12.0
70	35.0	122.5	0.0	14.0
80	40.0	140.0	0.0	16.0
90	45.0	157.5	0.0	18.0
100	50.0	175.0	0.0	20.0

* H_w is the water depth above the outlet invert level

** H_s is the sediment depth above the outlet invert level

Chapter 5: Analysis and Discussion of Results

With the deposited sediment at the soffit level of the outlet the estimated scour cone dimensions from the equations developed in **Section 5.3.9** are shown in **Table 5.35**. The maximum and minimum values indicate the error range which can be expected as observed during the regression analysis for the respective equations.

Table 5.35 Scour cone dimensions for example scenario

Parameter	Predicted	Min	Max
L_c (m)	13.92	12.25	15.17
W_c (m)	28.47	25.55	30.42
H_c (m)	7.57	6.19	8.22
D_c (m)	5.07	3.69	5.72
V_c (m ³)	979	848	1 195

Figure 5.28 visually represents the prototype scour cone volume for the above-mentioned scenario at different water and sediment levels. Similar graphs for the scour cone dimensions are shown in **Appendix M** and allow the user to directly read off the predicted values for the given scenario.

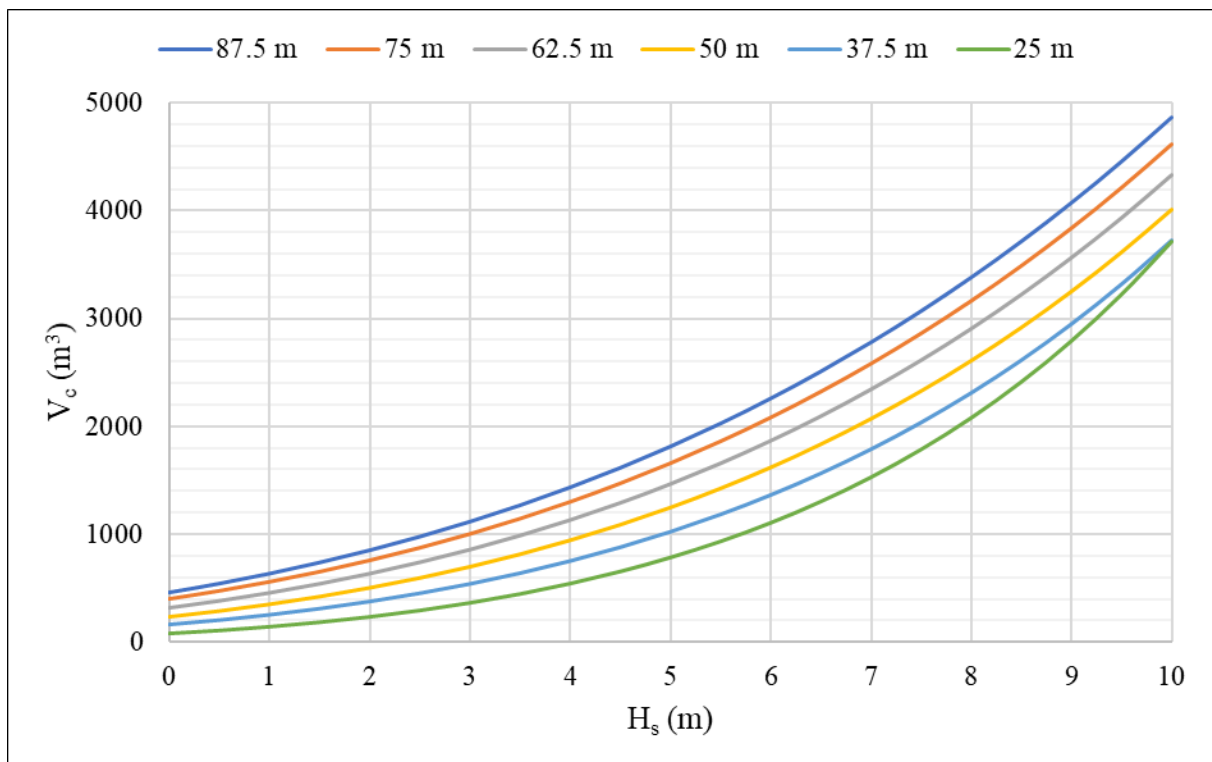


Figure 5.28 Prototype scour cone volume at different water depths for flat rectangular outlet at 1:50 scale (determined using Equation 5-28 and Table 5.26)

5.8.2 Proposed Layout of Flushing and HPP Intake

The main function of the low-level outlet is to protect the power intake from sediments and it is thus crucial to correctly position these two structures relative to each other. The scenario explained in **Section 5.8.1** is once again used for illustrative purposes. If the dam had three power intakes to protect, one low-level outlet could be located beneath each power intake as indicated in **Figure 5.29**. The scour cone shown is for the case where the sediment is level with the outlet invert. The scour cone width and height were taken as the minimum predicted by the equations and an overlap between the cones was also accounted for. In a prototype scenario the interaction between the outlets would cause the cones to be shaped differently than illustrated.

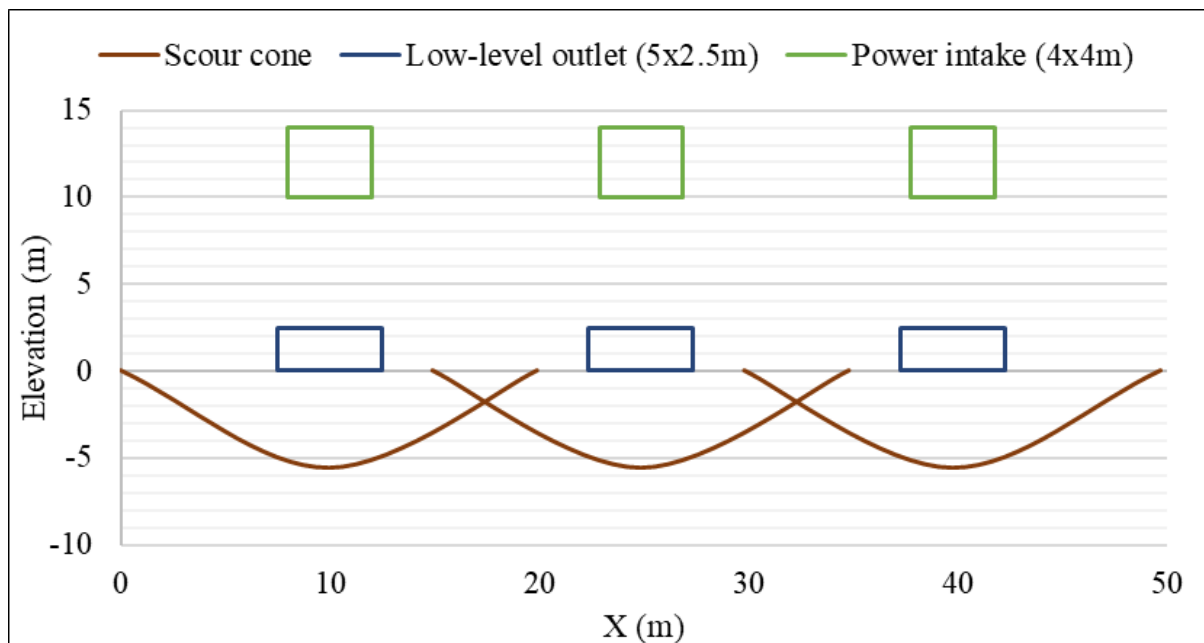


Figure 5.29 Elevation view of proposed layout of intake and outlet works

Since low-level outlets are expensive to construct and add major costs to any new HPP project, the number of low-level outlets should be reduced to the minimum that can maintain sediment free conditions at the intake works. **Figure 5.30** shows how one low-level outlet could also maintain sediment free conditions at the intakes even after sediment has deposited to the invert level of the HPP intakes. Designers of new hydropower dams should consider locating the low-level outlets based on the estimated scour cone dimensions and the position of the intake works.

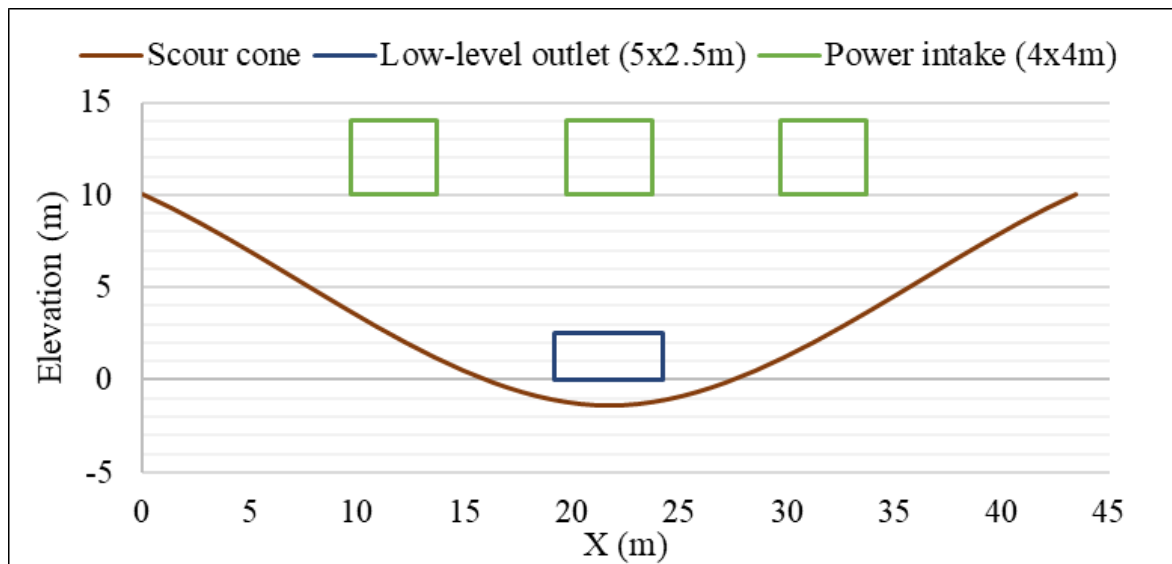
Chapter 5: Analysis and Discussion of Results

Figure 5.30 Elevation view of proposed layout of one low-level outlet and intakes

6 CONCLUSIONS AND RECOMMENDATIONS

Reservoir sedimentation poses a severe threat to the efficiency and productivity of HPPs due to hydro-abrasive turbine erosion and associated generation losses. Sedimentation management options range from preventing erosion in the catchment to removing already deposited sediment. Pressure flushing is an effective sediment management technique specifically focussed on periodic removal of deposited sediment in front of power intakes. The geometry of the scour cone formed in a pressure flushing event is specifically important for the design of intake and low-level outlet structures of new HPPs, so that a sediment free condition can be maintained at the power intake. In this study, experiments were conducted on a physical model to observe the differences in scour cone geometry for different outlet shapes. Four different outlet shapes (square, round, flat rectangular and upright rectangular) were tested at three water depths (0.5, 1.125 and 1.75 *m*) and three sediment levels (0, 0.1 and 0.2 *m*). The results were presented, analysed and compared with the literature.

6.1 Conclusions from the Literature Review

From the literature review the following conclusions were made that are important to this study:

- Reservoir sedimentation can cause major problems at hydropower intake works if not managed properly. Coarse sediments cause hydro-abrasive erosion of the turbines and other hydraulic machinery when passed through the intake structures. The damage to the turbines is mainly dependent on the type of turbine, flow characteristics and sediment type.
- Guidelines on low-level outlet design at dams are not specific about the outlet shape and layout with respect to the power intake. The suggestion that low-level outlets should be as low and wide as possible is contradicted by Chinese designs, which are generally higher than what they are wide.
- Pressure flushing is a method of removing previously deposited sediment in the vicinity of a low-level outlet at a dam to maintain sediment free conditions at the power intake. Since pressure flushing only creates a local scour cone just upstream of the outlet, it is not very effective in recovering large amounts of lost storage capacity, but can play a major role in the sustainability and productivity of HPPs.

- Several authors have conducted physical model tests of pressure flushing and suggested equations for predicting the scour cone geometry under specific conditions. Many of the equations have several shortcomings and limitations in terms of their applicability. Equations that take the shape of the low-level outlet into account do not exist.

6.2 Conclusions from the Physical Model Experiments

The results from the physical model experiments provided some insight into pressure flushing with different shaped outlets. The following important conclusions were drawn from the results:

- An increase in discharge through the low-level outlet and increase in initial sediment level increased the scour cone dimensions. The effect of increasing the discharge as well as the effect of the outlet shape reduced with an increase in sediment level. Interestingly, the depth of scour below the outlet was influenced by the initial sediment level, with higher sediment levels associated with less deep scour cones.
- The flat rectangular outlet shape was found to be the overall best performer since it created the longest, widest and deepest scour cones in most scenarios. The scour cone geometry of the square outlet tests was only slightly less than that of the flat rectangular outlet in most cases. A wide low-level outlet is recommended for HPP designs where pressure flushing of sediments will be implemented.
- The scour cone geometry results were compared with the literature in **Section 5.2** and it was found that existing equations do not compensate for the outlet shape, thus greatly over- or underestimating the scour cone dimensions. Designers must be extremely careful of applying existing formulas for scour cone prediction since many have only a very limited range of application.
- Non-dimensional equations for the scour cone dimensions and volume were developed by multi-linear regression analysis in **Section 5.3**. According to the author's best knowledge, these are the first scour cone geometry equations developed for pressure flushing that specifically take the outlet shape into account. The presented equations have high correlation coefficients and predicted the scour cone geometry with an acceptable degree of accuracy. Furthermore, outlet shape specific equations with slightly lower prediction errors were developed for the scour cone geometry in **Section 5.3.9**. All equations can be scaled up to prototype values to estimate the scour cone in a real world pressure flushing scenario as explained in **Section 5.8**.

Chapter 6: Conclusions and Recommendations

- Equations defining the non-dimensional centreline and cross-sectional bed profiles were developed in **Section 5.4** and **5.5** respectively. The aspect ratio of the scour cone was analysed for different conditions and compared to the ratios found by other authors. The flushing efficiency was also investigated as a measure to determine the best outlet shape. Flushing efficiency increased with increase in sediment level or a decrease in water depth. The flat rectangular outlet was the most efficient.

6.3 Recommendations for Further Research

The findings of this thesis have given insight into the effect of low-level outlet shape on the scour upstream of the dam. To further improve the knowledge and understanding of pressure flushing through low-level outlets the following recommendations are made:

- Since only one sediment type could be tested in the physical model due to time constraints, it is suggested that different sediment types (non-cohesive and cohesive) are also tested and compared. This will enable the development of equations that incorporate particle diameter, thus not limiting the equations to a specific sediment. Testing of cohesive sediment should also be considered, because many dams have a muddy lake that forms near the low-level outlets.
- The possibility of designing structures on the upstream end of the low-level outlet, such as suggested by Madadi *et al.* (2016, 2017), to improve flushing, preventing gate blockage and keeping boulders away should be further investigated by physical model studies. Such structures can significantly increase the size of the scour cone and thereby improve flushing efficiency, whilst providing several other benefits.
- Several dams (especially in China) have been designed with numerous upright rectangular outlets closely to each other, which could potentially act similar to one large flat rectangular outlet. Thus, the configuration of several closely spaced narrow low-level outlets that essentially act as one large wide sluice when opened together should be investigated.
- The ideal scenario under which pressure flushing is to be conducted is where the water level is relatively high and power generation at the dam continues as normal during the flushing event. During a pressure flushing event the flow inside the scour cone is turbulent and particles are re-suspended in the vicinity of the dam. If the power intake is located too close to the low-level outlet, pressure flushing may be detrimental to the turbines if any coarse sediment pass through the HPP intake. Further research on the

Chapter 6: Conclusions and Recommendations

physical model should be conducted to determine the minimum height required between the low-level outlet and the power intake.

- In order to make pressure flushing a viable option, the scour cone that forms should be large enough so that it is not immediately filled with sediment again. Even though it will be reservoir dependent, research into the time that the scour cone will take to refill with sediment is a very important design consideration since it will determine the frequency of pressure flushing events required.
- The correct structural and mechanical design of low-level outlets is extremely important for the safety and sustainability of a project. The cost of these structures are major contributors to overall project cost. Conduit and gate design are very important for the correct functioning of the reservoir. Further research into the structural and mechanical components of low-level outlets is required so that optimal pressure flushing can take place whilst also avoiding blockage, abrasion and cavitation.

7 REFERENCES

- Abdolahpour, M. & Roshan, R. 2014. Flow Aeration after Gate in Bottom Outlet Tunnels. *Arabian Journal for Science and Engineering*. 39(5):3441–3448.
- Agrawal, Y., Slade, W., Pottsmith, C. & Dana, D. 2016. Technologies and experience with monitoring sediments for protecting turbines from abrasion. *IOP Conference Series: Earth and Environmental Science*. 49(12).
- Albrecht, M.C., Nachtsheim, C.J., Albrecht, T.A. & Cook, R.D. 2013. Experimental design for engineering dimensional analysis. *Technometrics*. 55(3):257–270.
- Amirsayafi, P. 2015. Measures for Success in Dam Bottom Outlet Design. *GSTF Journal of Engineering Research*. 3(3):111–117.
- Annandale, G.W. 2005. 88 : Reservoir Sedimentation. In M.G. Anderson (ed.). John Wiley & Sons Ltd. *Encyclopedia of Hydrological Sciences*.
- Annandale, G.W., Morris, G.L. & Karki, P. 2016. *Extending the Life of Reservoirs: Sustainable Sediment Management for Dams and Run-of-River Hydropower*. World Bank Group.
- ASCE Hydropower Committee. 1995. *Guidelines for Design of Intakes for Hydroelectric Plants*. New York: American Society of Civil Engineers.
- Atkinson, E. 1996. *The feasibility of flushing sediment from reservoirs*.
- Baoligao, B., Xu, F., Chen, X., Wang, X. & Chen, W. 2016. Acute impacts of reservoir sediment flushing on fishes in the Yellow River. *Journal of Hydro-Environment Research*. 13:26–35.
- Basson, G.R. 2009. Management of siltation in existing and new reservoirs. In *Proc. of the 23rd Congress of the Int. Commission on Large Dams CIGB- ICOLD (vol. 2)*.
- Basson, G.R. & Rooseboom, A. 1999. *Dealing with reservoir sedimentation*.
- Basson, G.R. & Rooseboom, A. 2007. *Mathematical modelling of sediment transport and deposition in reservoirs*.
- Boeriu, P., Roelvink, D., Mulatu, C.A., Thilakasiri, C.N., Moldovanu, A. & Margaritescu, M. 2011. Modeling the flushing process of reservoirs. *Romanian Review Precision Mechanics, Optics and Mechatronics*. (40):54–64.
- Boes, R.M., Müller-Hagmann, M., Albayrak, I., Müller, B., Caspescha, L., Flepp, A., Jacobs, F. & Auel, C. 2018. Sediment Bypass Tunnels: Swiss Experience With Bypass Efficiency and Abrasion-Resistant Invert Materials. In *ICOLD 26th International Congress on Large Dams 4-6 July, Vienna, Austria*. 625–638.
- Boroujeni, H.S., Fathi-Moghadam, M. & Shafaei-Bejestan, M. 2009. Investigation on Bulk Density of Deposited Sediments in Dez Reservoir. *Trends in Applied Sciences Research*. 4(3):148–157.
- Bourdon, P., Farhat, M., Mossoba, Y. & Lavigne, P. 1999. Hydro Turbine Profitability and Cavitation Erosion. *Waterpower '99*. 1–10.
- Bouvard, M. 1992. *Mobile Barrages and Intakes on Sediment Transporting Rivers*. London: Routledge.

Chapter 7: References

- Brabben, T. 1988. *Reservoir desilting methods*. Wallingford.
- Brandt, S.A. 2000. Reservoir Desiltation By Means of Hydraulic Flushing: Sedimentological and Geomorphological Effects in Reservoirs and Downstream Reaches As Illustrated by the Cachí Reservoir and the Reventazón River, Costa Rica. Ph.D. Thesis. University of Copenhagen.
- Brater, E., King, H., Lindell, J. & Wei, C. 1996. *Handbook of Hydraulics*. 7th ed. USA: McGraw-Hill Book Co.
- Bratko, D. & Doko, A. 2013. Water intake structures for hydropower. In *2nd International Balkans Conference on Challenges of Civil Engineering, BCCCE*. 23–25.
- Braune, E. & Looser, U. 1989. Cost impacts of sediments in South African rivers. *Sediment and the Environment*. (184):131–143. [Online], Available: <http://scholar.google.com/scholar?hl=en&btnG=Search&q=intitle:Cost+impacts+of+sediments+in+South+African+rivers#0>.
- Breeze, P. 2014. Hydropower. In 2nd ed. Elsevier Ltd. *Power Generation Technologies*. 153–179.
- Brown, C.B. 1943. *The Control of Reservoir Silting*. Washington, D.C.
- Brown, P.P. & Lawler, D.F. 2003. Sphere Drag and Settling Velocity Revisited. *Journal of Environmental Engineering*. 129(3):222–231.
- Bruk, S. & Zebidi, H. 1996. Reservoir sedimentation. In Paris: UNESCO *International Hydrological Programme*.
- Bureau of Indian Standards. 1995. *Hydropower intakes - Criteria for hydraulic design*. New Delhi.
- Campbell, R.J. 2010. *Small Hydro and Low-Head Hydro Power Technologies and Prospects*. [Online], Available: www.crs.gov.
- Cao, Z., Pender, G. & Meng, J. 2006. Explicit Formulation of the Shields Diagram for Incipient Motion of Sediment. *Journal of Hydraulic Engineering*. 9429(June):553–562.
- Carter, A.C. 1950. *Angle of repose of noncohesive material*. Denver.
- Chadwick, A., Morfett, J. & Borthwick, M. 2013. *Hydraulics in Civil and Environmental Engineering*. CRC Press.
- Chamoun, S., De Cesare, G. & Schleiss, A.J. 2016. Managing reservoir sedimentation by venting turbidity currents: A review. *International Journal of Sediment Research*. 31(3):195–204.
- Chamoun, S., De Cesare, G. & Schleiss, A.J. 2017. Management of turbidity current venting in reservoirs under different bed slopes. *Journal of Environmental Management*. 204:519–530.
- Chanson, H. 1999. Physical modelling of hydraulics. *The Hydraulics of Open Channel Flow*. 261–283.
- Cleveland, C.J. & Morris, C. 2014. *Hydropower*. Vol. II.
- Darbre, G.R., Beckstein, A., de Goumoëns, P., Senn, J., Schlegel, B., Stahl, H., Klein, B., Walti, D., et al. 2018. The Supervision of Small Dams in Switzerland. In *ICOLD 26th International Congress on Large Dams 4-6 July, Vienna, Austria*. 475–494.
- Daware, K. 2016. *Hydroelectric Power Plant: Layout, Working and Types*. [Online], Available: <https://www.electricaleasy.com/2015/09/hydroelectric-power-plant-layout.html> [2018, August

Chapter 7: References

- 07].
- Dey, S. 2014. Bed-Load Transport. In Berlin, Heidelberg: Springer *Fluvial Hydrodynamics*. 261–326.
- Dodaran, A.A., Park, S.K., Mardashti, A. & Noshadi, M. 2012. Investigation of Dimension Changes in Under Pressure Hydraulic Sediment Flushing Cavity of Storage Dams Under Effect of Localized Vibrations in Sediment Layers. 2(2):71–81.
- Dodaran, A.A., Park, S.K., Mardashti, A., Noshadi, M. & Afsari, M. 2013. Experimental Investigation of Local Half-cone Scouring Against Dam under the Effect of Localized Vibrations in the Sediment Layers. *Journal of Ocean Engineering and Technology*. 27(2):107–113.
- Dodaran, A.A., Park, S.K. & Mardashti, A. 2014. Experimental Investigation of the Effect of Vibrator Machine for Desilting Sediment in the Pressure Flushing. *Journal of Scientific Research*. 6(3):475–485.
- Dorji, U. & Ghomashchi, R. 2014. Hydro turbine failure mechanisms: An overview. *Engineering Failure Analysis*. 44:136–147.
- DotProduct. 2017. *DPI-7/8 Imager User Manual - Phi.3D V2.0*.
- Duan, C.G. & Karelin, V.Y. 2002. *Abrasive erosion and corrosion of hydraulic machinery*. Vol. 2. London: Imperial College Press.
- Egré, D. & Milewski, J.C. 2002. The diversity of hydropower projects. *Energy Policy*. 30(14):1225–1230.
- Emamgholizadeh, S. & Fathi-Moghadam, M. 2014. Pressure flushing of cohesive sediment in large dam reservoirs. *Journal of Hydrologic Engineering*. 19(4):674–681.
- Emamgholizadeh, S., Bina, M., Fathi-Moghadam, M. & Ghomeyshi, M. 2006. Investigation and evaluation of the pressure flushing through storage reservoir. *ARPJ Journal of Engineering and Applied Sciences*. 1(4):7–16.
- Emamgholizadeh, S., Bateni, S.M. & Jeng, D. 2013. Artificial intelligence-based estimation of flushing half-cone geometry. *Engineering Applications of Artificial Intelligence*. 26(10):2551–2558.
- ESHA. 2004. *Guide on How to Develop a Small Hydropower Plant*. [Online], Available: <http://citeseerx.ist.psu.edu/viewdoc/download?doi=10.1.1.172.1731&rep=rep1&type=pdf>.
- Espa, P., Castelli, E., Crosa, G. & Gentili, G. 2013. Environmental effects of storage preservation practices: Controlled flushing of fine sediment from a small hydropower reservoir. *Environmental Management*. 52(1):261–276.
- Espa, P., Brignoli, M.L., Crosa, G., Gentili, G. & Quadroni, S. 2016. Controlled sediment flushing at the Cancano Reservoir (Italian Alps): Management of the operation and downstream environmental impact. *Journal of Environmental Management*. 182:1–12.
- Fan, J. 1985. Methods of preserving reservoir capacity. In S. Bruk (ed.). Paris: UNESCO *Methods of computing sedimentation in lakes and reservoirs*. 65–164.
- Fan, J. & Morris, G.L. 1992a. Reservoir sedimentation II: Reservoir Desiltation and Long-Term storage capacity. *Journal of Hydraulic Engineering*. 118(3):370–384.
- Fan, J. & Morris, G.L. 1992b. Reservoir Sedimentation I: Delta and Density Current Deposits. *Journal of Hydraulic Engineering*. 118(3):354–369.

Chapter 7: References

- Fang, D. & Cao, S. 1996. An Experimental Study On Scour Funnel In Front of A Sediment Flushing Outlet of A Reservoir. In Vol. 1. Las Vegas, Nevada *Proceedings of the 6th Federal Interagency Sedimentation Conference*. 78–84.
- Fathi-Moghadam, M., Emamgholizadeh, S., Bina, M. & Ghomeshi, M. 2010a. Physical modelling of pressure flushing for desilting of non-cohesive sediment. *Journal of Hydraulic Research*. 48(4):509–514.
- Fathi-Moghadam, M., Emamgholizadeh, S., Bina, M. & Ghomeshi, M. 2010b. Physical modelling of pressure flushing for desilting of non-cohesive sediment. *Journal of Hydraulic Research*. 48(4):509–514.
- Felix, D., Albayrak, I., Abgottspoon, A. & Boes, R.M. 2016. Hydro-abrasive erosion of hydraulic turbines caused by sediment - A century of research and development. *IOP Conference Series: Earth and Environmental Science*. 49(12).
- FMC AG. 2011. *Hydroelectric Power - A guide for developers and investors*. Stuttgart, Germany: International Finance Corporation.
- Garcia, M.H. 2008. *Sedimentation Engineering Processes, Measurements, Modeling and Practice*. Update on ed. M.H. Garcia (ed.). Virginia: American Society of Civil Engineers.
- Gatte, M.T. & Kadhim, R.A. 2012. Hydro Power. In A.Z. Ahmed (ed.). *InTech Energy Conservation*. 95–124.
- Gill, T.W. & Pugh, C.A. 2009. Sediment transport similitude for scaled physical hydraulic modeling. In Vancouver, Canada *33rd IAHR Congress: Water Engineering for a Sustainable Environment*.
- Guo, J. 2012. Recent achievements in hydraulic research in China. *Comprehensive Renewable Energy*. 6:485–505.
- Hajikandi, H., Vosoughi, H. & Jamali, S. 2017. Comparing the Scour Upstream of Circular and Square Orifices. *International Journal of Civil Engineering*. 0(0):0.
- Healy, K.M., Cox, A.L., Hanes, D.M. & Chambers, L.G. 2014. *State of the practice of sediment management in reservoirs: Minimizing sedimentation and removing deposits*.
- Heller, V. 2011. Scale effects in physical hydraulic engineering models. *Journal of Hydraulic Research*. 49(3):293–306.
- Hussain, A., Ahmad, Z. & Asawa, G.L. 2010. Discharge characteristics of sharp-crested circular side orifices in open channels. *Flow Measurement and Instrumentation*. 21(3):418–424.
- Hussain, A., Ahmad, Z. & Ojha, C.S.P. 2016. Flow through lateral circular orifice under free and submerged flow conditions. *Flow Measurement and Instrumentation*. 52:57–66.
- ICOLD. 2017. *Technical Advancements in Spillway Design - Progress and Innovations from 1985 to 2015*. Prepared by ICOLD Technical Committee on Hydraulics for Dams. ICOLD.
- ICOLD Sedimentation Committee. 2009. *Sedimentation and Sustainable Use of Reservoirs and River Systems*. G.R. Basson (ed)
- International Hydropower Association. 2015. *A brief history of hydropower*. [Online], Available: <https://www.hydropower.org/a-brief-history-of-hydropower> [2017, June 25].
- International Hydropower Association. 2017a. *Hydropower Status Report*.

Chapter 7: References

- International Hydropower Association. 2017b. *2017 Key Trends in Hydropower*.
- IRENA. 2012. *Renewable Energy Technologies: Cost Analysis Series - Hydropower*.
- Jenzer Althaus, J.M.I., Cesare, G. De & Schleiss, A.J. 2015. Sediment Evacuation from Reservoirs through Intakes by Jet-Induced Flow. *Journal of Hydraulic Engineering*. 141(2):04014078.
- Jiang, N. 1980. Some investigations of reservoir sedimentation on heavy silt laden stream. *Journal of Sediment Research*. 1.
- Jiang, N.S. & Fu, L.Y. 1998. Problems of reservoir sedimentation in China. *Chinese Geographical Science*. 8(2):117–125.
- Jin, L. 1992. Local scour upstream of a bottom sluice gate in reservoirs. In Karlsruhe: University of Karlsruhe, Institute of Hydraulic Structures and Agricultural Engineering *Sediment Management, Proceedings of the 5th International Symposium on River Sedimentation*. 791–798.
- Johnson, P.L. 1988. Hydro-power intake design considerations. *Journal of Hydraulic Engineering*. 114(6):651–661.
- Julien, P. & Tuzson, J. 2002. *River Mechanics*. Vol. 56. Cambridge University Press.
- Kamble, S.A., Kunjeer, P.S., B, S. & Isaac, N. 2017. Hydraulic model studies for estimating scour cone development during pressure flushing of reservoirs. *ISH Journal of Hydraulic Engineering*. 5010:1–8.
- Khosrojerdi, A. & Ahmad-Abad, E.A. 2012. Cavitation study in bottom outlet gate slots by pressure fluctuation. *Indian Journal of Science and Technology*. 5(3):2273–2280.
- Kistner, S. 2013. Dam sediment flushing outlet. Bachelor's Thesis. University of Stellenbosch.
- Kjølle, A. 2001. *Hydropower in Norway - Mechanical Equipment*. [Online], Available: <http://www.magnu.polymtl.ca/contenu/ressources/docDivers/doc/Turbines101.pdf>.
- Kondolf, G.M. 1997. Hungry water: Effects of dams and gravel mining on river channels. *Environmental Management*. 21(4):533–551.
- Kondolf, G.M., Gao, Y., Annandale, G.W., Morris, G.L., Jiang, E., Zhang, J., Cao, Y., Carling, P., et al. 2014. Sustainable sediment management in reservoirs and regulated rivers : Experiences from five continents Earth's Future. *Earth's Future*. 256–280.
- Kriewitz, C.R., Gabl, W.F. & Lazaro, P. 2018. Sediment Transport Restoration - Experience and Lesson Learned at Simmeweir Intake and at Vasasca Dam in Switzerland. In *ICOLD 26th International Congress on Large Dams 4-6 July, Vienna, Austria*. 565–575.
- Kumar, A. & Singal, S.K. 2013. *STANDARDS/MANUALS/ GUIDELINES FOR SMALL HYDRO DEVELOPMENT*.
- Kumar, A., Schei, T., Ahenkorah, A., Caceres Rodriguez, R., Devernay, J.-M., Freitas, M., Hall, D., Killingtveit, Å., et al. 2011. Hydropower. In IPCC Special Report on Renewable Energy Sources and Climate Change Mitigation. In O. Edenhofer, R. Pichs-Madruga, Y. Sokona, K. Seyboth, P. Matschoss, S. Kadner, T. Zwickel, P. Eickemeier, G. Hansen, S. Schlömer, & C. von Stechow (eds.). Cambridge, United Kingdom and New York, NY, USA: Cambridge University Press *Renewable Energy Sources and Climate Change Mitigation*. 437–496.
- Lai, J.-S. & Shen, H.W. 1996. Flushing sediment through reservoirs. *Journal of Hydraulic Research*.

Chapter 7: References

- 34(2):237–255.
- Lane, E.W. & Koelzer, V.A. 1943. *Density of sediments deposited in reservoirs*. Iowa.
- Lara, J.M. & Pemberton, E.L. 1963. Initial weight of deposited sediments. In Denver, USA: U.S. Department of Agriculture *Proceedings of Federal Interagency Conference*. 933.
- Madadi, M.R., Rahimpour, M. & Qaderi, K. 2016. Sediment flushing upstream of large orifices: An experimental study. *Flow Measurement and Instrumentation*. 52(October):180–189.
- Madadi, M.R., Rahimpour, M. & Qaderi, K. 2017. Improving the Pressurized Flushing Efficiency in Reservoirs: an Experimental Study. *Water Resources Management*. 31(14):4633–4647.
- Mahmood, K. 1987. *Reservoir sedimentation; Impact, Extent, and Mitigation*.
- Majumder, M. & Ghosh, S. 2013. Decision Making Algorithms for Hydro-Power Plant Location. 15–20.
- Meshkati, M.E., Dehghani, A.A., Naser, G., Emamgholizadeh, S. & Mosaedi, A. 2009. Evolution of Developing Flushing Cone during the Pressurized Flushing in Reservoir Storage. *International Journal of Environmental, Chemical, Ecological, Geological and Geophysical Engineering*. 3(10):355–359.
- Meshkati Shahmirzadi, M.E., Dehghani, A.A., Sumi, T., Mosaedi, A. & Meftah H, M. 2010. Experimental Investigation of Pressure Flushing Technique in Reservoir Storages. *Water and Geoscience*. (54):132–137.
- Meshkati Shahmirzadi, M.E., Dehghani, A.A., Sumi, T., Naser, G. & Ahadpour, A. 2010. *Experimental investigation of local half-cone scouring against dam*. Dittrich, Koll, Aberle & Geisenhainer.
- Miller, C.R. 1953. Determination of the Unit Weight of Sediment for use in Sediment Volume Compaction. In R.I. Strand & E.L. Penibertori (eds.). Denver, USA: USBR *Reservoir Sedimentation: Technical Guideline for Bureau of Reclamation*.
- Miller, R.L. & Byrne, R.J. 1966. The Angle of Repose for a Single Grain on a Fixed Rough Bed. *Sedimentology*. 6(4):303–314.
- Mohammad, B.T., Daham, F.A. & Bilal, Z.Z. 2017. Experimental Investigation to study the Hydraulic Performance of Pressure Flushing in Straight Wall Reservoirs. In Vol. 1. Dam and water resources Department, College of Engineering, Salahaddin University-Hawler *1st International Conference of Water and Energy in Kurdistan, Challenges and Alternatives (ICWEK2017)*. 1–19.
- Morris, G.L. 2015. Management alternatives to combat reservoir sedimentation. In Zurich *First International Workshop on Sediment Bypass Tunnels*. 181–193.
- Morris, G.L. & Fan, J. 1998. *Reservoir Sedimentation Handbook*. 1st ed. New York: McGraw-Hill Book Co.
- Morris, G., Annandale, G. & Hotchkiss, R. 2008. Reservoir Sedimentation. In American Society of Civil Engineers (ed.). Reston, USA *Sedimentation Engineering: Processes, Measurements, Modeling, and Practice*.
- Msadala, V.P. 2009. Sediment Yield Prediction Based on Analytical Methods and Mathematical Modelling. Master's Thesis. University of Stellenbosch.
- Novák, P. & Cabelka, J. 1981. *Models in hydraulic engineering: physical principles and design*

Chapter 7: References

- applications*. London: Pitman Publishing Limited.
- Okumura, H. & Sumi, T. 2012. *Reservoir Sedimentation Management in Hydropower Plant Regarding Flood Risk and Loss of Power Generation*. Kyoto.
- Padhy, M.K. & Saini, R.P. 2008. A review on silt erosion in hydro turbines. *Renewable and Sustainable Energy Reviews*. 12:1974–1987.
- Partheniades, E. 2009. *Cohesive Sediments in Open Channels: Erosion, Transport and Deposition*. Butterworth-Heinemann.
- Paul, T.C. & Dhillon, G.S. 1988. Sluice dimensioning for desilting reservoirs. *International Water Power and Dam Construction*. 40–44.
- Pitt, J.D. & Thompson, G. 1984. The impact of sediment on reservoir life. Challenges in African Hydrology and Water Resources. In IAHS Publi ed. D.E. Walling, S.S.D. Foster, & P. Wurzel (eds.). Harare, Zimbabwe *Proceedings of the Harare Symposium, July*. 541–548.
- Poudel, L., Thapa, B., Shrestha, B.P., Thapa, B.S., Shrestha, K.P. & Shrestha, N.K. 2012. Computational and experimental study of effects of sediment shape on erosion of hydraulic turbines. *26th Iahr Symposium on Hydraulic Machinery and Systems, Pts 1-7*. 15:1–5.
- Powell, D. 2007. Sediment transport upstream of orifices. Clemson University. [Online], Available: <http://etd.lib.clemson.edu/documents/1202498786/umi-clemson-1443.pdf>.
- Powell, D.N. & Khan, A.A. 2012. Scour upstream of a circular orifice under constant head. *Journal of Hydraulic Research*. 50(1):28–34.
- Pugh, C.A. 2008. Sediment transport scaling for physical models. *Sedimentation Engineering: Processes, Measurements, Modeling, and Practice*. 5:1057–1065.
- Qian, N. 1982. Reservoir sedimentation and slope stability; technical and environmental effects. *Fourth International Congress on Large Dams, Rio de Janeiro, Brazil*. 3:639–690.
- Quadroni, S., Brignoli, M.L., Crosa, G., Gentili, G., Salmaso, F., Zaccara, S. & Espa, P. 2016. Effects of sediment flushing from a small Alpine reservoir on downstream aquatic fauna. *Ecohydrology*. 9(7):1276–1288.
- Ramos, H. & Betâmio de Almeida, A. 2000. *Guidelines for the design of Small Hydropower Plants*. Belfast, Northern Ireland: WREAN and DED.
- Rathore, P., Sahu, G., Sen, P.K., Sharma, R. & Bohidar, S. 2015. A Review on Steam Turbine Blade Desing and It's Principle. *International Journal of Science Technology & Engineering*. 2(5):4–8.
- Raudkivi, A.J. 1993. *Sedimentation: Exclusion and Removal of Sediment from Diverted Water*. CRC Press.
- Reda, A.L.L., Viña, F.D.S., Alves, R.L.F. & Ribeiro, R.G.C. 2016. Santo Antônio Hydroelectric Power Plant Reservoir Life Time: An Independent Sediment Budget Estimate on the Madeira River, Brazil. In Salvador *XIV International Conference on Engineering and Technology Education, February 28 – March 02, 2016, Salvador, Brazil*. 30–34.
- Rettedal, B. & Nielsen, L.E. 2012. Different Aspects of Flushing of Hydropower Intakes. Norwegian University of Science and Technology.
- Van Rijn, L.C. 1993. *Principles of sediment transport in rivers, estuaries and coastal seas*. Amsterdam:

Chapter 7: References

- Aqua Publications.
- Rollo, C., Bonnani, S., Sayah, S.M., Arboli, J. & Braghini, M. 2018. Sedimentation Management of Cerro Del Aguila Reservoir in Peru: A “Mobile Dam” for a Highly Erosive Andean Watershed. In *ICOLD 26th International Congress on Large Dams 4-6 July, Vienna, Austria*. 262–278.
- Rooseboom, A., Basson, M.S., Loots, C.H., Wiggett, J.H. & Bosman, J. 1983. *National Transport Commission Road Drainage Manual*. 2nd Editio ed. Pretoria: Director-General: Transport. Chief Directorate: National Roads: South African National Roads Agency.
- Rulot, F., Dewals, B.J., Erpicum, S., Archambeau, P. & Piroton, M. 2012. Long-term sediment management for sustainable hydropower. In Liege: Elsevier Ltd. *Comprehensive Renewable Energy*. 355–376.
- Samto Atmodjo, P. & Suripin. 2012. The Effect of Water Level on The Effectiveness of Sediment Flushing. *Internat. J. Waste of Resources*. 2(2):20–31.
- Sangal, S., Singhal, M.K. & Saini, R.P. 2018. Hydro-abrasive erosion in hydro turbines: a review. *International Journal of Green Energy*. 15(4):1–22.
- SANRAL. 2013. *Drainage Manual*. 6th ed. Pretoria: South African National Roads Agency.
- Sarkardeh, H. 2017. Minimum Reservoir Water Level in Hydropower Dams. *Chinese Journal of Mechanical Engineering (English Edition)*. 30(4):1017–1024.
- Sawadogo, O. 2015. Coupled Fully Three-Dimensional Mathematical Modelling of Sediment Deposition and Erosion in Reservoirs. Ph.D. Thesis. University of Stellenbosch.
- Sayah, S.M., Calvo, S., Bonanni, S. & Fenelli, A. 2015. *Design and erection of the 6 bottom outlets of Cerro del Águila dam for flood routing during construction and future sediment flushing*.
- Schellenberg, G., Donnelly, C.R., Holder, C., Briand, M.-H. & Ahsan, R. 2017. Sedimentation and Hydropower: Impacts and Solutions Sedimentation, Dam Safety and Hydropower: Issues, Impacts and Solutions. 24. [Online], Available: [http://www.hydroworld.com/content/dam/hydroworld/online-articles/2017/04/Sedimentation Dam Safety and Hydropower- Issues Impacts and Solutions.pdf](http://www.hydroworld.com/content/dam/hydroworld/online-articles/2017/04/Sedimentation%20Dam%20Safety%20and%20Hydropower-%20Issues%20Impacts%20and%20Solutions.pdf).
- Schellenberg, G., Donnelly, C.R., Holder, C. & Ahsan, R. 2017. *Dealing with Sediment : Effects on Dams and Hydropower Generation*.
- Scheuerlein, H. 1993. Estimation of flushing efficiency in silted reservoirs. In Washington, D.C. *Proceedings of the First International Conference on Hydro-Science and Engineering*.
- Scheuerlein, H., Tritthart, M. & Nuñez Gonzalez, F. 2004. Numerical and physical modelling concerning the removal of sediment deposits from reservoirs. In F. Yazdandoost & J. Attari (eds.). Taylor & Francis Group *Hydraulics of Dams and River Structures- Proceedings of the International Conference, Tehran, Iran, 26-28 April 2004*. 328–341.
- Schleiss, A.J., Franca, M.J., Juez, C. & De Cesare, G. 2016. Reservoir sedimentation. *Journal of Hydraulic Research*. 54(6):595–614.
- Shahraki, S.M., Ahadpour, A. & Mardashty, A. 2014. Pressure Hydraulic Sediment Flushing on short dams. *Journal of River Engineering*. 2(9).
- Shammaa, Y., Zhu, D.Z. & Rajaratnam, N. 2005. Flow upstream of orifices and sluice gates. *Journal of Hydraulic Engineering*. 131(2):127–133.

Chapter 7: References

- Sharma, H.D. & Sharma, H.R. 1977. Sediment problems at intakes for hydropower plants. *Hydrological Sciences Journal*. 122:330–337.
- Shen, H.W. 1999. Flushing sediment through reservoirs. *Journal of Hydraulic Research*. 37(6):743–757.
- Di Silvio, G. 1990. Modeling desiltation of reservoirs by bottom-outlet flushing. In H.W. Shen (ed.). Dordrecht: Kluwer Academic Publishers *Movable bed physical models*. 159–171.
- Singh, R., Tiwari, S.K. & Mishra, S.K. 2012. Cavitation erosion in hydraulic turbine components and mitigation by coatings: Current status and future needs. *Journal of Materials Engineering and Performance*. 21(7):1539–1551.
- Srivastav, A. & Nayak, A. 2015. Bottom Outlet of Koldam HEPP – Scheme, Challenges and Performance – A Case Study. In *Global Energy Technology Summit*.
- Sumi, T. & Hirose, T. 2000. Accumulation of sediment in reservoirs. In *Encyclopedia of Life Support Systems Water storage, transport and distribution*.
- Sumi, T. & Kantoush, S.A. 2010. Integrated Management of Reservoir Sediment Routing by Flushing, Replenishing, and Bypassing Sediments in Japanese River Basins Dam. In *Proceedings of the 8th International Symposium on Ecohydraulics, Seoul, Korea*. 831–838.
- Tiğrek, Ş., Göbelez, Ö. & Aras, T. 2009. Sustainable management of reservoirs and preservation of water quality. 53:41–53. [Online], Available: <http://om.ciheam.org/article.php?IDPDF=801179>.
- Tomlinson, R.A. 1976. The Perachora Waterworks: Addenda. *The Annual of the British School at Athens*. 71:147–148.
- USACE. 2003. *Engineering and Design: Structural Design and Evaluation of Outlet Works*. Washington DC.
- USBR. 1987. *Design of Small Dams*. 3rd ed. United States Department of the Interior.
- USBR. 2005. *Hydroelectric Power*.
- Vanoni, V.A. 2006. *Sedimentation Engineering*. Classic Ed ed. ASCE.
- Vischer, D.L. & Hager, W.H. 1998. *Dam Hydraulics*. Zurich: John Wiley & Sons Ltd.
- Walker, K. 2016. *Intake vortex formation and suppression at hydropower facilities*.
- Webber, N.B. 1971. Hydraulic Models. In London: Chapman and Hall *Fluid Mechanics for Civil Engineers*. 297–304.
- Wetstone, G., Thornton, K., Hinrichs-rahlwes, R., Sawyer, S., Sander, M., Taylor, R., Rodgers, D., Alers, M., et al. 2016. *Renewables 2016 GLObal Status Report*.
- White, R. 2001. *Evacuation of sediments from reservoirs*. London: Thomas Telford publishing.
- White, W.R. & Bettess, R. 1984. The feasibility of flushing sediments through reservoirs. *International Association of Hydrological Sciences*. (144):577–587.
- Xu, M. & Lu, X. 1991. *Reservoir sedimentation control strategies in China*.
- Yang, C.T. 2003. *Sediment Transport: Theory and Practice*. Malabar, Florida: Krieger Publishing

Chapter 7: References

Company.

Yin, X.A., Yang, Z.F., Petts, G.E. & Kondolf, G.M. 2014. A reservoir operating method for riverine ecosystem protection, reservoir sedimentation control and water supply. *Journal of Hydrology*. 512:379–387.

8 APPENDICES

Appendix A Summary of Tunnel Spillways	182
Appendix B Experimental Setup Photos	185
Appendix C Sediment Specification Sheet	188
Appendix D Scanner Specifications.....	189
Appendix E Scour Cone Photos	190
Appendix F Scour Cone Contour Plots	193
Appendix G Comparison with Other Studies.....	199
Appendix H Statistical Parameters Definitions.....	205
Appendix I Sreferetastical Parameters of the Regression Analysis	207
Appendix J Statistical Parameters for the Outlet Specific Regression Analysis.....	208
Appendix K Centreline Bed Profiles.....	210
Appendix L Cross-Sectional Bed Profiles	215
Appendix M Scour Cone Slope Comparison	220
Appendix N Prototype Scaled Graphs	221

Appendix A Summary of Tunnel Spillways

Table A.1 Characteristics of typical large scale tunnel spillways ordered by height ICOLD (2017)

Project Name	Country	Type of dam	Dam height (m)	Type of tunnel spillway (see Figure A.1)	Number of tunnel spillways	Shape	Tunnel dimensions, BxH (m)	Q_{\max} (m^3/s)	Type of aeration	Year of completion	Width/height ratio (rectangular only)
Rogun	Tajikistan	ER	335	V(a)	1	Horseshoe	D14×17	4040	Aerator in vortex	u.d.	-
Rogun	Tajikistan	ER	335	V	1	Horseshoe	D14×17	1800	Aerator in vortex	u.d.	-
Rogun	Tajikistan	ER	335	V	1	Horseshoe	D14×17	2000	Aerator in vortex	u.d.	-
Jinping I	China	AV	305	IV	1	Rectangular	14×12	3651	Offset, ramp	u.c.	1.17
Nurek	Tajikistan	ER	300	III	1	Rectangular	11×10	2000	Aerator ds of radial gate	1980	1.10
Nurek	Tajikistan	ER	300	II	1	Rectangular	10×10.5	2020	Aerator ds of radial gate	1980	0.95
Xiaowan	China	AV	292	IV	1	Rectangular	13×13.5	3811	2-steps offset	2011	0.96
Xiluodu	China	AV	278	IV	4	Rectangular	14×12.5	4×3860	Offset, ramp	u.c.	1.12
Tehri	India	ER	261.5	IV	1	Circular	8.5	1100	-	2008	-
Tehri	India	ER	260.5	V	4	Horseshoe	D11	1800	Deaerator between vertical shaft and horizontal tunnel	2008	-
Mica	Canada	ER	244	V	1	-	-	850	Concrete plug	1977	-
Mica	Canada	ER	244	III	1	-	-	-	Offset	1977	-

Appendix A: Summary of Tunnel Spillways

Ertan	China	AV	240	III	2	Rectangular	13×13.5	3700	Offset, ramp	1999	0.96
Sayano-Shushenskaya	Russia	AV	240	II	2	Rectangular	10×12	1900	In stepped chute	2011	0.83
Chirkeyskaaya	Russia	AV	232	III	1	Rectangular	11.2×12.6	2900	-	1978	0.89
Hoover	United States	PG	221	III	2	Circular	15.56	5500	Circular aerator	1936	-
Glen Canyon	United States	AV	216	III	1	Circular	12.5	3900	Circular aerator	1966	-
Irape	Brazil	TE	208	II	2	Rectangular	10×11.4	2000	Offset	2005	0.88
Irape	Brazil	TE	208	II	1	Rectangular	12×11.4	2000	Offset	2005	1.05
Longyangxia	China	PG	178	III	1	Rectangular	5×7	1340	Offset at gate	1989	0.71
Charvakskaaya	Uzbekistan	ER	168	IV	1	Circular	9	1100	Downstream steel liner	1976	-
Charvakskaaya	Uzbekistan	ER	168	V	1	Circular	11	1200	Downstream steel liner	1976	-
Xiaolangdi	China	ER	160	II	1	Rectangular	10×12	2680	Offset	2000	0.83
Xiaolangdi	China	ER	161	II	1	Rectangular	8×9	1973	Offset	2000	0.89
Xiaolangdi	China	ER	162	II	1	Rectangular	8×9.5	1796	Offset	2000	0.84
Xiaolangdi	China	ER	163	V	1	Circular	14.5	1727	Offset at gate	2000	-
Xiaolangdi	China	ER	164	V	2	Circular	14.5	1549	Offset at gate	2000	-
Yellowtail	United States	AV	160	III	2	Circular	15.56	2600	Circular aerator	1968	-
Zipingpu	China	CFRD	156	III	1	Horseshoe	D10.7	1672	U-shape sidewall ramp	2006	-
Liujiaxia	China	PG	147	III	1	Rectangular	8×12.9	2105	Aerator	1974	0.62
Cousar	Iran	PG	140	II	2	Rectangular	10×10	1900	-	2006	1.00
Aldeadavila	Spain	-	139.5	III	1	Circular	10.4	2800	-	1962	-

Appendix A: Summary of Tunnel Spillways

Gongboxia	China	CFRD	132.2	V	1	Rectangular	11×14	1090	Circular aerator on lower part of shaft	2006	0.79
Shapai	China	RCC/VA	132	V	1	Rectangular	4×5.5	242	Air vent downstream	2002	0.73

Where: *PG* = gravity dam, *RCC* = roller compacted concrete dam, *VA* = arch dam, *CFRD* = concrete faced rockfill dam, *ER* = rock-filled dam, *TE* = earth-filled dam, *u.c.* = under construction, *u.d.* = under design.

The type of tunnel spillway refers to the types shown in **Figure A.1**.

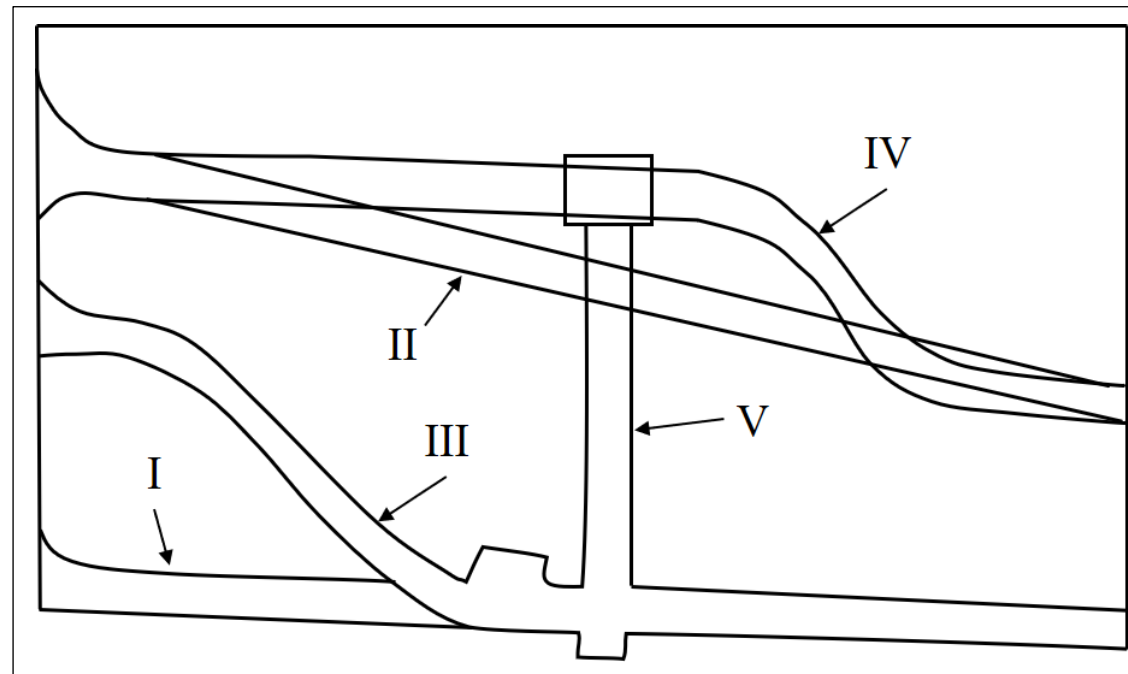


Figure A.1 Tunnel spillway types according to ICOLD (2017)

Appendix B Experimental Setup Photos



Figure B.1 View downstream towards plate showing concrete flow straighteners in flume



Figure B.2 View downstream towards plate showing the levelled sediment bed at the invert level ($H_s = 0$ m) before the start of Test 1

Appendix B: Experimental Setup Photos



Figure B.3 View of levelled sediment bed with thin steel plate used to keep sediment out of the outlet (acting as a control gate)



(a)



(b)

Figure B.4 (a) SAFMAG flow meter used for measuring outflowing discharge (b) butterfly valve used to control outflow

Appendix B: Experimental Setup Photos



Figure B.5 Settling basin used to trap outflowing sediment



Figure B.6 Outflow at settling basin during testing

Appendix C Sediment Specification Sheet

No 2 Foundry sand (Consol)				
<u>Grading Limits</u>			<u>Other</u>	
-212 μ m 80% Min			AFS No. 85-105	
Typical Grading Analysis			Typical Chemical Analysis	
(U.S.) Mesh	Aperture (μ m)	% Retained	Component	%
4	4750		SiO ₂	99.45
5	4000		Al ₂ O ₃	0.158
6	3350		Fe ₂ O ₃	0.048
7	2800		TiO ₂	0.043
8	2300		ZrO ₂	0.006
10	2000		CaO	0.025
12	1700		MgO	0.001
14	1400		L.O.I	0.213
16	1180			
18	1000			
20	850			
25	710	0		
30	600	-		
35	500	0.8		
40	425	-		
45	355	2.9		
50	300	-		
60	250	4.9		
70	212	2.9		
80	180	-		
100	150	25.9		
120	125	-		
140	106	45.6		
200	75	13.4		
(-200)	-75	3.5		
			<u>Other typical data</u>	
			Loose bulk density	1461 kg/m ³
			Coefficient of Uniformity	1.63
			A.F.S. Number	96.3
			Size Range	0.0-0.5 mm
			Total fines	3.5

Figure C.1 Sediment specification sheet as provided by supplier

Appendix D Scanner Specifications

PRODUCT SPECIFICATIONS	DPI-8 PRODUCT SPECIFICATIONS – GENERAL	DPI-8 PRODUCT SPECIFICATIONS – PHYSICAL															
Screen Size: 8 inch	Imager type Compact, near infrared structured light and rgb 3D imaging system User Interface Android 4.4/Android 4.2 operating system Data Storage Onboard 16 GB or 32 GB flash drive Data Transfer USB 2.0/3.0, microUSB connector	Mass <1kg (2.2 lbs)															
Device Size: 20 cm x 24 cm x 6 cm		Dimensions 20 cm x 24 cm x 6 cm (8 in x 9.5 in x 2.4 in)															
Interfaces: USB, WiFi, 3G		Temperature Tested operating range: 15°C to 32°C (60°F to 85°F)															
Capacity: 16 GB or 32 GB		Lighting Not Operational in direct sunlight															
Export Formats: 16 GB or 32 GB		Humidity Non-condensing															
Sensor Range: 60 cm to 5 m (2 ft to 15 ft)	<table border="1"> <thead> <tr> <th>RANGE</th> <th>TYPICAL ACCURACY (RMS)</th> <th>MINIMUM ACCURACY</th> </tr> </thead> <tbody> <tr> <td>< 1 m (3.3 ft)</td> <td>0.2%</td> <td>0.4%</td> </tr> <tr> <td>1 m to 2 m (6.6 ft)</td> <td>0.5%</td> <td>0.8%</td> </tr> <tr> <td>2 m to 3.3 m (11 ft)</td> <td>0.8%</td> <td>1.2%</td> </tr> <tr> <td>>3.3 m (11 ft)</td> <td>Not specified</td> <td>Not specified</td> </tr> </tbody> </table>		RANGE	TYPICAL ACCURACY (RMS)	MINIMUM ACCURACY	< 1 m (3.3 ft)	0.2%	0.4%	1 m to 2 m (6.6 ft)	0.5%	0.8%	2 m to 3.3 m (11 ft)	0.8%	1.2%	>3.3 m (11 ft)	Not specified	Not specified
RANGE	TYPICAL ACCURACY (RMS)	MINIMUM ACCURACY															
< 1 m (3.3 ft)	0.2%	0.4%															
1 m to 2 m (6.6 ft)	0.5%	0.8%															
2 m to 3.3 m (11 ft)	0.8%	1.2%															
>3.3 m (11 ft)	Not specified	Not specified															
Op. Temperature: 5°C to 40°C (41°F - 104°F)																	
Horizontal FOV: 57.5 degrees																	
Point Density: ≤ 1.7mm at 1m distance ≤ 3.4mm at 2m distance																	
Power Supply: Using tablet battery																	

Figure D.1 DPI-8 handheld 3D scanner specifications (DotProduct, 2017)

Appendix E Scour Cone Photos

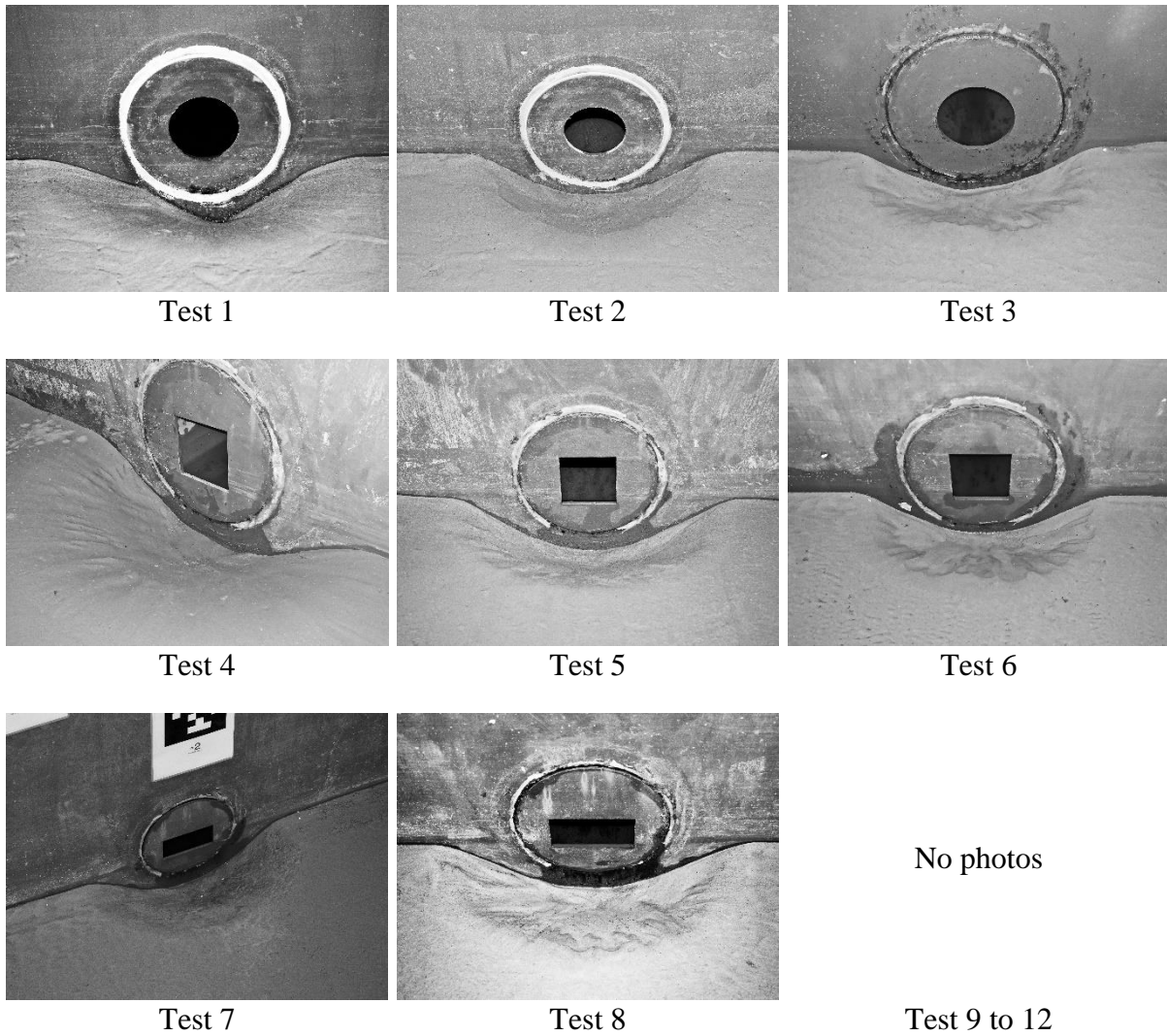


Figure E.1 Scour cone photos for the first set of tests where $H_s = 0$ m

Appendix E: Scour Cone Photos

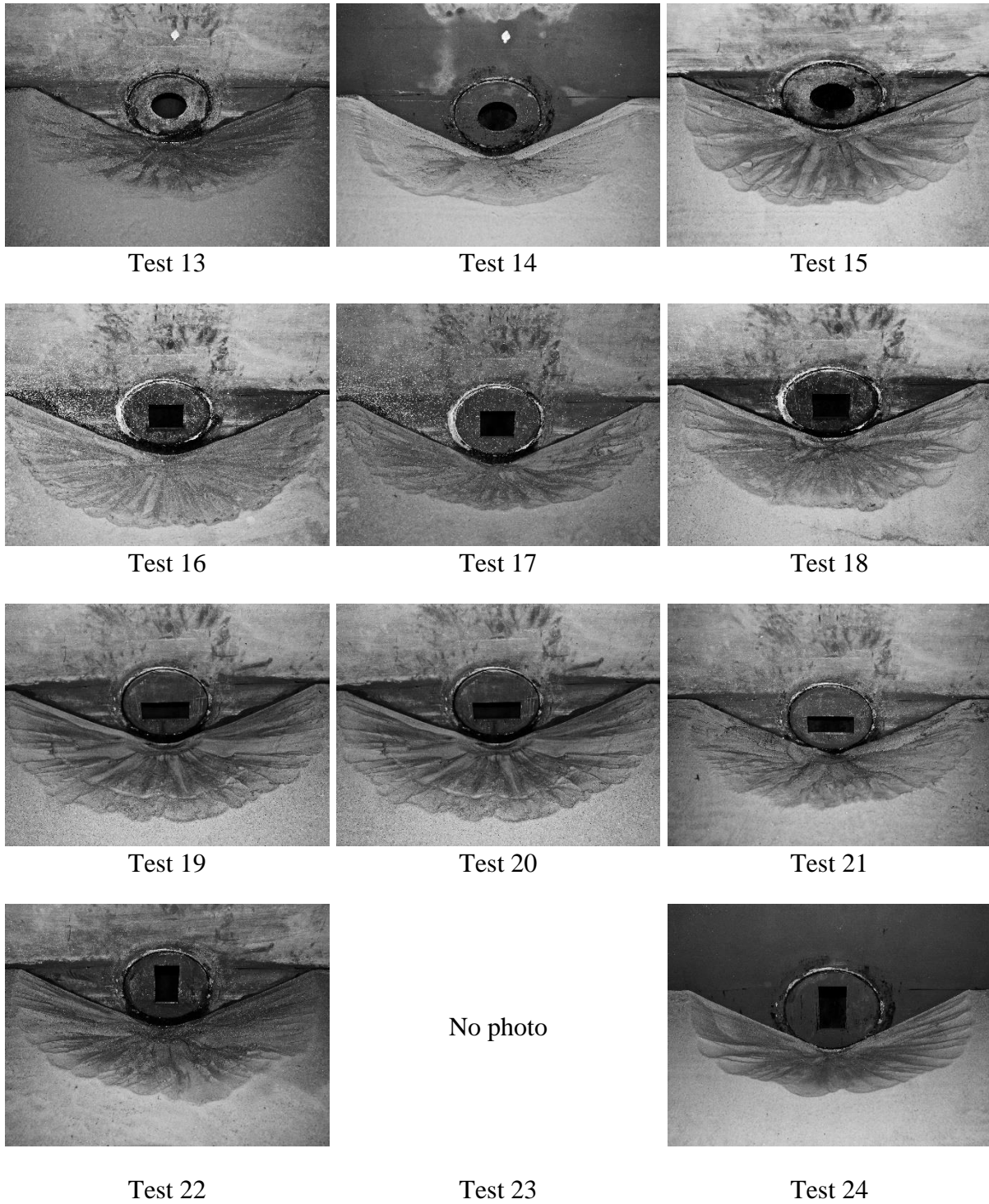


Figure E.2 Scour cone photos for the first set of tests where $H_s = 0.1$ m

Appendix E: Scour Cone Photos

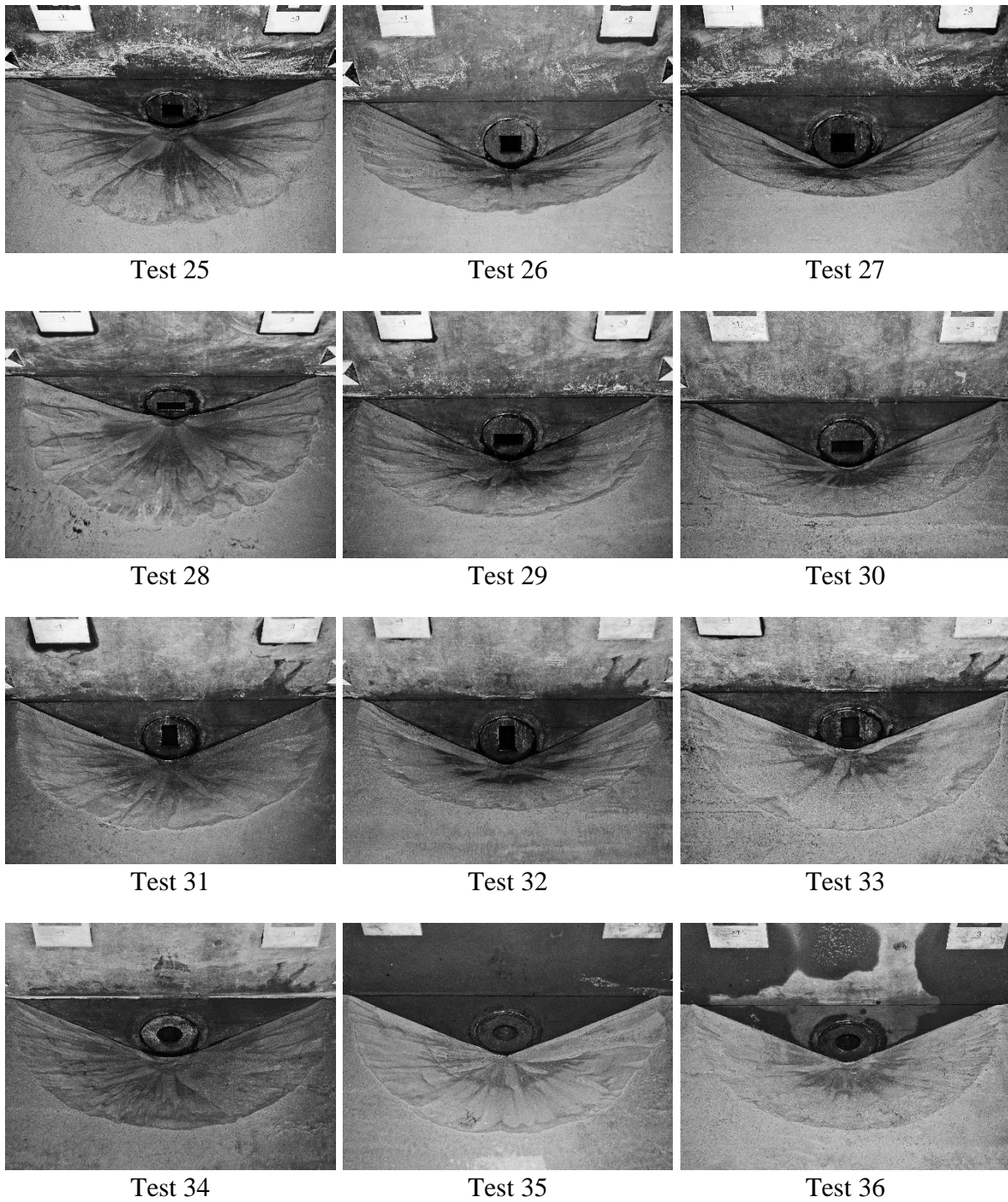


Figure E.3 Scour cone photos for the first set of tests where $H_s = 0.2$ m

Appendix F Scour Cone Contour Plots

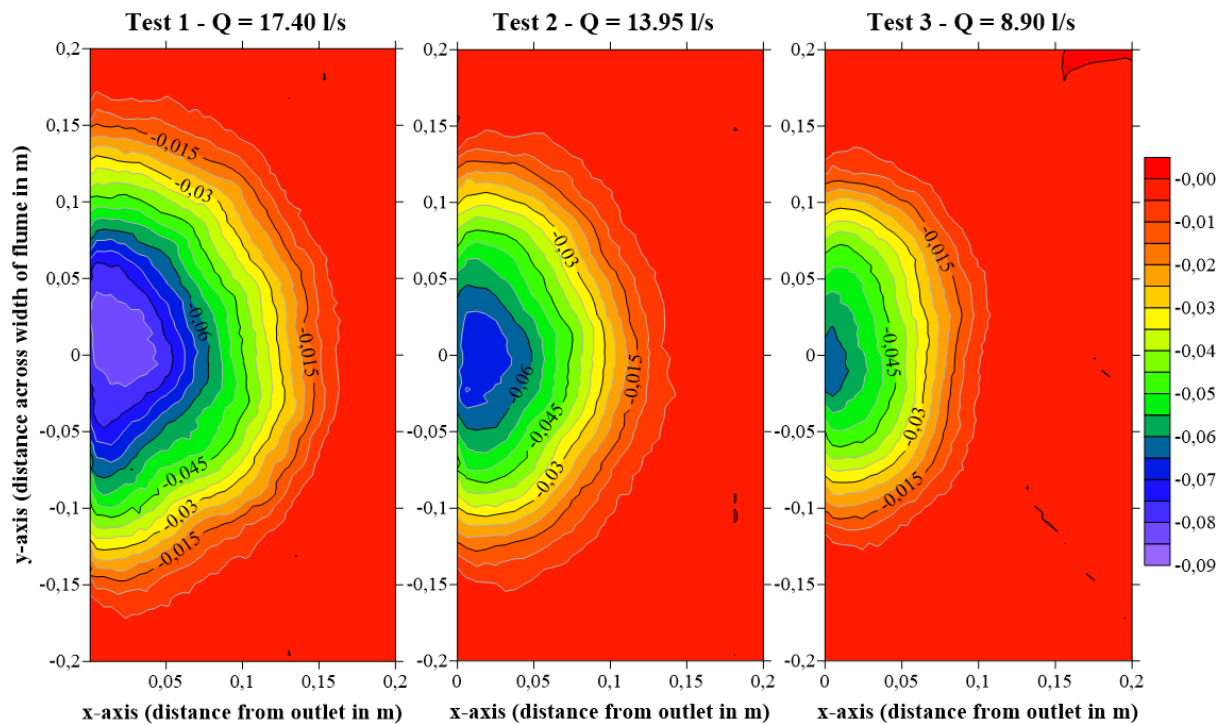


Figure F.1 Scour cone contour plots for Tests 1 to 3 (Round outlet)

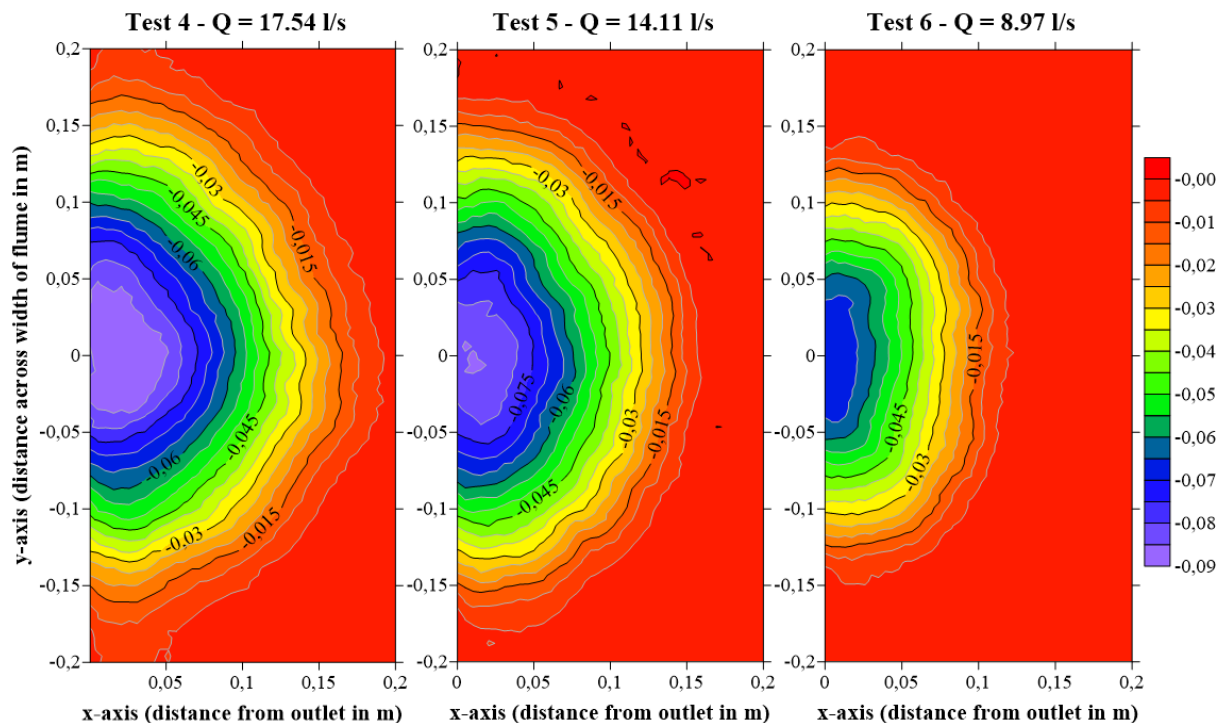


Figure F.2 Scour cone contour plots for Tests 4 to 6 (Square outlet)

Appendix F: Scour Cone Contour Plots

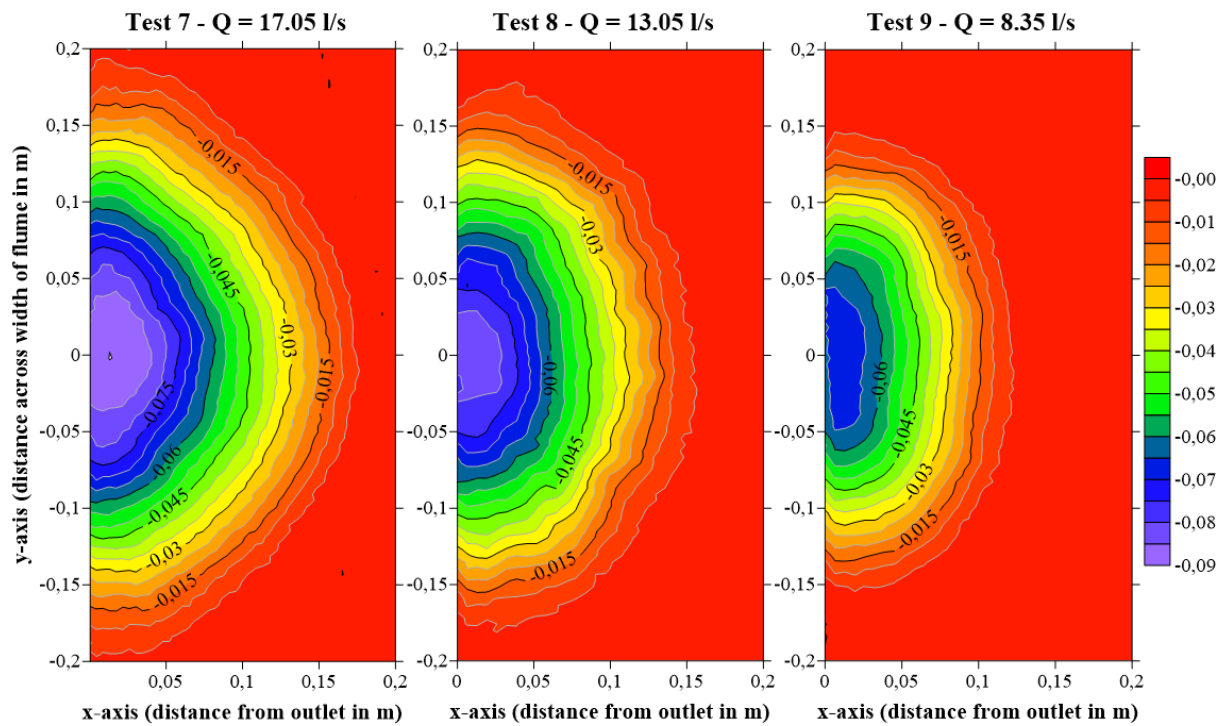


Figure F.3 Scour cone contour plots for Tests 5 to 7 (Flat rectangular outlet)

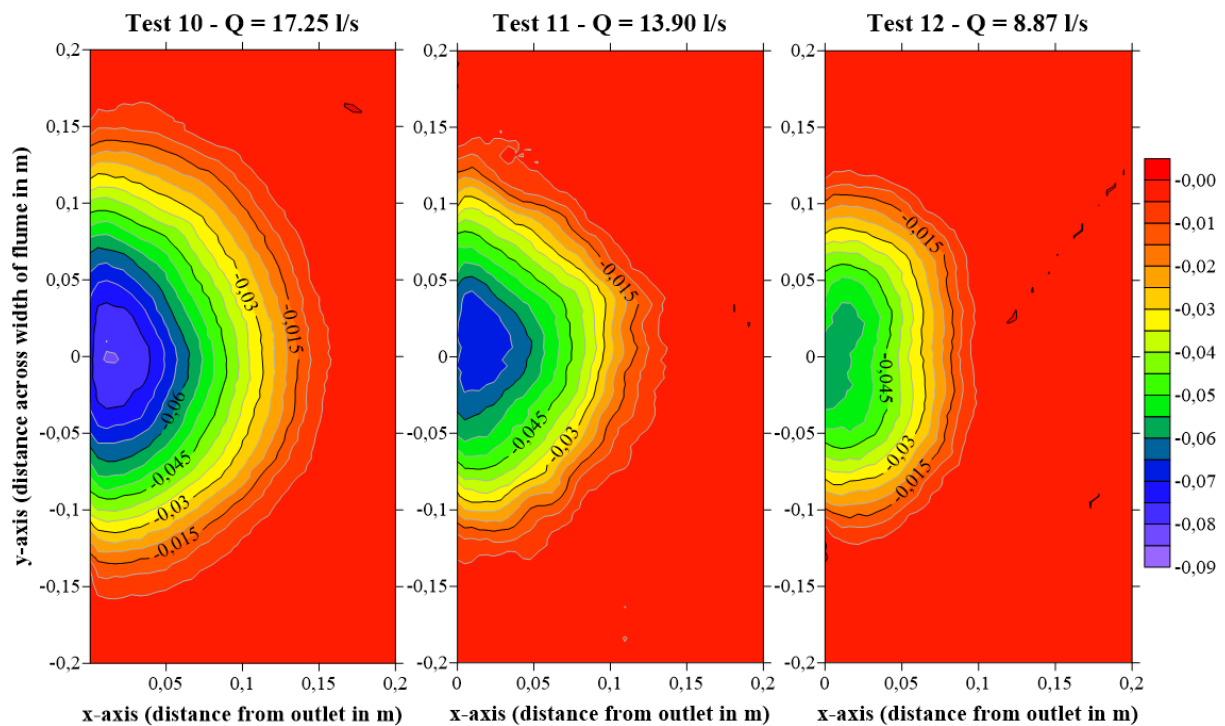


Figure F.4 Scour cone contour plots for Tests 10 to 12 (Upright rectangular outlet)

Appendix F: Scour Cone Contour Plots

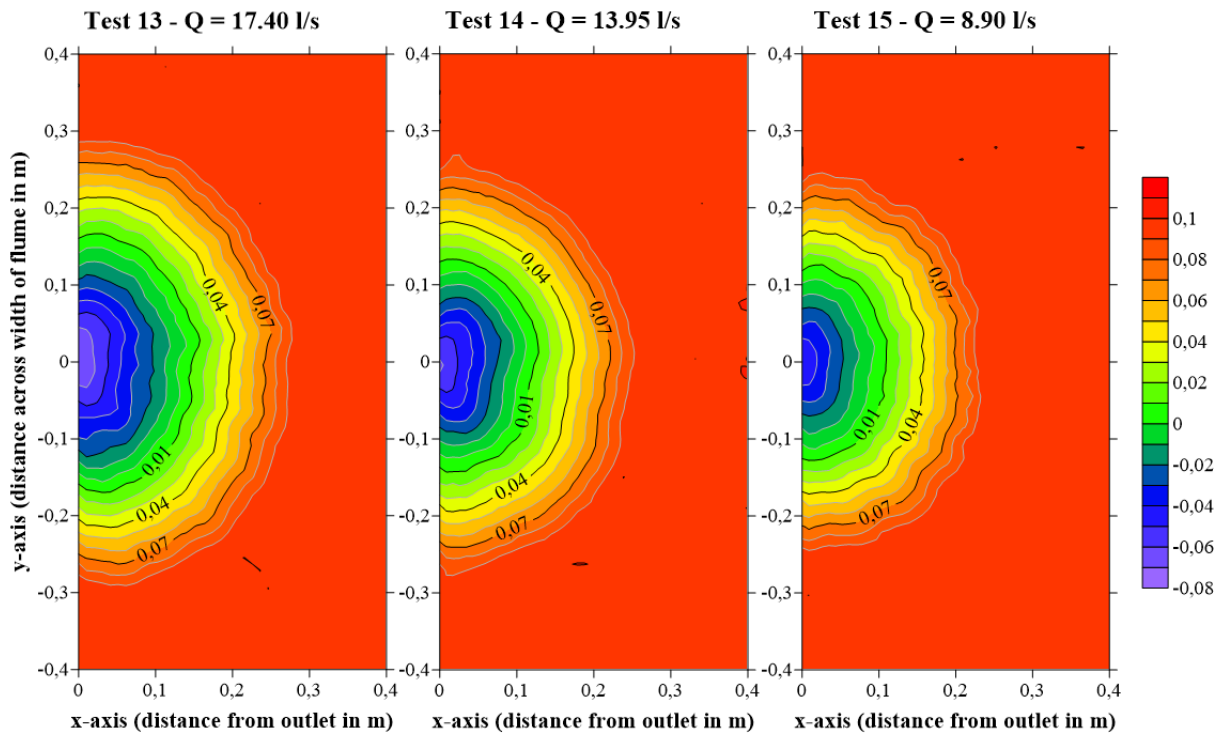


Figure F.5 Scour cone contour plots for Tests 13 to 15 (Round outlet)

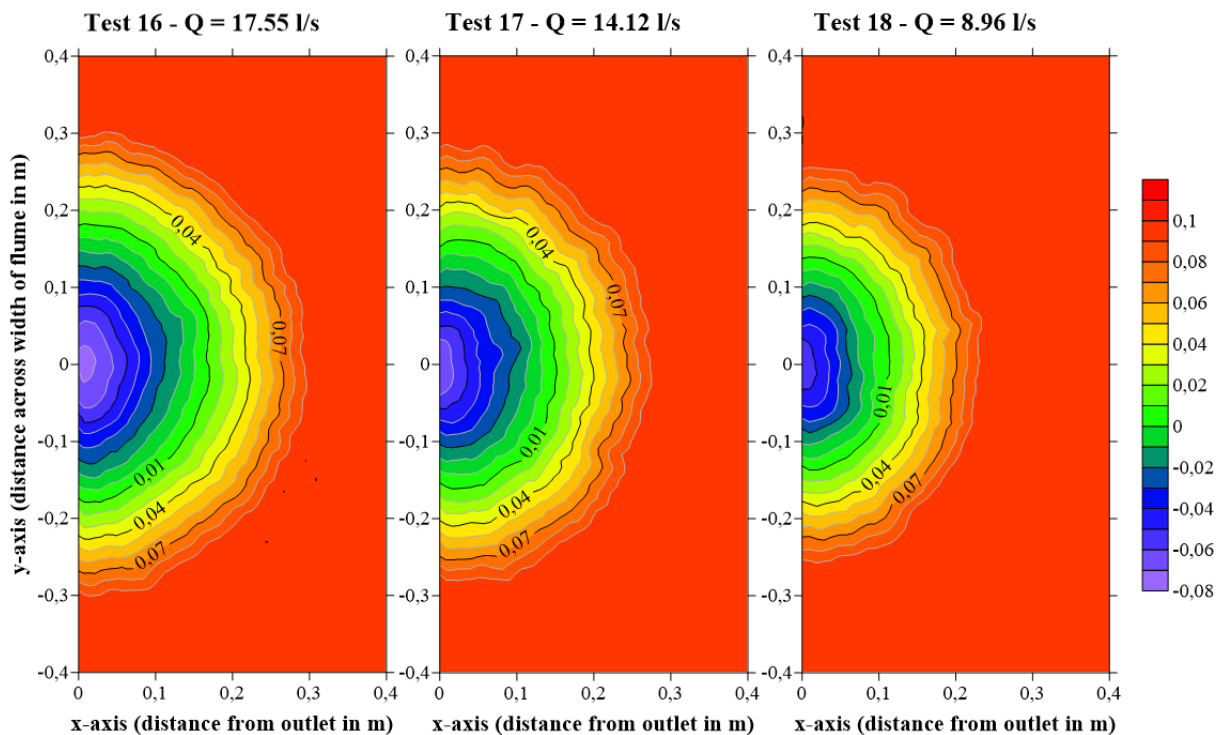


Figure F.6 Scour cone contour plots for Tests 16 to 18 (Square outlet)

Appendix F: Scour Cone Contour Plots

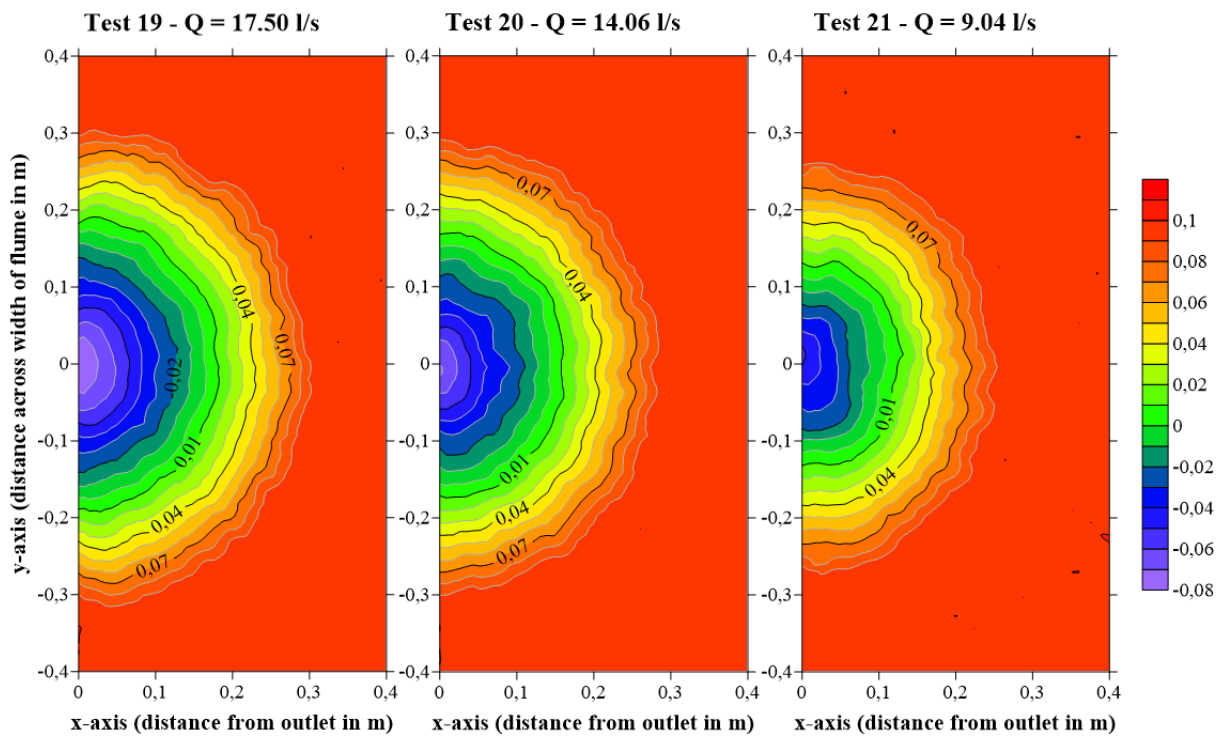


Figure F.7 Scour cone contour plots for Tests 19 to 21 (Flat rectangular outlet)

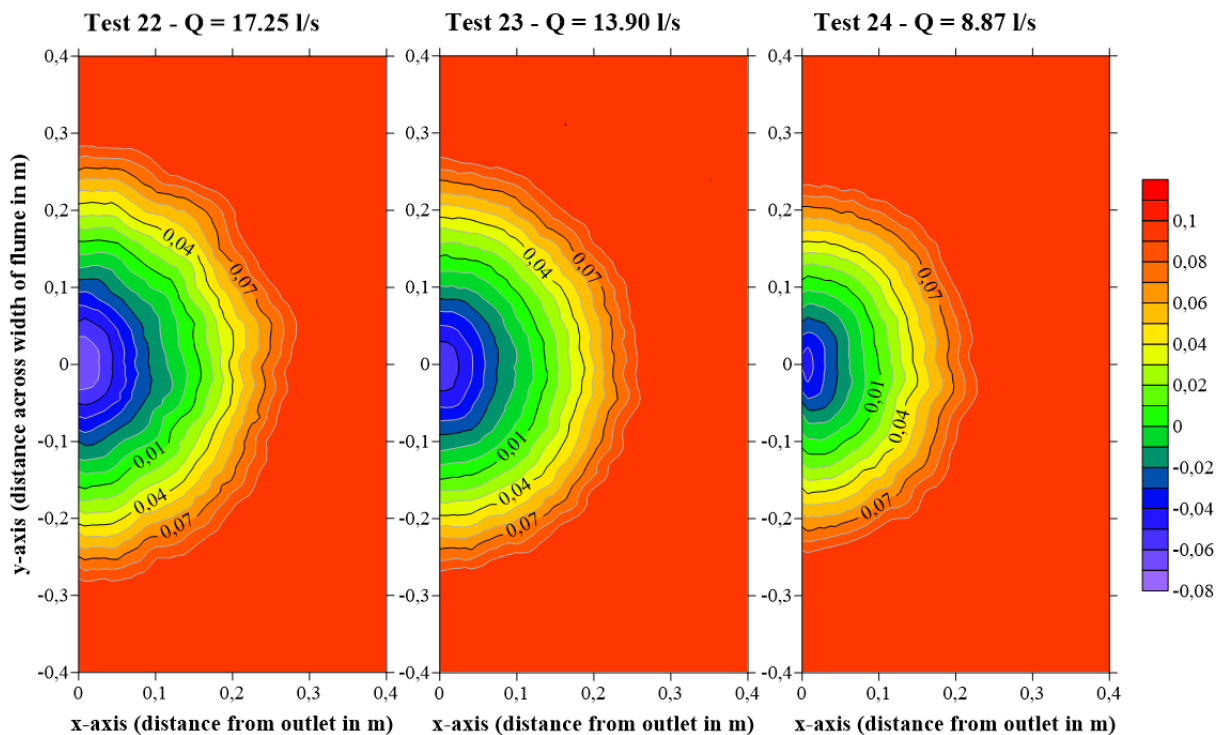


Figure F.8 Scour cone contour plots for Tests 22 to 24 (Upright rectangular outlet)

Appendix F: Scour Cone Contour Plots

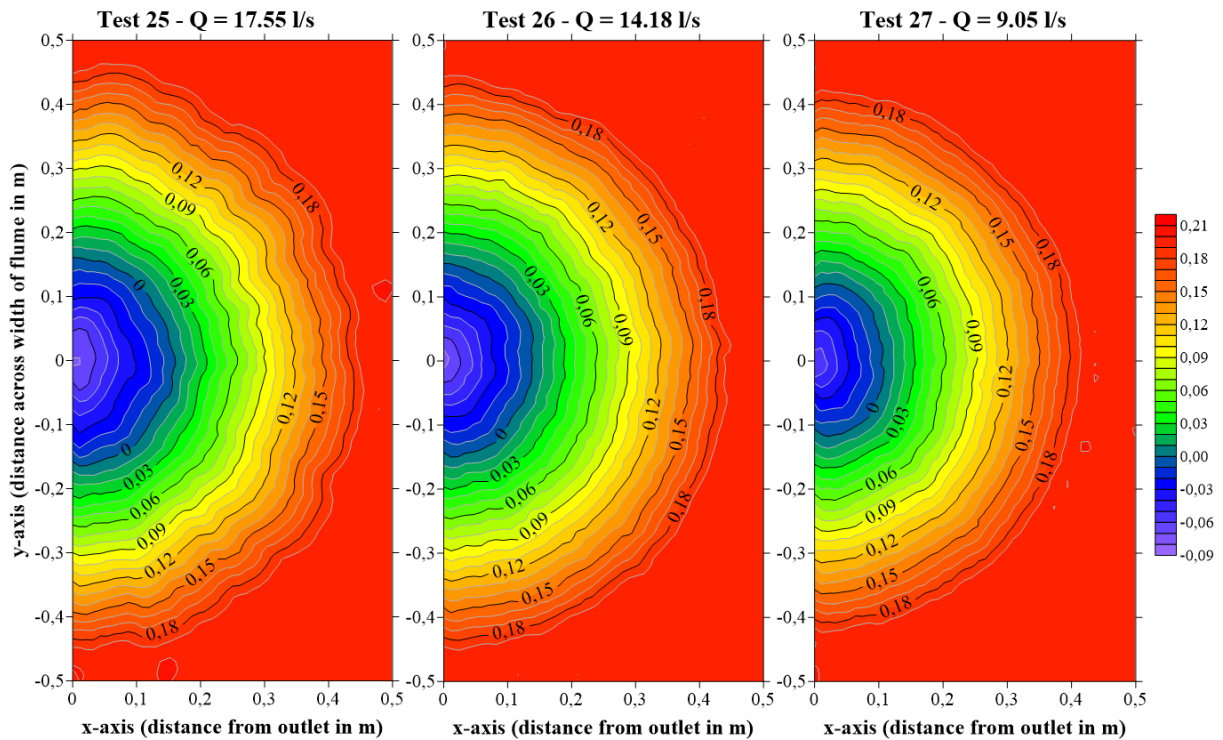


Figure F.9 Scour cone contour plots for Tests 25 to 27 (Square outlet)

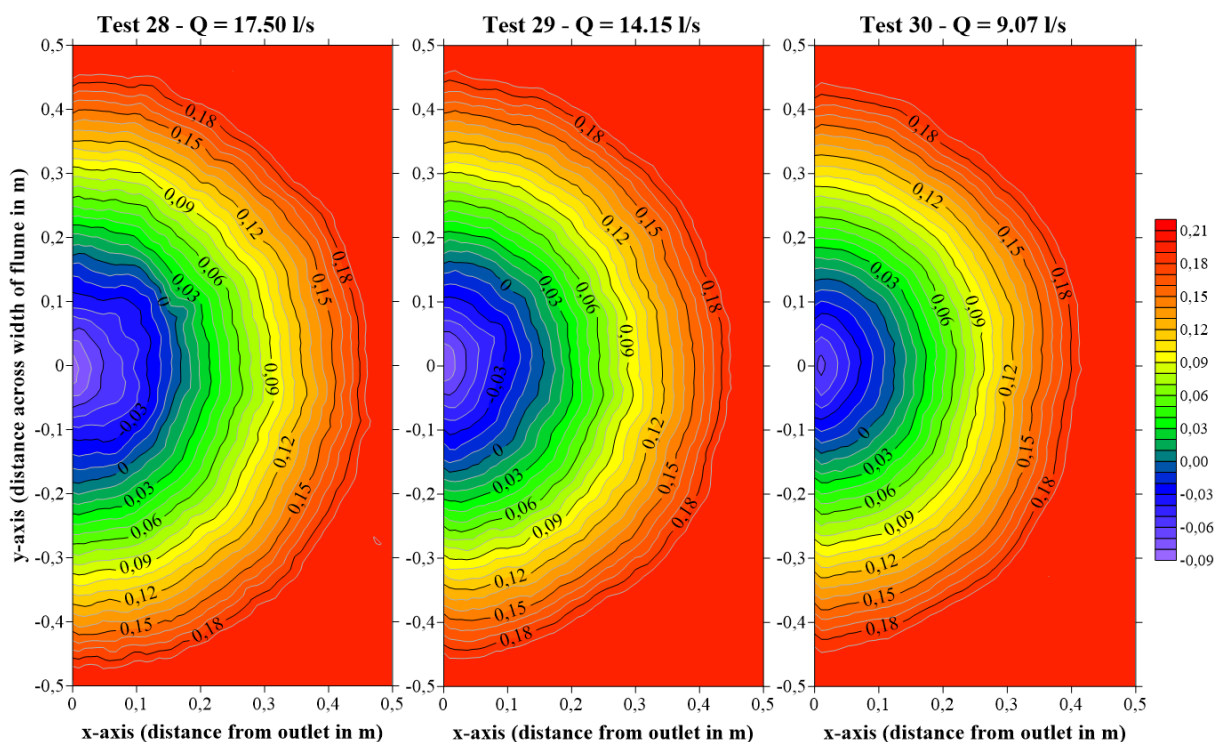


Figure F.10 Scour cone contour plots for Tests 28 to 30 (Flat rectangular outlet)

Appendix F: Scour Cone Contour Plots

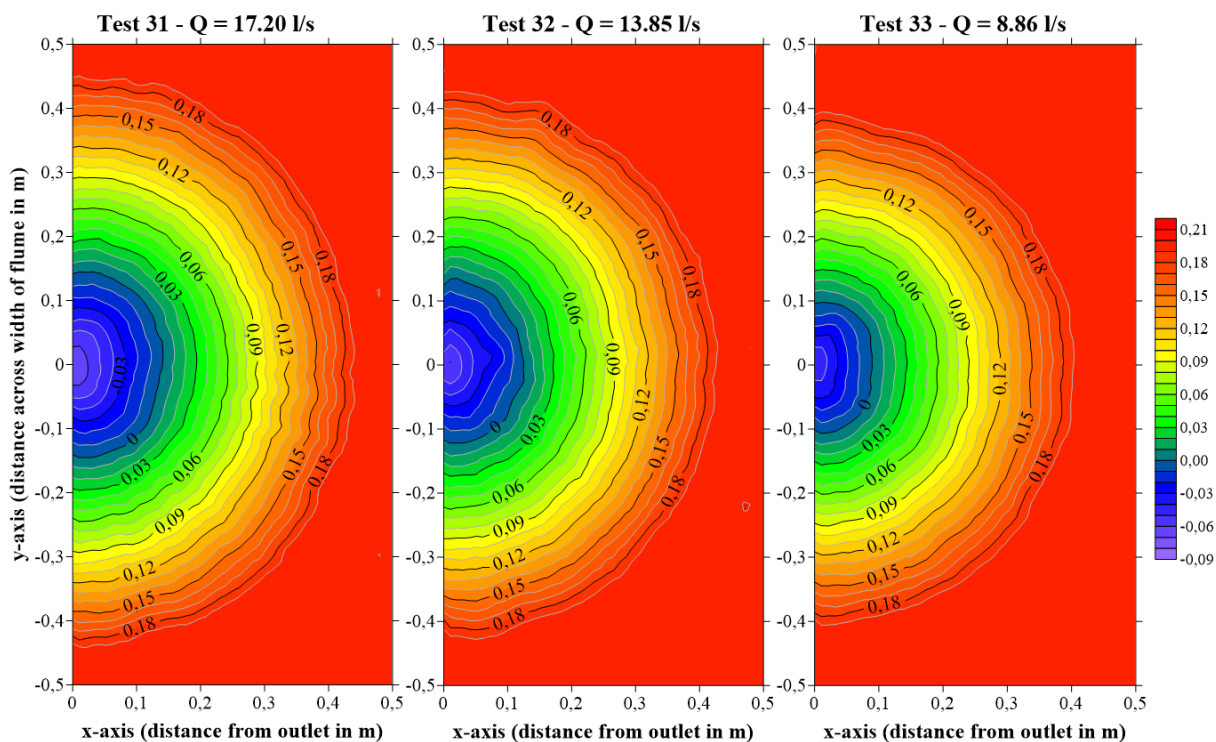


Figure F.11 Scour cone contour plots for Tests 31 to 33 (Upright rectangular outlet)

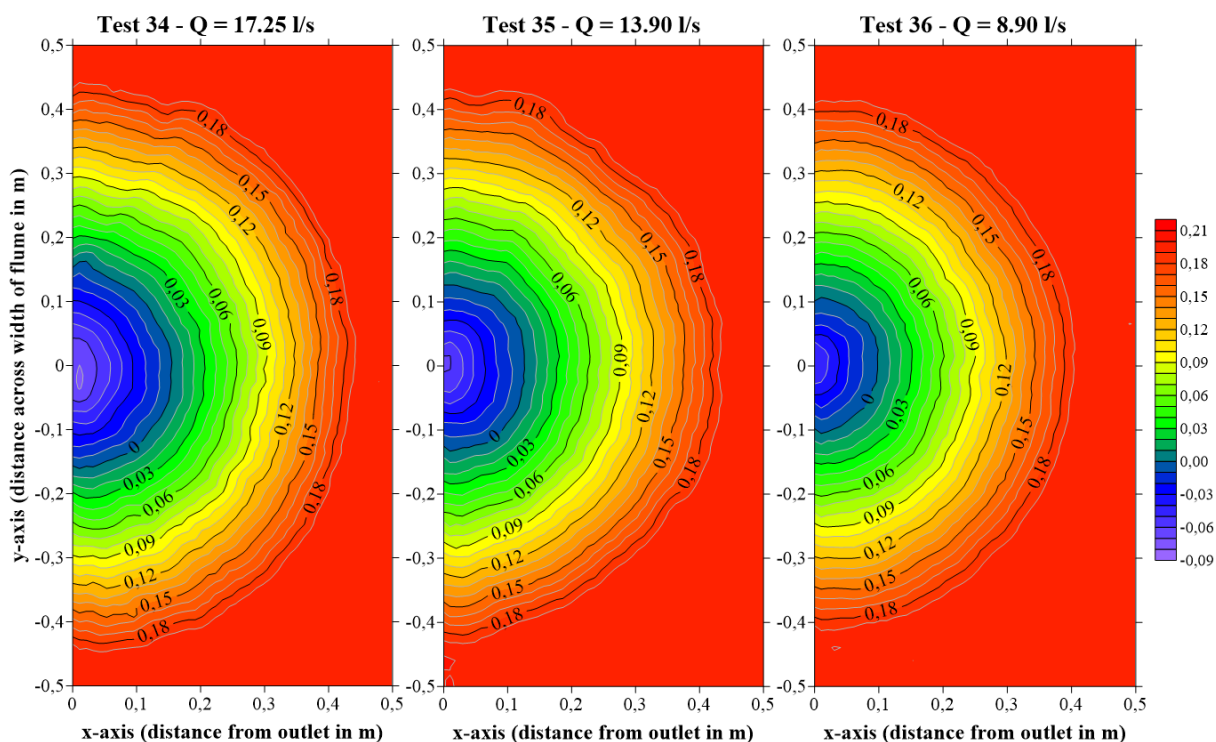


Figure F.12 Scour cone contour plots for Tests 34 to 36 (Round outlet)

Appendix G Comparison with Other Studies

Table G.1 Scour cone length comparison between observed values from this study and predicted values from the equations of other authors (*mm*)

Test number	This study	Kistner (2013) Equation 2-51		Fathi-Moghadam et al. (2010a) Equation 2-50		Meshkati-Shahmirzadi et al. (2010) Equation 2-47		Kamble et al. (2017) Equation 2-59	
		Value	Error %	Value	Error %	Value	Error %	Value	Error %
		4	196	633	223%	Not applicable where Hs = 0			
5	171	371	117%						
6	138	132	-4%						
16	306	771	152%	936	206%	256	-16%	174	-43%
17	284	512	80%	929	227%	259	-9%	184	-35%
18	240	281	17%	912	280%	263	10%	209	-13%
25	468	918	96%	958	105%	426	-9%	247	-47%
26	455	667	47%	951	109%	431	-5%	261	-43%
27	433	475	10%	934	116%	438	1%	296	-32%
7	188	634	237%	Not applicable where Hs = 0					
8	162	372	130%						
9	142	133	-6%						
19	318	772	143%	937	195%	256	-19%	173	-46%
20	290	512	77%	930	221%	259	-11%	183	-37%
21	270	283	5%	914	238%	263	-2%	207	-23%
28	476	919	93%	958	101%	426	-11%	246	-48%
29	460	668	45%	952	107%	431	-6%	260	-43%
30	435	476	9%	935	115%	438	1%	294	-32%
1	178	632	255%	Not applicable where Hs = 0					
2	155	370	138%						
3	118	132	12%						
13	288	769	167%	935	225%	256	-11%	174	-40%
14	270	510	89%	928	244%	259	-4%	185	-32%
15	244	281	15%	912	274%	263	8%	209	-14%
34	453	914	102%	956	111%	425	-6%	249	-45%
35	443	664	50%	950	114%	430	-3%	263	-41%
36	420	474	13%	933	122%	437	4%	298	-29%
10	179	631	252%	Not applicable where Hs = 0					
11	149	370	148%						
12	109	132	21%						
22	296	769	160%	935	216%	256	-14%	174	-41%
23	272	510	88%	929	241%	259	-5%	184	-32%
24	232	281	21%	912	293%	263	13%	209	-10%
31	451	914	103%	957	112%	425	-6%	248	-45%
32	442	664	50%	950	115%	430	-3%	262	-41%
33	415	474	14%	933	125%	437	5%	297	-28%

Appendix G: Comparison with Other Studies

Table G.2 Scour cone width comparison between observed values from this study and predicted values from the equations of other authors (*mm*)

Test number	This study	Kistner (2013)		Meshkati-Shahmirzadi et al. (2010)	
		Equation 2-52		Equation 2-48	
		Value	Error %	Value	Error %
4	400	6476	1519%	Not applicable where $H_s = 0$	
5	378	3924	938%		
6	298	1522	411%		
16	624	6706	975%	513	-18%
17	588	4157	607%	519	-12%
18	536	1769	230%	527	-2%
25	935	6949	643%	852	-9%
26	920	4418	380%	863	-6%
27	860	2093	143%	876	2%
7	392	6485	1554%	Not applicable where $H_s = 0$	
8	362	3930	986%		
9	296	1529	416%		
19	644	6715	943%	513	-20%
20	616	4161	576%	518	-16%
21	544	1777	227%	527	-3%
28	940	6958	640%	852	-9%
29	925	4425	378%	862	-7%
30	905	2098	132%	876	-3%
1	368	6469	1658%	Not applicable where $H_s = 0$	
2	320	3913	1123%		
3	280	1520	443%		
13	619	6696	982%	512	-17%
14	552	4147	651%	518	-6%
15	515	1767	243%	526	2%
34	905	6924	665%	851	-6%
35	875	4399	403%	861	-2%
36	845	2086	147%	875	4%
10	336	6462	1823%	Not applicable where $H_s = 0$	
11	288	3916	1260%		
12	268	1520	467%		
22	592	6690	1030%	512	-14%
23	580	4148	615%	518	-11%
24	508	1768	248%	526	4%
31	905	6928	666%	850	-6%
32	860	4401	412%	860	0%
33	805	2087	159%	874	9%

Appendix G: Comparison with Other Studies

Table G.3 Scour cone depth comparison between observed values from this study and predicted values from the equations of other authors (mm)

Test number	This study	Kistner (2013)		Meshkati-Shahmirzadi et al. (2010)	
		Equation 2-52		Equation 2-48	
		Value	Error %	Value	Error %
4	88	257	192%	Not applicable where $H_s = 0$	
5	85	153	80%		
6	67	58	-14%		
16	73	262	259%	513	-73%
17	64	157	147%	519	-62%
18	55	62	12%	527	-38%
25	70	267	280%	852	-44%
26	72	162	125%	863	-33%
27	56	67	20%	876	22%
7	90	258	187%	Not applicable where $H_s = 0$	
8	79	153	94%		
9	67	58	-13%		
19	77	262	241%	513	-74%
20	69	157	127%	518	-65%
21	49	62	26%	527	-30%
28	82	267	226%	852	-52%
29	72	163	126%	862	-33%
30	59	67	15%	876	16%
1	83	257	211%	Not applicable where $H_s = 0$	
2	68	153	125%		
3	64	58	-9%		
13	65	261	300%	512	-69%
14	60	157	161%	518	-60%
15	43	62	44%	526	-20%
34	69	265	287%	851	-43%
35	60	161	171%	861	-19%
36	46	67	44%	875	45%
10	80	257	220%	Not applicable where $H_s = 0$	
11	68	153	126%		
12	57	58	2%		
22	67	261	291%	512	-70%
23	57	157	173%	518	-58%
24	43	62	44%	526	-20%
31	67	266	295%	850	-42%
32	60	161	171%	860	-20%
33	45	67	49%	874	50%

Appendix G: Comparison with Other Studies

Table G.4 Scour cone volume comparison between observed values from this study and predicted values from the equations of other authors ($10^{-3} m^3$)

Test number	This study	Kistner (2013) Equation 2-55		Fathi-Moghadam et al. (2010a) Equation 2-49		Meshkati Shahmirzadi et al. (2010) Equation 2-46		Emamgholizadeh et al. (2006) Equation 2-40	
		Value	Error %	Value	Error %	Value	Error %	Value	Error %
4	2.15	110.71	5054%	Not applicable where Hs = 0					
5	1.72	24.29	1315%						
6	0.98	1.43	47%						
16	10.60	160.48	1414%	3.72	-65%	1.06	-90%	6.11	-42%
17	9.10	43.69	380%	3.72	-59%	1.28	-86%	6.14	-32%
18	6.48	5.83	-10%	3.69	-43%	1.81	-72%	6.11	-6%
25	35.04	237.94	579%	3.84	-89%	8.98	-74%	54.63	56%
26	33.03	83.72	153%	3.84	-88%	10.88	-67%	55.01	67%
27	27.01	36.04	33%	3.81	-86%	15.32	-43%	54.80	103%
7	2.00	111.18	5467%	Not applicable where Hs = 0					
8	1.65	24.42	1376%						
9	1.07	1.45	35%						
19	11.21	161.23	1339%	3.72	-67%	1.06	-91%	6.12	-45%
20	9.50	43.84	361%	3.72	-61%	1.28	-86%	6.15	-35%
21	6.82	5.92	-13%	3.69	-46%	1.81	-74%	6.14	-10%
28	37.82	239.06	532%	3.84	-90%	8.98	-76%	54.71	45%
29	34.99	84.17	141%	3.84	-89%	10.87	-69%	55.11	58%
30	29.54	36.37	23%	3.81	-87%	15.32	-48%	54.97	86%
1	1.72	110.27	6315%	Not applicable where Hs = 0					
2	1.18	24.09	1945%						
3	0.70	1.43	103%						
13	8.51	159.67	1777%	3.72	-56%	1.06	-88%	6.10	-28%
14	7.03	43.33	516%	3.71	-47%	1.28	-82%	6.13	-13%
15	5.66	5.81	3%	3.68	-35%	1.80	-68%	6.10	8%
34	34.55	234.95	580%	3.84	-89%	8.96	-74%	54.40	57%
35	30.33	82.47	172%	3.83	-87%	10.84	-64%	54.74	81%
36	25.60	35.60	39%	3.80	-85%	15.28	-40%	54.58	113%
10	1.43	109.89	7611%	Not applicable where Hs = 0					
11	1.00	24.14	2319%						
12	0.64	1.43	122%						
22	8.82	159.20	1705%	3.72	-58%	1.06	-88%	6.09	-31%
23	7.56	43.40	474%	3.71	-51%	1.28	-83%	6.13	-19%
24	5.67	5.82	3%	3.68	-35%	1.80	-68%	6.11	8%
31	33.12	235.45	611%	3.84	-88%	8.96	-73%	54.44	64%
32	29.53	82.60	180%	3.83	-87%	10.84	-63%	54.77	85%
33	24.69	35.63	44%	3.80	-85%	15.26	-38%	54.59	121%

Appendix G: Comparison with Other Studies

Table G.5 Scour cone length comparison between observed values for the round outlet from this study and predicted values from the equations of other authors (*mm*)

Test number	This study	Powell (2007)		Fathi-Moghadam et al. (2010a)		Emamgholizadeh and Fathi-Moghadam (2014)	
		Equation 2-42		Equation 2-50		Equation 2-57	
		Value	Error %	Value	Error %	Value	Error %
1	196	633	223%	Not applicable where $H_s = 0$			
2	171	371	117%				
3	138	132	-4%				
13	306	Not applicable for $H_s > 0$		94	-69%	71	-77%
14	284			93	-67%	85	-70%
15	240			91	-62%	117	-51%
34	468			96	-80%	94	-80%
35	455			95	-79%	112	-75%
36	433			93	-78%	155	-64%

Table G.6 Scour cone width comparison between observed values for the round outlet from this study and predicted values from the equations of other authors (*mm*)

Test number	This study	Powell (2007)		Meshkati Shahmirzadi et al. (2010)	
		Equation 2-43		Equation 2-45	
		Value	Error %	Value	Error %
1	345	943	173%	Not applicable where $H_s = 0$	
2	302	767	154%		
3	262	587	124%		
13	577	Not applicable for $H_s > 0$		450	-22%
14	544			458	-16%
15	483			471	-3%
34	889			756	-15%
35	865			770	-11%
36	827			792	-4%

Appendix G: Comparison with Other Studies

Table G.7 Scour cone volume comparison between observed values for the round outlet from this study and predicted values from the equations of other authors ($10^{-3} m^3$)

Test number	This study	Meshkati Shahmirzadi et al. (2010) Equation 2-44		Fathi-Moghadam et al. (2010a) Equation 2-49		Emamgholizadeh and Fathi-Moghadam (2014) Equation 2-56	
		Value	Error %	Value	Error %	Value	Error %
		1	1.72	Not applicable where $H_s = 0$			
2	1.18						
3	0.70						
13	8.51	7.51	-12%	3.72	-56%	6.40	-25%
14	7.03	7.46	6%	3.71	-47%	8.30	18%
15	5.66	7.30	29%	3.68	-35%	13.39	137%
34	34.55	34.44	0%	3.84	-89%	9.63	-72%
35	30.33	34.25	13%	3.83	-87%	12.49	-59%
36	25.60	33.55	31%	3.80	-85%	20.16	-21%

Appendix H Statistical Parameters Definitions

The coefficient of determination, R^2 , is given by

$$R^2 = \left[\frac{1}{n} \cdot \frac{\sum (x_i - \bar{x}) \cdot (y_i - \bar{y})}{\sigma_x \cdot \sigma_y} \right]^2 \quad \text{H-1}$$

where:

- R = correlation coefficient
- n = number of observations
- Σ = summation symbol
- x_i = x value for observation i
- \bar{x} = mean x value
- y_i = number of observations
- \bar{y} = y value for observation i
- σ_x = standard of deviation of x
- σ_y = standard of deviation of y

Adjusted R^2 is given by

$$R_{adj}^2 = 1 - \left[\frac{(1 - R^2) \cdot (n - 1)}{n - k - 1} \right] \quad \text{H-2}$$

where:

- k = number of independent regressors, i.e. the number of variables in the model excluding the constant

Mean absolute error (MAE) is given by

$$MAE = \frac{1}{n} \sum_{j=1}^n |z_j - z| \quad \text{H-3}$$

where:

- z_j = predicted value
- z = observed value

Appendix H: Statistical Parameters Definitions

Root mean squared error (RMSE) is given by

$$RMSE = \sqrt{\frac{1}{n} \sum_{j=1}^n (z_j - z)^2} \quad \text{H-4}$$

Appendix I Statistical Parameters of the Regression Analysis

Table I.1 Regression analysis summary for the Linear Model

		L_c	W_c	H_c	D_c	V_c
Regression Coefficients	a	0.9484	1.8462	0.5934	0.0025	0.2242
	b	-1.0035	-1.9469	-0.6385	0.0351	-0.3446
	c	0.3872	0.9632	0.1832	0.2553	1.0949
Statistical parameters	Multiple R	0.998	0.997	0.997	0.978	0.885
	R Square	0.996	0.995	0.994	0.956	0.783
	Adjusted R Square	0.966	0.964	0.963	0.923	0.740
	Standard Error	0.025	0.061	0.018	0.017	0.036
	RMSE	0.029	0.064	0.021	0.013	0.044
	MAE	0.021	0.050	0.017	0.011	0.029

Table I.2 Regression analysis summary for the Linear Logarithmic Model

		L_c	W_c	H_c	D_c	V_c
Regression Coefficients	a	1.2060	2.3065	0.7615	-0.0386	0.3805
	b	-1.4594	-3.4197	-0.7519	-0.7511	0.0226
	c	0.0536	0.1360	0.0278	0.0317	-0.2855
Statistical parameters	Multiple R	0.999	0.999	0.999	0.993	0.872
	R Square	0.998	0.998	0.998	0.985	0.760
	Adjusted R Square	0.967	0.967	0.968	0.954	0.715
	Standard Error	0.020	0.040	0.010	0.010	0.038
	RMSE	0.019	0.043	0.012	0.009	0.077
	MAE	0.015	0.033	0.008	0.007	0.046

Table I.3 Regression analysis summary for the Logarithmic Transformed Model

		L_c	W_c	H_c	D_c	V_c
Regression Coefficients	a	3.0851	2.8288	3.5875	-0.2144	1.9529
	b	4.5569	0.8333	7.5888	5.5876	-0.3787
	c	0.4097	0.3835	0.4543	0.7782	1.3663
Statistical parameters	Multiple R	0.985	0.963	0.987	0.995	1.000
	R Square	0.971	0.927	0.974	0.990	0.999
	Adjusted R Square	0.939	0.893	0.942	0.959	0.969
	Standard Error	0.257	0.238	0.343	0.289	0.147
	MAE	0.077	0.141	0.058	0.021	0.002
	RMSE	0.058	0.111	0.043	0.016	0.002

Appendix J Statistical Parameters for the Outlet Specific Regression Analysis

Table J.1 Regression analysis summary for the square outlet

		L_c	W_c	H_c	D_c	V_c
Coefficients	a	1.2149	2.3170	0.7710	-0.0303	1.9405
	b	-1.4297	-3.4061	-0.7848	-0.7906	-0.4151
	c	0.0503	0.1332	0.0300	0.0347	1.3871
Statistical parameters	Multiple R	0.9985	0.9992	0.9992	0.9953	0.9998
	R Square	0.9970	0.9984	0.9984	0.9906	0.9995
	Adjusted R Square	0.8293	0.8311	0.8312	0.8208	0.8327
	Standard Error	0.0267	0.0404	0.0116	0.0098	0.1370
	RMSE	0.0248	0.0512	0.0145	0.0106	0.0030
	MAE	0.0243	0.0459	0.0120	0.0109	0.0024

Table J.2 Regression analysis summary for the flat rectangular outlet

		L_c	W_c	H_c	D_c	V_c
Coefficients	a	1.2149	2.3170	0.7710	-0.0303	1.9405
	b	-1.4297	-3.4061	-0.7848	-0.7906	-0.4151
	c	0.0503	0.1332	0.0300	0.0347	1.3871
Statistical parameters	Multiple R	0.9985	0.9992	0.9992	0.9953	0.9998
	R Square	0.9970	0.9984	0.9984	0.9906	0.9995
	Adjusted R Square	0.8293	0.8311	0.8312	0.8208	0.8327
	Standard Error	0.0267	0.0404	0.0116	0.0098	0.1370
	RMSE	0.0248	0.0512	0.0145	0.0106	0.0030
	MAE	0.0243	0.0459	0.0120	0.0109	0.0024

Table J.3 Regression analysis summary for the round outlet

		L_c	W_c	H_c	D_c	V_c
Coefficients	a	1.2149	2.3170	0.7710	-0.0303	1.9405
	b	-1.4297	-3.4061	-0.7848	-0.7906	-0.4151
	c	0.0503	0.1332	0.0300	0.0347	1.3871
Statistical parameters	Multiple R	0.9985	0.9992	0.9992	0.9953	0.9998
	R Square	0.9970	0.9984	0.9984	0.9906	0.9995
	Adjusted R Square	0.8293	0.8311	0.8312	0.8208	0.8327
	Standard Error	0.0267	0.0404	0.0116	0.0098	0.1370
	RMSE	0.0248	0.0512	0.0145	0.0106	0.0030
	MAE	0.0243	0.0459	0.0120	0.0109	0.0024

Appendix J: Statistical Parameters for the Outlet Specific Regression Analysis**Table J.4 Regression analysis summary for the upright rectangular outlet**

		L_c	W_c	H_c	D_c	V_c
Coefficients	a	1.2149	2.3170	0.7710	-0.0303	1.9405
	b	-1.4297	-3.4061	-0.7848	-0.7906	-0.4151
	c	0.0503	0.1332	0.0300	0.0347	1.3871
Statistical parameters	Multiple R	0.9985	0.9992	0.9992	0.9953	0.9998
	R Square	0.9970	0.9984	0.9984	0.9906	0.9995
	Adjusted R Square	0.8293	0.8311	0.8312	0.8208	0.8327
	Standard Error	0.0267	0.0404	0.0116	0.0098	0.1370
	RMSE	0.0248	0.0512	0.0145	0.0106	0.0030
	MAE	0.0243	0.0459	0.0120	0.0109	0.0024

Appendix K Centreline Bed Profiles

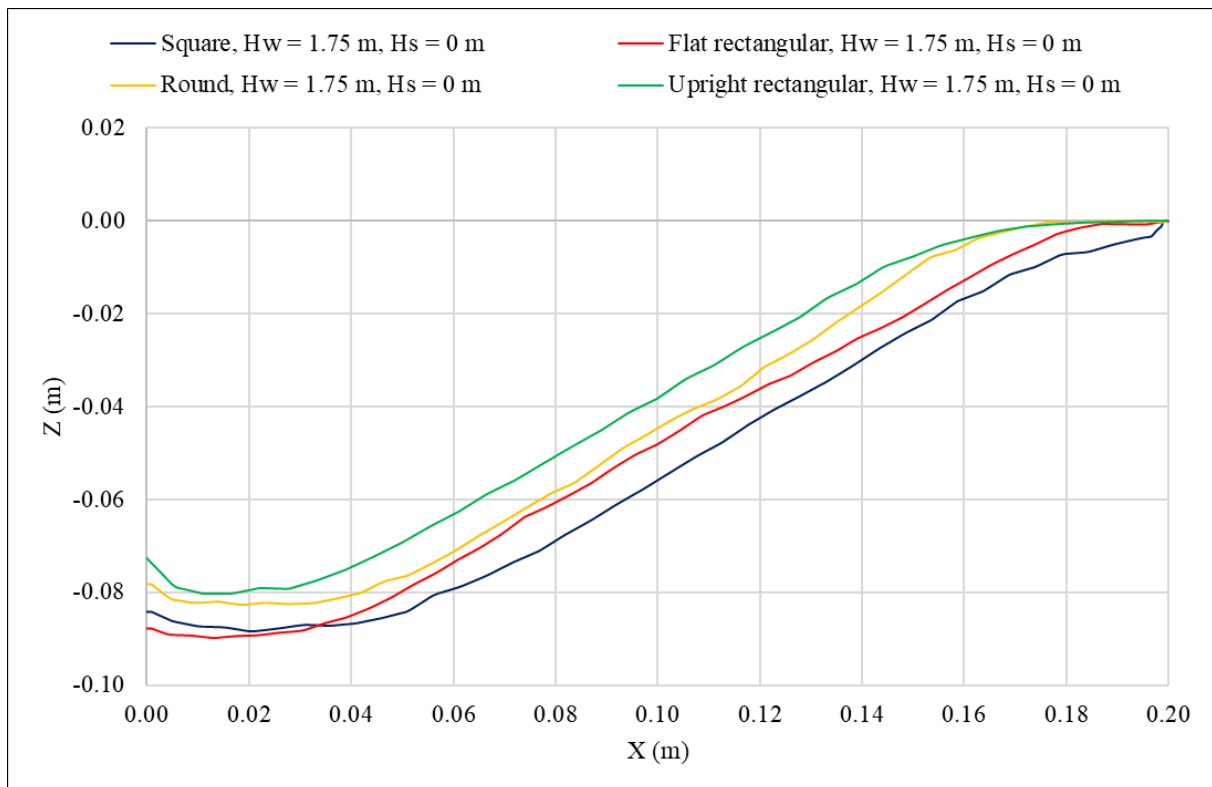


Figure K.1 Centreline bed profiles for $H_w = 1.75$ m and $H_s = 0$ m

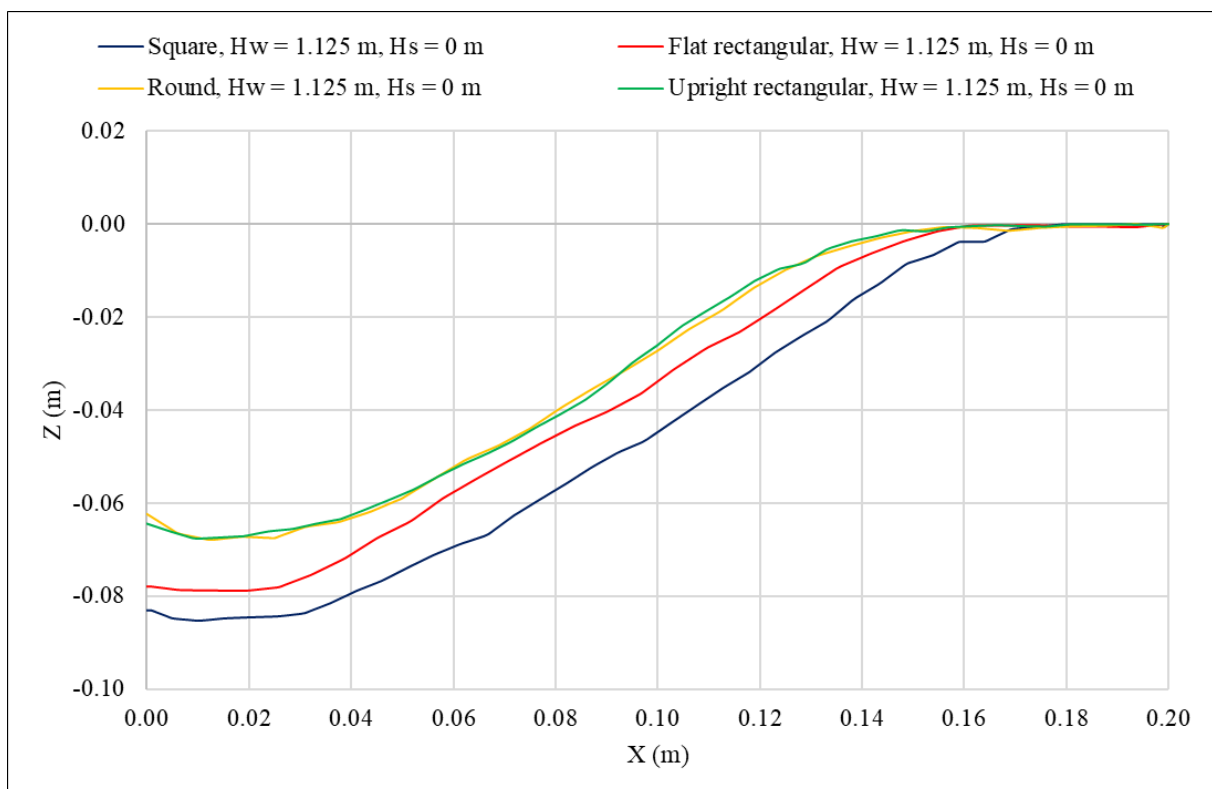
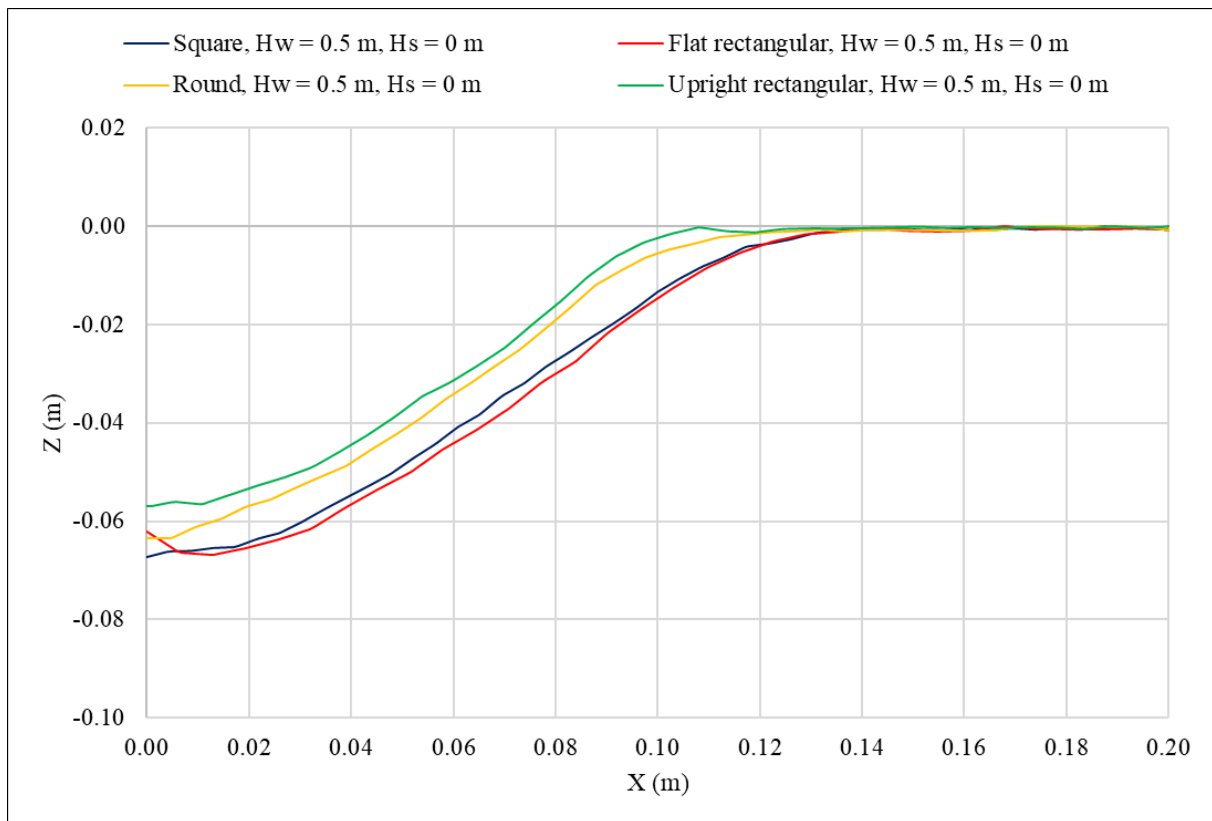
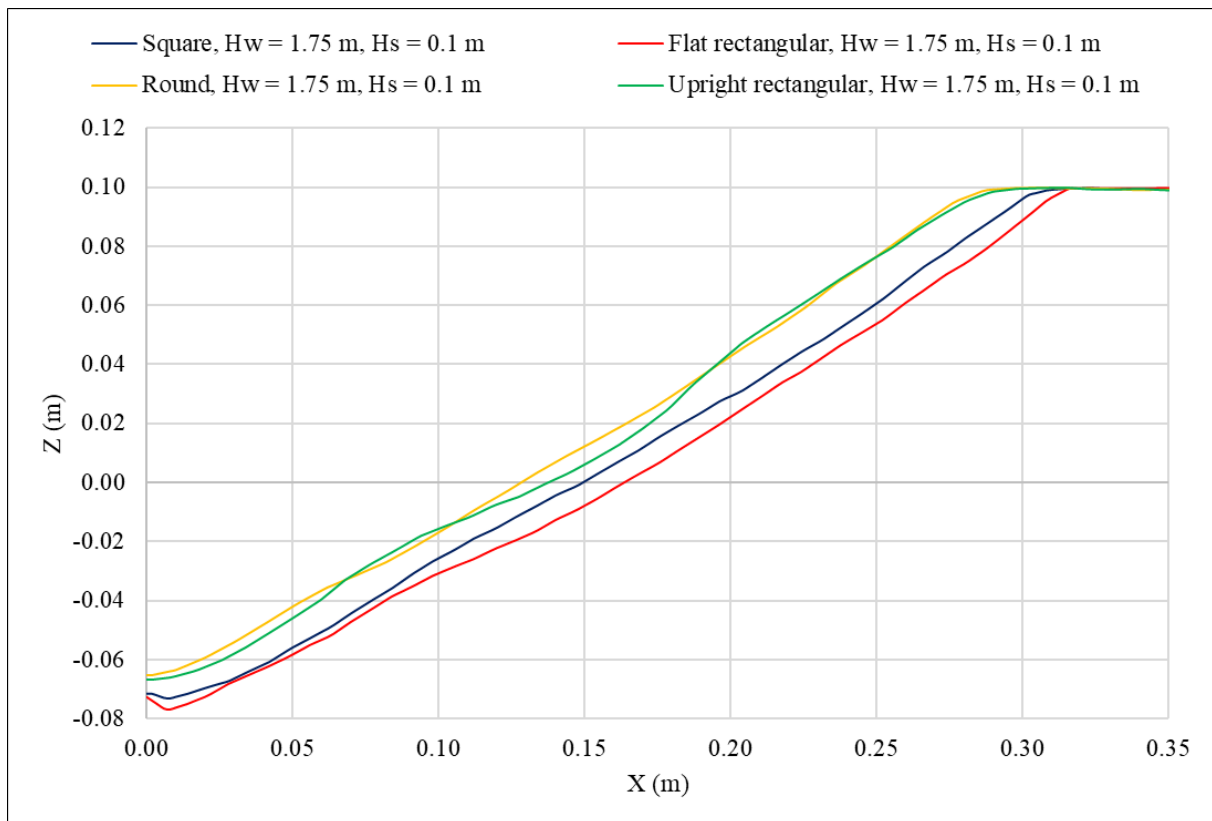
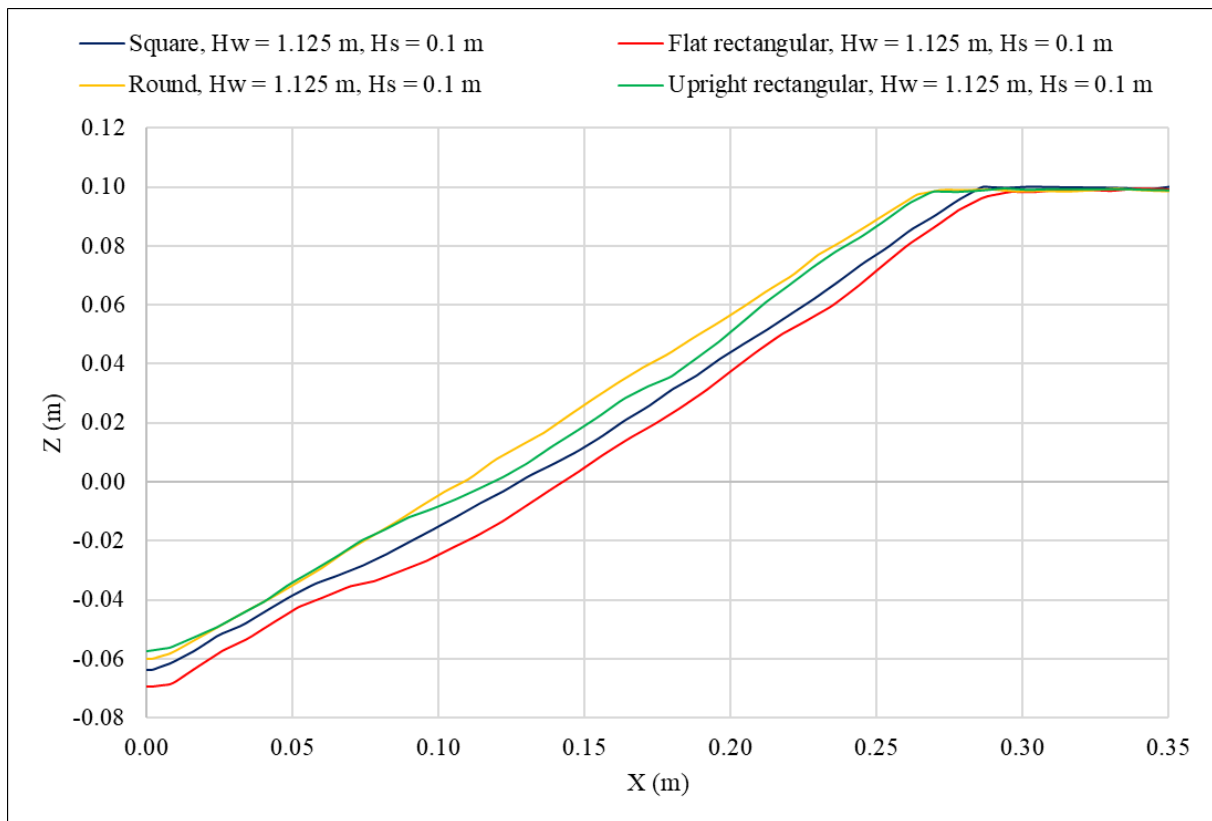
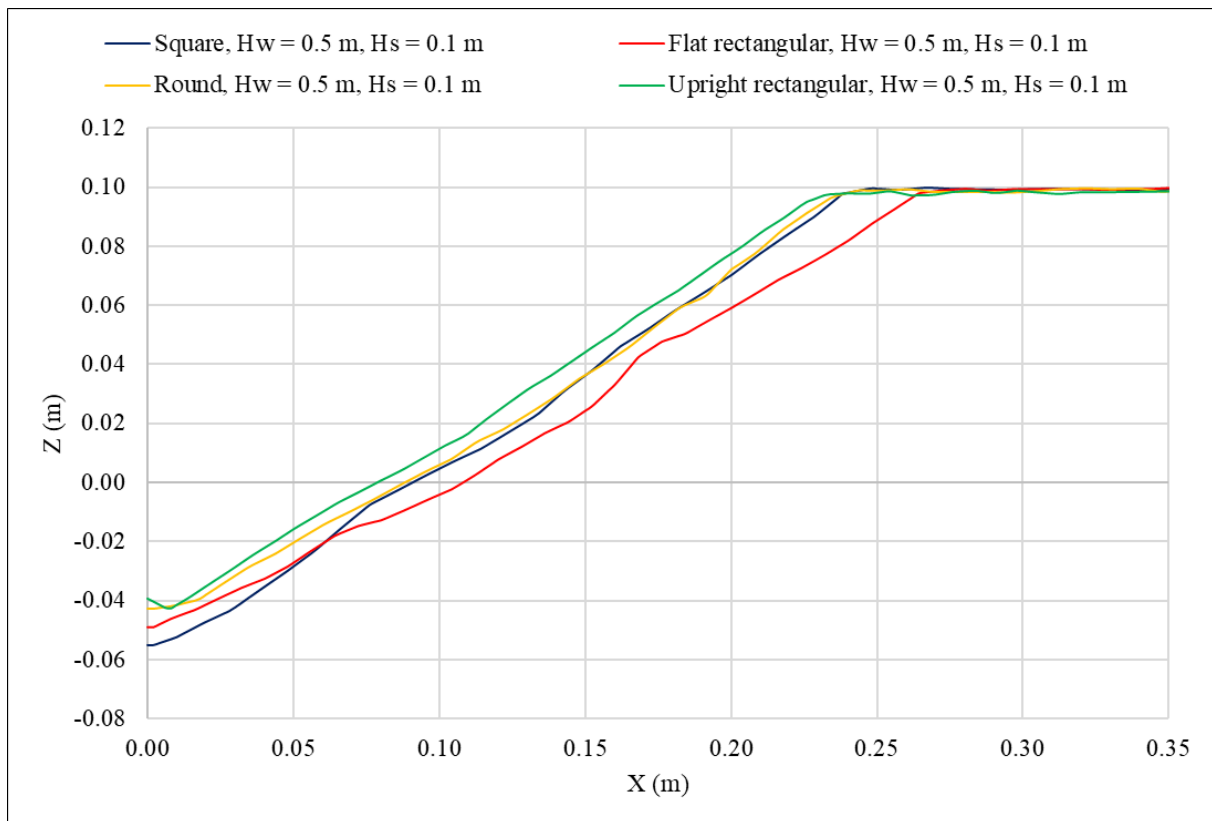
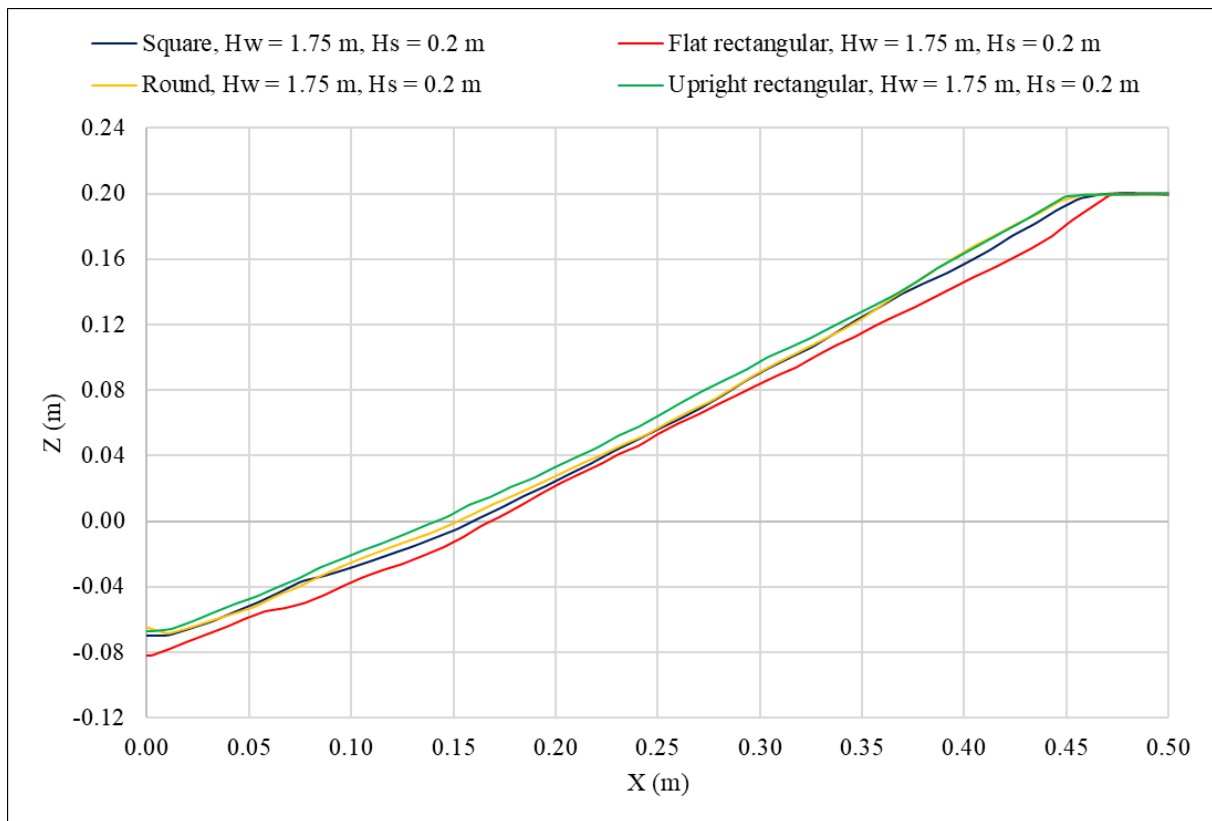
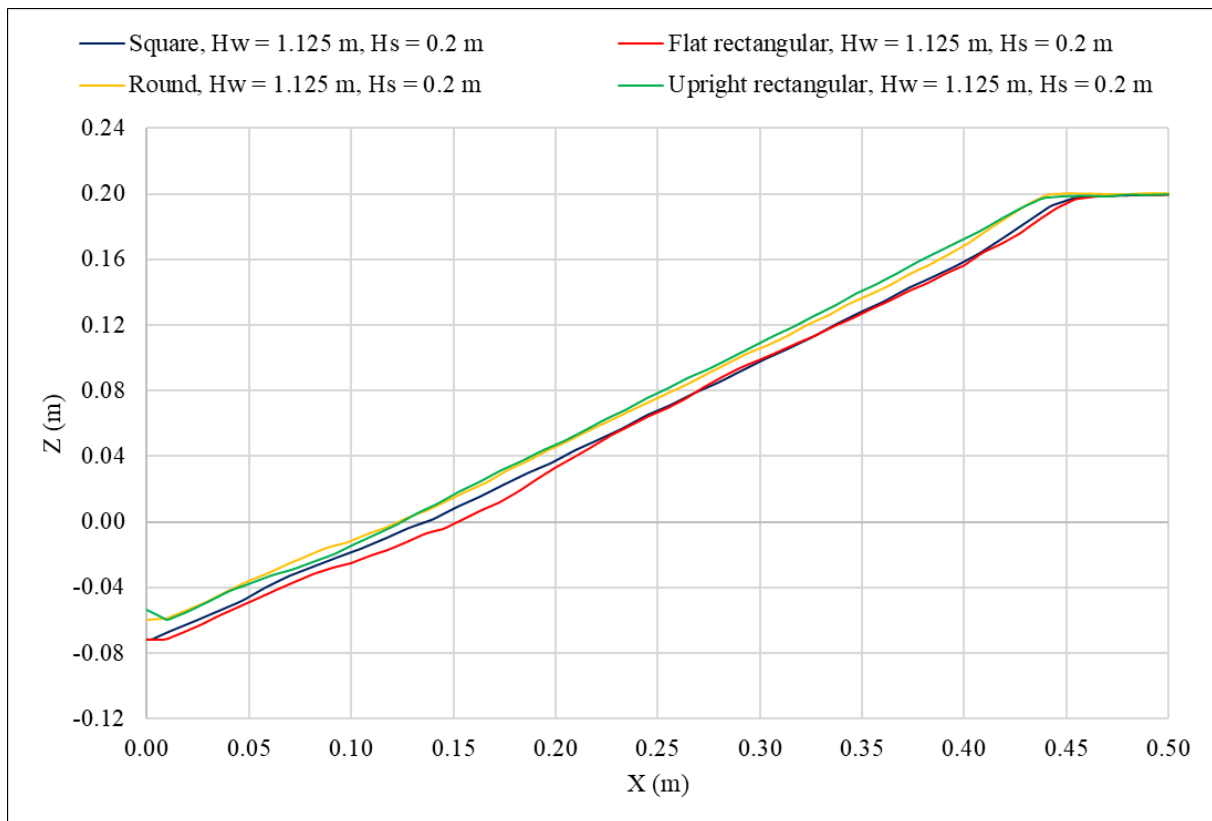


Figure K.2 Centreline bed profiles for $H_w = 1.125$ m and $H_s = 0$ m

Appendix K: Centreline Bed Profiles**Figure K.3 Centreline bed profiles for $H_w = 0.5\text{ m}$ and $H_s = 0\text{ m}$** **Figure K.4 Centreline bed profiles for $H_w = 1.75\text{ m}$ and $H_s = 0.1\text{ m}$**

Appendix K: Centreline Bed Profiles**Figure K.5 Centreline bed profiles for $H_w = 1.125$ m and $H_s = 0.1$ m****Figure K.6 Centreline bed profiles for $H_w = 0.5$ m and $H_s = 0.1$ m**

Appendix K: Centreline Bed Profiles**Figure K.7 Centreline bed profiles for $H_w = 1.75\text{ m}$ and $H_s = 0.2\text{ m}$** **Figure K.8 Centreline bed profiles for $H_w = 1.125\text{ m}$ and $H_s = 0.2\text{ m}$**

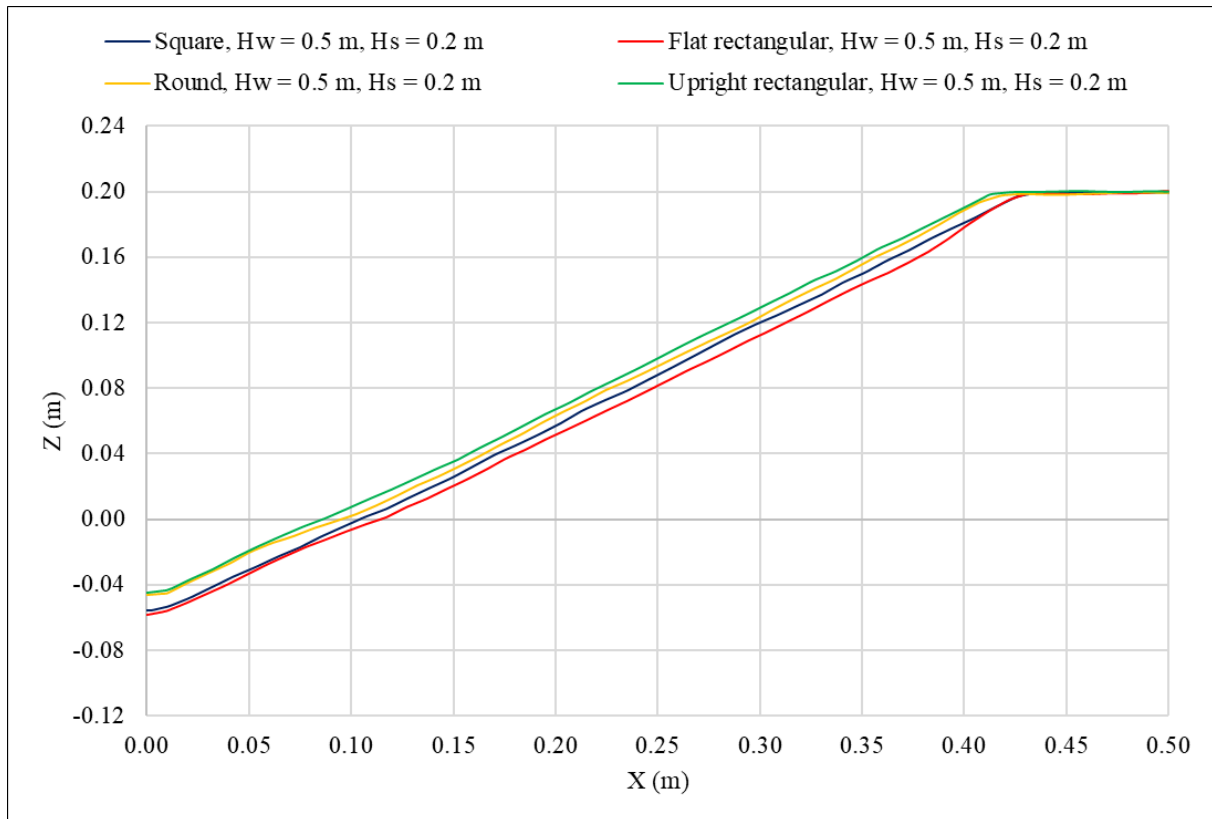
Appendix K: Centreline Bed Profiles

Figure K.9 Centreline bed profiles for $H_w = 0.5$ m and $H_s = 0.2$ m

Appendix L Cross-Sectional Bed Profiles

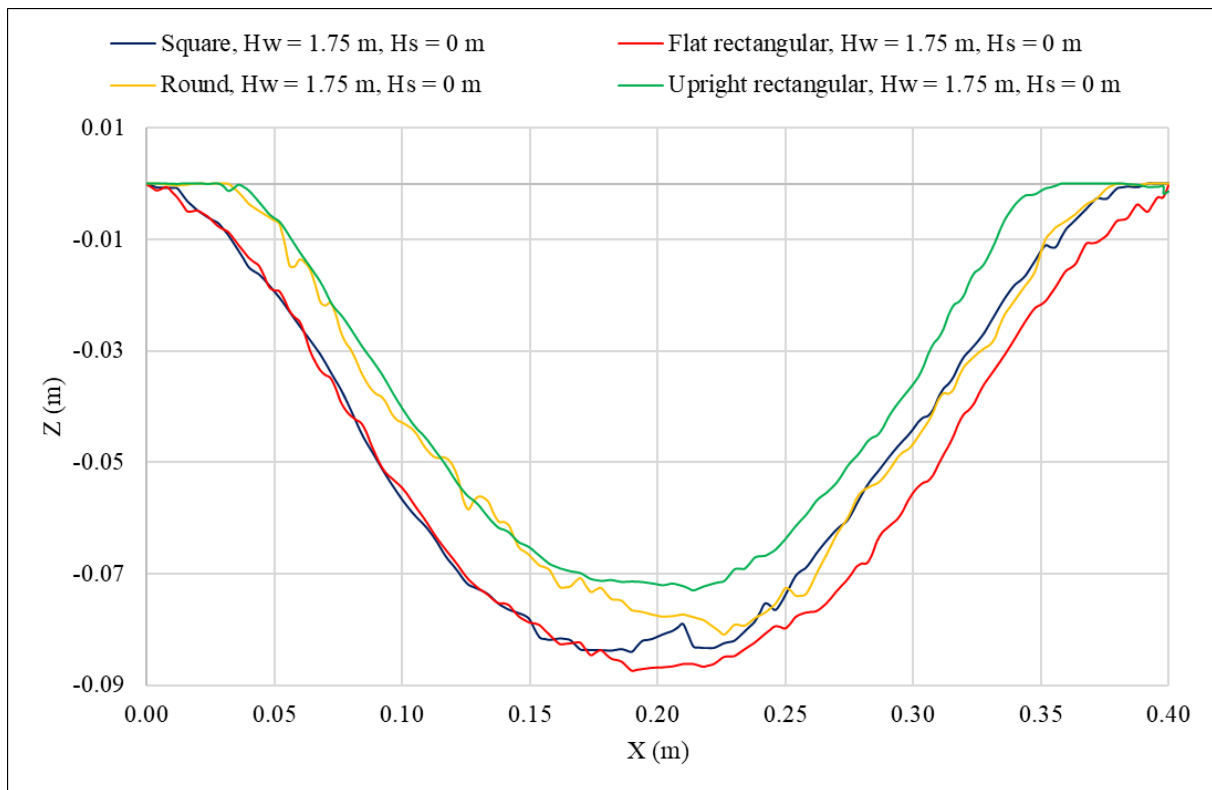


Figure L.1 Cross-sectional bed profiles for $H_w = 1.75$ m and $H_s = 0$ m

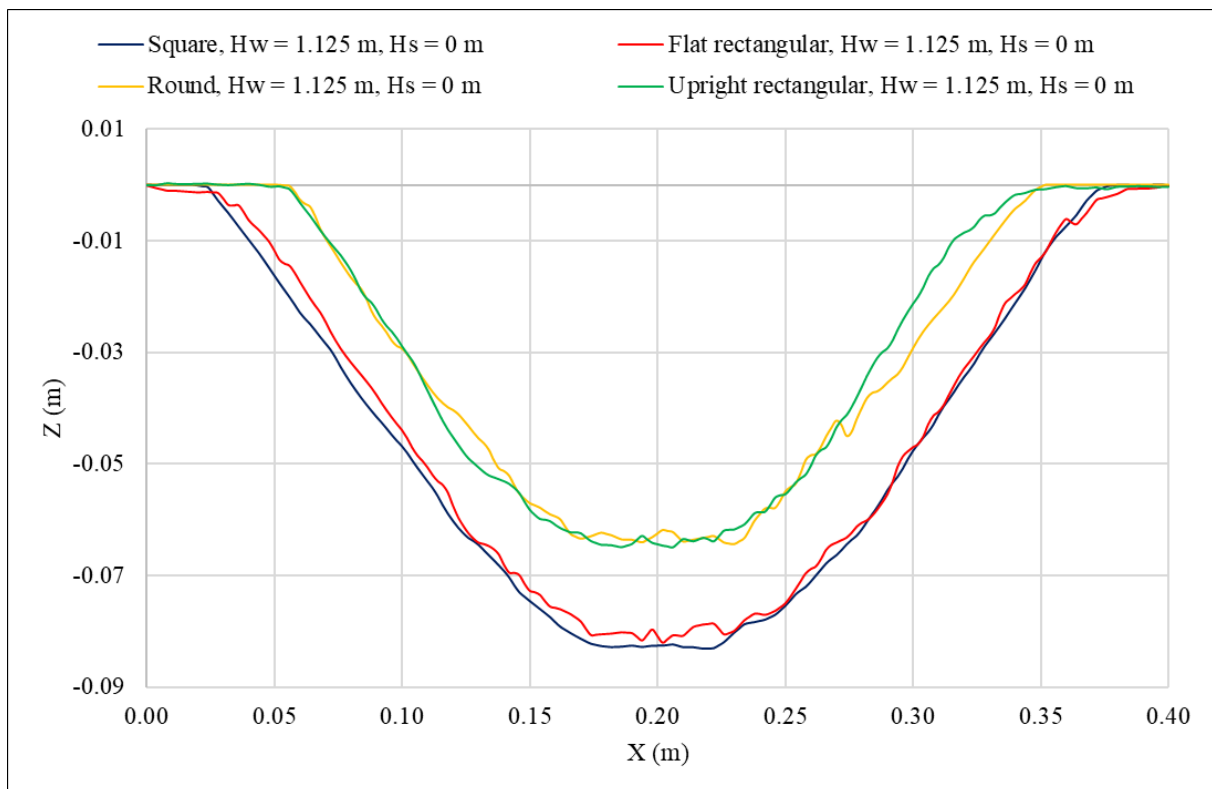
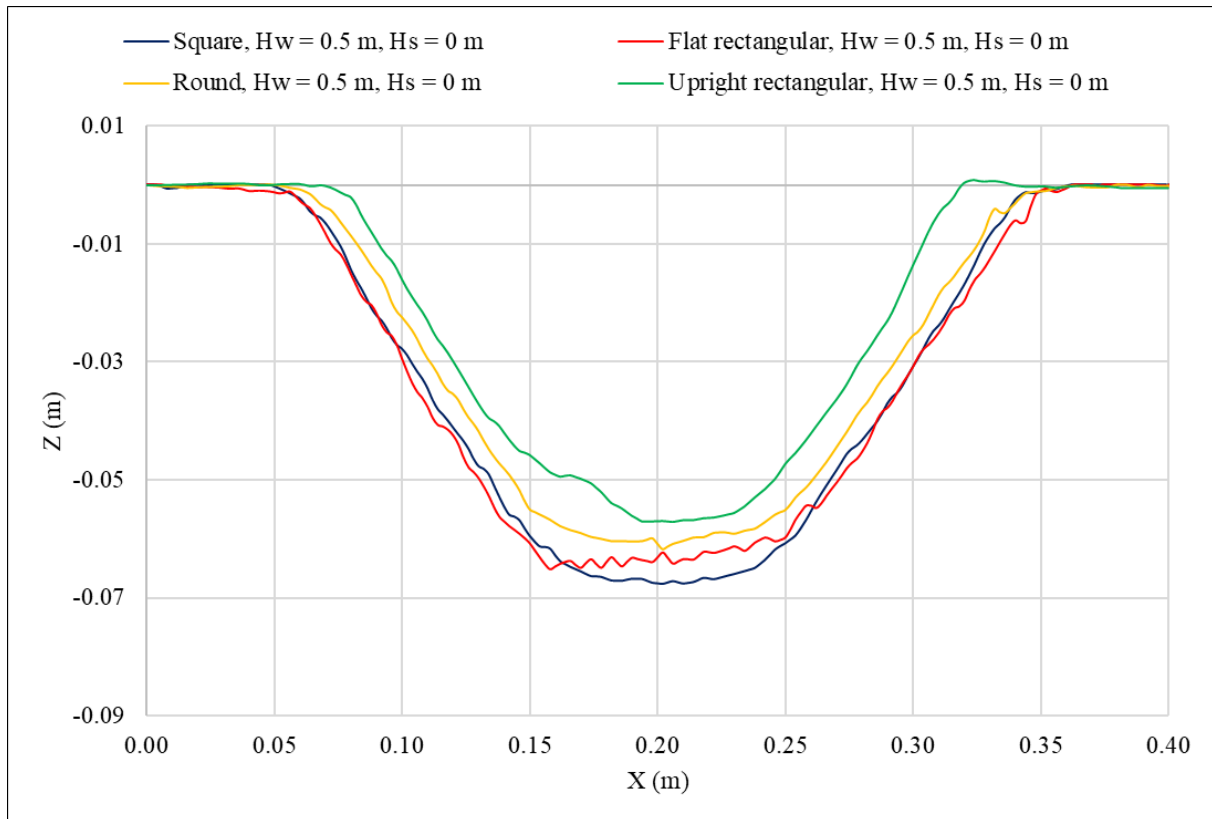
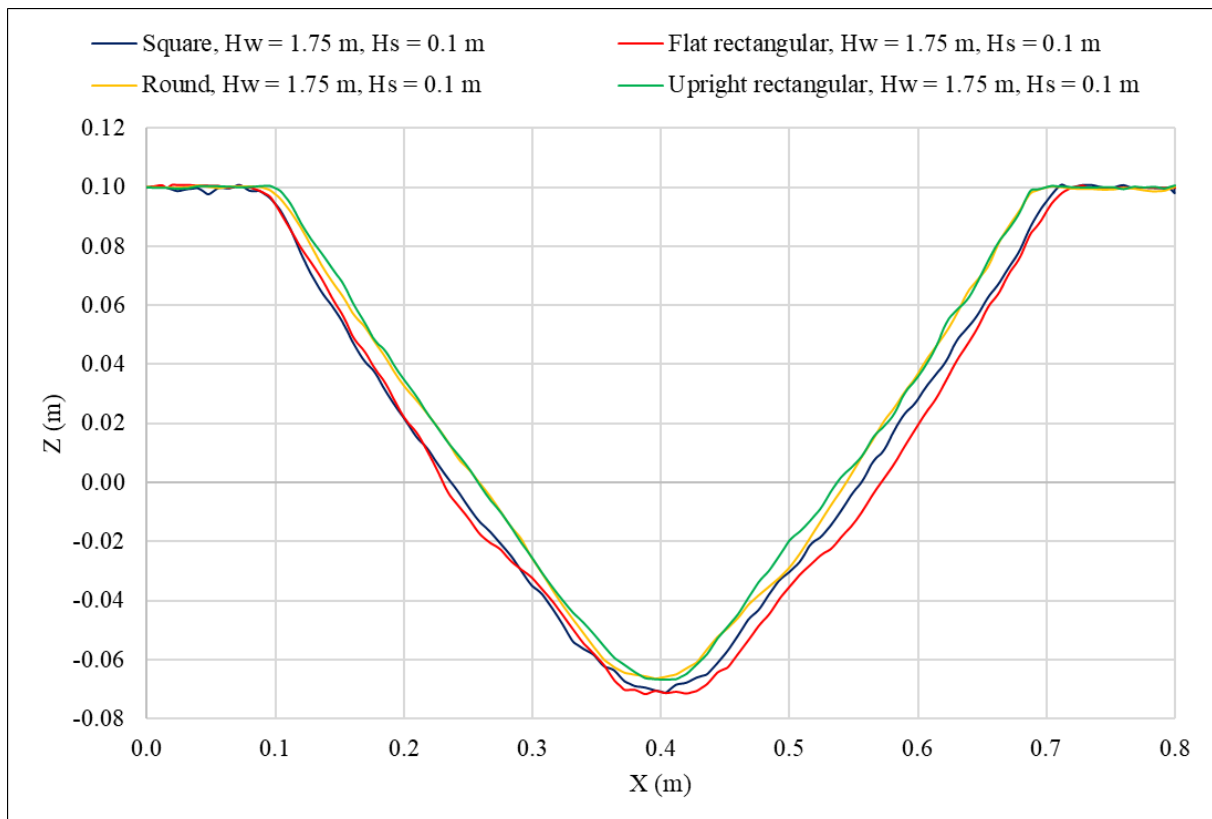
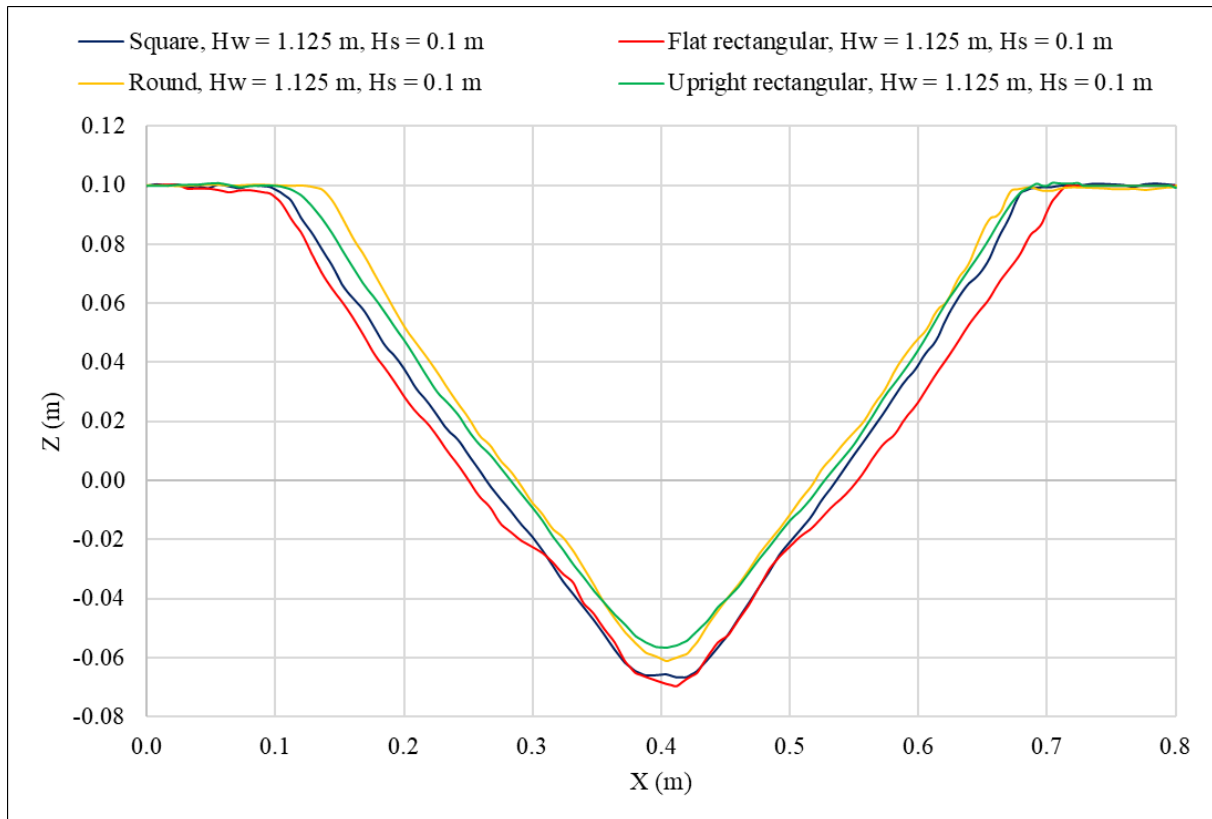
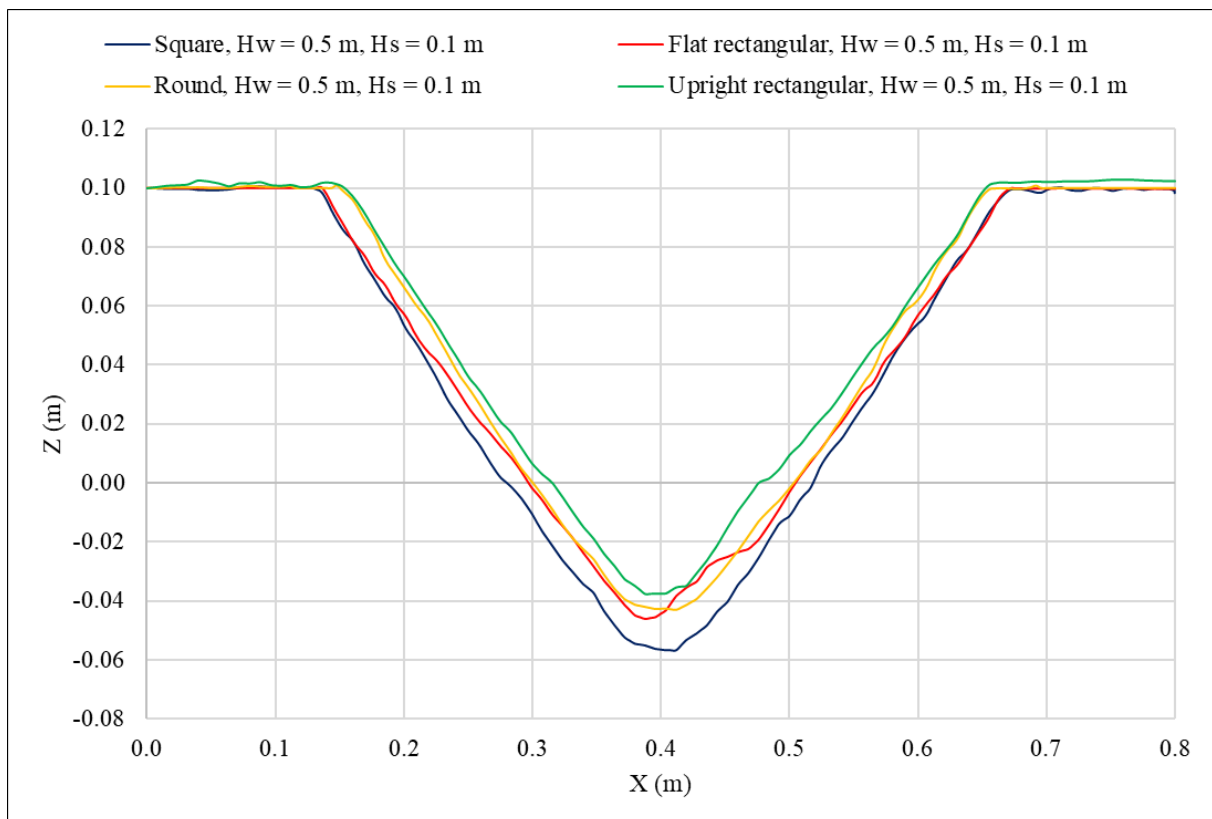
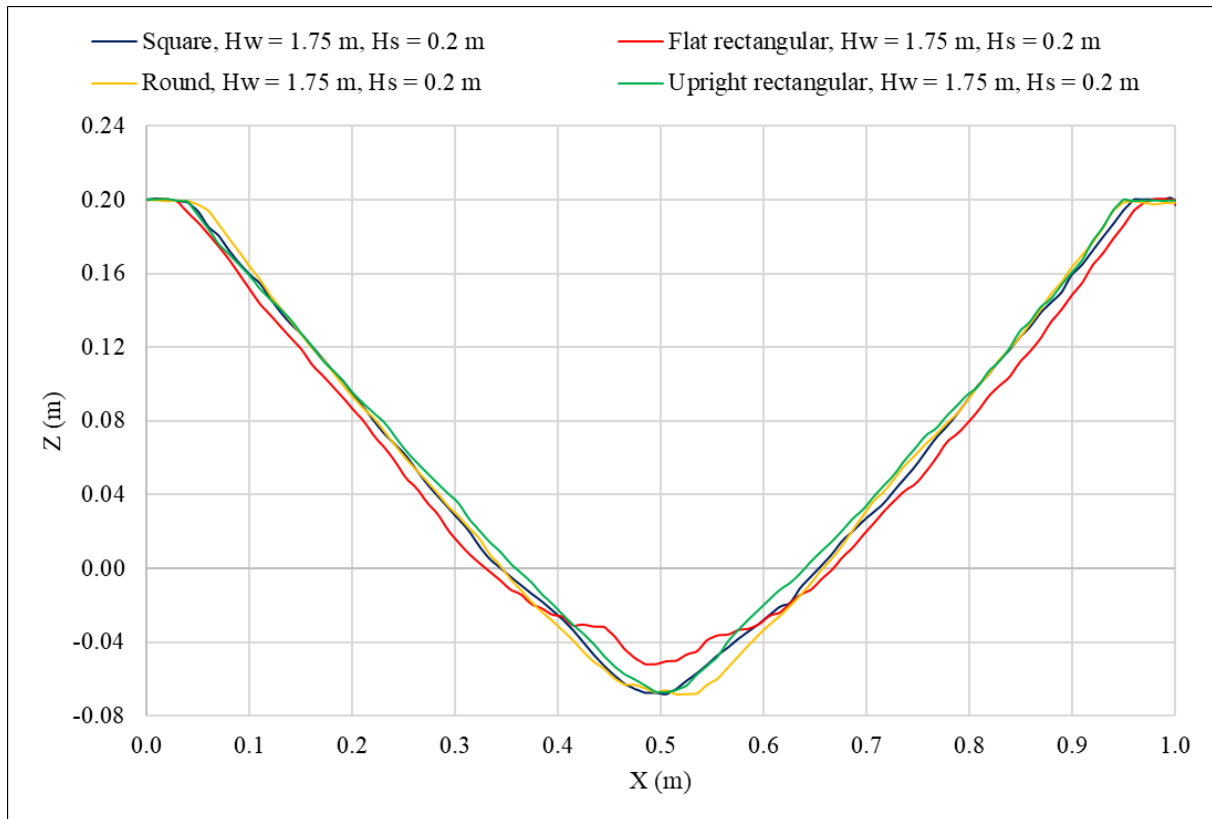
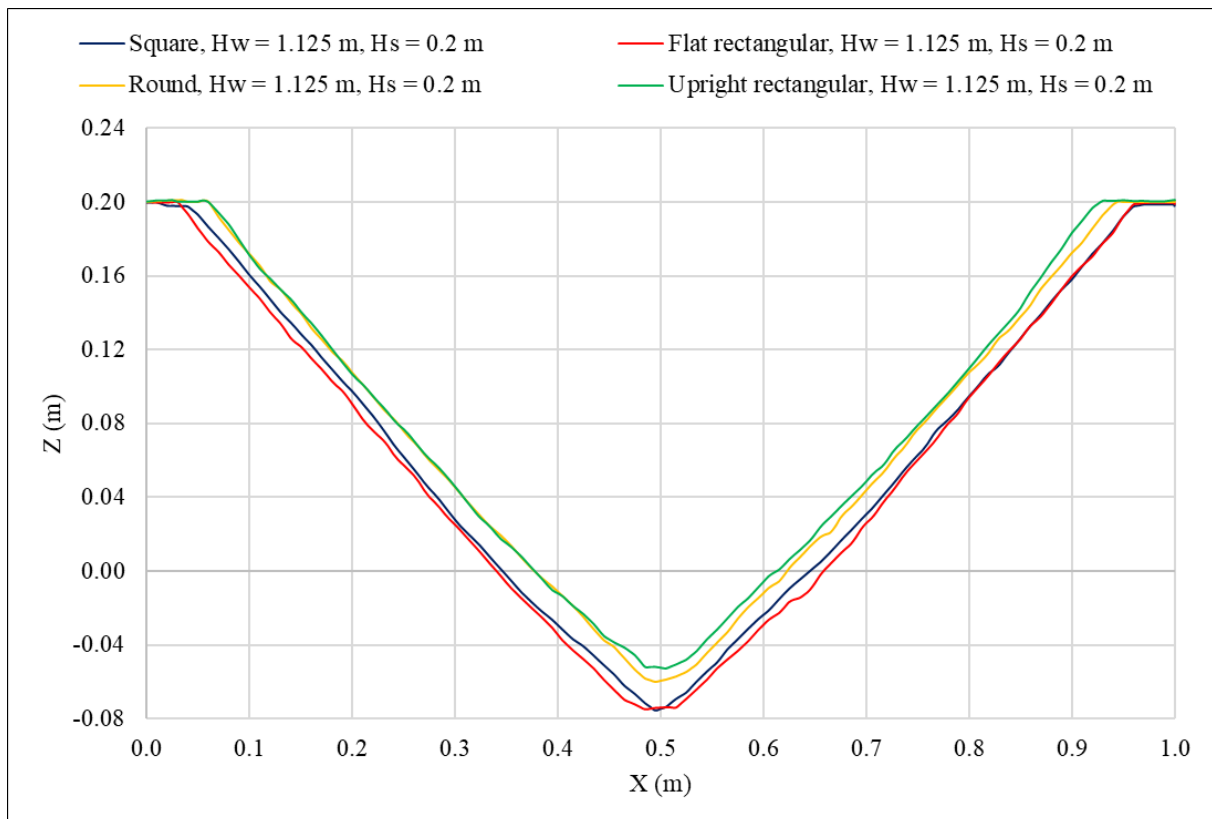
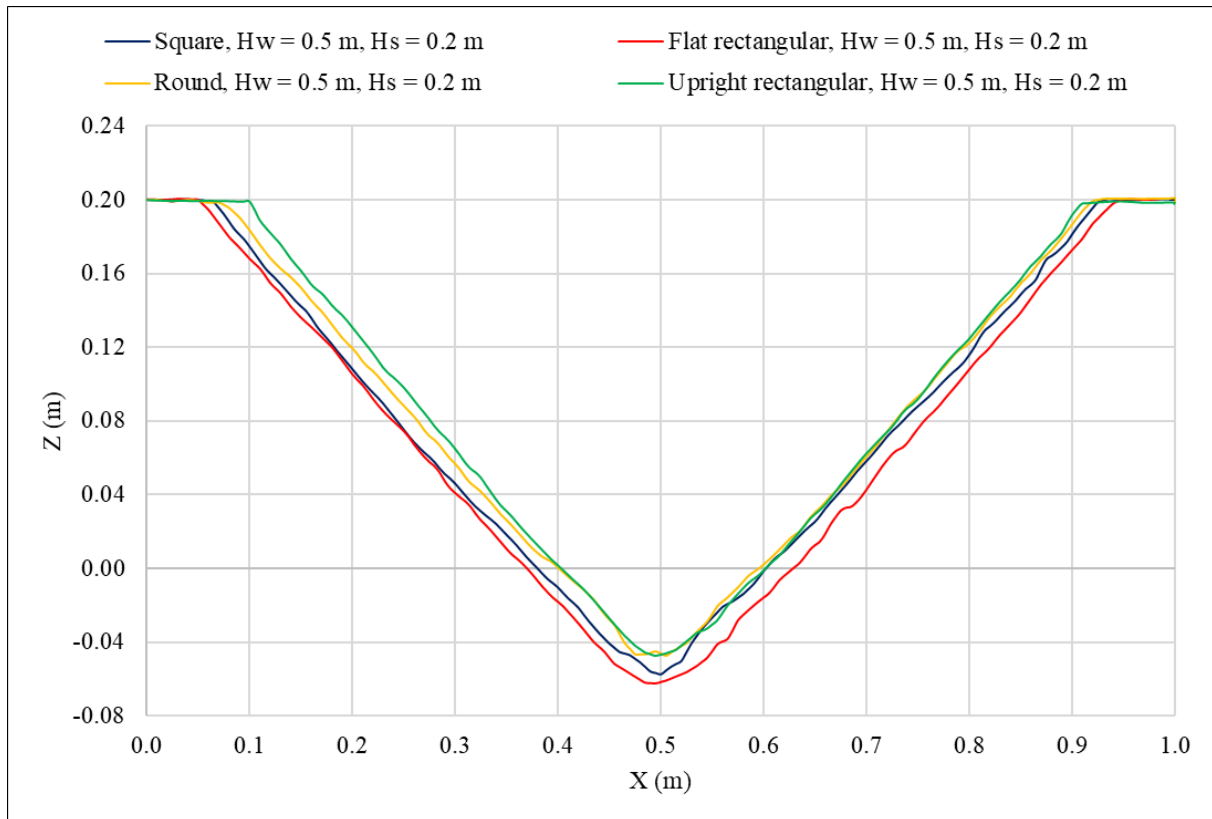


Figure L.2 Cross-sectional bed profiles for $H_w = 1.125$ m and $H_s = 0$ m

Appendix L: Cross-Sectional Bed Profiles**Figure L.3 Cross-sectional bed profiles for $H_w = 0.5$ m and $H_s = 0$ m****Figure L.4 Cross-sectional bed profiles for $H_w = 1.75$ m and $H_s = 0.1$ m**

Appendix L: Cross-Sectional Bed Profiles**Figure L.5 Cross-sectional bed profiles for $H_w = 1.125$ m and $H_s = 0.1$ m****Figure L.6 Cross-sectional bed profiles for $H_w = 0.5$ m and $H_s = 0.1$ m**

Appendix L: Cross-Sectional Bed Profiles**Figure L.7 Cross-sectional bed profiles for $H_w = 1.75\text{ m}$ and $H_s = 0.2\text{ m}$** **Figure L.8 Cross-sectional bed profiles for $H_w = 1.125\text{ m}$ and $H_s = 0.2\text{ m}$**

Appendix L: Cross-Sectional Bed Profiles**Figure L.9 Cross-sectional bed profiles for $H_w = 0.5$ m and $H_s = 0.2$ m**

Appendix M Scour Cone Slope Comparison

Table M.1 Longitudinal and transverse slopes of the scour cones for all tests

Test number	Test ID	Longitudinal slope	Transverse slope	Difference between longitudinal and transverse
1	RoHs1Hw1	33.3	33.3	0.00%
2	RoHs1Hw2	33.2	31.4	5.71%
3	RoHs1Hw3	32.2	30.7	4.89%
4	SqHs1Hw1	32.0	30.7	4.11%
5	SqHs1Hw2	32.7	31.2	4.72%
6	SqHs1Hw3	33.8	32.0	5.74%
7	FrHs1Hw1	31.2	30.7	1.76%
8	FrHs1Hw2	32.7	30.4	7.71%
9	FrHs1Hw3	34.9	31.9	9.34%
10	UrHs1Hw1	31.7	32.0	-0.92%
11	UrHs1Hw2	32.4	32.8	-0.94%
12	UrHs1Hw3	34.9	32.5	7.30%
13	RoHs2Hw1	30.7	32.3	-5.15%
14	RoHs2Hw2	31.8	31.3	1.46%
15	RoHs2Hw3	30.6	33.1	-7.57%
16	SqHs2Hw1	31.1	28.0	10.92%
17	SqHs2Hw2	30.2	32.0	-5.45%
18	SqHs2Hw3	33.4	32.5	2.51%
19	FrHs2Hw1	30.0	30.3	-1.14%
20	FrHs2Hw2	30.4	29.4	3.26%
21	FrHs2Hw3	29.5	30.6	-3.53%
22	UrHs2Hw1	31.7	30.7	3.31%
23	UrHs2Hw2	35.7	31.6	12.90%
24	UrHs2Hw3	32.3	30.1	7.14%
25	SqHs3Hw1	31.4	32.1	-2.20%
26	SqHs3Hw2	30.9	31.0	-0.23%
27	SqHs3Hw3	30.1	31.0	-2.80%
28	FrHs3Hw1	29.6	33.0	-10.33%
29	FrHs3Hw2	31.3	32.3	-2.92%
30	FrHs3Hw3	30.5	30.5	0.10%
31	UrHs3Hw1	31.4	31.8	-1.15%
32	UrHs3Hw2	30.6	31.3	-2.27%
33	UrHs3Hw3	30.9	31.4	-1.77%
34	RoHs3Hw1	32.0	32.8	-2.60%
35	RoHs3Hw2	30.8	31.9	-3.40%
36	RoHs3Hw3	30.9	30.6	0.88%

Appendix N Prototype Scaled Graphs

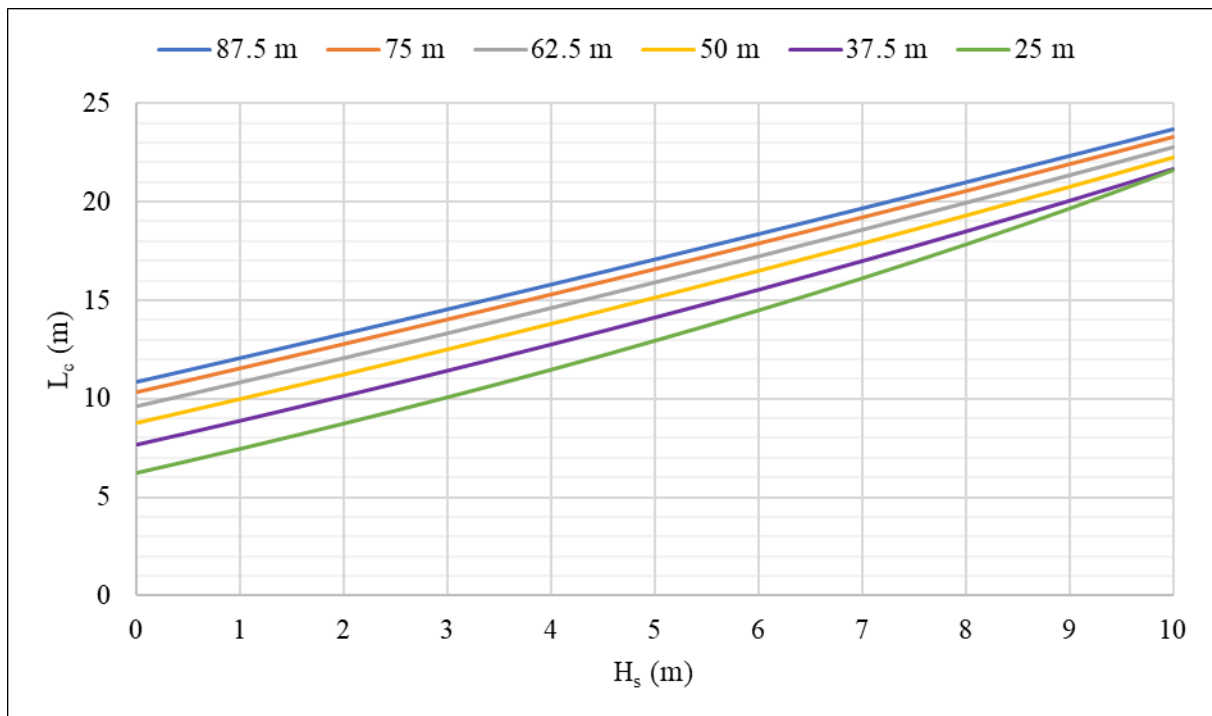


Figure N.1 Prototype scour cone length at different water depths for flat rectangular outlet at 1:50 scale (determined using Equation 5-27 and coefficients in Table 5.26)

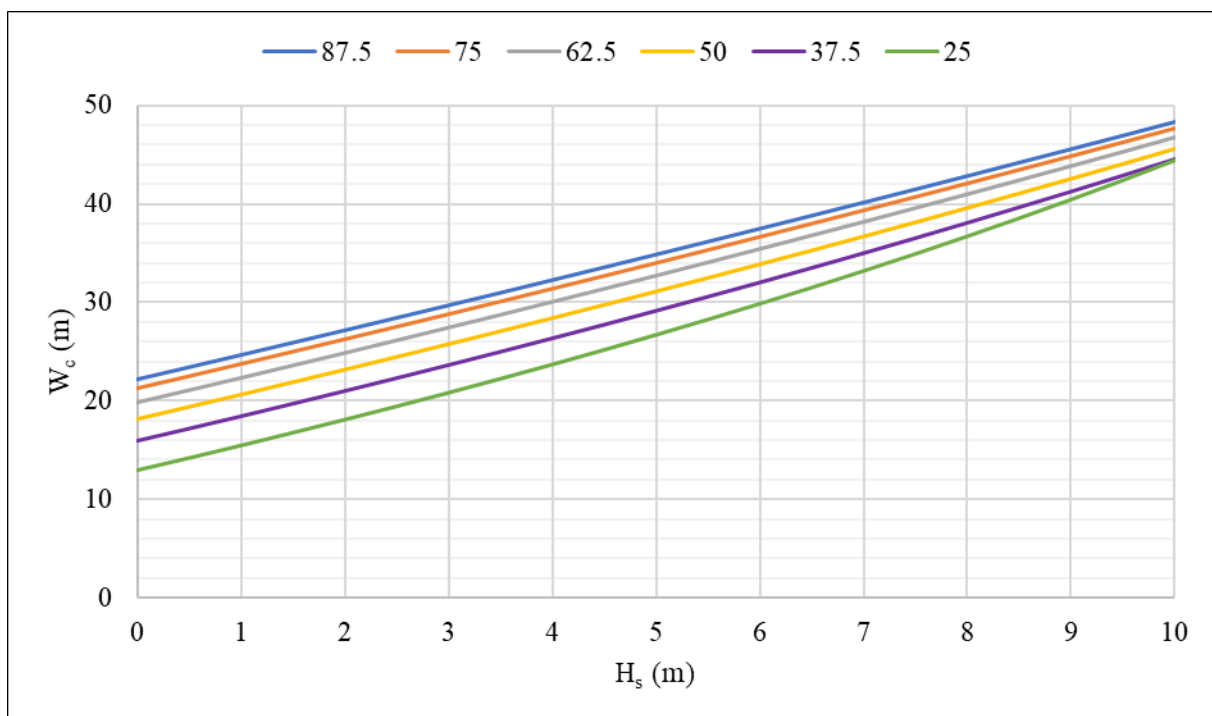


Figure N.2 Prototype scour cone width at different water depths for flat rectangular outlet at 1:50 scale (determined using Equation 5-27 and coefficients in Table 5.26)

Appendix N: Prototype Scaled Graphs

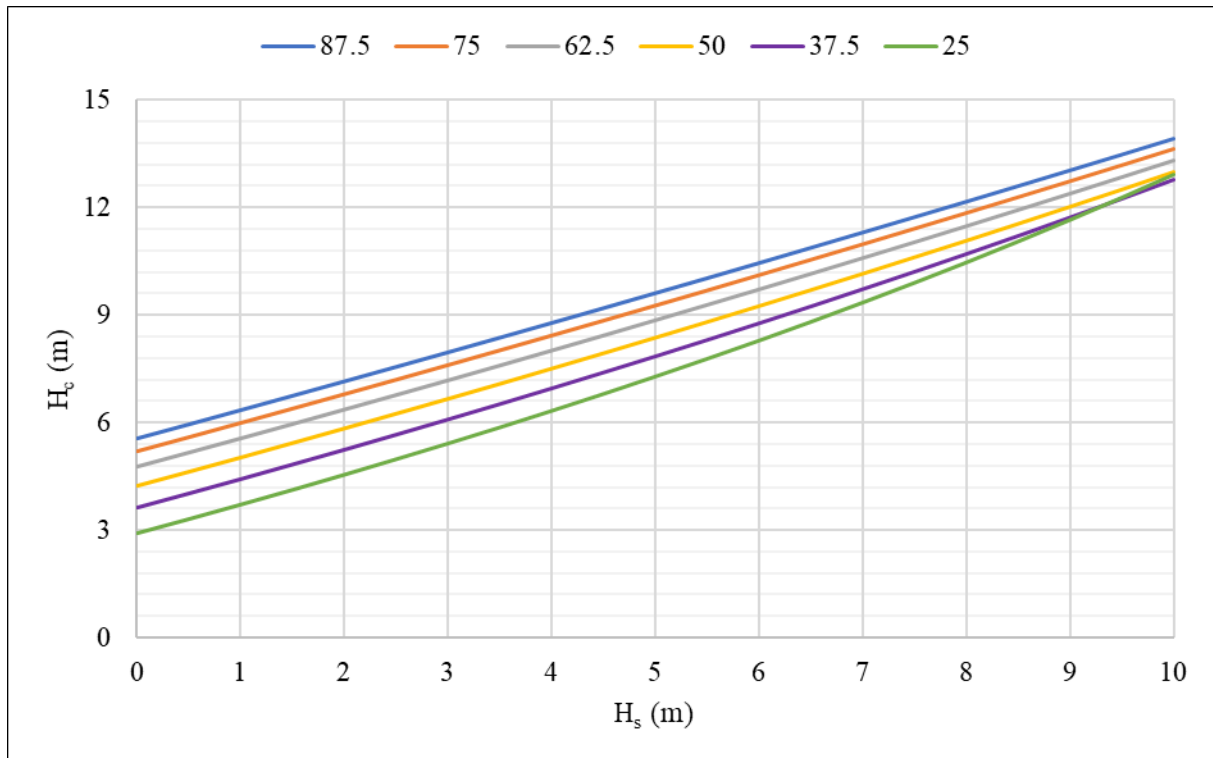


Figure N.3 Prototype scour cone height at different water depths for flat rectangular outlet at 1:50 scale (determined using Equation 5-27 and coefficients in Table 5.26)

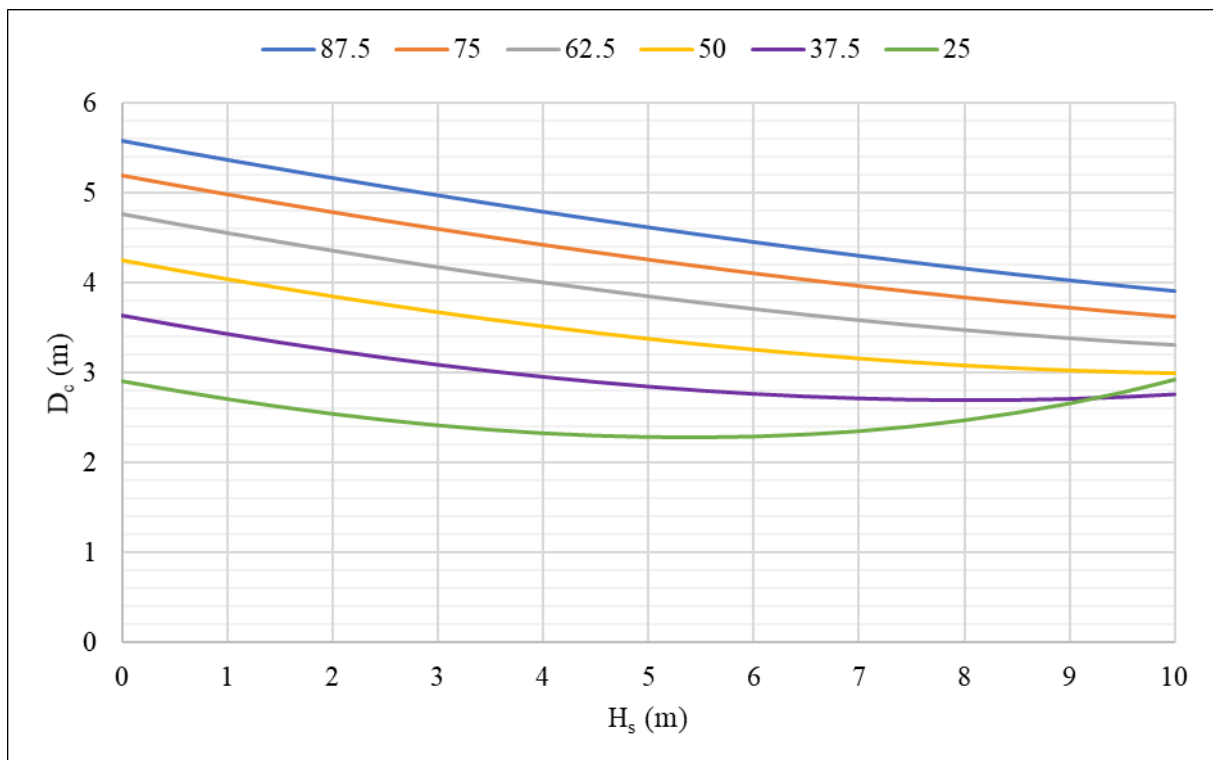


Figure N.4 Prototype scour cone depth at different water depths for flat rectangular outlet at 1:50 scale (determined using Equation 5-27 and coefficients in Table 5.26)